

# ResearchOnline@JCU

This file is part of the following reference:

**Stark, Clair (2016) *Spatial and temporal water quality changes during a large scale dredging operation*. PhD thesis, James Cook University.**

Access to this file is available from:

<http://researchonline.jcu.edu.au/50022/>

*The author has certified to JCU that they have made a reasonable effort to gain permission and acknowledge the owner of any third party copyright material included in this document. If you believe that this is not the case, please contact*

*[ResearchOnline@jcu.edu.au](mailto:ResearchOnline@jcu.edu.au) and quote  
<http://researchonline.jcu.edu.au/50022/>*

# **Spatial and temporal water quality changes during a large scale dredging operation**

Thesis submitted by

Clair Stark BSc (Hons)

in December 2016

for the degree of Doctor of Philosophy

in the College of Science and Engineering

James Cook University

Supervisors: Prof. Peter Ridd, Dr. Ross Jones, Dr. James Whinney, Prof. Ron White

# Acknowledgments

This PhD would not have been possible without the support of my parents, Al and Disy. You have not only housed me and fed me, but have provided ongoing emotional support and advice throughout my undergraduate and PhD. You have weathered my stress levels and listened to my whinging. Thank you! Also thank you to my wonderful siblings for their continued support.

A special thanks to my primary supervisor, Professor Peter Ridd, who I imagine is the best supervisor anyone has ever had. Thank you for your patience and understanding and always putting your students first. Your feedback was always thorough, fast and with the continued development of your students in mind. I have learnt a lot, not only about scientific research, but personally from knowing you I have seen your excellent work ethic, professional communication, and teaching.

I would also like to thank the Western Australian Marine Science Institution for giving me the opportunity to work on this project.

## Statement on the contribution of others

This thesis was conducted in collaboration with the Western Australian Marine Science Institution's (WAMSI) Dredging Science Node (DSN) under Theme 4: Coral Reefs, and included the following contributions of others:

*Data analysis:* JCU nephelometer sensor data was quality controlled and error corrected by the JCU Marine Geophysics Lab and Dr. Rebecca Fisher at WAMSI. Water quality data at Barrow Island and Hay Point was collected by sensors from the JCU Marine Geophysics Lab.

*Contributions to co-authored publications and reports:*

Two WAMSI DSN reports and 4 journal articles have resulted from the work in this thesis, as follows:

### **WAMSI DSN reports:**

- Fisher R, Stark C, Ridd P, Jones R (2014). *Project 4.2. Effects of dredging and dredging related activities on water quality: Phase 1 - spatial and temporal patterns* (published).
- Stark C, Whinney J, Ridd P, Jones R (submitted 2016). *Project 4.4. Estimating sediment deposition fields around dredging projects.*

### **Journal publications:**

Stark C, Ridd P, Fisher R, Jones R (in preparation). *Dredging spatial impacts on light attenuation*

Stark C, Whinney J, Ridd P, Jones R (in preparation). *Estimating sediment deposition fields around dredging projects.*

Fisher R, Stark C, Ridd P, Jones R (2015). *Spatial patterns in water quality changes during dredging in tropical environments.* PLoS One.

Jones RJ, Fisher R, Stark C, Ridd P V (2015). *Temporal Patterns in Seawater Quality from Dredging in Tropical Environments*. PLoS One.

# Abstract

Dredging poses an environmental risk by increasing suspended sediment which has a range of effects on sensitive benthic communities, particularly coral reefs. Understanding spatial and temporal sediment related dredging impacts is essential to improve environmental impact assessment (EIA), monitoring and management of dredge operations. Despite the scale of global dredging projects, our understanding of the impacts is limited due to a lack of sufficiently large water quality datasets, the site specific nature of water quality changes during dredging, and the complex response of corals to the various associated suspended sediment pressures (i.e. reduced light, increased sediment deposition). Of particular importance during the EIA phase, and while monitoring dredging impacts, is understanding the distance to dredge effects i.e. how far the dredge related sediment impacts extend to more accurately predict environmental impacts and provide greater protection to coral reefs during dredging operations.

The distance to dredge effects on water quality conditions (i.e. the spatial impacts of dredging) was investigated at Barrow Island, Western Australia, to determine how dredging affects turbidity, submarine light and sediment deposition conditions. Analysis was made possible using the largest water quality dataset ever collected prior to and during a large scale dredging operation. Water quality conditions prior to and during 18 months of dredging at Barrow Island, Western Australia, as well as the distance to dredge effects, were analysed to determine the impacts of dredging on turbidity, submarine light and sediment deposition. A high proportion of water quality sites (10/29) were located within 1.5 km south of dredging,

allowing a high resolution of spatial dredging impact analysis close to the dredge zone. During dredging, water quality impacts were primarily confined to sites within 2 – 5 km south of the dredge zone, gradually decreasing to ambient levels at sites north of the dredge zone and sites > 10 km south. Turbidity maximums, means and standard deviations were up to 4 – 6 x higher, median light attenuation coefficients 1.5 x higher, median deposition levels up to 7 x higher and median overburden (dredge related turbidity, calculated using a simple statistical turbidity model which estimates natural turbidity during dredging) were 3 – 4 x higher at sites within 2 – 5 km south of dredging. Sites north of the dredge zone (extending up to 30 km north), sites > 10 km south of the dredge zone (extending up to 30 km south), and 2 dredge disposal perimeter sites were unaffected by dredging. There was also a strong relationship between light attenuation and turbidity at almost all of the 25 Barrow Island sites used to study light levels; 24 of the 25 sites had  $R^2 > 0.5$  and 17 had  $R^2 \geq 0.50$ .

Turbidity conditions at Barrow Island were also characterised by using a range of different temporal analysis, including running mean and spectral analysis. By applying running means using increasing window sizes (from 1 hour to 30 days) separately to the baseline and dredge periods, it was revealed that dredging increases both the intensity and the duration of turbidity, with monthly, daily and hourly turbidity conditions higher at sites within 2 km of dredging; monthly averages were up to 25 NTU (compared to ~ 10 NTU at reference sites), daily averages up to 200 NTU (compared to maximum ~ 30 NTU at reference sites) and hourly averages up to 400 NTU (compared to maximum 100 NTU at reference sites). Spectral analysis also revealed the occurrence of horizontal advection during dredging at sites within 2 km of dredging.

The use of a simple, statistical turbidity model to estimate natural turbidity (due to the natural resuspension processes of waves and tides) during dredging, and as a possible turbidity and deposition threshold exceedance monitoring tool, was investigated. The model is designed to be simple – an alternative method to the more complex three dimensional hydrodynamic models which require numerous inputs – and as such has expected limitations. Despite these limitations, the purpose of the model in this study is to decouple the natural turbidity and dredge induced turbidity, and possibly as an exceedance threshold tool. Model performance was tested in 2 different hydrodynamic settings – a clear water environment (Barrow Island) during a dredge operation and a turbid, energetic environment (Hay Point, Queensland) during a baseline water quality monitoring study. The model was successful at estimating daily turbidity at a few of the Hay Point and Barrow Island sites, with  $R^2 > 0.5$  between modelled and measured turbidity at 83% of sites during the model test phase at Hay Point (although model skill scores were  $> 0.5$  at only 1 site during the test phase), but only 38 % of sites had  $R^2 > 0.5$  at Barrow Island and , but improvements could be made to both the input data and possibly more sophisticated parameter estimation tools (such as Bayesian analysis).

The impact of dredging on submarine light levels was also investigated. Light attenuation coefficients ( $k$ ) were analysed in lieu of measured PAR values due to non-uniform sensor depths across the water quality sites (depths ranged from  $\sim 4$  to 14 m), which introduces a depth dependence to the distance to dredge analysis. Median light attenuation coefficients at sites closest to the main dredge zone (within 2 – 5 km) were between  $0.4 - 0.55 \text{ m}^{-1}$  compared to all other sites which had levels  $0.35 - 0.4 \text{ m}^{-1}$ . As well as calculating  $k$  (using the



Beer-Lambert Law) for the spatial analysis, the strong relationship between midday turbidity and  $k$  ( $R^2 > 0.5$  at 96 % of sites and  $\geq 0.7$  at 68 %) was used to derive regression models of light attenuation from measured (midday) turbidity. The use of a double exponential method, which is an extension of the Beer Lambert Law developed by Paulson and Simpson (1977), was also investigated for estimating the light attenuation coefficients but was unsuitable for the Barrow Island study sites.

# Contents

|   |     |
|---|-----|
| Acknowledgments .....   | ii  |
| Statement on the contribution of others .....   | iii |
| Abstract .....  | v   |
| Contents .....  | ix  |
| List of Figures.....  | xi  |
| List of Tables .....  | xiv |
| Chapter 1. Introduction.....  | 1   |
| 1.1 Background .....  | 1   |
| 1.2 Motivation.....   | 2   |
| 1.3 Knowledge gaps .....  | 3   |
| 1.4 Aims and objectives .....   | 7   |
| 1.5 Document Organisation .....   | 18  |
| Chapter 2. Sites and data .....   | 20  |
| 2.1 Study sites .....   | 20  |
| 2.2 Data .....  | 24  |
| 2.2.1 <i>Turbidity and deposition measurement and calibration</i> .....                 | 24  |
| 2.2.2 <i>Photosynthetically active radiation and water pressure</i> .....               | 25  |
| Chapter 3. Temporal and spatial impacts of dredging on turbidity .....                  | 27  |
| 3.1 Synopsis.....   | 27  |
| 3.2 Methods .....   | 28  |
| 3.2.1 <i>Running mean temporal analysis</i> .....                                       | 28  |
| 3.2.2 <i>Spectral analysis</i> .....  | 29  |
| 3.2.3 <i>Time averaged wavelet power</i> .....  | 31  |
| 3.2.4 <i>Turbidity model</i> .....  | 32  |
| 3.3 Results.....  | 37  |
| 3.3.1 <i>Turbidity at Barrow Island</i> .....   | 37  |
| 3.3.2 <i>Turbidity at Hay Point</i> .....   | 42  |
| 3.3.3 <i>Turbidity model</i> .....  | 44  |
| 3.3.4 <i>Running mean analysis</i> .....  | 59  |
| 3.4 Discussion.....   | 77  |
| 3.4.1 <i>Barrow Island turbidity conditions</i> .....                                   | 77  |
| 3.4.2 <i>Running mean analysis</i> .....  | 78  |
| 3.4.3 <i>Turbidity model</i> .....  | 81  |
| Chapter 4. Light attenuation during dredging: spatial variations in PAR .....           | 85  |
| 4.1 Synopsis.....   | 85  |
| 4.2 Methods .....   | 86  |
| 4.2.1 <i>Light attenuation coefficient</i> .....  | 86  |
| 4.2.2 <i>Depth dependence of light absorption</i> .....                                 | 89  |
| 4.2.3 <i>Double exponential method</i> .....  | 90  |
| 4.3 Results.....  | 92  |
| 4.3.1 <i>Relationship between k and turbidity</i> .....                                 | 92  |
| 4.3.2 <i>Particle Size Distribution effects on light attenuation coefficients</i> ..... | 97  |
| 4.3.3 <i>Depth dependence of k</i> .....  | 98  |
| 4.3.4 <i>Double exponential Paulson Simpson method</i> .....                            | 101 |

|            |  |     |
|------------|--|-----|
| 4.3.5      | <i>Spatial dredging impacts on k and turbidity</i> .....                                 | 103 |
| 4.4        | Discussion.....  | 104 |
| Chapter 5. | Dredge deposition zone detection using in-situ data and turbidity model overburden ..... | 111 |
| 5.1        | Synopsis.....  | 111 |
| 5.2        | Methods .....  | 112 |
| 5.2.1      | <i>Overburden (from turbidity model)</i> .....   | 112 |
| 5.2.2      | <i>Daily surface sediment density (SSD)</i> .....  | 113 |
| 5.3        | Results.....   | 114 |
| 5.3.1      | <i>Surface sediment density</i> .....  | 114 |
| 5.3.2      | <i>Overburden</i> .....  | 119 |
| 5.3.3      | <i>Surface sediment density and overburden</i> .....                                     | 122 |
| 5.4        | Discussion.....  | 126 |
| Chapter 6. | Conclusion.....  | 130 |
| 6.1        | Summary of work.....   | 130 |
| 6.2        | Recommendations and future work .....  | 134 |
| Chapter 7. | References .....   | 136 |

# List of Figures

|  |    |
|--|----|
| <i>Figure 2-1 Location map showing the Barrow Island water quality sites (A - C) on the eastern side of the island and the Hay Point sites (D).</i>  | 21 |
| <i>Figure 3-1 Measured turbidity (raw, at 10 minute intervals) time series during the entire monitoring period at Barrow Island</i>  | 39 |
| <i>Figure 3-2 Maximum (A) and average (B) turbidity during the baseline (white dots) and dredge (black dots) periods, plotted by distance of the site from the dredge zone.</i>  | 40 |
| <i>Figure 3-3 Measured turbidity (raw, at 10 minute intervals) time series during the baseline period (July 2014 to August 2015) at Hay Point water quality sites</i>  | 43 |
| <i>Figure 3-4 Hay Point project. Turbidity model and model terms at 3 representative sites</i>   | 48 |
| <i>Figure 3-5 A-E Barrow Island Project. Turbidity model and model terms at 6 representative sites</i>   | 55 |
| <i>Figure 3-6 Relationship between daily averaged RMS pressure fluctuation measurements and daily averaged turbidity at three representative Hay Point sites</i>   | 57 |
| <i>Figure 3-7 Relationship between daily averaged RMS pressure fluctuation measurements and daily averaged turbidity at three representative Barrow Island sites</i>   | 58 |
| <i>Figure 3-8 E Turbidity running mean percentile analysis using increasing window sizes (from 1 hour to 30 days) comparing the baseline (dotted lines) and dredge periods (solid lines) at representative Barrow Island site</i>  | 64 |
| <i>Figure 3-9 Percentiles of turbidity running means (vertical axis) calculated using (A) 1 hour running mean window size and (B) 1 day running mean window size, plotted according to the site distance from the dredge zone during the baseline period (dots) and dredge period (circles).</i> | 66 |
| <i>Figure 3-10 Percentiles of turbidity running means (vertical axis) calculated using increasing window sizes (1 hour to 30 days) plotted according to the site distance from the dredge zone</i>   | 67 |
| <i>Figure 3-11 Normalised turbidity global (time-averaged) spectral power curves across all sites for the baseline period (A) and dredge period (B).</i>   | 69 |
| <i>Figure 3-12 Normalised wave global (time-averaged) spectral power curves across all sites for the baseline period (A) and dredge period (B).</i>  | 71 |
| <i>Figure 3-13 Normalised water height global (time-averaged) spectral power curves across all sites for the baseline period (A) and dredge period (B).</i>  | 72 |
| <i>Figure 3-14 Normalised wind global (time-averaged) spectral power curves at Barrow Island airport showing the zonal (blue) and meridional (red) directions during the baseline period (solid line) and dredge period (broken line).</i>   | 73 |
| <i>Figure 3-15 Turbidity spectral analysis for the Barrow Island project, showing reference sites C) DUG and D) SBS.</i>   | 76 |
| <i>Figure 4-1 Relationship between midday light attenuation coefficients (k) and turbidity (black dots) at two sites close to dredging.</i>  | 94 |

Figure 4-2 (A) Terrestrial PAR, (B) benthic PAR, (C) turbidity and (D) midday  $k$  values at MOFA (see Figure 2-1 for site locations) from September to December 2010. 96

Figure 4-3 (A) Time series of midday (10:00–14:00 h) turbidity (primary vertical axis) and light attenuation coefficients ( $k$ , secondary vertical axis) at MOFA (located ~ 500 m south of dredge zone), (B) scatter plot of turbidity and  $k$  at MOFA, (C) time series of midday (10:00–14:00 h) turbidity (primary vertical axis) and light attenuation coefficients ( $k$ , secondary vertical axis) at reference site REFS, and (D) scatter plot of turbidity and  $k$  at REFS (~25 km south of dredge zone). See Figure 2-1 for site locations. 97

Figure 4-4 Scatter plot showing the relationship between midday turbidity and light attenuation coefficients for the aggregated data during dredging, separated into near field (MOF and LNG sites < 1.4 km south of dredging, blue dots) and far field sites (all other sites, red asterix). The inset shows the zoomed region between turbidity = 0 - 4 NTU and  $k = 0 - 0.5 \text{ m}^{-1}$  as they are difficult to compare in the main figure. Sites have been grouped to investigate whether a particle size dependency exists in the light attenuation coefficients. 98

Figure 4-5 Relationship between turbidity and the light attenuation coefficient ( $k$ ) at four sites close to dredging 99

Figure 4-6 Clear water light attenuation coefficient ( $k_0$ ,  $k$  when turbidity = 0 NTU) plotted against the average of the dredge period midday logger depths ( $z$ ) at each site. 100

Figure 4-7 Relationship between observed  $I_z$  at depth  $z$  and modelled  $I$  using the three regression methods: linear / power comparisons are blue dots, rational function method are red dots and the Paulson Simpson double exponential method are orange dots at sites A) LNG0 and B) LNG2 during the dredge period. 103

Figure 4-8 Median midday (A)  $k$  (depth corrected) and (B) turbidity plotted according to the distance of the site from the dredge zone 104

Figure 5-1 An example of the sawtooth pattern occurring in the SSD data during significant sediment accumulation events. 114

Figure 5-2 Average daily SSD ( $\text{mg cm}^{-2}$ ) during the baseline period (white circles) and dredge period (black circles) during the Barrow Island project plotted according to the distance of the sites from the dredge zone 115

Figure 5-3 SSD data at MOFA demonstrating the rapid removal of accumulated sediment during a two hour accumulation period 118

Figure 5-4 (A) Turbidity (black line) and deposition (orange line) at site MOFC from 19-20 August 2010, demonstrating the sawtooth pattern in the deposition data resulting from sediment accumulation and wiper action, and (B) the wavelet transform of the sawtooth pattern in deposition data, showing higher energy (yellow bands) in the 2,1 and half hour periods. 118

Figure 5-5 Daily average overburden (NTU) during the baseline period (white circles) and dredge period (black circles) during the Barrow Island project plotted according to the distance (km, see Figure 2-1) of the sites from the dredge zone 120

Figure 5-6 Overburden and daily averaged surface sediment density comparing all overburden values (black circles) and only days when overburden > 5 NTU (orange circles) at sites DUG (A) and DSGS (B). The relationship improved significantly at both sites when comparing overburden and SSD only on days when overburden > 5 NTU, from  $R^2 = 0$  (typical of all sites) to  $R^2 = 0.5$  at DUG and  $R^2 = 0.7$  at DSGS. 123

Figure 5-7 Daily averaged SSD (solid line) and daily overburden (broken line) at site DUG (A, 9.3 km south of the dredge zone) and MOF1 (B, 0.8 km of dredge zone and on the perimeter of the spoil disposal ground) during the dredge period. 124

Figure 5-8 Daily overburden (A) and daily averaged sediment surface density (B) at Barrow Island sites from December 2007 to December 2011 plotted according to the distance of site from the dredge zone. Negative

*values are north of the dredge zone (which is at origin) and positive values are south. The black dotted line separates the baseline period (December 2007 to 19 May 2010) and dredge period (19 May 2010 to December 2011).*

125

# List of Tables

|  |     |
|--|-----|
| <i>Table 2-1 Barrow Island water quality monitoring site details, including site distance from dredge zone, average logger depth, baseline monitoring length and dredge period monitoring length.</i>  | 23  |
| <i>Table 2-2 Hay Point monitoring site details, including average logger depth and monitoring length in days.</i>  | 24  |
| <i>Table 3-1 Summary table showing maximum (raw and daily averaged), mean and standard deviation turbidity during the baseline (train and test periods) and dredging periods</i>   | 41  |
| <i>Table 3-2 Summary table showing maximum (raw and daily averaged), mean and standard deviation turbidity at Hay Point sites during the baseline (train and test) period, and <math>R^2</math> values between the measured and modelled turbidity</i>   | 44  |
| <i>Table 3-3 Turbidity model performance at Hay Point sites based on the <math>R^2</math> and skills score between modelled and measured turbidity</i>   | 49  |
| <i>Table 3-4 Turbidity model performance at Barrow Island sites based on the <math>R^2</math> and skills scores between modelled and measured turbidity</i>  | 56  |
| <i>Table 3-5 <math>R^2</math> and root mean square error (RMSE) between RMS pressure fluctuations (estimates of seafloor wave motion) and turbidity measurements</i>   | 58  |
| <i>Table 3-6 <math>R^2</math> and root mean square error between RMS pressure fluctuations (quasi-estimates of wave motion at the seafloor) and turbidity measurements at Barrow Island</i>  | 59  |
| <i>Table 4-1 Dredge period average PAR, median and maximum midday light attenuation coefficients (<math>k</math>) and turbidity, <math>k</math> in clear water (<math>k_0</math>), and the number of days the midday averaged turbidity exceeded 50 NTU at all study sites and aggregated across all Barrow Island sites</i> | 94  |
| <i>Table 4-2 Relationship between midday light attenuation coefficients (<math>k</math>) and turbidity at Barrow Island</i>  | 95  |
| <i>Table 4-3 <math>R^2</math> and RMSE between modelled <math>I</math> and measured <math>I_z</math></i>   | 102 |
| <i>Table 5-1 Summary table showing mean, median and maximum SSD during the baseline and dredging periods listed according to site distances (km) from north to south of the dredge zone.</i>   | 116 |
| <i>Table 5-2 Summary table showing mean and maximum overburden (i.e. difference between measured and modelled turbidity in NTU) during the dredge period</i>   | 121 |

# Chapter 1. Introduction

## 1.1 Background

Dredging is necessary to create or expand ports and harbours and deepen shipping channels but the altered water quality conditions can be harmful to the environment, particularly sensitive benthic habitats such as coral reefs (Rogers 1990, Foster et al. 2010, Erftemeijer et al. 2012), due to increased sediment related impacts. Despite the large number of dredging projects in Australia and around the world, and concerns about associated environmental impacts, our knowledge of water quality changes during dredging and impacts to coral reefs is limited. Fortunately we now have access to the largest (spatial and temporal) water quality dataset ever collected prior to and during a large scale ( $\sim 7 \text{ Mm}^3$ ) capital dredging project at Barrow Island, Western Australia, allowing a comprehensive study into water quality changes (specifically light and deposition) during dredging, as well as development of new dredge impact analysis techniques (i.e. turbidity model) to understand the environmental impact of dredging. The main focus of this thesis will be to look at aspects of this dataset to temporally compare turbidity, light attenuation and sediment deposition prior to and during dredging, and to spatially compare these conditions to describe the distance to dredge effects at increasing distance from the dredge zone.

Due to the recent resources boom, there have been numerous large scale capital dredging projects, particularly along the Queensland coast and on Western Australia's North West Shelf (NWS) (see McCook et al. 2015 for details). In the 2014-15 financial year, Australia's resources minerals and petroleum sector was worth  $\sim \$100$  billion, and 86 % of Australia's LNG exports were from the NWS



(DSD 2016). The potential environmental threat of dredging has attracted contentious public interest, mostly due to our limited understanding of how dredging alters sediment related processes such as turbidity, benthic light availability and sediment deposition, and the associated environmental impacts, particularly to coral reefs. Understanding these impacts is important for managing marine ecosystems in the short- and long- term, and at regional (Fabricius et al. 2014) and local scales (Sofonia & Unsworth 2010, Fabricius et al. 2014, Chartrand et al. 2016). Knowledge gaps lead not only to public scrutiny, which can influence government decisions, but can also cause unnecessary environmental damage, operational delays and greater cost to proponents during dredging operations (due to inaccurate thresholds), as well as costly and lengthy environmental approvals process.

## **1.2 Motivation**

The ability to forecast the environmental impact of dredging is an important component of modelling at the EIA stage, or when dredging is underway, and is based upon the ability to understand how pressure fields (such as light reduction and elevated deposition) relate to suspended sediment concentrations (SSCs), and how these propagate in the environment. This information can be used to describe the relationship between coral health and dredging water quality pressures. Being able to predict the scale of potential impacts from dredging near coral reefs is important for dredging management, and establishing an evidence-based footprint is increasingly becoming important for public perception of the nature and scale of dredging projects (Fisher et al. 2015, Spearman 2015).

Dredging proponents are required to manage projects under a spatially defined zonation scheme (EPA 2011), and limited understanding about dredging impacts can lead to inaccurate water quality thresholds, possibly resulting in unnecessary damage, operational delays and great expense to proponents. Water quality thresholds are often set conservatively (for example based on the 80<sup>th</sup> percentile of typical ambient conditions, ANZECC 1994) rather than based on evidence of environmental tolerance levels (EPA 2011). If thresholds are set too high corals may be regularly exposed to potentially stressful conditions, possibly leading to mortality. Inaccurate thresholds can also delay dredging operations and be costly for proponents; setting thresholds well below tolerance limits can prompt increased monitoring and reporting frequency (for example fortnightly, see Chevron Australia Pty Ltd 2011a), and, in the worst case scenario, can suspend dredging operations.

### **1.3 Knowledge gaps**

The most significant knowledge gap related to dredging impacts is the spatial extent of dredge effects. Our understanding of the distance to dredge effects is necessary for impact prediction during the EIA process, and for optimal design of dredging operation location and water quality monitoring site locations. There are a number of reasons for our limited understanding of dredging impacts. For one, there are few large (temporal and spatial) in-situ water quality datasets collected during dredging available; it is challenging placing water quality sensors close to a dredge, and data collected by industry aren't always publicly available (Condie et al. 2006). Furthermore, water quality changes during dredging are site specific, dependent on local hydrodynamic conditions. Therefore improved understanding requires comprehensive studies on a variety of dredging projects with adequate water quality monitoring site locations. Also, (although not addressed in this

thesis but rather driving the need for this study) further complexities exist because coral response to water quality changes are site- and species- specific, and there are multiple cause-effect pathways which can affect corals (is reduced light or increased deposition the greatest threat?).

Complex sediment pressure and coral response relationships further challenge our understanding and management of dredging impacts. The temporary release of sediment into the water column during dredging can have a range of environmental effects on sensitive communities such as coral reefs (Marszalek 1981, Rogers 1990, Foster et al. 2010, McCook et al. 2015). The two primary causes of stress or mortality to corals during dredging are reduced light and deposition (Erftemeijer et al. 2012, Jones et al. 2016). Light (specifically photosynthetically active radiation (PAR), 400 – 700 nm) is essential for benthic primary production and light reduction, which occurs during dredging due to increased turbidity and deposition (Stoddart 1969, Kirk 1977a, Cloern 1987, Anthony & Fabricius 2000, Gattuso et al. 2006, Saulquin et al. 2013), inhibits the primary energy source for corals (Hallock & Schlager 1986, Te 1997, Anthony & Fabricius 2000, Anthony et al. 2004, Gattuso et al. 2006, Gilmour et al. 2006, Storlazzi et al. 2015). Sustained and frequent PAR reductions have well-known effects on the functioning and distribution of marine ecosystems (Kinzie 1973, Chalker 1981, Chalker et al. 1984, Graus et al. 1989, Rogers 1990, Erftemeijer et al. 2012). Deposition of the re-suspended sediment is also a well-known hazard, requiring benthic organisms to expend energy self-cleaning or become progressively smothered in sediments, which can clog their breathing and feeding apparatus. Smothering is sometimes observed in dredging projects close to reefs (Dodge & Vaisnys 1977, Bak 1978) and the reduction in gas (solute) exchange, under some circumstances, quickly lead to local tissue mortality and lesion formation (Weber et al. 2012). Deposition during calm conditions

can be immediate and in-situ, as the lack of resuspension hydrodynamics – wind, waves and tidal currents – are insufficient to maintain the sediment in suspension (Masselink et al. 2011)

Another factor limiting our understanding of dredging impacts is the site specific nature of water quality conditions. Local bathymetric profiles and hydrodynamics determine natural water quality conditions and influence the direction and behaviour of dredge plumes which can lead to different spatial results for different dredging operations. For example, a study using satellite images of suspended sediments has suggested the dredging plume at Barrow Island travelled as far as 30 km south (Evans et al. 2012), while others have claimed, in scientific journals and the media that, using numerical simulations, very fine buoyant particles such as coal dust can travel as far as from the coast to the outer Great Barrier Reef (Burns 2014). These statements further emphasise the need for large, high spatial and temporal resolution in-situ water quality data to more accurately study the environmental impacts of dredging.

Coral response to dredging is also complex, as it is site- and species- specific. Different corals exhibit different morphological responses to sediment related pressures or different light environments (due to different depths), and these responses can also be developed differently according to the ambient water quality conditions (Falkowski et al. 1984). Cooper et al. (2008) suggest that chronic (long term) turbidity levels  $> 3$  and  $> 5$  NTU result in sub-lethal and severe stress to corals, and Flores et al (2012) found similar results from lab experiments with total mortality occurring after 12 weeks of exposure to 30 & 100  $\text{mg L}^{-1}$  (which approximately converts to 30 – 200 NTU for the Barrow

Island data based on the provided conversion values) depending on the species. In contrast, Browne reported little to no mortality to corals exposed to pulsed moderate turbidity ( $\sim 50 \text{ mg L}^{-1}$ ) in the lab for up to 1 month. Furthermore, the response of corals to changes in water quality can be location specific; the same species can become adapted to naturally clearer water or more turbid environments (Newell et al. 1998).

Although corals can survive from naturally elevated sediment-related disturbances caused by storms and cyclones (Shinn 1976, Woodley et al. 1981, Riddle 1988, Carter et al. 2009, Connell 1997), dredging can increase SSC to unnatural levels for prolonged periods, restricting recovery time between events (Gilmour et al. 2006, Jones, Fisher, et al. 2015). Natural resuspension can increase SSC to levels as high as occurs during dredging (Gagan et al. 1990, Green 1995, Orpin et al. 1999, McKinnon et al. 2003, Gilmour et al. 2006, Guillén et al. 2006, Carter et al. 2009), and, although there have been reports of coral reef destruction (depending on the severity of the storm and habitat depth) (Harmelin-Vivien & Laboute 1986, Done 1992, Dollar & Tribble 1993, Tomascik et al. 1994), such events are usually short lived (Dollar & Tribble 1993, Onuf 1994, Anthony et al. 2004) and the ecosystems are typically adapted to these conditions and can even benefit from the removal of sediment during storms. Resuspension due to dredging, however, may occur for longer, more frequently and during calm conditions. Previous studies show dredge related water quality changes were confined to an area close to dredge zones; in Cleveland Bay, deposition rates were 10 x higher at sites within 500 m of dredging than at sites 1.5 km away (Kettle et al. 2001) and, in Mermaid Sound (Dampier Archipelago on Western Australia's NWS), Stoddart and Anstee (2004) reported

average turbidity levels decreased from 3.75 NTU at sites within 1 km of dredging to 1.24 NTU at far field sites.

The consequences of our lack of understanding of dredging impacts are significant. The health of the Great Barrier Reef (GBR) and our oceans are important to the Australian public, but we are also reliant on the resources sector and large minerals and mining exports, which requires ship movements and suitable ports for export. Recently there has been increased public scrutiny about the impacts of dredging on coral reefs due to the expansion of a number of Queensland ports (e.g. Abbot Point and Gladstone Harbour) and associated dredging operations. Multiple pressures from the public and environmental lobby groups about the impacts of dredging and dredge spoil disposal have resulted in government intervention, particularly related to the Abbot Point and Gladstone Harbour dredging programs despite inconclusive evidence from multiple scientific organisations (including research by the Queensland Department of Environment and Heritage Protection, Queensland Department of Agriculture, Fisheries and Forestry, CSIRO, and the University of Tasmania) that dredging or dredge spoil disposal directly impacts local ecosystems (Environment and Communications References Committee 2014). This public scrutiny and lack of evidence into the impacts of dredging highlights the need for large water quality studies during dredging operations and comparisons to local ambient water quality conditions.

#### **1.4 Aims and objectives**

Using the largest water quality dataset ever collected prior to and during a large scale capital dredging project, this thesis aims to describe the distance to dredge effects on sediment related pressures. Although this data was not studied while the dredging operation was underway due to

limited time and resources, many aspects of the data are described here to better understand the temporal and especially the spatial impacts of dredging on water quality conditions.

The aims of this thesis are briefly outlined here and each aim is expanded below:

1. To broadly describe (spatially and temporally) turbidity changes during dredging at Barrow Island to better understand dredging related sediment pressures. Temporal analysis involves comparing baseline (pre-dredge) turbidity to dredge turbidity, and spatial analysis compares turbidity conditions at increasing distances from the dredge zone.
2. More specific temporal investigation of turbidity used a running mean analysis with increasing running mean window sizes to investigate turbidity extremes over increasing time frames.
3. Spectral methods were also used to study the temporal behaviour of turbidity. A wavelet analysis technique identified natural periodic resuspension drivers (i.e. semi-diurnal tides, daily sea breeze etc.), and comparison between the baseline and dredge periods investigated the impacts of dredging on these.
4. A simple empirical turbidity model was developed to estimate natural turbidity conditions from seafloor pressure measurements (estimates of the influence of waves and tides on the seafloor). The model is designed to be a simple alternative to the complex three dimensional hydrodynamic models typically used for suspended sediment estimates which require vast measurements across a large spatial area (which are often not available), and can provide an simple estimate of dredge induced turbidity as a first response threshold exceedance tool and can contribute to research into dredge impacts on coral reefs.

5. The impacts of dredging on underwater light conditions was also temporally and spatially analysed. Light attenuation coefficients were investigated in lieu of PAR measurements to study the distance to dredge impacts on submarine light levels.
6. Sediment deposition conditions prior to and during dredging, and at increasing distance from the dredge zone, were also studied using in-situ sediment surface density measurements and overburden calculations from the turbidity model. The ability of the overburden to be used during future dredging operations to monitor dredge related deposition was also investigated by comparing overburden to SSD measurements.

To better understand the impacts of dredging, this thesis explores distance to dredge effects on sediment-related processes during dredging, and investigates the use of a simple, statistical turbidity model to estimate natural turbidity during dredging so that turbidity levels caused solely by dredging can be estimated and used to further study the impacts of dredge sediment pressures on coral health. The spatial and temporal impacts on turbidity, light attenuation and sediment deposition conditions are investigated by comparing baseline (pre-dredge) conditions to dredge conditions, and spatially the distance to dredge effects are explored by comparing conditions at increasing distances from the main dredge zone. The model was developed and optimised in two different hydrodynamic settings (Barrow Island and Hay Point) to assess performance in different environments. Use of the model to estimate dredge related deposition was also investigated.



Temporal and spatial analysis of turbidity conditions were analysed at Barrow Island prior to and during dredging to characterise the ambient water quality conditions and better understand dredging impacts on these. Baseline turbidity levels were compared to dredging conditions, and, for both monitoring periods, turbidity levels compared at increasing distance from the dredge zone to investigate the distance to dredge effects. Common statistical methods were used (e.g. mean, median and standard deviation) as well as an running mean analysis and spectral analysis.

Running mean temporal analysis (with increasing running mean window sizes) was adopted to investigate turbidity characteristics and extremes over a range of time frames, due to the complex response of corals to changes in their environment (e.g. corals may be able to withstand acute changes but may suffer under prolonged or frequent baseline exceedance). Spectral analysis was also performed on turbidity, wind, wave and water height (tidal) data to better understand natural resuspension drivers and the impact of dredging on these. Spectral analysis can reveal the natural turbidity conditions in a region: i.e. are the daily resuspension events due to sea breezes or diurnal tides, and do the semi-diurnal and spring / neap tides influence resuspension? Comparing the baseline spectral results to those during dredging can also provide insight into the impact dredging has on natural resuspension events.

A simple empirical turbidity model was developed to predict natural turbidity events from seafloor pressure measurements induced by waves and tides (Larcombe et al. 1995, Jing & Ridd 1996, Ogston et al. 2004, Presto et al. 2006, Condie & Andrewartha 2008, Fettweis et al. 2010, Verspecht &

Pattiaratchi 2010, Erftemeijer et al. 2012). Seafloor pressure measurements provided model predictor variables – estimates of the influence of waves, water height, tidal range and tidal currents on sediment resuspension. Sediment suspension occurs due to high frequency wave orbital velocities and wind and tidal current velocities occurring in the bottom boundary layer immediately above the seafloor, which induce a shear stress on seafloor sediment that results in sediment suspension once a critical threshold is exceeded (Grant & Madsen 1986). Typically, complex three dimensional hydrodynamic and wave models are used to estimate sediment suspension and sediment transport, however these models require vast inputs which are often unavailable (either not collected or privately owned) and expensive to collect, particularly during dredging operations which are already very expensive operations. Therefore, a simple empirical model using only seafloor pressure measurements (estimates of the influence of waves and tides on the seafloor) was tested as an inexpensive alternative. Although wave orbital velocities were unable to be measured using pressure measurements due to the low sampling frequency, and therefore high resolution estimates of natural turbidity conditions are likely not possible, lower resolution (daily) estimates of natural turbidity conditions were attempted.

Model predictors were calibrated to baseline turbidity measurements and model performance was validated using out-of-sample baseline data i.e. a future section of the baseline time-series which was not used to train the model input variables to the measured turbidity. The model was applied in two different hydrodynamic settings – the clear waters of Barrow Island and the highly turbid environment of Hay Point, North Queensland. A feature of the model is its simplicity; it only requires collection of at least two variables – seafloor turbidity and water pressure – and the model provides

a simple method to decouple natural and dredge related turbidity events. As turbidity measured during dredging is a combination of both natural and dredged turbidity, coupling makes it difficult to assess if threshold exceedance or environmental damage is caused by dredging or due to natural disturbance (for example Onuf 1994). The difference between the measured (dredged + natural) and modelled (natural) turbidity provides an estimate of turbidity caused solely by dredging – called overburden from herein – offering improved insights into dredging impacts.

Further understanding of dredging impacts were achieved by studying changes to submarine light conditions prior to and during dredging, and analysing the relationship between light and turbidity conditions. Light attenuation was used to describe the light environment in this thesis, assuming that light decay in coastal waters can be approximated (at least to a first order) by the attenuation coefficients calculated using the Beer Lambert Law (Gallegos 2001). Attenuation coefficients were used in lieu of PAR or daily light integrals (DLI), due to the non-uniform water quality sensor depths (ranging from 3.5 – 14 m) and due to their inherent exclusion of atmospherically derived interference in the submarine light levels (i.e. because the attenuation coefficient is only concerned with irradiance decay from the surface to depth  $z$  it is unaffected by attenuation due to cloud cover). In contrast, PARs or DLIs provide simply a measure of the light at depth  $z$ , and, although sufficient to demonstrate benthic light conditions, do not specify the source of the light decay therefore possibly obscure dredging impact analysis.

Light is attenuated in the water column through scattering and absorption by water (Kirk 1977b) and water contents. In coastal waters, absorption is mostly by water molecules and scattering by suspended sediments (Kirk 1977b, Cloern 1987, Mobley 2001, Margvelashvili et al. 2006, Lawson et al. 2007, Saulquin et al. 2013). Coastal water attenuation coefficients typically range from 0.1 – 6  $\text{m}^{-1}$  (Kirk 1977b, Baker & Lavelle 1984, Anthony et al. 2004, Piniak & Storlazzi 2008, Devlin et al. 2008, Saulquin et al. 2013), while on the NWS (Cape Lambert) coefficients were between 0.1 and 3.5  $\text{m}^{-1}$  (In-Situ Marine Optics 2011) and in Queensland between 0.3 and 1  $\text{m}^{-1}$  (Anthony et al. 2004). Inland waters have much higher attenuation coefficients – up to 15  $\text{m}^{-1}$  (Devlin et al. 2008), due to the high absorption and scattering properties of yellow substances, or gilvin (Kirk 1977b, Bowers et al. 2000). In contrast, in the clear, deep open ocean waters, phytoplankton are relatively important in absorbing and scattering light (Smith & Baker 1978, Cloern 1987, Saulquin et al. 2013). Previous studies in Cleveland Bay have found light attenuation to be strongly related to suspended sediments, with 74 – 79 % variance in light attributed to SSCs (Anthony et al. 2004). The scattering of light by suspended particles not only reduces benthic light availability by diffracting light away from the benthos, but the consequent extended path length increases the probability that light will be absorbed by water molecules (Kirk 1985).

Dredging can dramatically decrease submarine light levels. Chartrand et al. (2008) reported light levels reduced to near darkness for most of the dredging program at Hay Point, measured using two light sensors approximately 16 km apart on the edges (southern and western) of the dredge plume impact area (although it is unclear the depth of the light sensors). Bak (1978) found that surface

irradiance had reduced from 30 % to 1 % at a depth of 12 – 13 m, and Onuf (1994) estimated attenuation coefficients increased from 1 – 1.35 m<sup>-1</sup> before dredging to 1.5 – 2.1 m<sup>-1</sup> after.

Attenuation of light due to absorption by water molecules is wavelength dependent, and therefore depth dependent (Sverdrup 1953, Kinzie 1973, Kirk 1977b, Saulquin et al. 2013, Storlazzi et al. 2015). Longer wavelengths (the red part of the spectrum) are absorbed more strongly than the shorter waves (Kirk 1977b, Saulquin et al. 2013, Storlazzi et al. 2015), and are therefore rapidly absorbed in the surface layers. This increases the absorption attenuation rate and depletes red light in the upper layers, leaving the less easily absorbed shorter wavelength light (blue-green) in the underlying layers. Consequently, the attenuation rate is higher in the surface layers, introducing a depth dependence to the attenuation coefficient (Kinzie 1973, figure 4 in Jewson et al. 1984, Schanz 1985). Paulson and Simpson (1977) provide an alternative double exponential function derived from the Beer Lambert Law to allow for this depth dependence. The Beer Lambert Law was converted into the double exponential function which includes a term for higher attenuation near the surface (upper 5 m according to the authors) and a separate term for the lower attenuation rate of the remaining blue-green light at depths > 10 m:

$$I/I_0 = Re^{z/\zeta_1} + (1 - R)e^{z/\zeta_2} \quad (1)$$

The first term on the right hand side (RHS) represents the higher attenuation in the upper layers and the second term represents the lower attenuation rate in the deeper layers. Values for  $R$  and  $\zeta_2$  were obtained by a least squares fit of  $I/I_0 = (1 - R)e^{z/\zeta_2}$  to observed light levels at depths > 10 m, then a second least squares fit of equation 1 was applied to observed light levels < 6 m to get

a value for  $\zeta_1$ . In addition to using the original Beer Lambert Law in this study to investigate light attenuation during dredging, the alternative Paulson and Simpson method was also investigated (see Chapter 4).

Previous studies have suggested that sediment particle size distribution can also influence light scattering (Jonasz & Fournier 2007, Kirk 2010). Storlazzi (2015) and Te (1997) both found higher attenuation coefficients for smaller grain size (e.g. mud compared to sand for Storlazzi, and terrigenous vs carbonate silt for Te). As dredging can alter sediment particle size distribution (PSD) by increasing the proportion of fine particles close to the dredge zone (Jones et al. 2016), differences in attenuation coefficient ranges were compared at sites close to dredging to further reference sites.

Excess suspended sediment during dredging can also lead to increased deposition as the sediment falls out of suspension, depositing on the benthos and corals. Sediment accumulation on corals can be as harmful, if not more, to corals as other suspended sediment related impacts such as reduced light (Jones et al. 2016). Deposition during dredging is more likely to be immediate and less dispersed than during natural deposition events (i.e. storms and cyclones) as the lack of resuspension hydrodynamics – wind, waves and tidal currents – are insufficient to maintain the sediment in suspension (Masselink et al. 2011). Furthermore, in the absence of high waves or strong currents the deposited material will likely remain on sensitive benthic communities.

In this study, several dredge related deposition analysis methods were investigated, including deposition sensor data and use of the turbidity model overburden. Model overburden (calculated by subtracting daily modelled from measured turbidity) estimates excess turbidity caused by dredging, and could also predict dredge related deposition. This is based on the assumption that excess turbidity above natural levels – particularly in calm conditions – is likely to result in immediate in-situ deposition due to the absence of resuspension hydrodynamics – high wind, wave and tidal activity (Green 1995, Larcombe & Woolfe 1999, Pearce et al. 2003, Storlazzi et al. 2004, Orpin et al. 2004, Condie & Andrewartha 2008, Fettweis et al. 2010). These turbulent conditions are necessary to maintain sediment in suspension and to disperse sediment from the source. Without them, excess turbidity is likely to immediately deposit and remain at the deposition site until sufficient wave activity can remove it (Spearman 2015, Jones et al. 2016).

The work in this thesis is also presented in 2 reports (1 submitted, 1 published) for the Western Australian Marine Science Institution’s Dredging Science Node, 1 report for the North Queensland Bulk Ports Corporation (NQBP) (published), and 4 journal articles (2 published, 2 in preparation). Further details on which reports and papers the contents of this thesis appear in, as well as my contribution to each, are provided here:

**WAMSI DSN reports:**

- Fisher R, Stark C, Ridd P, Jones R (2014). *Project 4.2. Effects of dredging and dredging related activities on water quality: Phase 1 - spatial and temporal patterns* (published).
  - *The running mean varying temporal analysis, spectral analysis and light attenuation analysis in this report were produced by myself and are included in this thesis in [chapter 3](#) (running mean and spectral analysis) and [Chapter 4](#) (light attenuation*

analysis). The running mean analysis is also included in the journal article Jones et al. (2015) listed below.

- Stark C, Whinney J, Ridd P, Jones R (submitted 2016). *Project 4.4. Estimating sediment deposition fields around dredging projects.*
  - *Analysis and results of the turbidity model at Barrow Island presented in the report appears in [Chapter 3](#) of this thesis, and model overburden and in-situ deposition analysis and results are used to describe a dredge deposition zone in [Chapter 5](#). This report will be submitted for publication as a journal article, listed below.*

**NQBP report:**

- Waltham, N., McKenna, S., York, P., Devlin, M., Campbell, S., Rasheed, M., Da Silva, E., Petus, C., Ridd, P., 2015, 'Port of Mackay and Hay Point Ambient Marine Water Quality Monitoring Program (July 2014 to July 2015)', Centre for Tropical Water and Aquatic Ecosystem Research (TropWATER) Publication 15/16, James Cook University, Townsville, 96 pp
- Waltham, N., McKenna, S., York, P., Devlin, M., Campbell, S., Stark, C., Rasheed, M., Da Silva, E., Petus, C., Ridd, P., (submitted), 'Port of Mackay and Hay Point Ambient Marine Water Quality Monitoring Program (July 2015 to July 2016)', Centre for Tropical Water and Aquatic Ecosystem Research (TropWATER)
  - *The turbidity model analysis and results at Hay Point from [Chapter 3](#) of this thesis are presented in these reports*

**Journal publications:**

- Stark C, Ridd P, Fisher R, Jones R (in preparation). *Dredging spatial impacts on light attenuation*
  - [Chapter 4](#) of this thesis will be submitted as a journal article and is in preparation.
- Stark C, Whinney J, Ridd P, Jones R (in preparation). *Estimating sediment deposition fields around dredging projects.*
  - [Chapter 5](#) of this thesis will be submitted as a journal article and is in preparation.
- Fisher R, Stark C, Ridd P, Jones R (2015). *Spatial patterns in water quality changes during dredging in tropical environments.* PLoS One.



- My contribution to this paper included construction and analysis of raw turbidity across all Barrow Island sites for the baseline and dredge periods (Figure 6) which also appears in this thesis as Figure 3-1.
- Jones RJ, Fisher R, Stark C, Ridd P V (2015). *Temporal Patterns in Seawater Quality from Dredging in Tropical Environments*. PLoS One.
  - My contribution to this paper included the running mean varying temporal analysis which appears in this thesis in Chapter 3 section 3.3.4.

## **1.5 Document Organisation**

Chapter 1 summaries the rationale and context for this work and discusses the research objectives and scope of thesis.

Chapter 2 presents information about the study sites and data collection instruments (data analysis methods for chapters 3 – 5 are included in each chapter).

Chapter 3 presents spatial and temporal analysis of turbidity conditions prior to (baseline period) and during dredging at Barrow Island and briefly describes turbidity conditions at Hay Point, North Queensland (where water quality sites were used to further analyse model performance). Temporal analyses includes running mean analysis using increasing running mean window sizes to investigate extreme conditions and the temporal range of dredging effects, and spectral analysis was applied to turbidity, wind, wave and water height data to investigate periodic events and identify resuspension driving mechanisms, and whether dredging impacted natural resuspension events.

The turbidity model applied to the Barrow Island and Hay Point water quality sites is also presented in this chapter.

Chapter 4 presents analysis of underwater light conditions during dredging. This study is unique in that the depth dependence of the light attenuation coefficient was removed to improve the spatial accuracy of dredging impacts on submarine light levels. To investigate the relationship between dredging impacts and light, light attenuation coefficients were compared to turbidity levels.

Chapter 5 investigates the effects of dredging on deposition accumulation. In-situ sediment accumulation data as well as overburden (estimated excess turbidity from dredging) calculated from the turbidity model were analysed to identify a dredge deposition zone and to investigate the use of a simple turbidity model for monitoring dredge threshold exceedance.

Chapter 6 presents the conclusion of the research and recommendations for possible future work. Key findings are presented in this chapter.

## Chapter 2. Sites and data

### 2.1 Study sites

The primary data used during this thesis is globally the largest water quality dataset ever collected during a dredging operation. Dredging for construction of the materials offloading facility (MOF) and LNG jetty of the new Gorgon LNG plant at Barrow Island, Western Australia – the “largest single resource development in Australia’s history” (see <https://www.chevronaustralia.com/our-businesses/gorgon>) – lasted for 18 months from 19 May 2010 – 31 November 2011. Prior to and during dredging, water quality and water pressure measurements were collected at up to 29 sites along a 60 km north / south transect for up to 4 years. A high density of water quality sites were positioned close to the dredge area (10 of the 29 sites), and two water quality sites were placed on the perimeter of the dredge spoil disposal ground which is located ~ 5 km from the main dredge zone (see Figure 2-1). Baseline monitoring began as early as December 2007 at some sites.

Barrow Island is located approximately 120 km from the Pilbara in Western Australia. On the eastern side of the island (the location of the dredging project and water quality monitoring sites) it is considered a clear water environment (Hubbert et al. 2005) with naturally low ambient SSC levels typically < 5 mg L<sup>-1</sup> (Jones, Ricardo, et al. 2015). Hydrodynamics in the Barrow Island region are generally driven by strong currents and a moderate tidal range, and are also influenced by wind and wave action (DEC 2007). The shallow bathymetry ( $\leq 20$  m), coral reefs and shoals between the island and mainland produce complex flows (Hubbert et al. 2005). Tidal currents, moving from offshore in a cross-shelf direction (which are oriented east-west around Barrow Island, Condie & Andrewartha 2008), diffract around the north and south of the island and converge on the eastern side between

the Lowendal Shelf and Dugong Reef (abbreviated to DUG in Figure 2-1) (Hubbert et al. 2005). Some of the water quality monitoring sites are protected on the lee of the island from offshore waves (Pearce et al. 2003, DEC 2007), adding to the complex flows and clear waters. There are fringing sub-tidal coral reefs around Barrow Island – estimated by the former Department of Environment and Conservation (now Department of Environment and Regulation) at ~ 150 hard coral species within the Barrow Island and Montebello nature reserves in 2007 (DEC 2007).

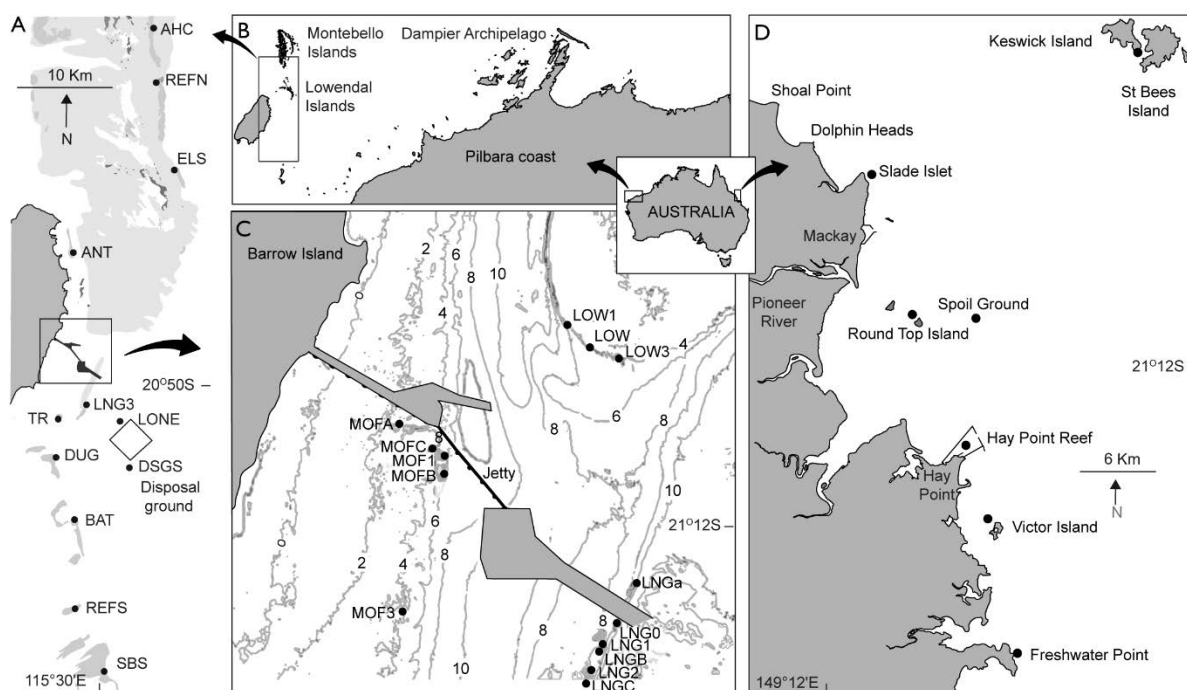


Figure 2-1 Location map showing the Barrow Island water quality sites (A - C) on the eastern side of the island and the Hay Point sites (D). Map A shows all water quality sites along the 60 km north / south transect. There are two main dredging areas with MOF and LNG water quality sites (map C), and a dredge spoil disposal ground approximately 5 km from the main dredging zone with sites LONE and DSGS on the perimeter. Map C also shows the depth contours of the higher resolution sites close to the materials offloading facility (MOF) and LNG access jetty. Map B shows the location of Barrow Island relative to the north western Australian Coast. Map D shows the Hay Point water quality sites (see Waltham et al. (2015) for further Hay Point site location details).

A second dataset was also used during this study to test and validate the turbidity model. Baseline water quality monitoring was conducted at Hay Point, Queensland, to ensure minimal

environmental impact during future routine maintenance dredging. Data was collected at 6 sites for 2 years from 05 July 2014 – 25 July 2015 and provided by the North Queensland Bulk Ports Corporation (Waltham et al. 2015). Note that the monitoring period for the Waltham et al. (2015) report only included the first year of data.

The Port of Hay Point, located ~ 40 km south of Mackay, is one of the largest global coal export facilities, transporting 115 million tonnes in 2014 / 2015 (NQBP 2015). Hay Point and Mackay are much more energetic, turbid environments than Barrow Island (Waltham et al. 2015), with significantly higher wave heights than other Queensland regions (Orpin et al. 1999, Chartrand et al. 2008, Macdonald et al. 2013, Waltham et al. 2015) where resuspension can occur at sites > 20 m depth (Orpin et al. 1999). Wind was predominantly from the S-SE during the study period (Waltham et al. 2015). Hay Point has fringing coral reefs, sparse seagrass and algal communities (Macdonald et al. 2013).

Water quality site details for both studies are provided in Table 2-1 (Barrow Island) and Table 2-2 (Hay Point), including average logger depth and deployment monitoring lengths in days. Barrow Island details also include distance of sites from the main dredge zone (see Table 2-1 for location of dredge zone) and the dredge period monitoring length.

Table 2-1 Barrow Island water quality monitoring site details, including site distance from dredge zone, average logger depth, baseline monitoring length and dredge period monitoring length.

| Sites                                | Distance from dredge zone (km) | Average logger depth (m) | Monitoring length (d) |        |
|--------------------------------------|--------------------------------|--------------------------|-----------------------|--------|
|                                      |                                |                          | Baseline              | Dredge |
| <b>Northern sites</b>                |                                |                          |                       |        |
| AHC                                  | 32.8                           | 7                        | 597                   | 484    |
| REFN                                 | 28                             | 7.5                      | 88                    | 356    |
| ELS                                  | 21                             | 7.8                      | 130                   | 346    |
| ANT                                  | 8.8                            | 4                        | 675                   | 364    |
| DIW                                  | 6.5                            | 2.1                      | 185                   | 377    |
| LOW                                  | 1.9                            | 3                        | 611                   | 447    |
| LOW1                                 | 1.6                            | 7                        | 214                   | 436    |
| LOW3                                 | 1.6                            | 4.5                      | 2                     | 459    |
| <b>Southern sites</b>                |                                |                          |                       |        |
| LNG0                                 | 0.2                            | 8.6                      | 427                   | 468    |
| LNGA                                 | 0.3                            | 11.8                     | 112                   | 475    |
| LNG1                                 | 0.5                            | 8.9                      | 583                   | 471    |
| LNGB                                 | 0.7                            | 10.2                     | 91                    | 486    |
| MOFA                                 | 0.6                            | 4.9                      | 138                   | 459    |
| MOFC                                 | 0.7                            | 6.9                      | 118                   | 449    |
| MOF1                                 | 0.8                            | 6.3                      | 635                   | 489    |
| MOFB                                 | 1                              | 7.5                      | 117                   | 506    |
| LNG2                                 | 1                              | 6.8                      | 575                   | 501    |
| LNGC                                 | 1.4                            | 10.7                     | 244                   | 475    |
| MOF3                                 | 1.5                            | 4.8                      | 559                   | 457    |
| LNG3                                 | 4                              | 6.3                      | 574                   | 483    |
| TR                                   | 5                              | 4.6                      | 253                   | 436    |
| DUG                                  | 9.2                            | 5.9                      | 766                   | 457    |
| BAT                                  | 15                             | 3.8                      | 543                   | 404    |
| REFS                                 | 24                             | 5                        | 137                   | 364    |
| SBS                                  | 30                             | 4.8                      | 561                   | 440    |
| <b>Dredge spoil disposal ground*</b> |                                |                          |                       |        |
| LONE                                 | 4.2                            | 9.9                      | 592                   | 473    |
| DSGS                                 | 9.2                            | 13.2                     | 120                   | 373    |

\* Distance to spoil ground = 0.1 km

Table 2-2 Hay Point monitoring site details, including average logger depth and monitoring length in days.

| Sites            | Average logger depth (m) | Monitoring length (d) |
|------------------|--------------------------|-----------------------|
| Hay Reef         | 10.1                     | 296                   |
| Freshwater Point | 6.8                      | 384                   |
| Keswick Island   | 8.6                      | 378                   |
| Round Top Island | 11.9                     | 386                   |
| Slade Islet      | 9.3                      | 387                   |
| Victor Island    | 6.4                      | 386                   |

\*No dredging occurred during the Hay Point monitoring, the spoil ground site is purely for baseline analysis

## 2.2 Data

Both Barrow Island and Hay Point monitoring used the James Cook University Marine Geophysics Lab water quality monitoring sensors. These sensors have also been used for water quality studies for the Port of Townsville (GHD 2009a) and Western Basin dredging in Gladstone Port (GHD 2009b). Turbidity, PAR, sediment deposition and water pressure were measured every 10 minutes with sensors mounted to a logger placed on the seafloor. Sensors sit approximately 40 cm above the bed, and all sensors have mechanical antifoul wipers attached, which activate every 2 hours to prevent biofouling, allowing much longer deployments without the need for regular cleaning (Ridd & Larcombe 1994, Chevron Australia Pty Ltd 2011b, Waltham et al. 2015).

### 2.2.1 Turbidity and deposition measurement and calibration

Turbidity and sediment deposition are both measured using optical backscatter sensors, which transmit infra-red light and detects the intensity of light scattered at 180° to the transmission sensor. Typically, OBS measure nephelometric turbidity units (NTU) with detectors oriented at 90° from the transmitter, however the JCU detectors are oriented at 180° to enable cleaning of the sensor plate (Waltham et al. 2015) the wiper.

The turbidity sensor (in units of NTU) faces horizontally and therefore measure light scattering due to water column turbidity while the deposition sensor (also in units of NTU) faces vertically and measure the amount of sediment depositing on the sensor (Ridd et al. 2001, Thomas et al. 2003). From these two measurements, surface sediment density (SSD, in  $\text{mg cm}^{-2}$ ) are calculated and calibrated. First the water column turbidity reading (from the horizontal facing OBS) is subtracted from the deposition sensor reading (vertical facing OBS) to calculate sediment accumulation (i.e. without the water column turbidity). Then these raw OBS calculations are converted to SSD by multiplying by a site-specific calibration factor to convert to SSD in  $\text{mg cm}^{-2}$ . The calibration factor is derived from the relationship between NTU and SSD, which is determined by calibrating the turbidity measurements with SSD measurements. In a vertical fall tower approximately 3 m high, an OBS is placed alongside a standard mass balance at the bottom of the tower. The tower is filled with water, and sediment from the site is released into the tower. Simultaneous measurements from the OBS and mass balance are recorded, and the slope of the resulting sediment density / turbidity curve provides the calibration factor to convert deposition OBS readings in NTU to SSD readings in  $\text{mg cm}^{-2}$ .

### **2.2.2 Photosynthetically active radiation and water pressure**

PAR were measured using an upwards facing light sensor measuring in units of  $\mu\text{E m}^{-2}\text{s}^{-1}$ , and water pressure fluctuations were measured using an absolute pressure sensor, which were converted to water depth in metres. The ten minute water depth measurements consisted of 1 second readings for 10 seconds, which were also used to calculate wave height. The root mean square pressure



fluctuation (RMS), which measures the variance in water height from the mean, provides an estimate of wave affects at the seafloor:

$$X_{rms}(t) = \sqrt{\frac{1}{n} \sum_{i=1}^n (x_i - \bar{x})^2} \quad (2)$$

where  $X_{rms}(t)$  is the RMS pressure fluctuation at time  $t$ ,  $n$  is the number of samples (ten),  $x_i$  is the  $i^{th}$  pressure sample, and  $\bar{x}$  is the mean of the ten pressure samples.

Terrestrial PAR data, used as the surface light to calculate the light attenuation coefficients, was collected on Barrow Island (339974E, 7701581N) every 15 minutes from April 2010 to February 2012 during the dredging period only (Chevron Australia Pty Ltd 2011c).

Wind data, used as a model input variable and for spectral analysis at Barrow Island, was recorded every 3 hours at Barrow Island airport and provided by the Bureau of Meteorology (Station ID: 005094, Bureau of Meteorology 2014).

## **Chapter 3. Temporal and spatial impacts of dredging on turbidity**

### **3.1 Synopsis**

To better understand environmental dredging impacts and to improve monitoring accuracy of future dredging operations, this chapter sought to describe the turbidity environment during a large scale capital dredging operation, to determine the spatial extent of dredging effects, and to compare dredging conditions to baseline (ambient) conditions.

A variety of temporal analyses were used, including running means using increasing running mean window sizes, to analyse extreme turbidity events and temporal changes in turbidity levels over a range of timeframes, as well as spectral analysis (using a wavelet method) – to understand the behaviour of natural turbidity drivers (daily seabreeze, semi-diurnal and spring / neap tides), and to determine whether dredging had an impact on these. A turbidity model was developed to estimate natural turbidity conditions.

A simple, statistical turbidity model was also developed to predict natural turbidity events, and its performance investigated in two different hydrodynamic settings – the clear waters of Barrow Island and the more turbid environment of Hay Point, North Queensland. The turbidity model provides a simple method to monitor dredge induced turbidity threshold exceedance during

dredging operations, by decoupling the natural and dredge related turbidity levels. The use of the model to also monitor dredge related deposition is investigated in 5.3.2 Overburden.

## 3.2 Methods

### 3.2.1 Running mean temporal analysis

The temporal behaviour of turbidity events over increasing intervals were analysed to characterise the duration of heightened turbidity levels during dredging. The running means of the raw turbidity data were calculated at each site using increasing running mean window sizes (from 1 hour to 30 days):

$$\bar{x}_T(t) = \frac{1}{N_T} \sum_{i=1}^{N_T} x_i(t) \quad (3)$$

where  $\bar{x}_T(t)$  is the mean value calculated over the previous  $T$  hours of the data from time  $t-T$  to time  $t$  hours, and  $x_i(t)$  are the  $N_T$  data points up to and including time  $t$ . To avoid false averages and percentile estimates, no  $\bar{x}_T$  value was recorded if more than 20% of the data points for any particular running mean period were missing.

The different running mean window sizes are used to describe turbidity conditions over a range of temporal scales. Running mean window sizes ranged from 1 hour to 30 days, and windows were increased using either a 1 hour increment for window sizes from 1 – 24 hours or a 1 day increment for larger window sizes from 1 – 30 days. For example, the first running mean applied to the turbidity data used a 1 hour window size (i.e. 6 of the 10 minute interval data points were used for each

running average), then the window size was increased to 2 hours (i.e. 12 data points were used for each running average), up to 24 hours. The next running mean window size incremented to 2 days, then daily up to 30 days. Each running mean value was recorded as the mid-point of the window; for example between 10 am and 11 am, the one hour mean was recorded as 10:30 am. These running means were calculated separately for the baseline and dredge periods for comparison.

The percentiles of each running mean window were then calculated over all running mean temporal scales to characterise the duration of turbidity events, from 1 hour to 30 days. Percentile values chosen were maximum, 99<sup>th</sup>, 95<sup>th</sup> and 80<sup>th</sup> and were calculated for each turbidity average (i.e. the 4 percentiles were calculated for the 1 hour averages, then for the 2 hour averages etc. up to the 30 day averages).

### **3.2.2 Spectral analysis**

Temporal periodicities of turbidity, wind, wave and water height data were analysed at each site and compared between study sites to investigate the dominant periodic turbidity cycles, their driving mechanisms (tides, waves) and determine any differences between the baseline and dredge periods.

The wavelet transform method was developed by Torrence and Compo (1995), and bias correction developed by Liu et al. (2007) (detailed below). The wavelet transform detects periodic events

across a range of periods (called scales in the wavelet method) and provides their temporal location along a time series, as well as the relative power of each event relative to events at other temporal locations.

A mother wavelet is chosen and compared across the time series to detect the temporal locations of periodic events over a range of periods (by changing the scale of the mother wavelet). In this case the 'Morlet' wavelet with variable scales 's' (similar to period) is convoluted with the time series data to determine the presence and amplitude of each scale at time t in the time series. For each convolution with the time series, the scale of the mother wavelet are varied to detect a range of periodicities.

The Torrence and Compo method first performs a discrete Fourier transform of the time series,  $x_n$ , and mother wavelet  $\psi_0$ , then the wavelet coefficients (a measure of the relative power or amplitude of a periodic event) are calculated by performing an inverse transform of the convolution: (equation 4 in Torrence & Compo 1995).

$$W_n(s) = \sum_{k=0}^{N-1} x_k \psi^* (s\omega_k e^{i\omega_k \hat{n}\delta t}) \quad (4)$$

where  $W_n(s)$  is the wavelet transform at scale  $s$  and translation along the time series  $\hat{n}$ ,  $x_k$  is the Fourier transformed time series with time step  $\delta t$ ,  $\psi^*$  is the complex conjugate of the Fourier transformed Morlet wavelet  $\psi_0$ , and  $\omega_k$  is the angular frequency. The wavelet transforms at all

scales across the time series, which are then squared and  $\log_2$  transformed to display the wavelet spectral power – the wavelet coefficient.

### **3.2.3 Time averaged wavelet power**

To analyse the dominant periodicities in a time series (rather than compare a single period at different temporal locations, similar to an analysis in the frequency domain) the wavelet power at each scale is averaged over the whole time series. This is called a global wavelet spectrum and is described in Torrence & Compo (1995). Comparisons of the global wavelet spectrums were made between all sites during each monitoring period and comparisons were made between the baseline and dredge periods. Peak periodicities in the baseline period and dredge period for each variable were calculated separately to compare if the dominant oscillations were affected by dredging.

A bias exists in the global wavelet spectrum where energy in the longer period bands are enhanced and energy in the shorter period bands are attenuated. This bias has been corrected using methods developed by Liu et al. (2007) – by normalising the power spectrum at each scale (i.e. by dividing the wavelet power at each scale by that scale).

Edge effects (spectral leakage) resulting from the Fourier transformation of the finite-length time series at the outset of the wavelet transform can distort the power in the wavelet spectra at the minimum and maximum periods (Torrence & Compo 1995). To overcome these edge effects, the

Torrence and Compo method temporarily pads the end of the time series with zeros before removal again after performing the wavelet transform. Although there is an attempt to exclude these from the spectral figures using a cone of influence (black region in Figure 3-15), spectral leakage does still appear, especially in the high frequency end (left hand side) of the global wavelet (time-averaged) in Figure 3-12 and Figure 3-15.

Due to differences in baseline time series length at Barrow Island, with baseline data measurements at around half the sites beginning only six months prior to dredging (compared to some sites having up to 2.5 years of baseline data, see Table 2-1), which was a particularly a low energetic period, only sites with sufficient baseline time series were included in the global wavelet spectrum comparison. All sites were included in the dredge period comparison as the time series lengths were very similar (~ 18 months, Table 2-1).

#### **3.2.4 Turbidity model**

Water column turbidity was estimated using a simple statistical model. The model is based on the natural primary resuspension hydrodynamics – waves and tides, and uses seafloor pressure fluctuations as estimates of the influence of waves and tides on sediment resuspension. which combine non-linearly to create shear stress on the seabed (Wright 1995, Soulsby & Clarke 2005, Dalyander et al. 2013). Model inputs were derived from seafloor pressure fluctuations, and the optimised model parameters determined the contribution of each process to resuspension by

fitting the input variables to the measured turbidity. Except for wind, all model input variables were derived from water pressure measurements described in Chapter 2.

$$\hat{T}(t) = a_0 X_{rmspf}^{b_0}(t) + a_1 X_{rmspf}^{b_1}(t-1) + a_2 X_{wh}^{b_2}(t) + a_3 X_{\delta wh}^{b_3}(t) + a_4 X_{rmswh}^{b_4}(t) + a_4 X_w^{b_4}(t) + a_5 \quad (5)$$

where  $\hat{T}(t)$  is the daily estimated turbidity at time  $t$  (days). Model input variables are explained below.

Pressure fluctuations at the seafloor induced by surface gravity waves (*rmspf*) are one of the primary resuspension drivers (Soulsby & Damgaard 2005). Estimates of the influence of waves on the seafloor were calculated by the root mean square (RMS) of ten consecutive pressure readings over ten seconds (which occurred every ten minutes).

$$X_{rmspf}(t) = \sqrt{\frac{1}{m} \sum_{i=1}^m (x_i - \bar{x})^2} \quad (6)$$

where  $X_{rmspf}(t)$  is the RMS pressure fluctuation at time  $t$  (denoted by *wave(t)* and *wave(t-1)* in model figures),  $m$  is the number of samples (ten),  $x_i$  is the  $i^{th}$  pressure sample, and  $\bar{x}$  is the mean of the ten pressure samples. Due to excessive noise present in the 10 min sampling of the raw data (Whinney 2007), all model variables were daily averaged using the arithmetic mean:

$$\bar{x}_j = \frac{1}{n} \sum_{i=1}^n x_i \quad (7)$$



where  $\bar{x}_j$  is the  $j^{\text{th}}$  mean data point,  $n$  is the number of samples averaged (144 for water quality logger data and 8 for wind data (i.e. 1 day)),  $x_i$  is the  $i^{\text{th}}$  raw data point (once per ten minutes for water quality or 3 hours for wind). Three, six and twelve hourly averages of model input variables were also tested due to results from the spectral analysis (with semi-diurnal peaks appearing in the turbidity data) but the daily averages were found to produce the best model performance. The relationship between daily averaged turbidity and daily averaged RMS pressure fluctuations were investigated using a power regression.

The RMS pressure fluctuations from the previous day ( $t-1$ ) were included in both the Barrow Island and Hay Point models as  $X_{rmspf}(t-1)$  (denoted by *wave (t-1)* in model figures) to account for any possible temporal lags in pressure fluctuations resuspending sediment.

$X_{wh}$  is water height (denoted by *WH (t)* in model figures), which influences resuspension by amplifying or dampening the shear stress at the seabed. Deeper water reduces the influence of waves on the seabed, which disappear when the depth is greater than half the wavelength (Wolanski et al. 2005), while shallower water increases wave orbital velocities and increases the shear stress.  $X_{wh}$  is calculated as the arithmetic mean of the ten consecutive one second pressure readings.

$X_{\delta wh}$  refers to estimates of tidal current (denoted by TC (t) in model figures), which also contribute to vertical sediment resuspension by increasing bed shear stress, either alone or in combination with wave orbital velocities (Pattiaratchi & Collins 1984). Tidal currents were estimated by calculating the difference in water height between 20 minute samples, based on the assumption that changes in sea level will induce a current flow beneath.

Estimates of tidal range ( $X_{rmswh}$ , denoted by  $TR(t)$  in model figures) were included, as tidal range alters the strength of the tidal current, with maximum tidal current velocities occurring during spring tides (Dunn et al. 2015). The tidal range was calculated as the RMS of the water height estimates ( $X_{wh}$ ) using a 13 h window (to ensure each sample includes one peak and one trough of the semi-diurnal tidal changes).

$X_w$  is the wind parameter (denoted by Wind (t) in model figures), which was included only during the Barrow Island project (as no wind data was available for the Hay Point analysis). Wind was measured directly at Barrow Island airport and is included due to its influence on surface gravity waves. Wind at Barrow Island airport (Station ID: 005094) was recorded every 3 hours and provided by the Bureau of Meteorology (2014).

Model parameters,  $a_{0-4}$  and  $b_{0-4}$ , were optimised by training (fitting) the model input variables to the corresponding daily averaged turbidity measurements using the first half of the baseline data

(train / fit period) at Barrow Island and the first half of the entire dataset at Hay Point (because there was no dredging at Hay Point, all turbidity was assumed to be from natural causes).

The MATLAB non-linear least squares function 'lsqnonlin' (Mathworks 2016a) was used to optimise the model. A nonlinear method was used due to the number and complexity of the parameters being optimised, with five coefficients and five indices requiring optimisation, as well as the offset term  $a_5$ . Non-linear least squares optimisation estimates the model parameters that minimises the function:

$$\sum_{i=1}^m (T_i - \hat{T}_i)^2 \quad (8)$$

where  $\hat{T}_i$  is the  $i^{th}$  modelled turbidity value at time  $t$  (i.e. daily) and  $T_i$  is the daily averaged measured turbidity value at  $t$ . The success of the model was tested by calculating the  $R^2$  values between measured and modelled turbidity for the train and test period, and by visually comparing concurrent measured and modelled turbidity events during the baseline period. Absolute residual errors between the modelled turbidity and measured turbidity were calculated at each site.

The success of the fit was investigated visually and quantitatively by calculating  $R^2$  and skills score (SS) on both the fit and test samples (first half and second half of baseline data. The test data is out-of-sample data, meaning that it was not used to fit the model parameters to the measured turbidity data, and therefore provides an objective measure of model performance. The equation to calculate the skill score is:

$$SS = 1 - \frac{\sum(\hat{T} - T)^2}{\sum(T - \bar{T})^2} \quad (9)$$

where SS is skill score,  $\hat{T}$  are the daily modelled turbidity,  $T$  are the daily averaged measured turbidity, and  $\bar{T}$  is the averaged turbidity measurements.

### 3.3 Results

#### 3.3.1 Turbidity at Barrow Island

Dredging increased turbidity at sites within 2 – 5 km south of dredging compared to all northern sites and sites > 5 km south, which had similar conditions to baseline turbidity levels (Figure 3-1, Figure 3-2 and Table 3-1). There was a strong non-linear rapidly decaying relationship between turbidity and site distance from dredging (Figure 3-2) with average and maximum turbidity levels up to 6 – 7 x higher at sites within 2 – 5 km south compared to all sites north of the dredge zone and sites > 5 km south of dredging; these sites had maximum turbidity 100 - 550 NTU, average turbidity 3 - 7 NTU and standard deviations (SD) 4.1 – 14.4 NTU, while all northern sites and sites > 5 km south had conditions similar to baseline levels (which were similar across all sites) with maximum turbidity 40 - 125 NTU, average turbidity 1 – 3 NTU and SD 1.1 – 3.1 NTU (Figure 3-2 and Table 3-1). Occasional higher maximum turbidities occurred at reference sites during dredging (compared to the baseline conditions) due to storms on 27 January and 04 May 2011 (Figure 3-1). There were also a few turbidity peaks during the baseline period at some of the more exposed reference sites during a storm in May 2008 (Figure 3-1).

The dredge spoil disposal sites, LONE and DSGS (4.2 km and 9.2 km south-east of dredging, see Figure 2-1 for site locations), had lower maximum and average turbidity than sites located at similar distances but in the path of the dredge plume flow south of dredging (LNG3, TR and DUG at 4 – 10 km south / south-west) and similar to reference sites further south (Figure 3-1 and Figure 3-2). The relatively lower turbidity levels at these sites can also be seen in the maximum / average turbidity plotted with distance from dredging in Figure 3-2 – the 2 lower black dots at ~ 5 and 10 km south represent the dredge spoil disposal sites.

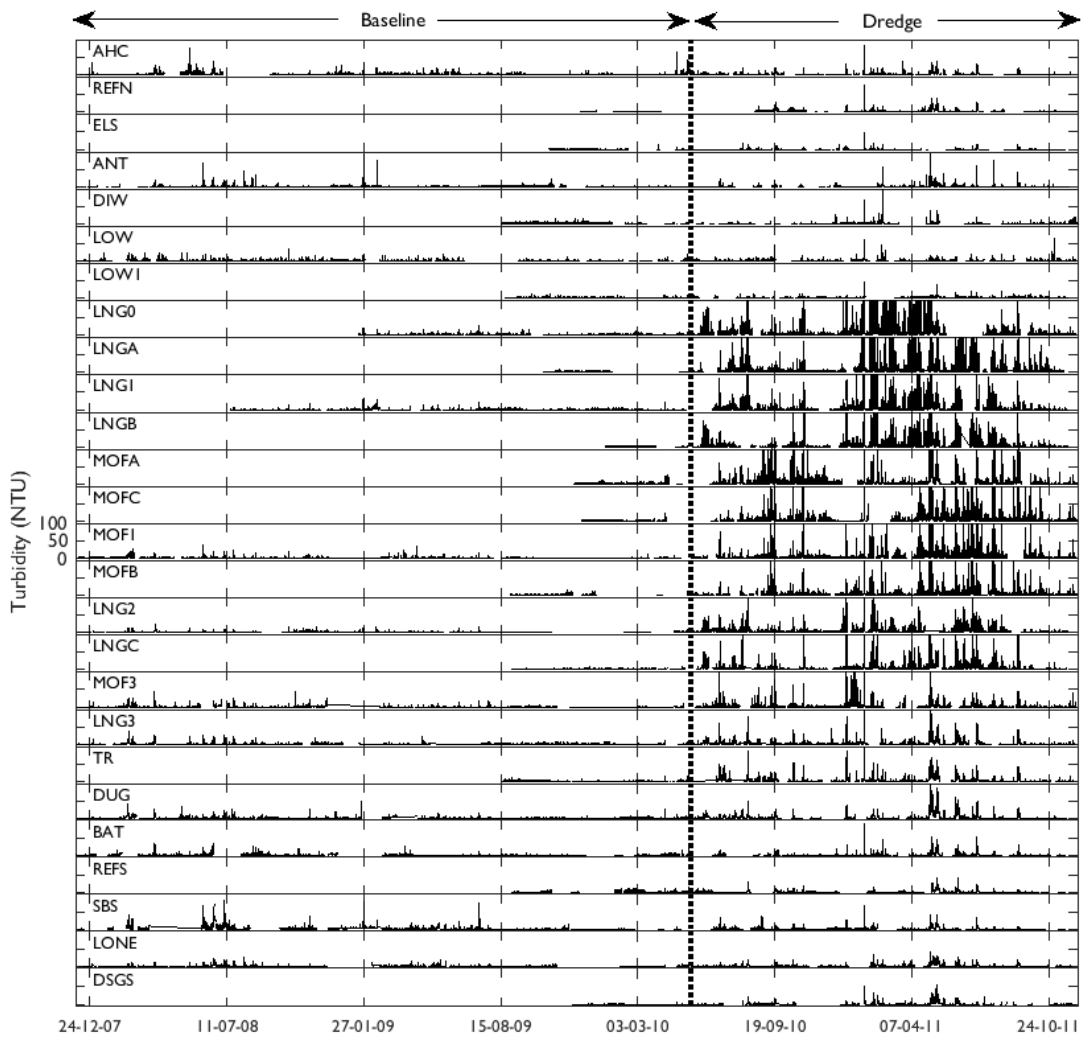


Figure 3-1 Measured turbidity (raw, at 10 minute intervals) time series during the entire monitoring period at Barrow Island, Western Australia (separated by the broken black line into baseline – December 2007 to 19 May 2010 – and dredge periods – 19 May 2010 to November 2011) at water quality sites on the eastern side of Barrow Island. Sites are arranged from north to south (see Table 2-1 for distances from dredge zone and Figure 2-1 for map). All Y axis limits are the same (0 – 100 NTU); axis limits have only been included on one representative panel to avoid overcrowding. Maximum turbidity has been truncated at 100 NTU to show lower turbidity levels.

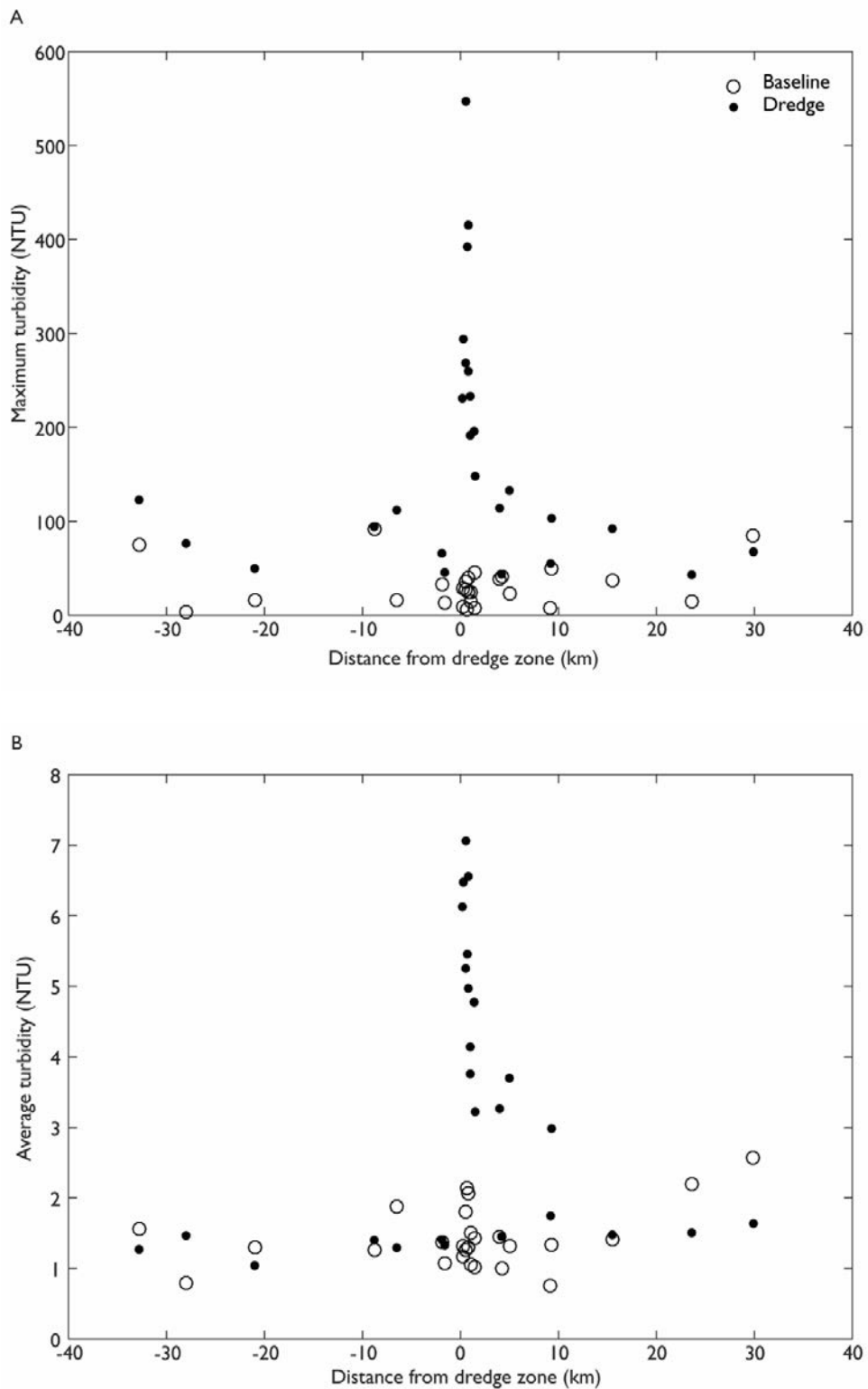


Figure 3-2 Maximum (A) and average (B) turbidity during the baseline (white dots) and dredge (black dots) periods, plotted by distance of the site from the dredge zone. Negative distances are north of the dredge zone (which is at origin) and positive distances are south.

Table 3-1 Summary table showing maximum (raw and daily averaged), mean and standard deviation turbidity during the baseline (train and test periods) and dredging periods, and R<sup>2</sup> values between measured and modelled turbidity for the fit (1<sup>st</sup> half of baseline data), test (2<sup>nd</sup> half of baseline data) and baseline (fit + test) period. The overburden (i.e. difference between daily measured and modelled turbidity during the dredge period) is shown for the Barrow Island sites only as average daily and maximum NTU. The numbers associated with the Barrow Island sites are distances (km) either N (north) or S (south) from the primary excavation site. Site LONE at Barrow Island was 4.2 km south of the primary site of dredging and also 0.1 km from the dredge material placement site (Figure 2-1).

| Sites                               | Distance (km) | Turbidity (NTU) |     |           |      |        |      |           |       |
|-------------------------------------|---------------|-----------------|-----|-----------|------|--------|------|-----------|-------|
|                                     |               | Baseline        |     |           |      | Dredge |      |           |       |
|                                     |               | Mean            | SD  | Max Daily | Max  | Mean   | SD   | Max Daily | Max   |
| <b>Northern sites</b>               |               |                 |     |           |      |        |      |           |       |
| AHC                                 | 32.8          | 1.6             | 2   | 18.5      | 74.9 | 1.3    | 2    | 13.1      | 122.9 |
| REFN                                | 28            | 0.8             | 0.3 | 1.5       | 3.4  | 1.5    | 2.2  | 28.5      | 76.5  |
| ELS                                 | 21            | 1.3             | 0.4 | 2.1       | 16.2 | 1      | 1.3  | 18.9      | 49.8  |
| ANT                                 | 8.8           | 1.2             | 0.8 | 13.3      | 91.2 | 1.4    | 1.5  | 13.9      | 94.1  |
| DIW                                 | 6.5           | 1.9             | 0.7 | 3.3       | 15.7 | 1.3    | 1.4  | 14.4      | 112.1 |
| LOW                                 | 1.9           | 1.4             | 1.2 | 11.8      | 32.7 | 1.4    | 1.7  | 21.4      | 66    |
| LOW1                                | 1.6           | 1.1             | 0.4 | 2         | 13.4 | 1.3    | 1.1  | 16.4      | 45.6  |
| <b>Southern sites</b>               |               |                 |     |           |      |        |      |           |       |
| LNGO                                | 0.2           | 1.2             | 0.8 | 8.5       | 28.4 | 6.1    | 7.9  | 60        | 231   |
| LNGA                                | 0.3           | 1.3             | 0.2 | 2.2       | 9.3  | 6.4    | 8.7  | 74.3      | 294   |
| LNG1                                | 0.5           | 1.2             | 1   | 13.1      | 35.1 | 5.2    | 6.8  | 52.8      | 268.6 |
| LNGB                                | 0.7           | 2.1             | 0.8 | 3.3       | 5.9  | 5.4    | 7.8  | 79.4      | 392.3 |
| MOFA                                | 0.6           | 1.8             | 0.6 | 5.6       | 27.6 | 7      | 14.4 | 153       | 547.2 |
| MOFC                                | 0.7           | 2.1             | 0.8 | 6.4       | 24.5 | 6.5    | 11   | 120.2     | 415.4 |
| MOF1                                | 0.8           | 1.3             | 1   | 9.4       | 39.8 | 4.9    | 7.2  | 74        | 259.8 |
| MOFB                                | 1             | 1.5             | 0.5 | 3.9       | 15.3 | 4.1    | 5.8  | 68.6      | 233.2 |
| LNG2                                | 1             | 1               | 0.8 | 6         | 24.6 | 3.7    | 4.1  | 32.1      | 191.6 |
| LNGC                                | 1.4           | 1               | 0.4 | 2.6       | 8.2  | 4.7    | 6.6  | 58.7      | 196   |
| MOF3                                | 1.5           | 1.4             | 1.2 | 11.6      | 45   | 3.2    | 4.4  | 50        | 148.1 |
| LNG3                                | 4             | 1.4             | 1.4 | 18.4      | 38.3 | 3.2    | 5.4  | 59.9      | 114.1 |
| TR                                  | 5             | 1.3             | 0.7 | 8.2       | 23.4 | 3.7    | 6.4  | 70.6      | 132.9 |
| DUG                                 | 9.2           | 1.4             | 1.4 | 10.9      | 49.3 | 2.9    | 6.3  | 53.5      | 103.3 |
| BAT                                 | 15            | 1.4             | 1.2 | 9.3       | 37.2 | 1.5    | 2.8  | 32.5      | 92.3  |
| REFS                                | 24            | 2.2             | 1.4 | 5.2       | 14.1 | 1.5    | 2.3  | 20        | 43.2  |
| SBS                                 | 30            | 2.7             | 4.6 | 26.9      | 84.2 | 1.6    | 2.3  | 30.5      | 67.7  |
| <b>Dredge spoil disposal sites*</b> |               |                 |     |           |      |        |      |           |       |
| LONE                                | 4.2           | 1               | 1   | 10        | 41.1 | 1.4    | 2    | 17.6      | 43.6  |
| DSGS                                | 9.2           | 0.8             | 0.3 | 1.5       | 7.8  | 1.8    | 3.1  | 25.3      | 55.1  |

\* Distance to spoil ground = 0.1 km



### 3.3.2 Turbidity at Hay Point

Conditions at Hay Point, North Queensland, are also briefly presented here because the turbidity model was analysed at the Hay Point water quality sites (although no dredging was carried out during testing, see Figure 2-1 for site locations). Baseline turbidity levels were significantly higher at Hay Point than during the Barrow Island baseline period (see Figure 3-1 for Barrow Island and Figure 3-3 for Hay Point), and were more similar to the dredging conditions at the nearfield Barrow Island sites. Maximum turbidities ranged from 30 – 556 NTU (with 5 of the 6 site maximums > 294 NTU, Table 3-1), average turbidities 1 – 12 NTU, and SD 1 – 25 NTU (with most sites having SD > 9 NTU, Table 3-1 and Figure 3-3). Conditions were similar across most of the Hay Point sites except for the Keswick Island site, which was more closely related to baseline Barrow Island conditions (Table 3-2), with average and maximum turbidity 1 NTU and 30 NTU (Figure 3-3 and Table 3-2).

Numerous short-term turbidity peaks > 20 NTU occurred at 5 of the 6 Hay Point sites (Figure 3-3 and also shown for representative sites at Hay Point in Figure 3-4 ). In contrast, during the baseline period at Barrow Island there were fewer turbidity peaks > 20 NTU, with a maximum of 830 peaks (which equates to ~ 0.8 % of turbidity measurements in 2 years), at the most southern site, most of which occurred during storms in June 2008.

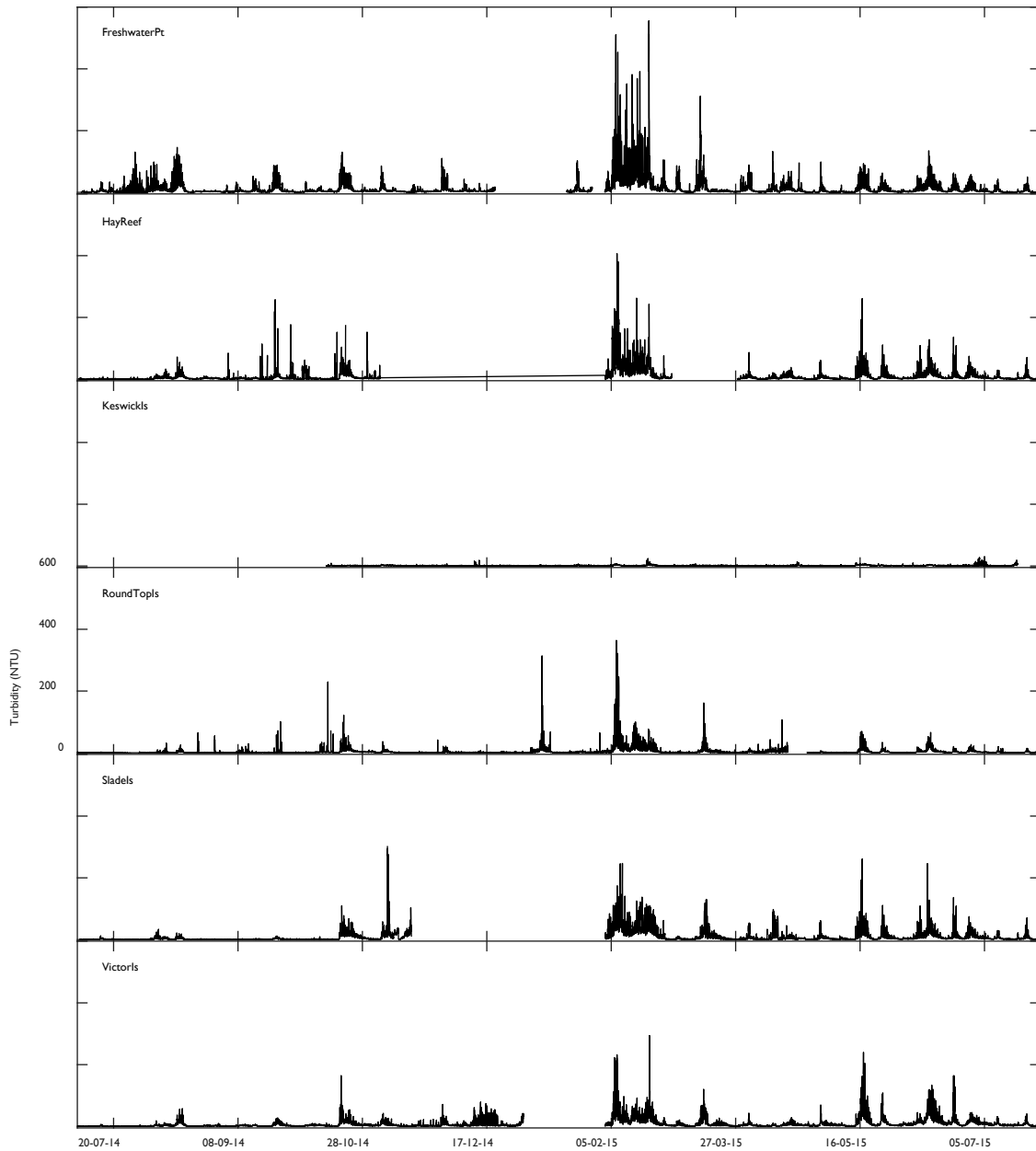


Figure 3-3 Measured turbidity (raw, at 10 minute intervals) time series during the baseline period (July 2014 to August 2015) at Hay Point water quality sites. Sites are arranged from north to south (see Figure 2-1 for map). All Y axis limits are the same (0 – 600 NTU) – axis limits have only been included on one representative panel to avoid overcrowding. Maximum turbidity has been truncated to 600 NTU to show lower turbidity levels.

Table 3-2 Summary table showing maximum (raw and daily averaged), mean and standard deviation turbidity at Hay Point sites during the baseline (train and test) period, and R<sup>2</sup> values between the measured and modelled turbidity for the fit (1<sup>st</sup> half of data), test (2<sup>nd</sup> half of data) and baseline period (fit + test periods) at Hay Point (see Figure 1).

| Sites            | Turbidity (NTU) |      |           |     |
|------------------|-----------------|------|-----------|-----|
|                  | Average         | SD   | Max daily | Max |
| Hay Point/Reef   | 8.4             | 16.9 | 97.6      | 406 |
| Freshwater Point | 11.4            | 25.1 | 127.7     | 556 |
| Keswick Island   | 1.1             | 1.3  | 6.1       | 30  |
| Round Top Island | 3.3             | 9.6  | 82.8      | 364 |
| Slade Point      | 8.6             | 16.4 | 85.9      | 303 |
| Victor Island    | 8.1             | 14.4 | 91.5      | 294 |

### 3.3.3 Turbidity model

The turbidity model predicts natural turbidity events based on seafloor pressure fluctuations caused by water motion from waves and currents, and was investigated in different hydrodynamic conditions to determine its performance in a clear water environment (Barrow Island) and a more turbid coastal setting (Hay Point).

At Hay Point the relationship between measured and modelled turbidity was moderate to strong at up to half (3/6) of the monitoring sites during the model fit (first half of time series) and test period (second half of time series). During the fit period, half the sites had R<sup>2</sup> > 0.5 (0.6 – 0.8) with skill score (SS) between 0.52 and 0.78 and during the test period, 5 of 6 sites had R<sup>2</sup> > 0.5 (0.56 – 0.68)

but only 1 site had a SS > 0.5 (0.57, Table 3-3). The best model performance was at Hay Point Reef (Table 3-3 and Figure 3-4 A) with the highest R<sup>2</sup> of all Hay Point sites during the fit period (0.79, Table 3-3), but lower during the test phase (0.45, Table 3-3), and moderate SS during both the fit and test periods (0.54 and 0.47, respectively). Two other representative sites are displayed in Figure 3-4 B & C, site Round Top Island and Slade Islet which are located approximately 11 and 22 km north of the Hay Point Reef site. Both sites had moderate to strong R<sup>2</sup> (0.56 and 0.64) but moderate to weak SS (0.45 and 0.31) during the test period. Performance was weaker during the fit phase at these sites, with R<sup>2</sup> of 0.32 and 0.07, respectively, and SS 0.13 and -0.04. The temporal location and magnitude of the modelled and measured turbidity peaks were very similar at site Hay Point Reef (Figure 3-4 A), and measured and modelled peaks had similar temporal locations at Round Top Island and Slade Islet but higher measured than modelled (Figure 3-4 B & C). Model and measured plots of the remaining Hay Point sites are provided in Appendix B.

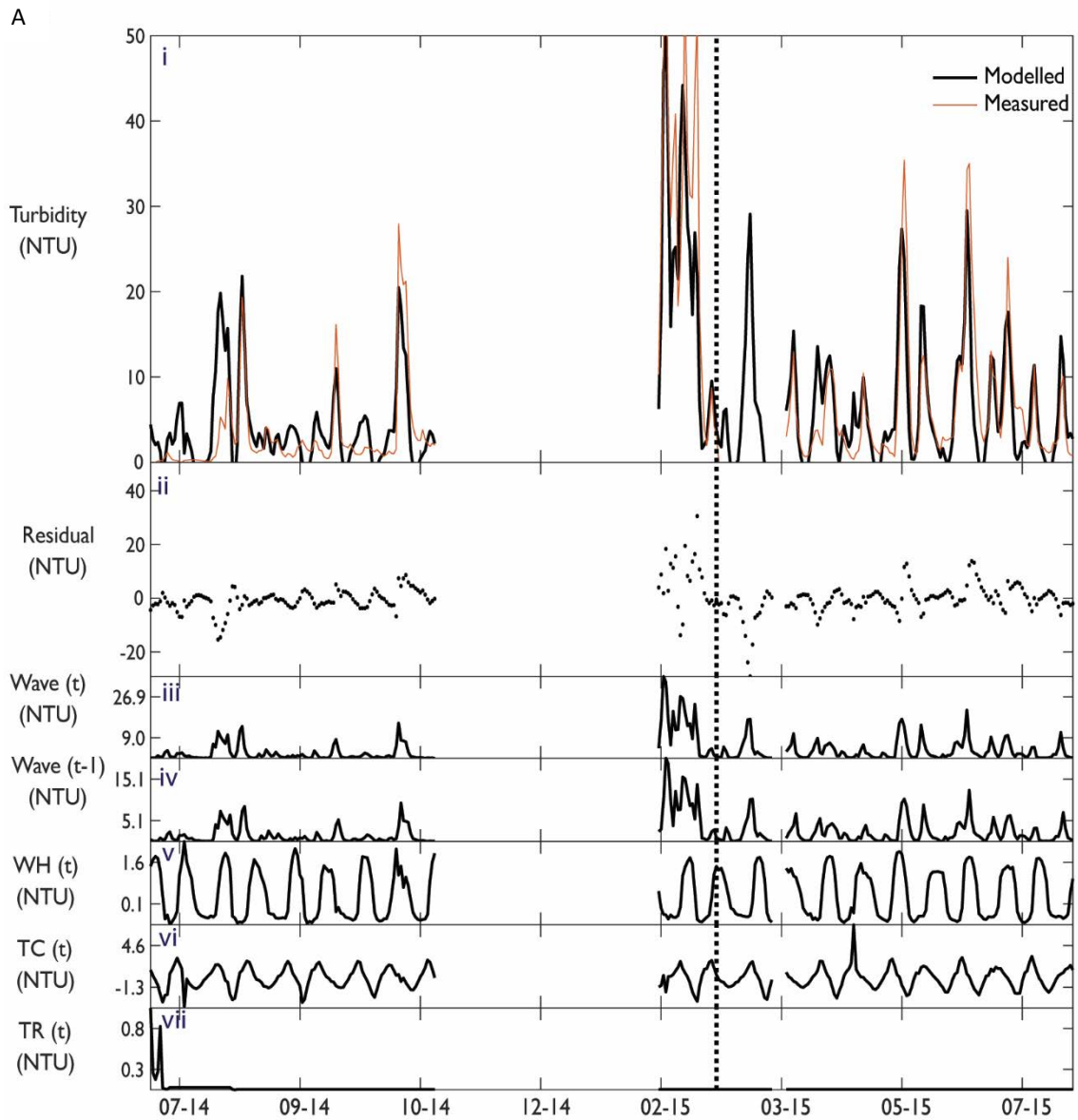
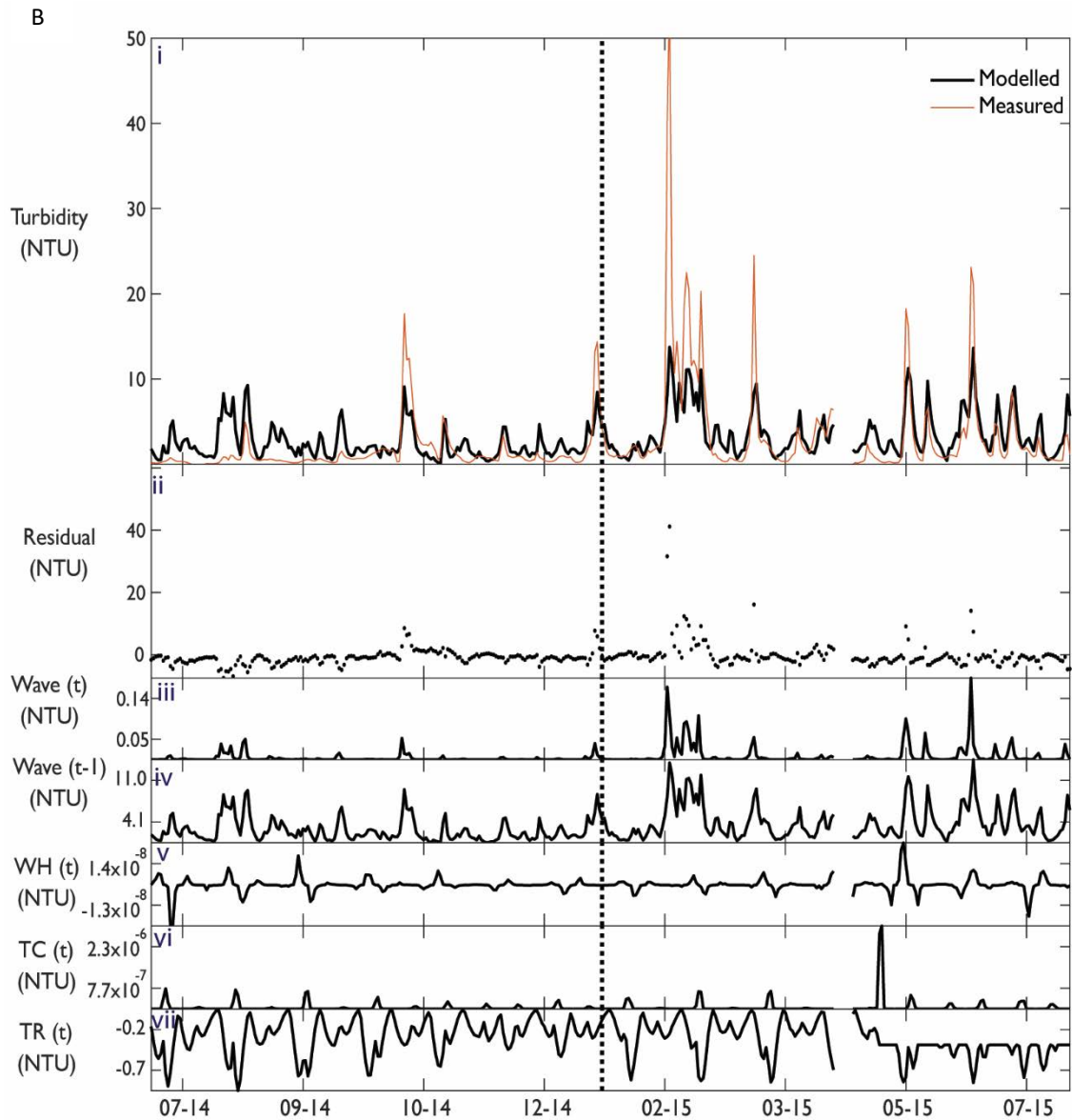


Figure 3-4 A. Hay Point project. Turbidity model (equation 5) at Hay Point Reef during the baseline train (left of the dotted line) and test (right of the dotted line) periods showing (from top to bottom): (i) the modelled (black line) and measured (orange line) turbidity levels, (ii) the residual turbidity, then each model term (with parameters applied) including (iii) RMS pressure fluctuations to represent the motion of surface gravity waves on the sea floor at time  $t$  (wave ( $t$ )), (iv) RMS pressure fluctuations from the previous day (wave( $t-1$ )), (v) water height at time  $t$ , (vi) tidal current quasi estimates at time  $t$  and (vii) tidal range at time  $t$ , all in units of NTU. Panel i showing measured and modelled turbidity is the same in all 3 figures and has been truncated to 50 NTU to show the smaller modelled turbidity levels.



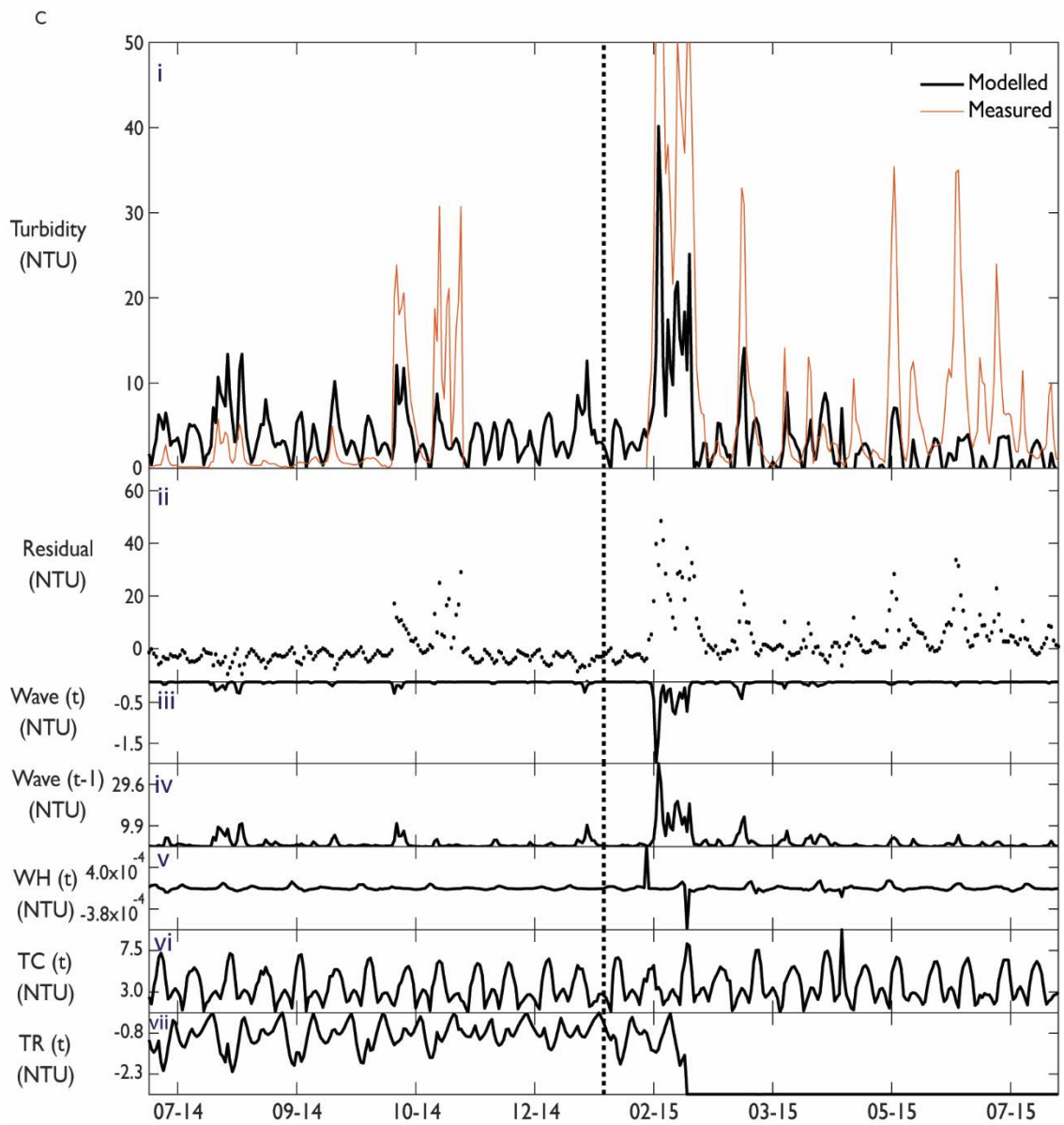


Figure 3-4 Hay Point project. Turbidity model (equation 5) at Slade Islet during the baseline train (left of the dotted line) and test (right of the dotted line) periods showing (from top to bottom): (i) the modelled (black line) and measured (orange line) turbidity levels, (ii) the residual turbidity, then each model term (with parameters applied) including (iii) RMS pressure fluctuations to represent the motion of surface gravity waves on the sea floor at time  $t$  (wave ( $t$ )), (iv) RMS pressure fluctuations from the previous day (wave( $t-1$ )), (v) water height at time  $t$ , (vi) tidal current quasi estimates at time  $t$  and (vii) tidal range at time  $t$ , all in units of NTU. Panel i showing measured and modelled turbidity is the same in all 3 figures and has been truncated to 50 NTU to show the smaller modelled turbidity levels.

Table 3-3 Turbidity model performance at Hay Point sites based on the R<sup>2</sup> and skills score between modelled and measured turbidity during the fit (first half of data, used to calibrate model parameters) and test (second half of data used to validate model performance) data.

| Site             | R <sup>2</sup> |      | Skills score |      |
|------------------|----------------|------|--------------|------|
|                  | Fit            | Test | Fit          | Test |
| Hay Point/Reef   | 0.60           | 0.68 | 0.54         | 0.47 |
| Freshwater Point | 0.79           | 0.45 | 0.78         | 0.36 |
| Keswick Island   | 0.61           | 0.57 | 0.52         | 0.57 |
| Round Top Island | 0.32           | 0.56 | 0.13         | 0.45 |
| Slade Point      | 0.07           | 0.64 | -0.04        | 0.31 |
| Victor Island    | 0.12           | 0.62 | -0.10        | 0.36 |

At Barrow Island the R<sup>2</sup> values were 0 – 0.78 (median 0.27) during the fit period and 0 – 0.65 (median 0.24) during the test period, while the skill scores were -0.78 – 0.76 (median -0.04) during the fit period and -0.31 – 0.48 (median -0.31) during the test period (Table 3-4). During the fit period 4 of 26 sites (LNG3, SBS, LONE and DSGS) had R<sup>2</sup> > 0.6 (0.59 – 0.78) and the same sites had skill scores > 0.58 (0.58 – 0.76, Table 3-1). During the test period, 3 sites had R<sup>2</sup> > 0.53 (0.53 – 0.60, sites LNG2, SBS and LONE) but those sites had poor skill scores (-0.32 – 0.20). The highest skill score during the test period occurred at site TR which had a test period R<sup>2</sup> of 0.48. The best model performance was at site LONE (perimeter of the dredge spoil disposal site), with R<sup>2</sup> = 0.78 and SS = 0.76 during the fit phase (but R<sup>2</sup> = 0.53 and SS = 0.20 during the test phase, Figure 3-5 A and Table 3-4). Similar to Hay Point Reef (Figure 3-4 A), the temporal location and magnitude of the measured and modelled peaks were very similar at site LONE (Figure 3-5 A).

Four other representative sites are also displayed in Figure 3-5 B to E. Sites MOF1 and LNG0 (Figure 3-5 B & C) are within 0.8 km south of dredging (0.2 and 0.8 km away, respectively), and sites AHC and DUG (Figure 3-5 D & E) are reference sites located 32 km north and 9.2 km south from dredging.



Despite their low to moderate  $R^2$  and SS values between measured and modelled turbidity, ranging from  $R^2 = 0.27 - 0.54$  during the fit period,  $R^2 = 0.14 - 0.38$  during the test period, and SS from  $0.24 - 0.5$  and  $-0.57 - 0.14$  during fit and test periods (respectively, Table 3-4), the magnitude and temporal location of the modelled peaks are similar to the measured peaks (typically  $< 10$  NTU, Figure 3-5). During the dredge period, the dredge impact sites have significantly higher measured turbidity than modelled turbidity, and the modelled turbidity peaks are similar magnitude to the baseline peaks (Figure 3-5 B & C) during the fit and test (i.e. entire baseline) periods, as expected. Model and measured plots of the remaining Hay Point sites are provided in Appendix B.

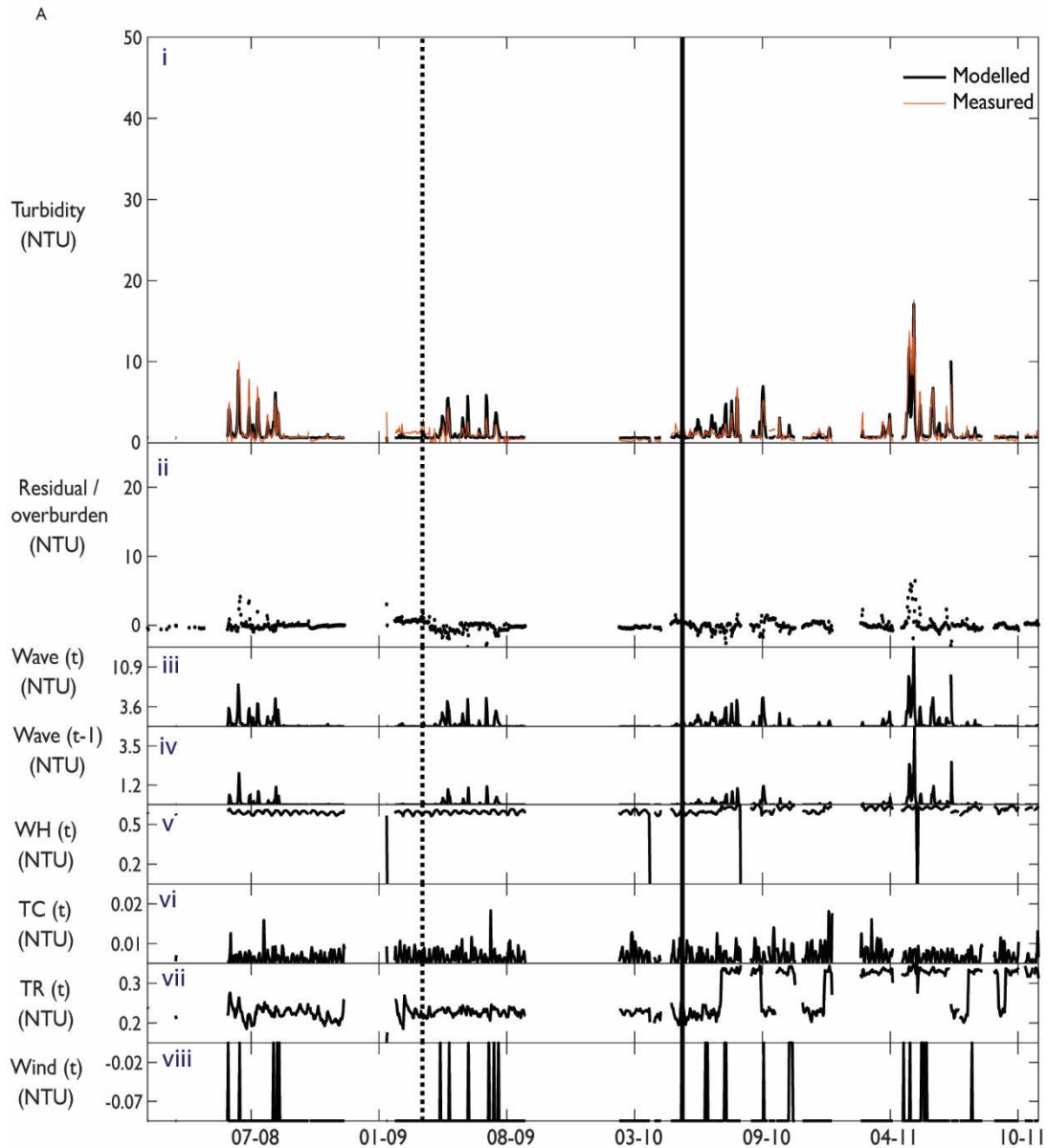


Figure 3-5 A Barrow Island Project. Turbidity model (equation 5) performance at site LONE during the baseline train (left of the dotted line), test (between dotted and solid lines), and dredge period (right of the solid line) showing (from top to bottom): the modelled (black line) and measured (orange line) turbidity levels, residual turbidity, or ‘overburden’ (which is the difference between the measured and modelled turbidity), and each model term (with parameters applied) including: (iii) RMS pressure fluctuations to represent the motion of surface gravity waves on the sea floor at time  $t$  (wave ( $t$ )), (iv) RMS pressure fluctuations from the previous day (wave( $t-1$ )), (v) water height at time  $t$ , (vi) tidal current quasi estimates at time  $t$ , (vii) tidal range at time  $t$  and (viii) wind at time  $t$ , all in units of NTU. The top panel showing measured and modelled turbidity has the same scale in all 5 figures, truncated to 50 NTU to show the smaller modelled turbidity events (most of which are < 10 NTU during the baseline period).

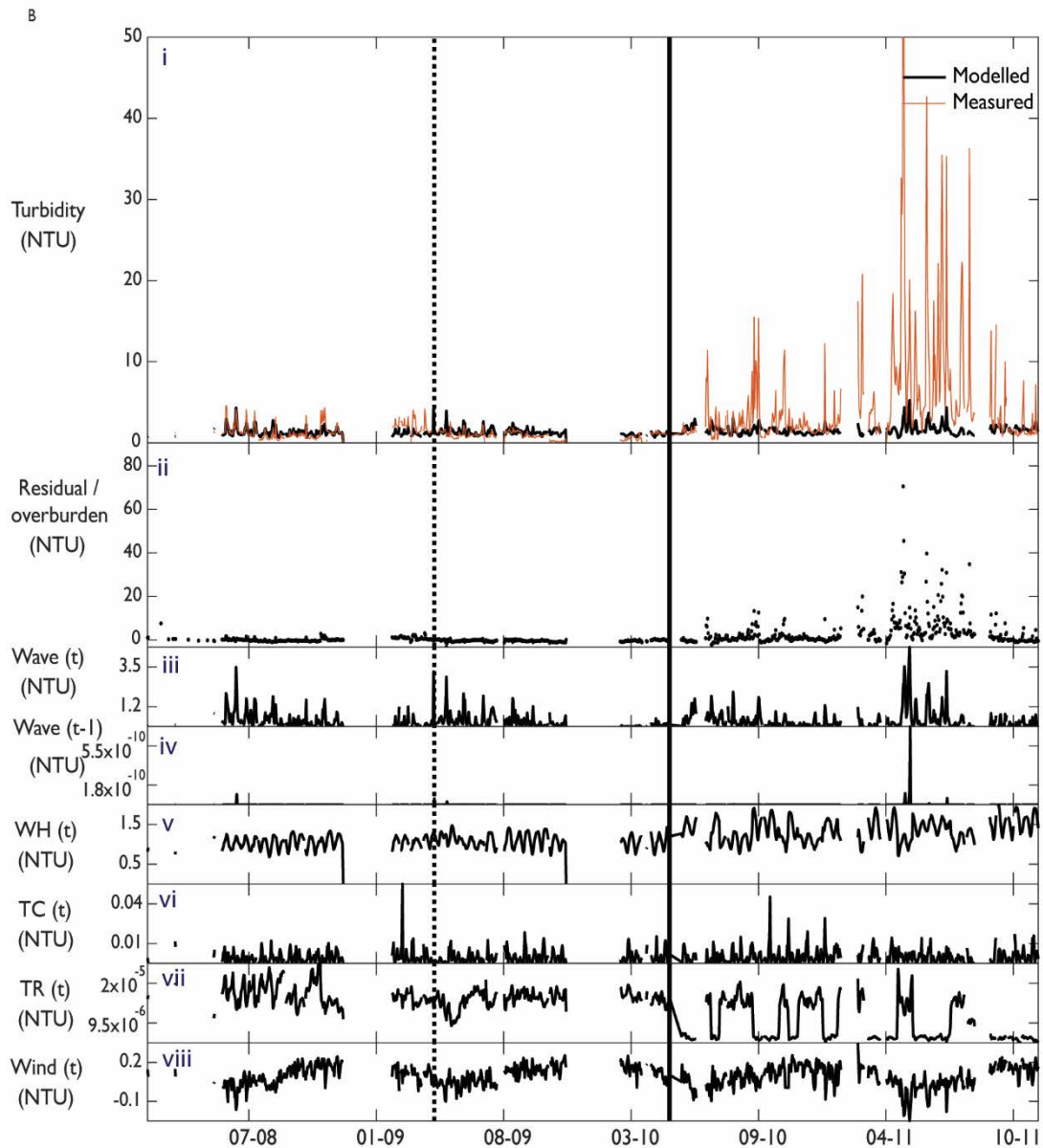


Figure 3-5 B Barrow Island Project. Turbidity model (equation 5) performance at MOF1 during the baseline train (left of the dotted line), test (between dotted and solid lines), and dredge period (right of the solid line) showing (from top to bottom): the modelled (black line) and measured (orange line) turbidity levels, residual turbidity, or ‘overburden’ (which is the difference between the measured and modelled turbidity), and each model term (with parameters applied) including: (iii) RMS pressure fluctuations to represent the motion of surface gravity waves on the sea floor at time  $t$  (wave ( $t$ )), (iv) RMS pressure fluctuations from the previous day (wave( $t-1$ )), (v) water height at time  $t$ , (vi) tidal current quasi estimates at time  $t$ , (vii) tidal range at time  $t$  and (viii) wind at time  $t$ , all in units of NTU. The top panel showing measured and modelled turbidity has the same scale in all 5 figures, truncated to 50 NTU to show the smaller modelled turbidity events (most of which are < 10 NTU during the baseline period).

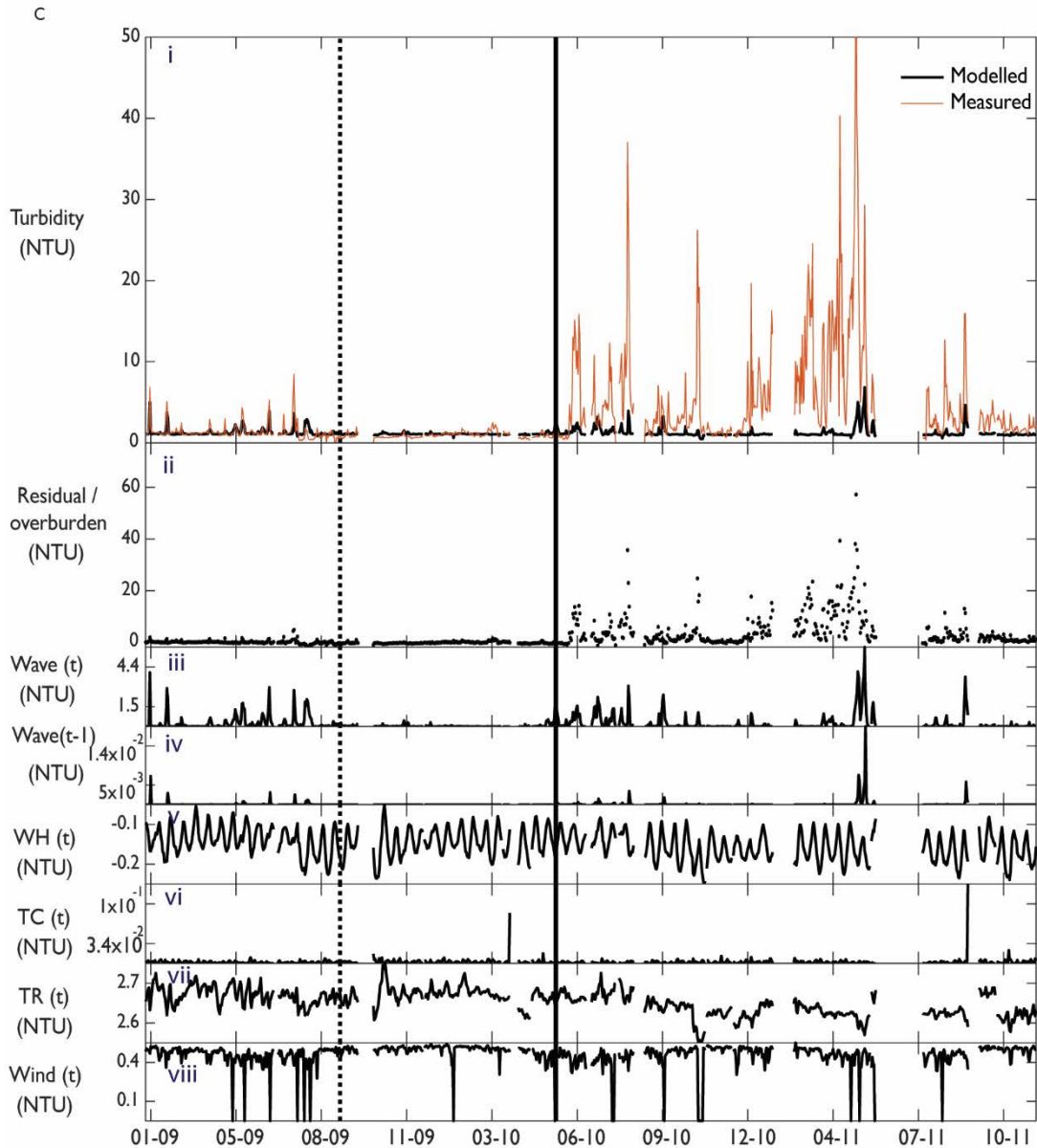


Figure 3-5 C Barrow Island Project. Turbidity model (equation 5) performance at LNG0 during the baseline train (left of the dotted line), test (between dotted and solid lines), and dredge period (right of the solid line) showing (from top to bottom): the modelled (black line) and measured (orange line) turbidity levels, residual turbidity, or ‘overburden’ (which is the difference between the measured and modelled turbidity), and each model term (with parameters applied) including: (iii) RMS pressure fluctuations to represent the motion of surface gravity waves on the sea floor at time  $t$  (wave ( $t$ )), (iv) RMS pressure fluctuations from the previous day (wave( $t-1$ )), (v) water height at time  $t$ , (vi) tidal current quasi estimates at time  $t$ , (vii) tidal range at time  $t$  and (viii) wind at time  $t$ , all in units of NTU. The top panel showing measured and modelled turbidity has the same scale in all 5 figures, truncated to 50 NTU to show the smaller modelled turbidity events (most of which are < 10 NTU during the baseline period).

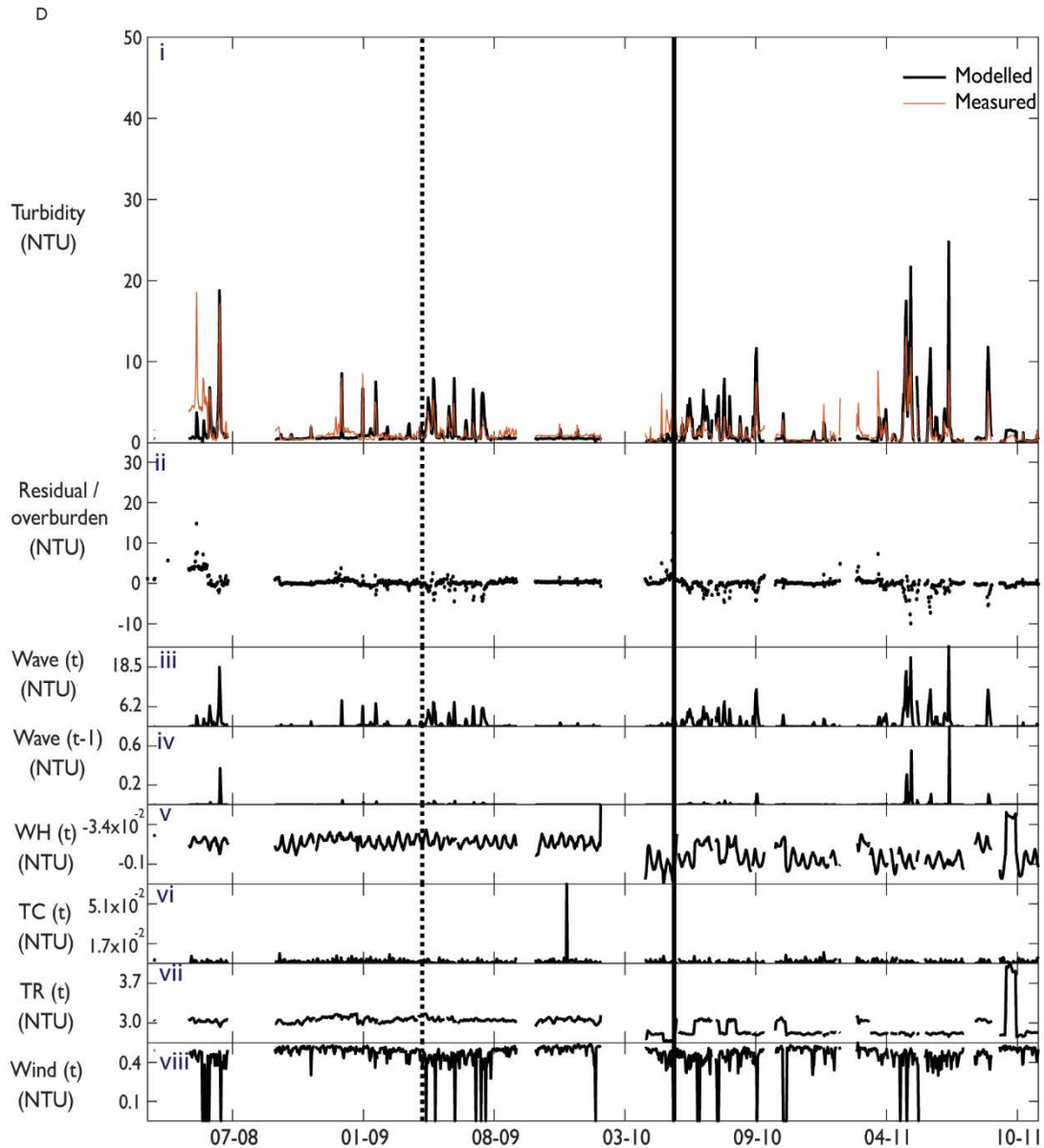


Figure 3-5 D Barrow Island Project. Turbidity model (equation 5) performance at AHC during the baseline train (left of the dotted line), test (between dotted and solid lines), and dredge period (right of the solid line) showing (from top to bottom): the modelled (black line) and measured (orange line) turbidity levels, residual turbidity, or ‘overburden’ (which is the difference between the measured and modelled turbidity), and each model term (with parameters applied) including: (iii) RMS pressure fluctuations to represent the motion of surface gravity waves on the sea floor at time  $t$  (wave ( $t$ )), (iv) RMS pressure fluctuations from the previous day (wave( $t-1$ )), (v) water height at time  $t$ , (vi) tidal current quasi estimates at time  $t$ , (vii) tidal range at time  $t$  and (viii) wind at time  $t$ , all in units of NTU. The top panel showing measured and modelled turbidity has the same scale in all 5 figures, truncated to 50 NTU to show the smaller modelled turbidity events (most of which are < 10 NTU during the baseline period).

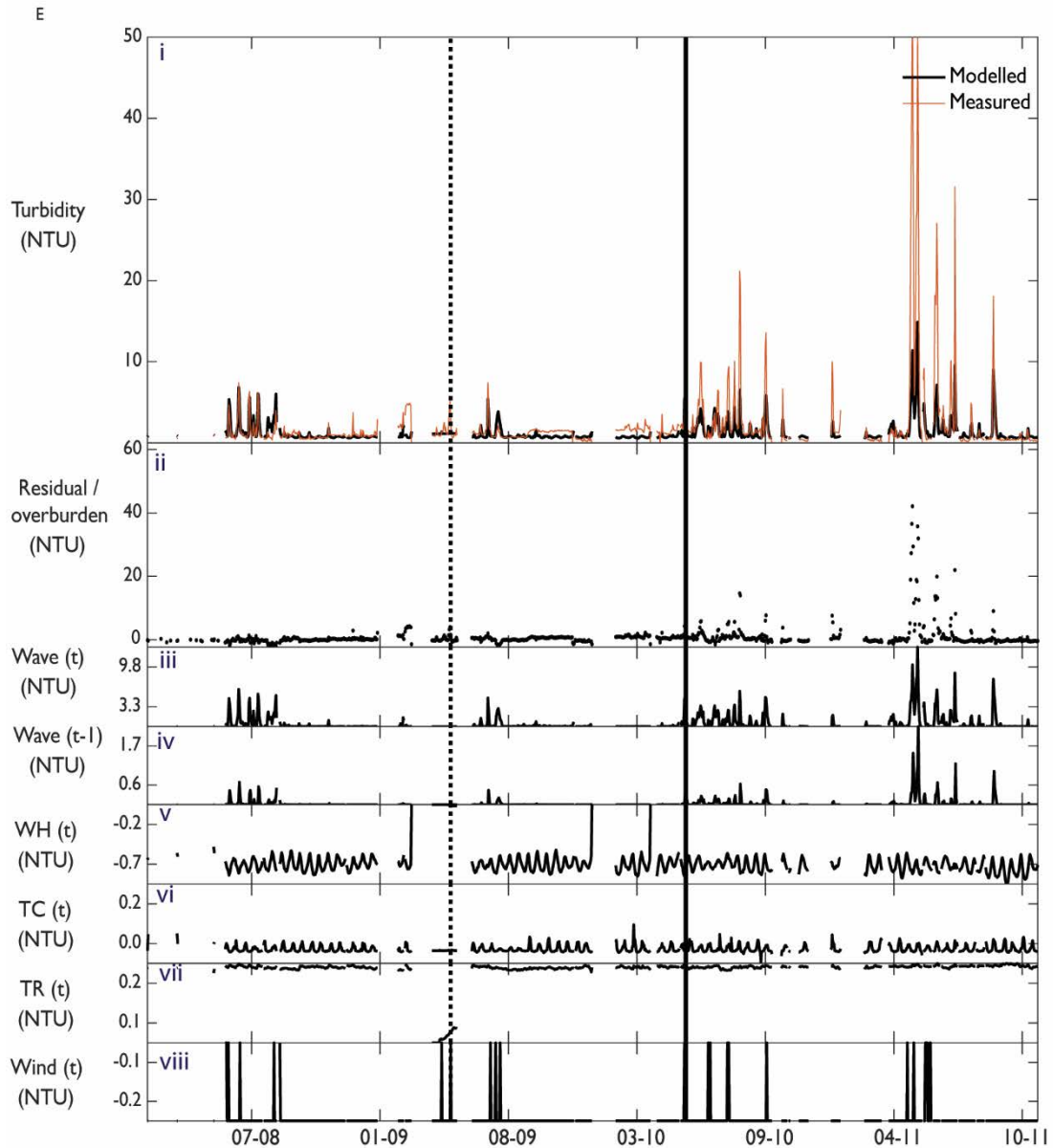


Figure 3-5 E Barrow Island Project. Turbidity model (equation 5) performance at DUG during the baseline train (left of the dotted line), test (between dotted and solid lines), and dredge period (right of the solid line) showing (from top to bottom): the modelled (black line) and measured (orange line) turbidity levels, residual turbidity, or ‘overburden’ (which is the difference between the measured and modelled turbidity), and each model term (with parameters applied) including: (iii) RMS pressure fluctuations to represent the motion of surface gravity waves on the sea floor at time  $t$  (wave ( $t$ )), (iv) RMS pressure fluctuations from the previous day (wave( $t-1$ )), (v) water height at time  $t$ , (vi) tidal current quasi estimates at time  $t$ , (vii) tidal range at time  $t$  and (viii) wind at time  $t$ , all in units of NTU. The top panel showing measured and modelled turbidity has the same scale in all 5 figures, truncated to 50 NTU to show the smaller modelled turbidity events (most of which are < 10 NTU during the baseline period).

Table 3-4 Turbidity model performance at Barrow Island sites based on the R<sup>2</sup> and skills scores between modelled and measured turbidity during the fit (first half of baseline data, used to calibrate model parameters), test (second half of baseline data used to validate model performance) and dredge (all of dredge period, 19 May 2010 – 31 November 2011) periods.

| Site                               | R <sup>2</sup> |      | Skills score |        |
|------------------------------------|----------------|------|--------------|--------|
|                                    | Fit            | Test | Fit          | Test   |
| <b>Northern sites</b>              |                |      |              |        |
| AHC                                | 0.46           | 0.22 | 0.38         | -0.09  |
| REFN                               | 0.58           | 0.65 | -28.23       | -18.4  |
| ELS                                | 0.2            | 0.43 | -15.53       | -24.4  |
| ANT                                | 0.49           | 0.11 | 0.33         | -0.25  |
| DIW                                | 0              | 0.24 | -10.4        | -1.72  |
| LOW                                | 0.2            | 0.4  | -0.58        | 0      |
| LOW1                               | 0.4            | 0.47 | -2.44        | -5.91  |
| <b>Northern sites</b>              |                |      |              |        |
| LNG0                               | 0.54           | 0.14 | 0.5          | 0      |
| LNGA                               | 0.27           | 0.43 | -46.63       | -31.03 |
| LNG1                               | 0.14           | 0.23 | -1.79        | -1.88  |
| LNGB                               | 0.45           | 0.25 | 0.42         | -0.3   |
| LNG2                               | 0.21           | 0.6  | -9           | -3.84  |
| LNGC                               | 0.04           | 0.2  | -42.19       | -30.72 |
| MOFA                               | 0.07           | 0.06 | -0.04        | 0.06   |
| MOFC                               | 0.22           | 0    | -78.37       | -0.07  |
| MOF1                               | 0.27           | 0.22 | 0.24         | -0.57  |
| MOFB                               | 0.16           | 0    | -9.26        | -0.17  |
| MOF3                               | 0.22           | 0.26 | -0.03        | -0.05  |
| LNG3                               | 0.72           | 0.09 | 0.67         | -0.18  |
| TR                                 | 0.27           | 0.48 | 0.26         | 0.42   |
| DUG                                | 0.37           | 0.38 | 0.31         | 0.14   |
| BAT                                | 0.34           | 0.19 | 0.31         | -1.16  |
| REFS                               | 0.25           | 0.13 | -2.02        | -1.46  |
| SBS                                | 0.64           | 0.57 | 0.62         | -0.32  |
| <b>Dredge spoil disposal sites</b> |                |      |              |        |
| LONE                               | 0.78           | 0.53 | 0.76         | 0.2    |
| DSGS                               | 0.59           | 0.01 | 0.58         | -1.08  |

RMS pressure fluctuations (estimates of wave motion at the seafloor, wave (t) in Figure 3-4 and Figure 3-5, panel iii) influenced the turbidity model more than the other input variables at Hay Point and Barrow Island sites, and at some of the Hay Point sites the RMS pressure fluctuations on the previous day (wave (t-1) in Figure 3-4 and Figure 3-5 panel iv) were also a significant component of the model, but had negligible influence at the Barrow Island sites. The relationship between daily

averaged RMS pressure fluctuations and daily averaged turbidity are presented in Figure 3-6 and Figure 3-7 for representative sites at Hay Point (Figure 3-6) and Barrow Island (Figure 3-7) to demonstrate the influence of seafloor pressure fluctuations at resuspending sediment. Quantitative comparisons of the pressure fluctuations and turbidity ( $R^2$  and root mean square errors) are provided in Table 3-5 for Hay Point sites and Table 3-6 for Barrow Island sites. In the Hay Point sites show in Figure 3-4, contribution from present day waves was the most significant at Hay Point Reef; modelled turbidity values reached over 50 NTU (Figure 3-4 A i), while values from the present day wave term ranged from 9 -27 NTU (Figure 3-4 A iii), from the previous day waves ranged from 5 – 15 NTU (Figure 3-4 A iv) and all other model inputs were < 1 NTU, Figure 3-4 A v – vii. The previous day waves were the most significant to the modelled turbidity at the other 2 represented Hay Point sites (Figure 3-4 B & C, panel iv), with values ranging between 4 – 11 NTU for turbidity ~ 10 NTU at Round Top Island (Figure 3-4 B), and 10 – 30 NTU contributing to modelled turbidity of up to 40 NTU at Slade Islet (Figure 3-4 C). Apart from the influence of the tidal current at Slade Islet (3 – 7.5 NTU, Figure 3-4 C vi), all other input variables contributed relatively little (Figure 3-4 B & C v - vii).

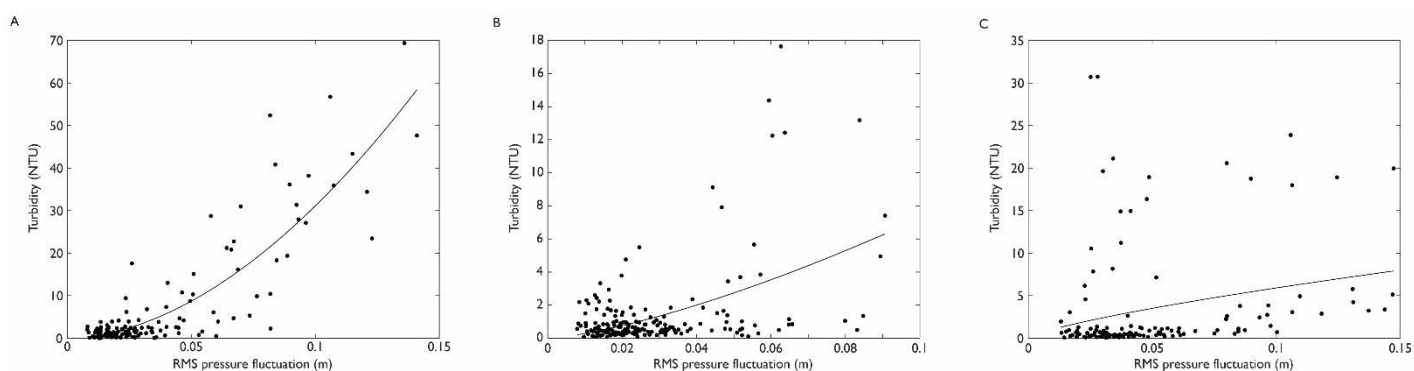


Figure 3-6 Relationship between daily averaged RMS pressure fluctuation measurements and daily averaged turbidity at three representative Hay Point sites (the same turbidity model representative sites) during the turbidity model fit period (first half of data): A) Hay Point Reef, B) RoundTop Island and C) Slade Islet. The RMS pressure fluctuations (an estimate of the influence of waves on the seafloor) were the most significant predictor of modelled turbidity at Hay Point.



Table 3-5 R<sup>2</sup> and root mean square error (RMSE) between RMS pressure fluctuations (estimates of seafloor wave motion) and turbidity measurements at Hay Point for the fit and test periods (first half and second half of data) using a power regression.

| Site             | R <sup>2</sup> |      | RMSE (NTU) |      |
|------------------|----------------|------|------------|------|
|                  | Fit            | Test | Fit        | Test |
| Hay Point/Reef   | 0.76           | 0.57 | 6.4        | 4.7  |
| Freshwater Point | 0.74           | 0.72 | 4.4        | 9.8  |
| Keswick Island   | 0.24           | 0.34 | 0.5        | 0.6  |
| Round Top Island | 0.21           | 0.64 | 2.3        | 4.0  |
| Slade Point      | 0.05           | 0.57 | 6.3        | 9.4  |
| Victor Island    | 0.18           | 0.75 | 5.4        | 6.4  |

At the representative Barrow Island sites, the present day waves were consistently the most significant contributor to the modelled turbidity (panel iii in Figure 3-5). Maximum wave term values ranged between 3.5 – 19 NTU (Figure 3-5 A – E iii) which were similar to the maximum modelled turbidities of between 5 – 20 NTU (Figure 3-5 A – E i). Only at site LONE did the previous day waves influence the modelled turbidity, contributing up to 3.5 NTU (Figure 3-5 A iii) for turbidity up to 20 NTU (Figure 3-5 A i), but had less influence than the present day waves. At sites LNG0 and AHC, the tidal range contributed to the modelled turbidity up to 3 NTU (Figure 3-5 C & D panel vii). At all sites shown in Figure 3-5 the water height (panel v), tidal current (panel vi) and wind (panel viii) terms did not contribute to modelled turbidity.

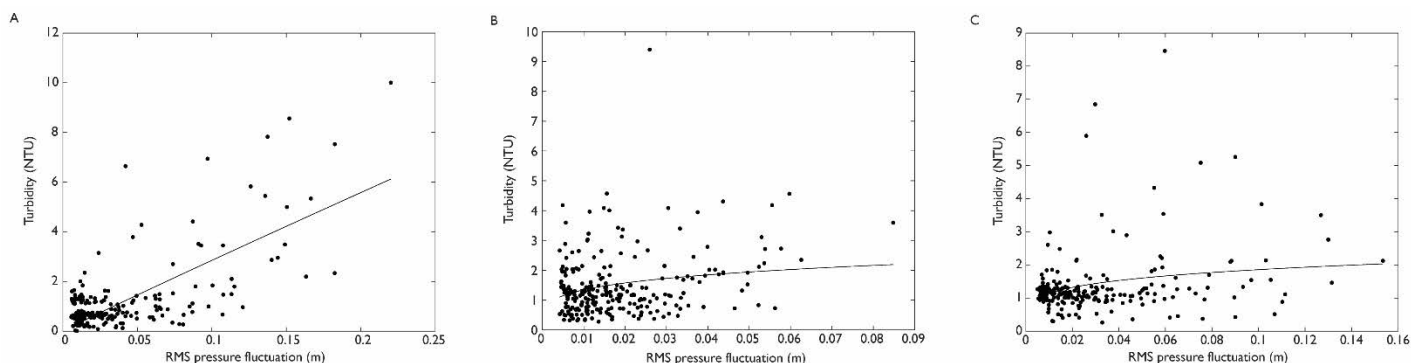


Figure 3-7 Relationship between daily averaged RMS pressure fluctuation measurements and daily averaged turbidity at three representative Barrow Island sites during the turbidity model fit period (first half of baseline data): A) LONE, B) MOF1 and C) LNG0. The RMS pressure fluctuations (a quasi-estimate of the influence of waves on the seafloor) were the most significant predictor of modelled turbidity at Barrow Island.

Table 3-6 R<sup>2</sup> and root mean square error between RMS pressure fluctuations (quasi-estimates of wave motion at the seafloor) and turbidity measurements at Barrow Island for the fit and test periods (first half and second half of baseline data) using a power regression.

| Site                                | R <sup>2</sup> |      | RMSE (NTU) |      |
|-------------------------------------|----------------|------|------------|------|
|                                     | Fit            | Test | Fit        | Test |
| <b>Northern sites</b>               |                |      |            |      |
| AHC                                 | 0.17           | 0.10 | 2.11       | 1.23 |
| REFN                                | 0.22           | 0.30 | 0.21       | 0.20 |
| ELS                                 | 0.05           | 0.15 | 0.16       | 0.22 |
| ANT                                 | 0.10           | 0.02 | 1.00       | 0.65 |
| DIW                                 | 0.05           | 0.26 | 0.45       | 0.49 |
| LOW                                 | 0.09           | 0.06 | 0.97       | 0.93 |
| LOW1                                | 0.02           | 0.00 | 0.33       | 0.36 |
| <b>Southern sites</b>               |                |      |            |      |
| LNG0                                | 0.06           | 0.01 | 0.94       | 0.37 |
| LNGA                                | 0.07           | 0.21 | 0.17       | 0.20 |
| LNG1                                | 0.02           | 0.03 | 1.34       | 0.57 |
| LNGB                                | 0.39           | 0.22 | 0.08       | 0.56 |
| LNG2                                | 0.01           | 0.28 | 0.70       | 0.60 |
| LNGC                                | 0.01           | 0.14 | 0.33       | 0.39 |
| MOFA                                | 0.01           | 0.02 | 0.25       | 0.82 |
| MOFC                                | 0.02           | 0.02 | 0.12       | 0.75 |
| MOF1                                | 0.04           | 0.13 | 1.01       | 0.41 |
| MOFB                                | 0.01           | 0.02 | 0.17       | 0.69 |
| MOF3                                | 0.02           | 0.07 | 1.41       | 0.60 |
| LNG3                                | 0.15           | 0.12 | 0.99       | 0.43 |
| TR                                  | 0.22           | 0.01 | 0.36       | 0.57 |
| DUG                                 | 0.04           | 0.05 | 1.15       | 0.85 |
| BAT                                 | 0.10           | 0.06 | 1.35       | 0.58 |
| REFS                                | 0.52           | 0.02 | 0.81       | 0.97 |
| SBS                                 | 0.29           | 0.18 | 3.57       | 1.62 |
| <b>Dredge spoil disposal sites*</b> |                |      |            |      |
| LONE                                | 0.44           | 0.44 | 1.07       | 0.55 |
| DSGS                                | 0.18           | 0.14 | 0.12       | 0.35 |

### 3.3.4 Running mean analysis

Running mean percentile plots for representative Barrow Island sites are shown in Figure 3-8. First, a brief explanation of the structure of the running mean plots are provided. Each data point in the figures represent a percentile (either maximum, 99<sup>th</sup>, 95<sup>th</sup> and 80<sup>th</sup> in Figure 3-8 or maximum and

95<sup>th</sup> in Figure 3-10) for each running mean window size (1 hour to 30 days, horizontal axis). For example, in Figure 3-8 A, the start of the solid lines (i.e. the very first data point at the left of the figure) represent the percentiles of the hourly running mean array during the dredge period at site MOF1. And each individual line represents a percentile of all running means; i.e. moving from left to right, the green solid line are the maximums of the running means from 1 hour to 30 days. Broken lines represent the baseline period.

At site MOFA (0.6 km from the dredge zone) maximum hourly running means reached over 400 NTU (solid green line, Figure 3-8 A) during dredging but did not exceed ~ 20 NTU during the baseline period (broken green line, Figure 3-8 A). Also at site MOFA the maximum 30 day running mean during dredging (~ 25 NTU, green solid line on the right of Figure 3-8 A) exceeded the hourly maximum baseline turbidity (~ 8 NTU, green dotted line on the left of Figure 3-8 A). Site MOFC (Figure 3-8 B) which is also within the dredge impact zone (0.6 km south), had similar conditions to MOFA with hourly percentiles during dredging from 6 – 400 NTU (solid lines in Figure 3-8 B) compared to the hourly percentiles during the baseline from 3 – 20 NTU (broken lines in Figure 3-8 B). Site LNGO (Figure 3-8 C), which is also within the dredge impact zone (0.2 km south) had slightly lower hourly percentiles during dredging, from 6 – 200 NTU (solid lines in Figure 3-8 C) but similar baseline hourly percentiles from 1 – 20 NTU (broken lines in Figure 3-8 B).

Site DSGS, which is on the perimeter of the spoil disposal ground and 4.2 km south of dredging, had lower dredge period hourly percentiles, from 1 – 40 NTU (solid lines in Figure 3-8 D) and 1 – 6 NTU

during the baseline period (broken lines in Figure 3-8 D). Site SBS, which is the furthest southern site ~ 30 km from the dredge zone, the dredge period running means were similar to or less than the baseline period running means with maximum hourly dredge period mean of ~ 50 NTU (green solid line in Figure 3-8 E) and the maximum hourly baseline mean of ~ 70 NTU (green broken line in Figure 3-8 E). Additional running mean percentile analysis of turbidity at the remaining Barrow Island sites can be found in Appendix A.

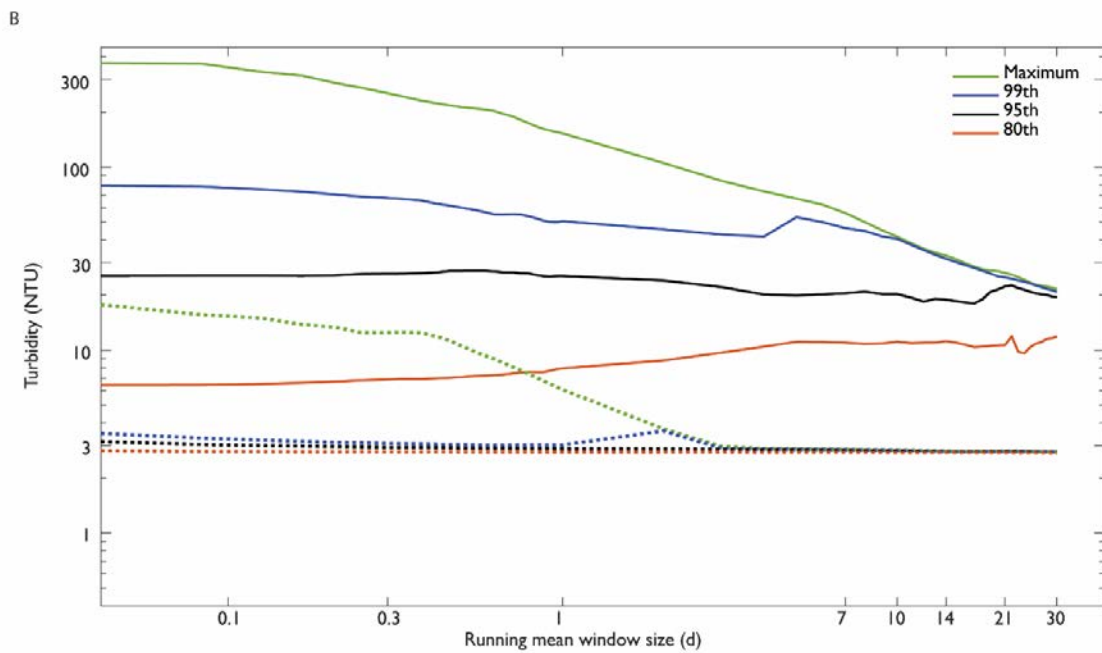
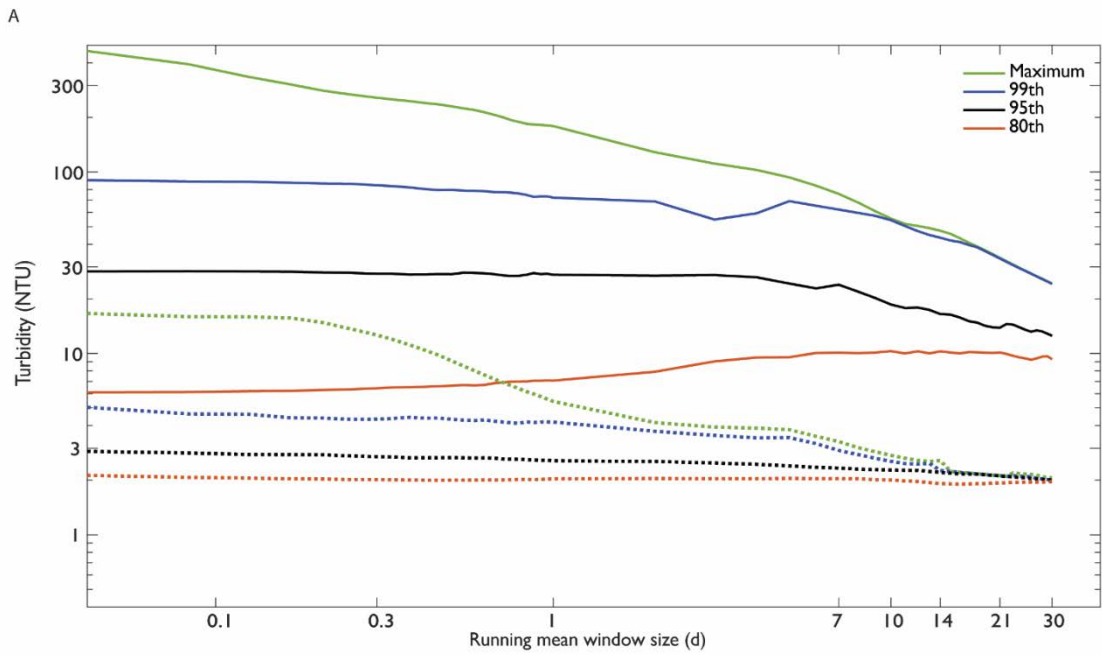


Figure 3-6 A and B. Turbidity running mean percentile analysis using increasing window sizes (from 1 hour to 30 days) comparing the baseline (dotted lines) and dredge periods (solid lines) at representative Barrow Island sites, including A) MOFA and B) MOFC which are within 1 km south of the dredge zone (see Figure 2-1 for site locations). The four lines for each period (baseline and dredge) are the maximum, 99th, 95th and 80th percentiles. Starting from the left of each figure to the right are the different running mean window sizes. Note that the 95<sup>th</sup> percentiles (black solid and broken line) represent the intensity of turbidity events.

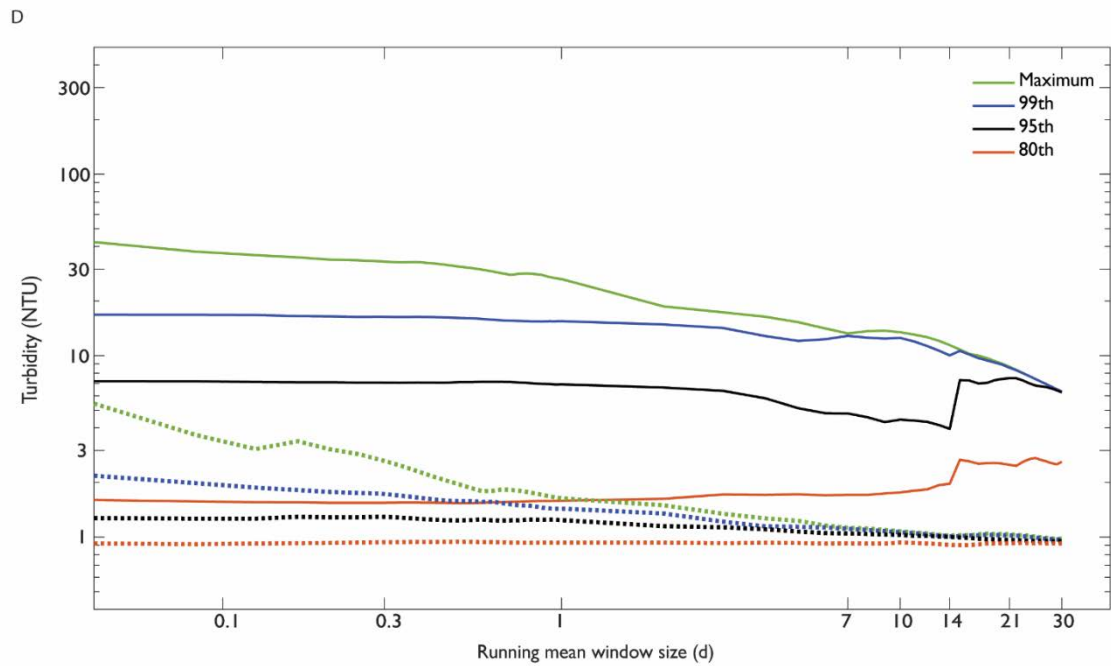
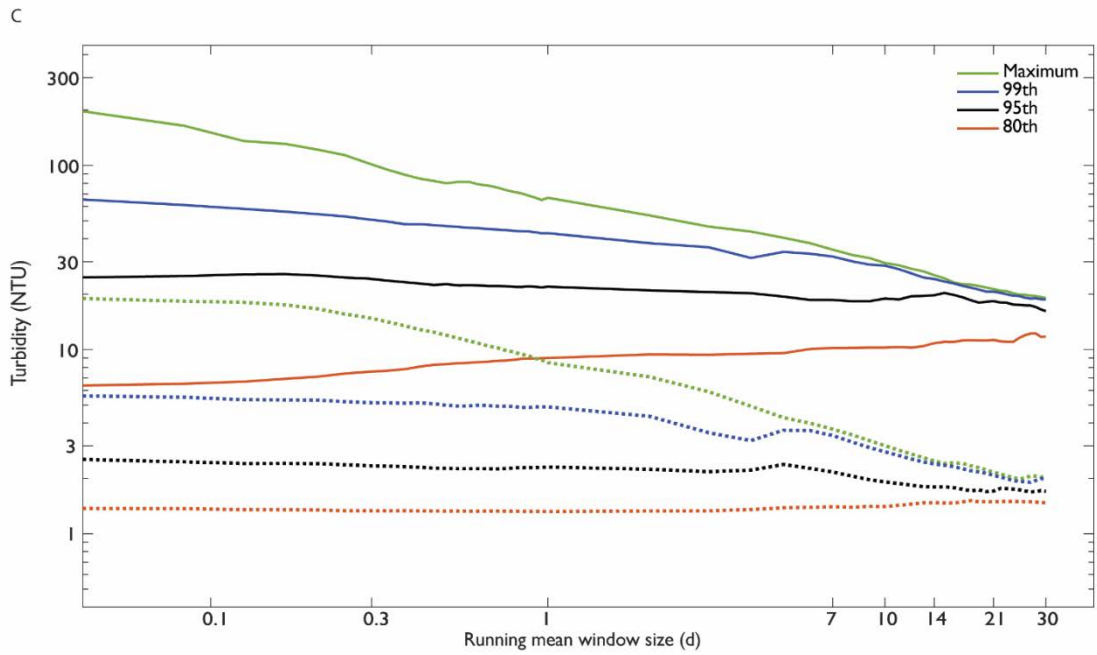


Figure 3-6 C and D Turbidity running mean percentile analysis using increasing window sizes (from 1 hour to 30 days) comparing the baseline (dotted lines) and dredge periods (solid lines) at representative Barrow Island sites, including C) LNG0 (within 1 km south of the dredge zone) and D) DSGS (on the perimeter of the spoil disposal ground and 4.2 km from the main dredge area) (see Figure 2-1 for site locations). The four lines for each period (baseline and dredge) are the maximum, 99th, 95th and 80th percentiles. Starting from the left of each figure to the right are the different running mean window sizes. Note that the 95<sup>th</sup> percentiles (black solid and broken line) represent the intensity of turbidity events.

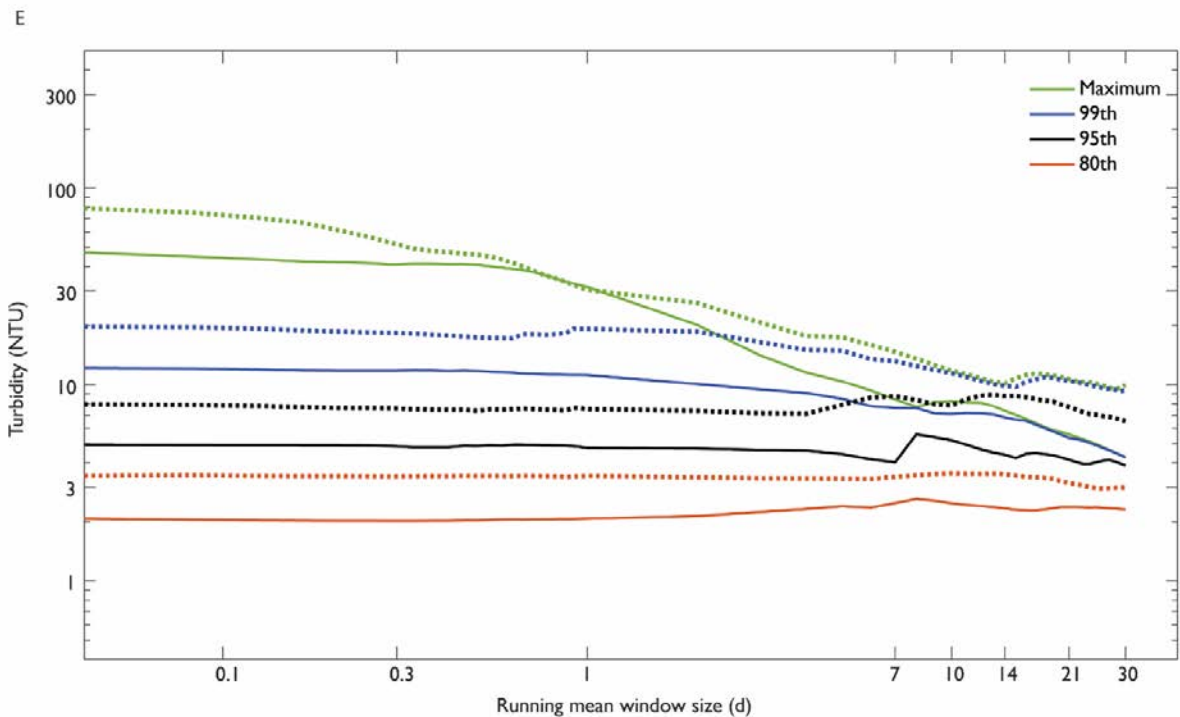


Figure 3-8 E Turbidity running mean percentile analysis using increasing window sizes (from 1 hour to 30 days) comparing the baseline (dotted lines) and dredge periods (solid lines) at representative Barrow Island site E) SBS, the furthest southern site (see Figure 2-1 for site locations). The four lines for each period (baseline and dredge) are the maximum, 99th, 95th and 80th percentiles. Starting from the left of each figure to the right are the different running mean window sizes. Note that the 95<sup>th</sup> percentiles (black solid and broken line) represent the intensity of turbidity events.

Percentile running mean analysis of turbidity at all Barrow Island monitoring sites revealed that running means also increased at sites within 2 km south of dredging during the dredge period. The distance from dredge effects of running mean percentiles are shown in Figure 3-9 and Figure 3-10. Figure 3-9 shows the percentiles of the 1 hour (panel A) and 1 day (panel B) running means plotted at all sites according to the site distance from the dredge zone, separately for the baseline (dots) and dredge periods (circles). The remaining running mean window sizes are added to Figure 3-10 (imagine Figure 3-9 being extended into the page with the addition of all other running mean percentiles (similar to the horizontal lines in Figure 3-8), however only the maximum and 95<sup>th</sup>

percentiles are included to avoid overcrowding. Figure 3-10 has been separated into baseline (panel A) and dredge periods (panel B).

The maximum 1 hour turbidity averages during the dredge period ranged from approximately 100 – 550 NTU at sites within 2 km of the dredge zone (green circles, Figure 3-9 A and green lines, Figure 3-10 B) and the maximum 1 day turbidity averages ranged from approximately 20 – 200 NTU for the same sites (green circles, Figure 3-9 B and green lines, Figure 3-10 B). In contrast, during dredging northern sites and sites > 5 km south of dredging had maximum hourly turbidity < 100 NTU (green dots, Figure 3-9 A and green lines, Figure 3-10 B) with 1 hour turbidity averages between around 5 – 30 NTU (green dots, Figure 3-9 A) and around 2 – 15 NTU 1 day turbidity averages (green dots, Figure 3-9 B).

Baseline running means were fairly consistent across all study sites, with the maximum turbidity percentiles of all window sizes  $\leq 30$  NTU across most sites, while the furthest northern and southern sites (AHC and SBS) had the highest maximum percentile for all running mean periods (Figure 3-10 A). Maximum baseline hourly averages at all sites ranged from 3 – 100 NTU (green dots, Figure 3-9 A and Figure 3-10 A) and maximum baseline daily averages from 3 – 30 NTU (green dots, Figure 3-9 B and Figure 3-10 A). Differences between the further reference sites baseline and dredge running mean percentiles could be due to differences in the length of each time series (the lengths of the baseline time series varied significantly between sites and compared to the dredge period, see Table 2-1 for time series lengths).



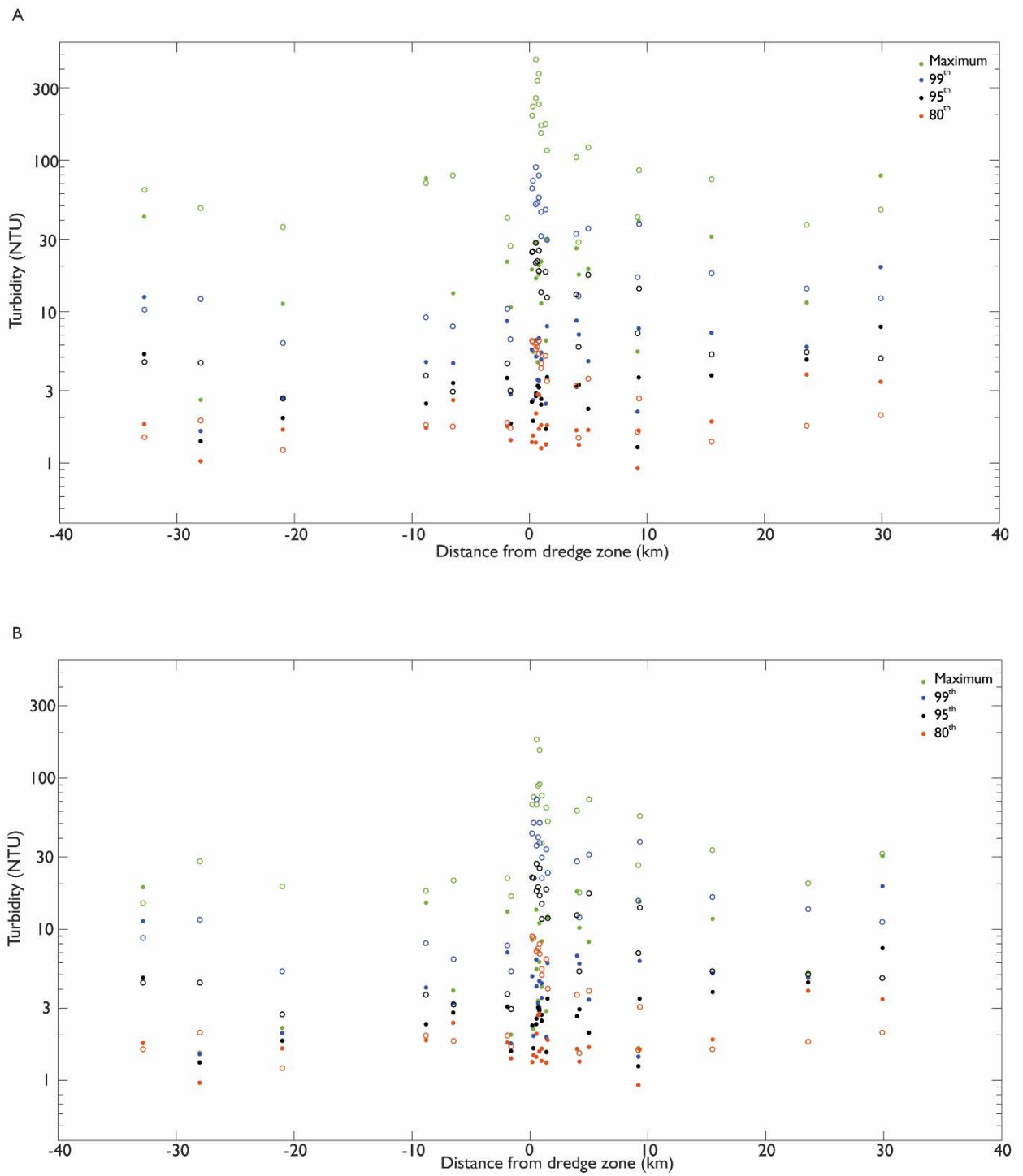


Figure 3-9 Percentiles of turbidity running means (vertical axis) calculated using (A) 1 hour running mean window size and (B) 1 day running mean window size, plotted according to the site distance from the dredge zone during the baseline period (dots) and dredge period (circles). Negative values on the horizontal axis are north of the dredge zone (which is at origin) and positive values are south.

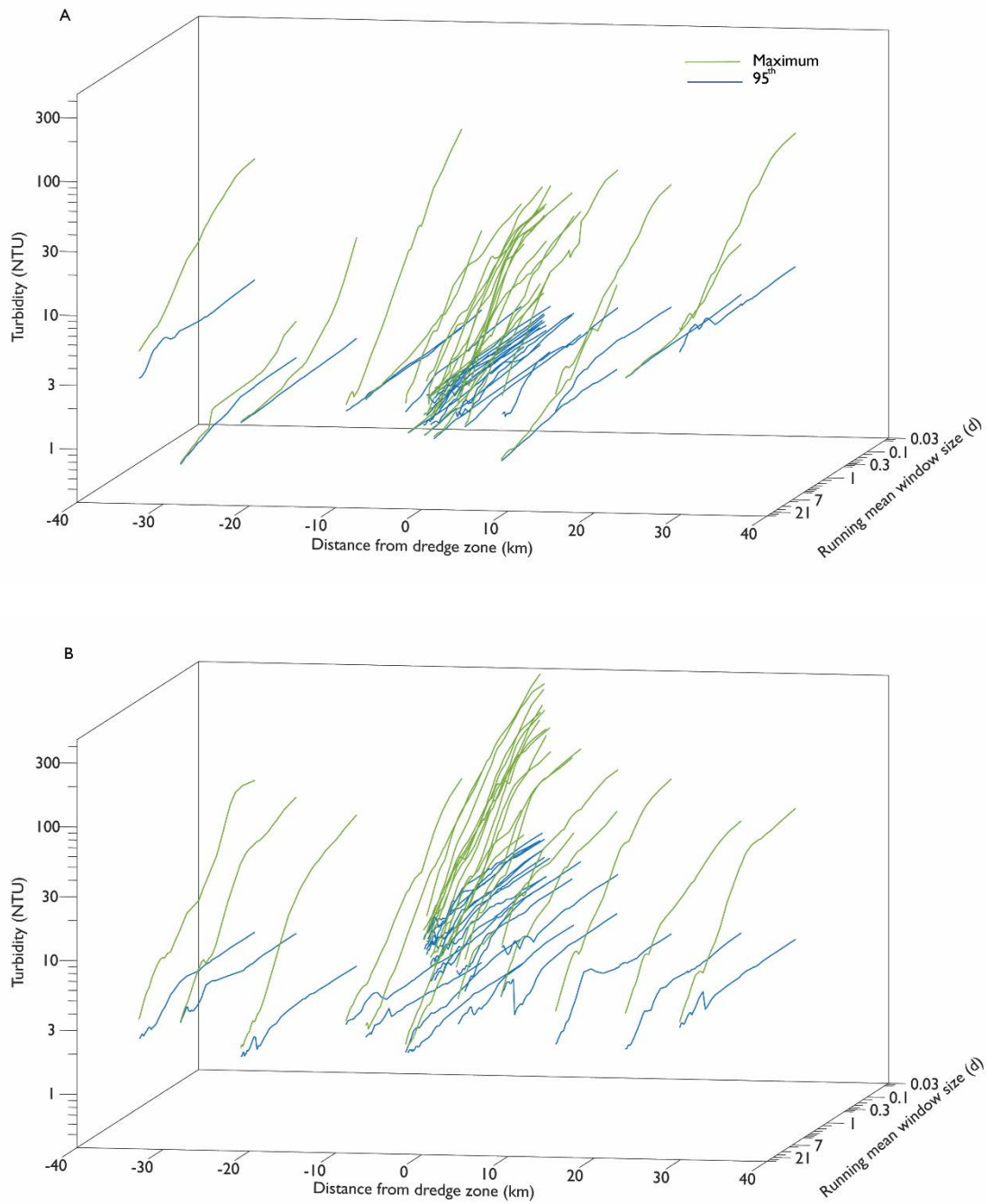


Figure 3-10 Percentiles of turbidity running means (vertical axis) calculated using increasing window sizes (1 hour to 30 days) plotted according to the site distance from the dredge zone (front axis) during the (A) baseline period and (B) dredge period. Negative values are north of the dredge zone (which is at origin) and positive values are south. Only the maximum and 95<sup>th</sup> percentiles of the running means for each site are shown to prevent overcrowding the plot.

### 3.3.5 Spectral analysis

Spectral analysis clearly identified periodic patterns in the turbidity data at the semi-diurnal (particularly during the dredge phase), diurnal, spring/neap and longer period weather band periods of 1 week to months (shown in the global wavelet spectrum in Figure 3-11). During baseline monitoring, the largest peaks in the turbidity global spectra across all sites occurred at the semi-diurnal, diurnal (tide and/or sea breeze) and fortnightly (spring / neap tide) periods, with no clear distinction based on site distance (i.e. sites within 2 km had the same relative spectral peaks as the reference sites located > 10 km away, Figure 3-15 A). However, during dredging, the semi-diurnal and diurnal peaks were significantly higher at sites within 2 km of dredging (red and orange lines, Figure 3-11 B) compared to sites > 2 km away (Figure 3-11 B) and compared to the baseline period (Figure 3-11 A). These semi-diurnal and diurnal peaks were also higher than the longer period fortnightly and monthly peaks during dredging (Figure 3-11 B). The semi-diurnal peak was stronger during the dredge phase at Barrow Island dredge impact LNG and MOF sites. During the baseline period, and at reference sites during dredging, this semi-diurnal peak was of similar strength or weaker than the diurnal peak and the longer period weather bands.

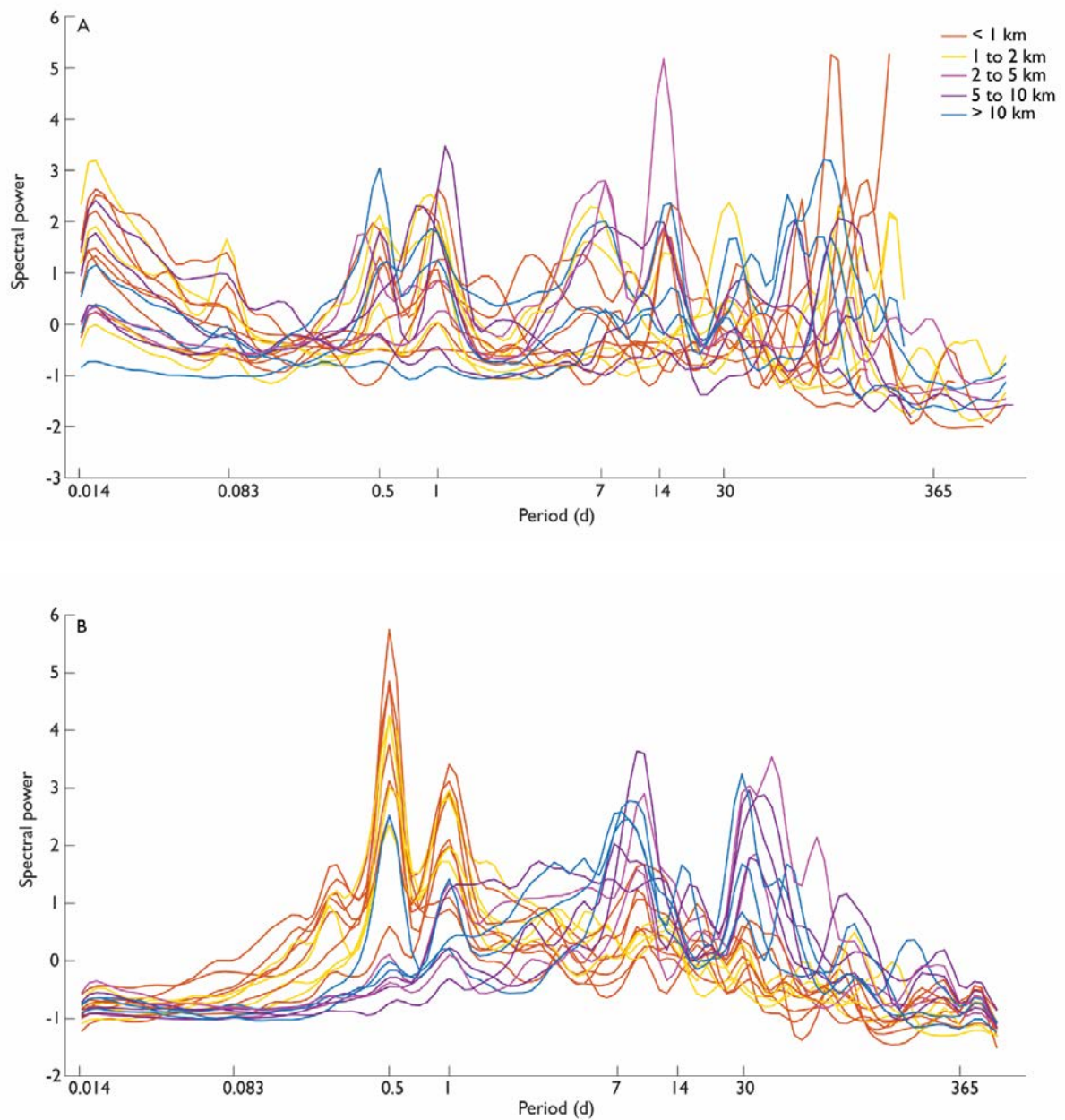


Figure 3-11 Normalised turbidity global (time-averaged) spectral power curves across all sites for the baseline period (A) and dredge period (B). Lines show normalised temporal spectral power values across the range of periods examined, with colours from blue (sites > 10 km from dredging) to red (sites < 1 km from dredging).

Peaks in the wave spectral plots were greatest at the semi-diurnal and diurnal periods compared to the longer periods, with most sites having a larger diurnal peak (Figure 3-12). Conditions were similar during the baseline and dredge periods. There were also smaller peaks during the baseline

and dredge periods at the weekly, spring/neap tide, monthly and annual seasonal cycles, which are better defined during the dredge period (probably because of the consistent lengths of the time series during the dredge measurement period compared to the baseline) (Figure 3-12). In the water height spectrum during both the baseline and dredge monitoring phases (Figure 3-13 A (baseline) and B (dredge)), the largest peak occurred at the semi-diurnal period, while the diurnal signal was insignificant. The longer period spring/neap tide and weather patterns were present but weaker than the semi-diurnal signal.

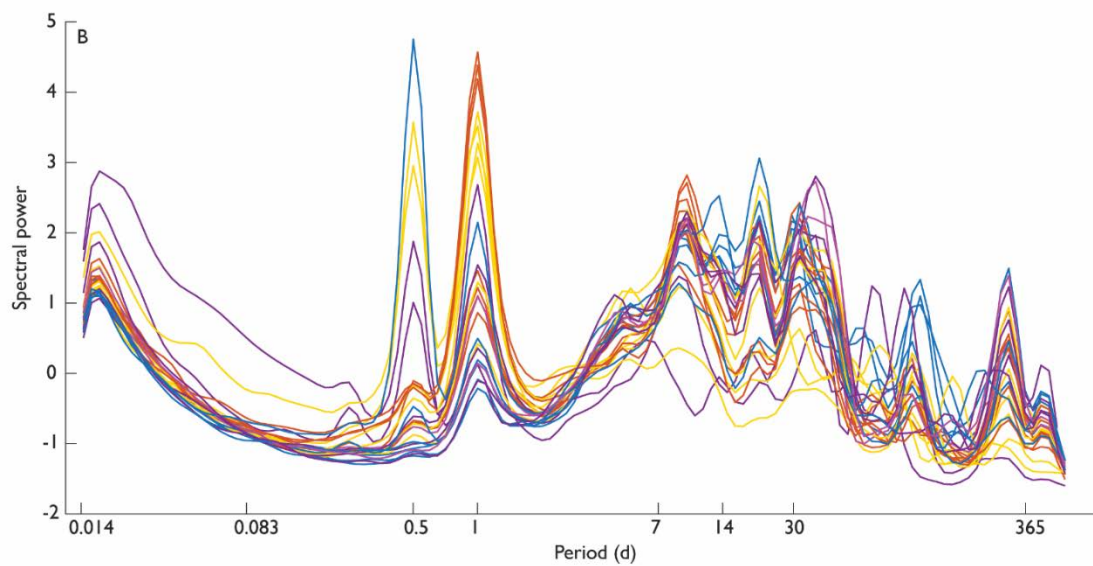
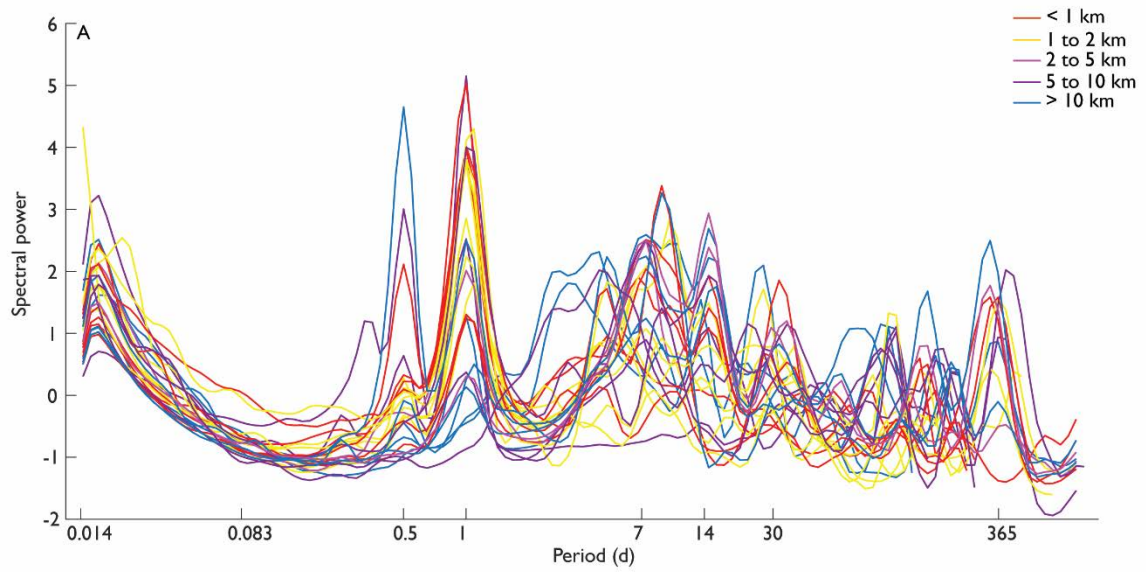


Figure 3-12 Normalised wave global (time-averaged) spectral power curves across all sites for the baseline period (A) and dredge period (B). Lines show normalised temporal spectral power values across the range of periods examined, with colours from blue (sites > 10 km from dredging) to red (sites < 1 km from dredging).

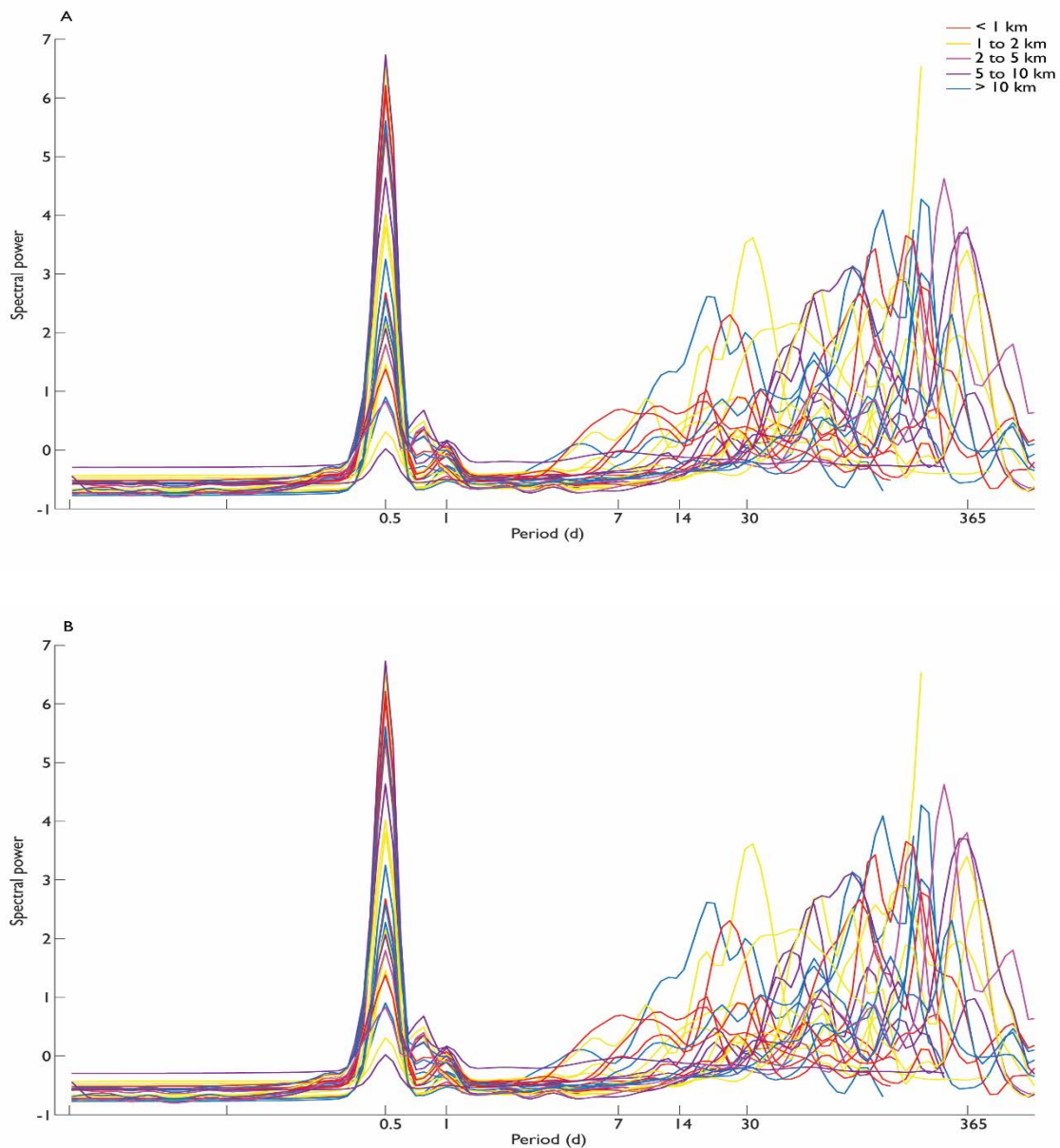


Figure 3-13 Normalised water height global (time-averaged) spectral power curves across all sites for the baseline period (A) and dredge period (B). Lines show normalised temporal spectral power values across the range of periods examined, with colours from blue (sites > 10 km from dredging) to red (sites < 1 km from dredging).

The dominant periodicities in the wind were the strong daily sea breeze in both the zonal and meridional directions, and the annual seasonal peak in the zonal direction (Figure 3-14). As expected, there was little difference in spectral power between the baseline and dredge periods (the slight difference in the zonal wind direction could be due to the length of the time series). Irregularly shaped intermittent energetic features were also present, with periods ranging from 4

to 100 days in both directions but were less energetic than the daily sea breeze and seasonal cycle (Figure 3-14).

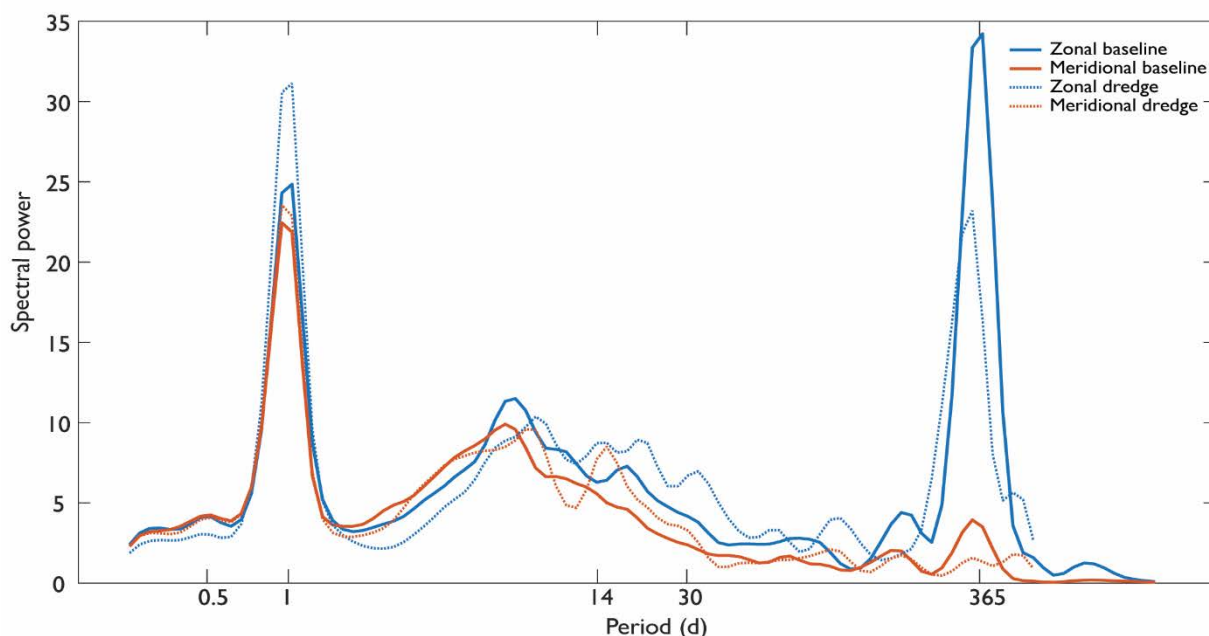


Figure 3-14 Normalised wind global (time-averaged) spectral power curves at Barrow Island airport showing the zonal (blue) and meridional (red) directions during the baseline period (solid line) and dredge period (broken line).

Individual spectral plots, including global wavelet power spectrums comparing baseline and dredge monitoring phases, are presented at some representative sites in Figure 3-15; LNG1 and MOF1 (Figure 3-15 A and B) are both in the dredge impact zone (0.5 and 0.8 km south) while sites DUG and SBS (Figure 3-15 C and D) are reference sites further south (9.2 and 30 km south). The two sites close to the dredge zone have relatively low power across all periods during the baseline monitoring compared to dredging, which is evident in Figure 3-15 A and B panel i by the lack of yellow on the left of the red dotted line (which separates the baseline and dredge monitoring periods) compared to the right of the dotted line, and by the absence of any peaks in the blue curve in the panel ii of Figure 3-15 A and B. In contrast during dredging the dominant periodicities occurred in the semi-diurnal and diurnal bands, demonstrated by the yellow bands in panel i and the peaks in the orange



curve in panel ii of Figure 3-15 A and B. There was also some lower power occurring in the synoptic 10 day weather, spring / neap tidal and longer period weather bands at both LNG1 and MOF1 during dredging (Figure 3-15 A and B, panels i and ii).

In contrast, site DUG had higher power occurring in the longer period weather bands compared to the semi-diurnal and diurnal bands during both the baseline and dredge periods (Figure 3-15 C), with the longer periodicities more dominant during the dredge phase than baseline. The lower power of the semi-diurnal and diurnal signals are similar during baseline and dredging, which is evident in the yellow horizontal bands in Figure 3-15 C panel i. Site SBS had similar power across baseline and dredging, with peaks in the semi-diurnal, diurnal, ten day synoptic pattern and the spring / neap cycle (Figure 3-15 D). The additional spectral analysis figures of turbidity at Barrow Island can be found in 0.

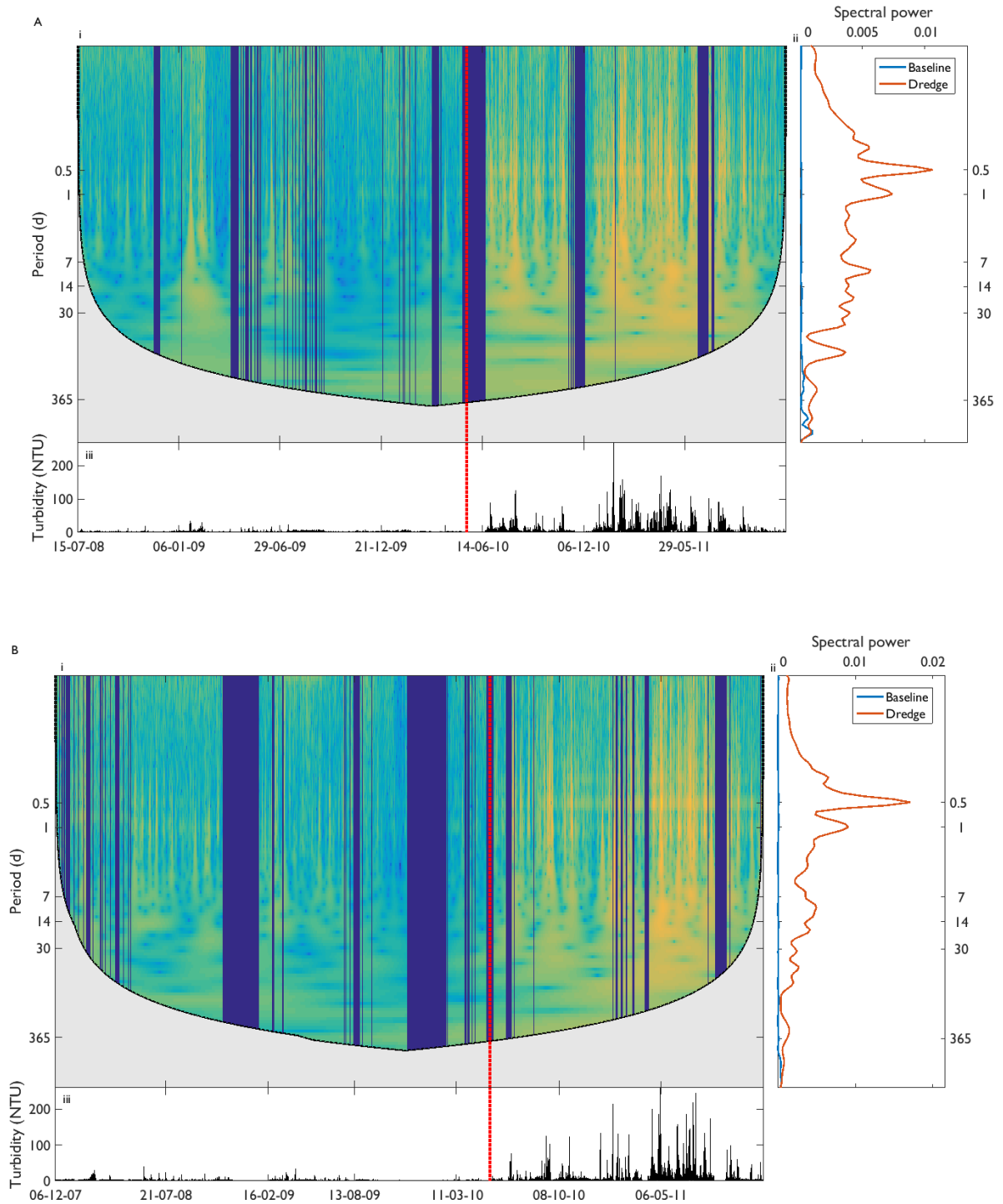


Figure 3-12 A and B Turbidity spectral analysis for the Barrow Island project, showing representative dredge impact sites A) LNG1 and B) MOF1. The three panels on each figure are: (i) wavelet spectrum, (ii) global wavelet spectrum and (iii) original time series. Areas of high energy are yellow, and low energy are light blue and green. The darker blue horizontal areas are gaps in the time series, and the grey curved area between the top and bottom plots is outside the cone of influence. The broken red line running from the wavelet spectrum through to the time series shows the start of dredging. The global wavelet spectral plot shows the peaks in the baseline data (blue line) and dredge data (orange line). 95% confidence contours have been removed as they obscure the high frequency energy regions. Full spectral analysis plots for all sites can be found in 0.

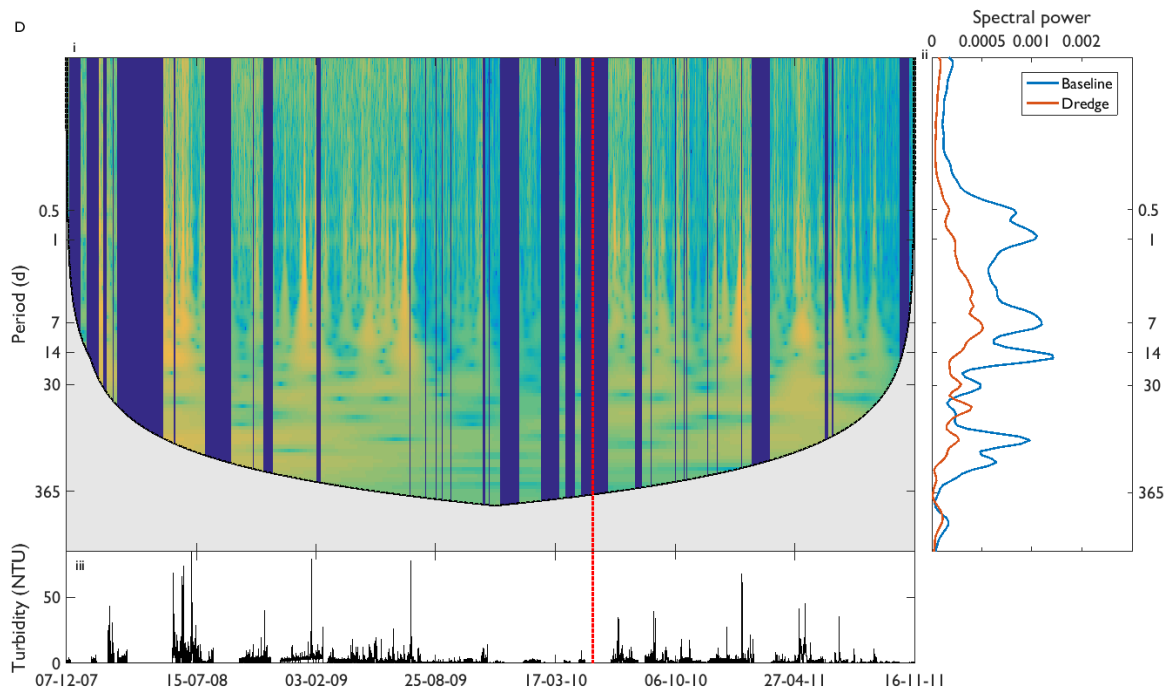
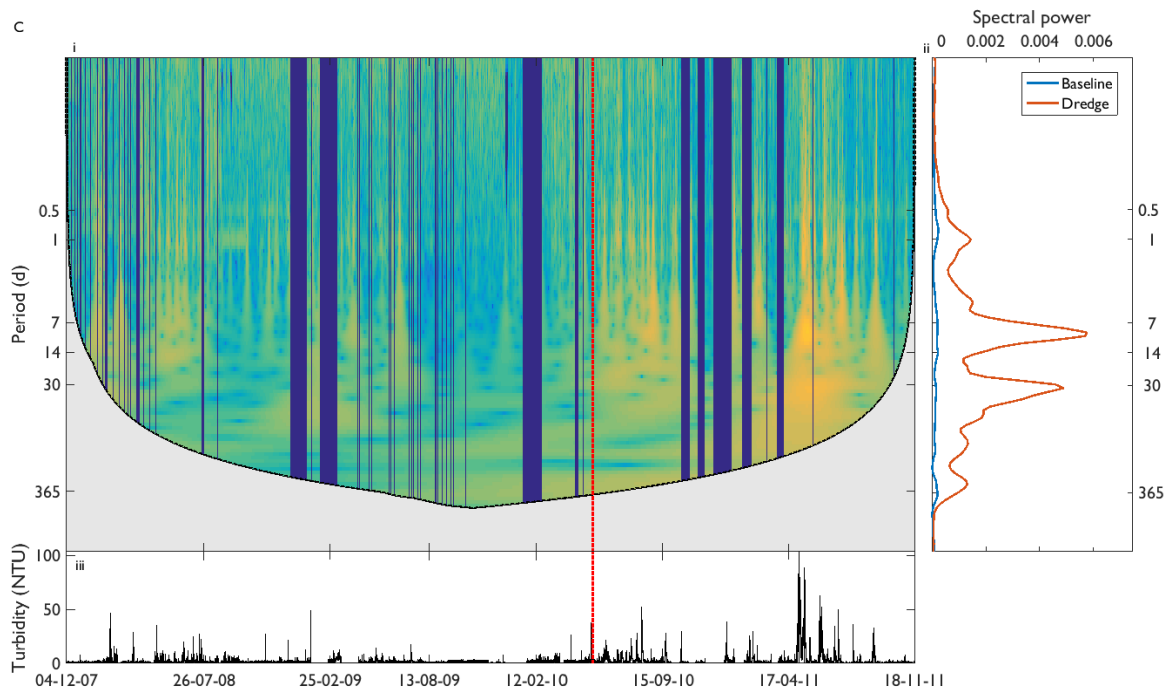


Figure 3-15 C and D Turbidity spectral analysis for the Barrow Island project, showing reference sites C) DUG and D) SBS. The three panels on each figure are: (i) wavelet spectrum, (ii) global wavelet spectrum and (iii) original time series. Areas of high energy are yellow, and low energy are light blue and green. The darker blue horizontal areas are gaps in the time series, and the grey curved area between the top and bottom plots is outside the cone of influence. The broken red line running from the wavelet spectrum through to the time series shows the start of dredging. The global wavelet spectral plot shows the peaks in the baseline data (blue line) and dredge data (orange line). 95% confidence contours have been removed as they obscure the high frequency energy regions. Full spectral analysis plots for all sites can be found in Appendix C.

### **3.4 Discussion**

#### **3.4.1 Barrow Island turbidity conditions**

The Barrow Island water quality sites are located in a shallow offshore environment with naturally low turbidity levels, typically  $< 5 \text{ mg L}^{-1}$  (Jones, Ricardo, et al. 2015). Spatial analysis clearly shows a dredge related increase in turbidity in a well-defined region within 2 – 5 km south of the dredge zone. Turbidity maximums, means and standard deviations were up to 4 – 6 x higher at sites within 2 – 5 km south of dredging compared to all northern sites and sites  $> 5 \text{ km}$  south, which had levels similar to the baseline period of 1 – 3 NTU, compared to dredge period averages 3 – 7 NTU (Table 3-1 and Figure 3-2). Turbidity levels declined sharply at the northern sites however a more gradual decline occurred at the southern sites 2 – 10 km from dredging (in the path of the dredge plume flow, see Evans et al. 2012, Fisher et al. 2015). Spatial results are supported by other studies, with a literature review by Spearman (Spearman 2015) reporting that no dredge effects were evident  $> 3 \text{ km}$  from dredging in a number of dredging projects.

There were small differences in maximum and average turbidity between sites during the baseline period due to storms. The impact of storms on turbidity levels is well documented (see Chapter 1 Introduction and Erftemeijer et al. 2012), and can be seen in some of the reference sites in Figure 3-1. Storms passing through the region during the dredge period could also be responsible for the slightly higher dredge period maximum turbidities at some reference sites (Figure 3-2 A) and the higher baseline period average at SBS (Figure 3-2 B), which is located beyond the southern tip of the island and is therefore more exposed to waves (Pearce et al. 2003).

The two dredge spoil disposal sites (LONE and DSGS located 4.2 and 9.2 km, respectively, southeast of dredging) had lower turbidity levels than sites located at similar distances but in a more southerly direction from the dredge zone (TR and DUG, see Figure 2-1 for site locations). During baseline monitoring site LONE had higher mean, maximum and SD turbidities than DSGS, while during dredging both sites were similar. Differences during baseline monitoring between the 2 sites and at DSGS between baseline and dredge periods could be due to differences in time series length because the shorter monitoring period would more likely exclude high turbidity events such as storms; DSGS had only 120 baseline monitoring days compared to 529 at LONE, and both sites had similar monitoring days during dredging (373 days at DSGS and 473 days at LONE).

#### **3.4.2 Running mean analysis**

It is important to understand not only how dredging affects the intensity of turbidity events, but also how dredging alters the duration and frequency of these events. How these changes correlate with coral health are necessary to thoroughly understanding the impacts of dredging on coral reefs (Rogers 1990, Erftemeijer et al. 2012). Large turbidity peaks of short duration (acute) may have little to no effect on corals but instead lower, prolonged (chronic) turbidity increases could lead to mortality. For example, upon reviewing the literature, Connell (1997) found that, of 65 coral assemblages after being exposed to both acute and chronic disturbances (with disturbance defined as any event causing damage or mortality), coral cover recovered after 69 % of the acute disturbances but only 27 % of the chronic events. This running mean analysis is designed to characterise the duration of extreme turbidity events occurring during dredging. Information from

this research will be used in conjunction with coral health studies at Barrow Island project by researchers at WAMSI DSN to determine the impact of dredging on coral health and to determine accurate and appropriate thresholds for future dredging operations.

The percentile running mean analysis demonstrated that during dredging turbidity increases were more frequent and lasted longer at sites within 2 km of dredging. Prolonged increases are shown in the running mean plot for site MOF1 (0.8 km south of dredging); the 95<sup>th</sup> percentile of the 30 day running mean during dredging wasn't much lower than the maximum hourly mean during the baseline period (~ 20 NTU, Figure 3-8 A). All sites within 2 km of dredging had higher maximum running means, with maximum hourly means between ~ 100 and 300 NTU (Figure 3-10 B). An increased frequency of turbidity levels during dredging were also evident in the running mean analysis. At site MOF1, the 95<sup>th</sup> and 80<sup>th</sup> percentiles increased with increasing running mean window size while during the baseline period and during both monitoring periods at site SBS (Figure 3-8 B), these lower percentiles either remained steady (with a slight increase between 5 and 7 days) or decreased with increasing window size. For the 95<sup>th</sup> percentile of the 30 day average to be higher than the 95<sup>th</sup> percentile of the hourly average, there must have been more frequent, high turbidity peaks captured within the 30 day averaging window than in the hourly window.

### **3.4.3 Spectral analysis**

Dominant periodicities in turbidity data during both baseline and dredge monitoring occurred at the semi-diurnal frequency, diurnal frequency (due to the strong daily sea breeze characteristic of

the WA coast, Verspecht & Pattiaratchi 2010), the spring/neap tidal frequency, the 10 day large scale synoptic pattern and the longer period monthly weather bands (Pattiaratchi 2011). Higher energy regions appearing in the 30 to 100 day period range were possibly due to the 30-60 Madden Julian Oscillation (MJO, Madden & Julian 1994, Zhang 2005), which is well known for its intra-seasonal and intra-annual characteristics, causing it to appear at uneven intervals (Zhang 2005). The longer period events were less energetic than the daily sea breeze and seasonal cycles, and were slightly more energetic in the east/west direction than north/south.

The spectral analysis performed separately on the baseline and dredge shows that M2 (semi-diurnal) peaks were stronger at sites within 2 km of dredging during the dredge period. The appearance of the semi-diurnal peak in the wave spectra and during the baseline period in the turbidity spectra suggests that the twice daily low water height amplifies wave resuspension, and the strengthening of the semi-diurnal peak during dredging at sites within 2 km of the dredge zone suggests that horizontal advection occurred at these sites. According to Weeks et al. (1993) the M2 peak in suspended sediment occurs due to horizontal advection of sediments, not because of the semi-diurnal tidal currents which would appear as 6 hourly peaks during both ebb and flood tidal current resuspension.

Wind, wave and water height spectral analysis were helpful in determining the cause of the turbidity spectral peaks, particularly the diurnal (i.e. whether the diurnal peaks are due to daily sea breeze or the diurnal tide). The diurnal peak was the dominant oscillation in the wind (zonal) and wave

spectra, but was relatively weak in the water height (tidal) data, suggesting that the daily sea breeze was the cause of the diurnal peak in turbidity. The strong semi-diurnal peak appeared in the water height (tidal) data, representing the semi-diurnal tidal height, and also in the wave spectra, suggesting that the influence of waves on the pressure fluctuations were stronger during low tide.

A large annual peak occurred in the wave and zonal wind data (Figure 3-12 and Figure 3-14), however this did not translate to the turbidity spectrum (Figure 3-11). Also, seasonal periodicities in the global wavelet spectra were weak and the locations of the peaks were inconsistent between monitoring sites. Seasonal variability between sites could be due to the length of the time series (analyses were performed separately on baseline and dredge periods, and dredge monitoring lasted for 18 months), but is also consistent with other research of seasonal turbidity cycles in the region. Margvelashvili et al (2006) found no seasonal effect on turbidity due to the lack of seasonal differences in the monthly bottom shear stress patterns responsible for sediment resuspension.

#### **3.4.4 Turbidity model**

The primary purpose of the turbidity model was to provide a simple, statistical predictor of natural turbidity driven by waves and tides. The model can be used during dredging operations to decouple the natural and dredge related turbidity events, allowing proponents to more accurately assess dredging impacts by altered water quality conditions, and scientists to better understand the impacts of dredging on resuspension. Water column turbidity measurements during dredging include both natural and dredge related turbidity, therefore subtracting the modelled (natural)



turbidity from measured (natural + dredge related) turbidity provides an estimate of turbidity caused solely by dredging. A similar method of using a simple turbidity model to estimate natural turbidity and monitor threshold exceedance was developed for dredging activities in Darwin Harbour (VanSenden et al. 2013). The difference between the turbidity model in this study and the turbidity model developed for the Darwin project is the form of the model and the dominant resuspension forcing mechanisms in the two regions; in our model, waves are the most significant forcing term at both the Barrow Island and Hay Point sites due to both regions being wave dominant (Orpin et al. 1999, DEC 2007, Chartrand et al. 2008, Macdonald et al. 2013, Waltham et al. 2015) whereas the Darwin turbidity model has a single input variable for the tidal range due to the large tidal influence on sediment resuspension in Darwin Harbour (VanSenden et al. 2013).

A feature of the model is its simplicity; it only requires collection of two variables – seafloor turbidity and water pressure. Water quality modelling typically involves multi-dimensional complex hydrodynamic models (e.g. DELFT3D) which require multiple inputs such as currents, waves, tides, boundary layer dynamics and sediment type / particle size information (van Rijn 1986, Luger et al. 1998, Luger & Ballegooyen 2000, Swanson et al. 2007, Erfteimeijer et al. 2012) which are expensive to collect and not always available. The turbidity and hydrodynamic data for this model are typically collected during a dredge operation, and the ability for this data to monitor dredge related turbidity and deposition events would replace the need for additional data collection and monitoring (e.g. sediment trap deployments which are expensive and often inaccurate, see below).

The turbidity model was tested at both Barrow Island and at Hay Point to compare model performance at different locations with varying water quality conditions. Model performance was strong at a few of the Hay Point and Barrow Island sites. During the test phase (2nd half of the baseline data), 83 % of the Hay Point sites had  $R^2 > 0.5$  compared to 38 % of the Barrow Island sites however the skill scores were moderate to weak at both Hay Point and Barrow Island sites during test periods. Model performance was stronger during the fit period than during the test period. At Hay Point half the sites had both  $R^2$  and skill scores  $> 0.5$ . At Barrow Island, during the test period no site had a skill score  $> 0.5$ , and 3 sites had  $R^2 > 0.5$ . Also, at the Hay Point sites the model significantly underestimated the measured turbidity levels, which could be a limitation of the pressure measurements to estimate higher turbidity levels. Due to the simplicity of both the model function (i.e. a simple empirical model) and the data inputs, the results aren't unexpected; as ten 1 second readings of pressure fluctuations were measured instead of higher frequency wave measurements for longer than 10 seconds, wave orbital velocities and therefore shear stresses could not be calculated, which limits the model to lower resolution (daily) turbidity estimates and possibly reduces model performance. However, the model was intended as a first order estimate of dredge induced turbidity and possibly as a simple, cost effective initial indicator of turbidity threshold exceedance during dredging operations, and could also provide further evidence of the impact of dredging on corals. Despite the quantitative results, the similarities between the magnitude and temporal location of modelled and measured turbidity peaks at Barrow Island (Figure 3-5), as well as the model scores at a few sites during the fit period, provide some evidence that the model has the potential to be used to estimate dredge related turbidity and as a first order threshold exceedance monitoring tool, providing daily exceedance estimates during monitoring operations.

This chapter provides an overview of the turbidity environment at Barrow Island (and briefly Hay Point), and compared changes in turbidity levels prior to and during a large scale capital dredging operation at Barrow Island. Although Barrow Island is a clear water environment with naturally low average turbidity levels, dredging significantly increased turbidity frequently and for prolonged periods during dredging. However, these increases were confined to a relatively small area 2 – 5 km south of dredging, along the principal axis of the dredge plume flow. Dredge spoil disposal sites were relatively unaffected by dredging, as were all northern sites and sites > 5 km south. Dredge plume advection occurred at sites within 2 km of dredging, demonstrated by higher amplitudes of the M2 frequency occurring in the turbidity data during dredging. The success of the model at a few sites at both Barrow Island and Hay Point demonstrate that, with further testing, the model could be a simple and cost-effective tool for monitoring dredge related turbidity (and possibly deposition – see Chapter 5 Dredge deposition zone detection using in-situ data and turbidity model overburden) threshold exceedance during future dredging operations.

The following chapters extend this investigation into dredging impacts on water quality by analysing changes in underwater light levels (specifically light attenuation coefficients, Chapter 4 Light attenuation during dredging: spatial variations in PAR) and a deposition dredge impact zone in Chapter 5 Dredge deposition zone detection using in-situ data and turbidity model overburden), where the model is also assessed as a tool to monitor deposition threshold exceedance.

## **Chapter 4. Light attenuation during dredging: spatial variations in PAR**

### **4.1 Synopsis**

This chapter characterises spatially the submarine light environment during dredging to better understand the impact dredging has on light levels – one of the most important requirements for coral survival. Light (specifically PAR) is essential for benthic primary production, and reduced PAR (lasting for days and weeks) can reduce photosynthesis and trigger a range of adaptive behaviours, including stress to corals, seagrasses and other marine organisms (Kinzie 1973, Rogers 1990, Anthony & Larcombe 2000, Anthony et al. 2004, Gilmour et al. 2006, Cooper et al. 2008, Erftemeijer et al. 2012). Reduced PAR levels have been implicated as the cause of coral mortality (Chalker 1981, Chalker et al. 1984, Erftemeijer et al. 2012).

Dredging increases suspended sediment which, in the coastal environment, is likely the primary cause of light attenuation (Kirk 1977b, Cloern 1987, Mobley 2001, Margvelashvili et al. 2006, Lawson et al. 2007, Saulquin et al. 2013). Anthony et al. (2004) discovered turbidity was responsible for 74 – 79 % variation in light levels in a coastal environment. To better understand how dredging affects submarine light levels, light attenuation coefficients were calculated at each site (from the Beer Lambert Law and using a double exponential method developed by Paulson and Simpson (1977)), compared to turbidity levels and the distance from dredge effects were analysed by comparing conditions at increasing distance from the dredge zone.

Light attenuation coefficients were calculated and analysed in lieu of the measured PARs because of the non-uniform sensor depths at the different monitoring sites. The PAR sensors measured light from the benthos and were therefore deployed at different depths (ranging from ~ 4 – 14 m) which introduces a depth dependence to the spatial analysis (because light continues to attenuate with depth regardless of the turbidity levels, obscuring the dredging impact analysis). Using the attenuation coefficients also has the advantage of only considering light reduction in the water column and excludes light reduction due to atmospheric conditions (as the Beer Lambert Law calculates light attenuation from the surface to depth  $z$ ). To ensure all depth dependence was removed from the spatial analysis, depth effects in the light attenuation coefficients (due to the preferential absorption and therefore higher attenuation rates of red light in the surface layers) were also investigated.

## 4.2 Methods

### 4.2.1 Light attenuation coefficient

The light attenuation coefficients ( $k$ ) were calculated using the Beer-Lambert Law (Mobley 2001, Devlin et al. 2008, Kirk 2010):

$$I_z = I_0 e^{-kz} \quad (10)$$

where  $I_z$  is the subsurface light at depth  $z$ ,  $I_0$  is the surface light (using terrestrial PAR),  $k$  is the attenuation coefficient, and  $z$  is the logger depth derived from the water pressure measurements (converted to water depth using the hydrostatic equation). Note that the Beer-Lambert Law

(equation 10) is wavelength dependent (Kirk 1977b), however, as our incident radiation measurements cover the PAR bandwidth, our attenuation coefficient represents a 300 – 700 nm average (derived in Kirk 1977b for natural systems).

All terrestrial PAR values were reduced by 5% to account for the proportion of incident light reflected from the sea surface (Sverdrup 1953, Nelson & Smith 1991, Humphrey et al. 2008, Kirk 2010). To ensure the origin of the incident light was as close to zenith as possible (satisfying the condition of the Beer Lambert Law that incident light is normal to the surface) only midday measurements (10 am – 2 pm) were used.

Midday  $k$  values (also referred to herein as daily values) were calculated using benthic PAR, water depth and terrestrial PAR measurements. A  $k$  value was calculated for every 10 minute benthic reading between 10 am and 2 pm using the Beer-Lambert Law. Because terrestrial PAR measurements were every 15 minutes, the benthic readings were matched with the nearest terrestrial PAR neighbour, allowing a gap of no more than ten minutes between benthic and terrestrial samples. The  $k$  values were then averaged to get a single midday  $k$ . Negative  $k$  values at each site (no more than 5 % per site) occurred if a terrestrial PAR measurement was lower than the benthic PAR value, due to either logger errors or patchy cloud covering only the terrestrial sensor (which is unlikely to prevail over the four hour period), and were therefore removed.

Midday  $k$  values were compared to midday turbidity averages at each site, and three different regression functions were investigated to determine the best fit. Initial visual inspection of the relationship, and comparison of  $R^2$  and root mean square errors (RMSEs), indicated that the optimal regression function was either linear or power, depending on the site. The best fitting function was applied at each site and the regression parameters derived from a least squares fit to observations. The use of a rational function (polynomial ratios, e.g.  $f(x) = ax/(b + x)$ ) was also tested at each site (Bolker 2008, Mathworks 2016b). Although rational functions are not commonly applied to water quality relationships, their flexible function shape (shape can be either linear or non-linear depending on the function parameters) make them useful when investigating the relationship between  $k$  and turbidity across multiple sites which have different relationships, which would otherwise require testing the relationship and possibly changing the regression function at each site. To demonstrate the flexibility and performance of the rational function, comparisons were made between the rational function and either linear or (non-linear) power regression functions, depending on the site (comparisons to the Paulson and Simpson (1977) method are described below in section 4.2.3 Double exponential method).

The three regression functions tested were:

**Rational:**  $\hat{k}(T) = (a_1T + a_2)/(T + a_3)$  ( 11 )

**Linear:**  $\hat{k}(T) = b_1T + b_2$  ( 12 )

**Power:**  $\hat{k}(T) = c_1T^{c_2}$  ( 13 )

where  $\hat{k}$  is the predicted light attenuation coefficient,  $T$  the turbidity, and  $a_{1-3}$ ,  $b_{1-2}$  and  $c_{1-2}$  the regression parameters which were determined using the curve fitting toolbox in MATLAB (Mathworks 2016b).

The performance of each regression was investigated by calculating  $\hat{I}$  at depth  $z$  ( $\hat{I}_z$ ) by substituting  $\hat{k}$  from each regression equation into equation 10, e.g.:

$$\hat{I}_z = I_0 e^{-((a_1 T + a_2)/(T + a_3))z} \quad (14)$$

then comparing  $R^2$  and RMSE between  $\hat{I}_z$  and measured  $I_z$  (from equation 10) at each site for each regression type. The rational function was then used instead of the linear or power function for this research due to its performance (see section 4.3.1 Relationship between  $k$  and turbidity), its ease of use and its flexibility.

#### 4.2.2 Depth dependence of light absorption

Based on the theory that the attenuation rate is higher in the surface layers due to the selective absorption of light by wavelength (with higher attenuation rates of shorter wavelength red light in the surface layers), the depth dependence of the clear water attenuation coefficient at each site ( $k_0$ , i.e. light absorption when turbidity = 0 NTU, calculated from the regression parameters of the rational function) was tested. A depth dependence of  $k_0$  would lead to a depth dependence of  $k$  and would interfere with the spatial analysis of dredging impacts, therefore  $k_0$  was derived at each site using the regression coefficients in equation 11 when  $T = 0$ , i.e.:

$$k_0 = a_2/a_3 \quad (15)$$

This relationship between  $k_0$  (equation 15) and depth  $z$  was then analysed by plotting  $k_0$  against each site's average logger depth (see Figure 4-6), fitting a linear regression and calculating  $R^2$ :

$$k_0(z) = bz + k_c \quad (16)$$



where  $b$  is the depth coefficient and  $k_c$  is  $k_0$  at the surface ( $z = 0$  m).

To correct for this depth dependence at each site,  $k_0$  was normalised to a single value – average  $k_0$  across all sites, 0.25). The normalised value of 0.25 was chosen as the average:

$$k_0(5) = 0.25 = a_2/a_3 \quad (17)$$

The depth corrected  $k$  was then modelled at each site using the ten minute turbidity measurements and used in the spatial analysis for more accurate distance to dredge effect investigation:

$$\hat{k}_d(T) = (a_1T + 0.25a_3)/(T + a_3) \quad (18)$$

Paulson and Simpson (1977) have derived an equation to account for the strong wavelength selective absorption in the upper layers

#### 4.2.3 Double exponential method

Paulson and Simpson (1977) extended the Beer Lambert Law to a double exponential function, with separate terms for the different attenuation rates at the surface (higher attenuation, top 6 m) and at deeper layers (lower attenuation, > 10 m):

$$\widehat{I/I_0} = Re^{z/\zeta_1} + (1 - R)e^{z/\zeta_2} \quad (19)$$

The 1<sup>st</sup> term on the right hand side (RHS) represents the higher attenuation of red light in the upper 6 m, and the 2<sup>nd</sup> term on the RHS is for the lower attenuation rate of blue-green light at depths > 10 m. The Paulson Simpson method (referred to herein as PS method) calculated submarine light at

increasing depths from the surface to 40 m at single locations, while submarine light data for this study are measured at a single depth at each site.

Paulson and Simpson derived the regression parameter values for the 2<sup>nd</sup> term on the RHS ( $R$  and  $\zeta_2$ ) by a least-squares fit of

$$\widehat{I/I_0} = (1 - R)e^{z/\zeta_2} \quad (20)$$

with observed  $I/I_0$  values at site depths  $> 10$  m, then derived a value for  $\zeta_2$  by a least squares fit of

$$\widehat{I/I_0} - (1 - R)e^{z/\zeta_2} = Re^{z/\zeta_1} \quad (21)$$

equation 19 with observed values at depths  $< 6$  m.

To derive the PS method regression parameters for this study ( $R$ ,  $\zeta_1$  and  $\zeta_2$ ), the midday averaged (10 am – 2 pm) measured PAR at each site were calculated using data between 21<sup>st</sup> April – 18 May 2010 to represent the observed  $I$ , and the midday averaged terrestrial PAR were calculated for the same observation period to represent the surface light ( $I_0$ ). The dates for the regression calibration (21<sup>st</sup> August – 18 May 2010) were chosen because this was the only period with both terrestrial and submarine light data collected prior to dredging. It was important to use ambient submarine PAR measurements to ensure minimum water quality variation (and therefore minimum PAR variation due to turbidity) existed between sites in an effort to represent multiple depth measurements at a single location, and the dredge period data was expected to have maximum PAR variation with lower PAR at sites closer to dredging. The adjustments to surface irradiance levels ( $I_0$ ) applied in the PS method were not applied here because each daily surface irradiance measurement was the same

for all sites (i.e. surface irradiance was represented by terrestrial light measurements made at a single location on Barrow Island).

The same method was used to derive the fit parameters as in Paulson and Simpson (1977). A least squares fit of equation 20 to the average  $\widehat{I/I_0}$  calculations was performed using sites with depths > 9.5 m to derive R and  $\zeta_2$ , then a second least squares fit of equation 21 using data at sites < 6 m produced a value for  $\zeta_1$ . Once all regression parameters were estimated, the final regression (equation 19) was applied to the average  $\widehat{I/I_0}$  for the ambient observation period. To improve the fit, the value for  $\zeta_1$  was adjusted between its 95<sup>th</sup> confidence interval limits. Once the best fit was obtained by adjusting the regression parameters, daily estimates of  $\widehat{I/I_0}$  were calculated at each site for the dredge period using equation 19. The method was validated by comparing  $\widehat{I}$  to measured  $I$  by multiplying both sides by  $I_0$  and calculating R<sup>2</sup> and RMSE at each site. Comparisons were then made between the PS method and the previously described light attenuation and turbidity regression methods (i.e. linear / power and rational function) by visual comparison as well as comparing the R<sup>2</sup> and RMSE from each method.

### **4.3 Results**

#### **4.3.1 Relationship between k and turbidity**

The relationship between daily (midday, 10 am – 2 pm)  $k$  and turbidity was investigated at all sites visually using scatter plots and quantitatively by calculating R<sup>2</sup> and root mean square error (RMSE) and the relationship varied between either linear or power depending on the site. Comparison between observations and regression using a rational function at each site (due to its flexibility and

therefore ease of application) was also tested. There were strong relationships between  $k$  and turbidity at almost all sites, with  $R^2 = 0.7$  for the aggregated sites (Table 4-2 and Figure 4-4),  $R^2 > 0.6$  at 21 of the 25 sites, and median RMSE of  $0.1 \text{ m}^{-1}$  across all sites (Table 4-2 and Figure 4-1 and Figure 4-5 for representative sites). There was very little difference (visually and quantitatively) between the linear / power regression relationship and the rational function regression relationship across the sites (see Table 4-2 and Figure 4-1) . Moderate relationships ( $R^2 \geq 0.5$ ) occurred at 92 % of sites and strong relationships ( $R^2 \geq 0.7$ ) at 64 % (Table 4-2). 16 of the 25 sites had median turbidity  $> 1$  NTU and 14 of those had  $k > 0.4 \text{ m}^{-1}$ , while high turbidity events ( $> 50$  NTU) occurred at 12 sites during dredging (Table 4-1). Most of these sites had only 2 – 7 days with high midday turbidity ( $> 50$  NTU), whereas site MOFA ( $\sim 500$  m south of the dredge zone) had the highest with 17 days (Table 4-1). All of the high turbidity days resulted in  $k > 1 \text{ m}^{-1}$  at MOFA. For example, three events ( $\sim 19$ th September, 19th October and 29th October 2010, shown in Figure 4-2 and Figure 4-3 A) coincided with  $k$  between  $1.5$  and  $3 \text{ m}^{-1}$  (Figure 4-3 A) and complete loss of benthic PAR (Figure 4-2 A and B). Lower turbidity events (20 - 50 NTU) resulted in  $k > 0.5 \text{ m}^{-1}$  and reduced instantaneous daily benthic PAR levels  $< 100 \mu\text{mol photons m}^{-2} \text{ s}^{-1}$  (Figure 4-2 A, D and B and Figure 4-3 A).

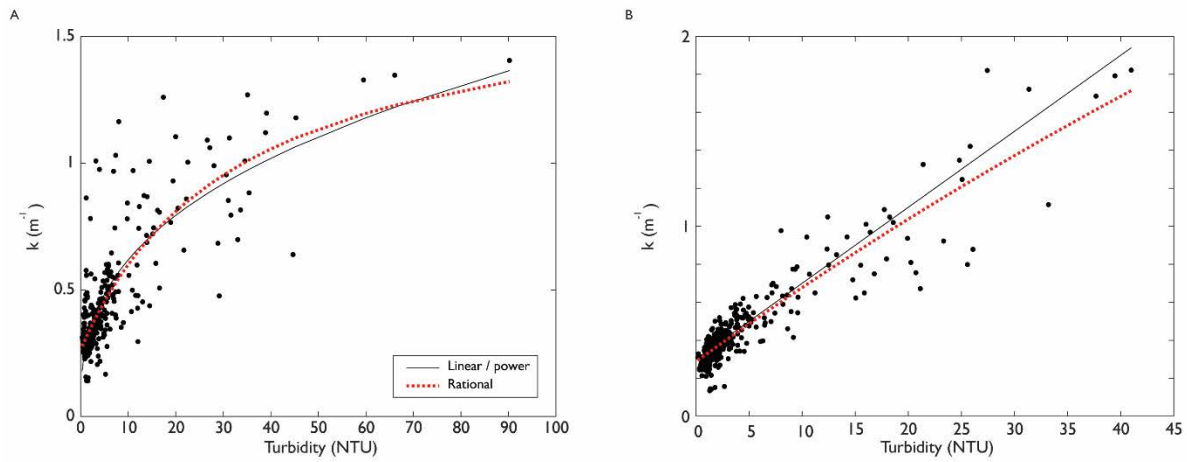


Figure 4-1 Relationship between midday light attenuation coefficients ( $k$ ) and turbidity (black dots) at two sites close to dredging. Sites are: (A) LNG0 (0.2 km from dredging) and (B) LNG2 (1.8 km from dredging, also shown in Figure 4-4) with either a linear or power fit (black line) and a rational function fit (red broken line).

Table 4-1 Dredge period average PAR, median and maximum midday light attenuation coefficients ( $k$ ) and turbidity,  $k$  in clear water ( $k_0$ ), and the number of days the midday averaged turbidity exceeded 50 NTU at all study sites and aggregated across all Barrow Island sites

| Site                  | PAR<br>( $\mu\text{E m}^{-2} \text{s}^{-1}$ ) | $k_0$ | $k$ ( $\text{m}^{-1}$ ) |     | Turbidity (NTU) |     | #days $T > 50$ NTU |
|-----------------------|---|-------|-------------------------|-----|-----------------|-----|--------------------|
|                       |   |       | Median                  | Max | Median          | Max |                    |
| All                   |   | 0.25  | 0.4                     | 2.3 | 1.5             | 187 | 51                 |
| <b>Northern sites</b> |   |       |                         |     |                 |     |                    |
| AHC                   | 343.8   | 0.23  | 0.36                    | 1.1 | 0.6             | 20  | 0                  |
| REFN                  | 378.4   | 0.18  | 0.37                    | 1.3 | 0.9             | 21  | 0                  |
| ELS                   | 415.4   | 0.19  | 0.37                    | 0.8 | 0.8             | 10  | 0                  |
| ANT                   | 256.7   | 0.35  | 0.35                    | 0.5 | 0.9             | 9   | 0                  |
| LOW3                  | 308.7   | 0.24  | 0.40                    | 1.4 | 1.0             | 16  | 0                  |
| LOW1                  | 334.2   | 0.23  | 0.40                    | 1.0 | 1.2             | 13  | 0                  |
| <b>Southern sites</b> |   |       |                         |     |                 |     |                    |
| LNG0                  | 206.4   | 0.26  | 0.44                    | 1.3 | 2.8             | 90  | 3                  |
| LNGA                  | 276.2   | 0.16  | 0.46                    | 0.9 | 3.0             | 75  | 2                  |
| LNG1                  | 225.7   | 0.25  | 0.42                    | 1.3 | 2.3             | 75  | 3                  |
| LNGB                  | 279.0   | 0.18  | 0.44                    | 1.0 | 2.4             | 92  | 3                  |
| LNG2                  | 125.3   | 0.29  | 0.42                    | 1.8 | 2.2             | 41  | 0                  |
| LNGC                  | 181.5   | 0.19  | 0.44                    | 1.1 | 2.1             | 95  | 5                  |
| MOFA                  | 204.4   | 0.30  | 0.53                    | 2.3 | 3.5             | 187 | 17                 |
| MOFC                  | 231.9   | 0.32  | 0.42                    | 1.7 | 2.0             | 68  | 3                  |
| MOF1                  | 215.8   | 0.25  | 0.47                    | 1.3 | 2.6             | 72  | 7                  |
| MOFB                  | 232.1   | 0.25  | 0.43                    | 1.3 | 2.1             | 91  | 3                  |
| MOF3                  | 213.5   | 0.33  | 0.40                    | 1.9 | 1.7             | 39  | 0                  |
| LNG3                  | 260.7   | 0.27  | 0.40                    | 2.1 | 1.5             | 51  | 1                  |
| TR                    | 223.0   | 0.31  | 0.39                    | 2.3 | 1.3             | 60  | 2                  |

|                                     |       |      |      |     |     |    |   |
|-------------------------------------|-------|------|------|-----|-----|----|---|
| DUG                                 | 269.8 | 0.24 | 0.36 | 2.0 | 0.8 | 63 | 2 |
| BAT                                 | 285.5 | 0.28 | 0.37 | 1.1 | 0.5 | 40 | 0 |
| REFS                                | 337.9 | 0.24 | 0.37 | 1.9 | 0.8 | 28 | 0 |
| SBS                                 | 331.2 | 0.26 | 0.37 | 0.9 | 0.9 | 14 | 0 |
| <b>Dredge spoil disposal sites*</b> |       |      |      |     |     |    |   |
| LONE                                | 392.9 | 0.18 | 0.36 | 1.2 | 0.8 | 20 | 0 |
| DSGS                                | 396.4 | 0.15 | 0.36 | 1.0 | 1.2 | 30 | 0 |

\* Distance to spoil ground = 0.1 km

Table 4-2 Relationship between midday light attenuation coefficients ( $k$ ) and turbidity, including function equation,  $R^2$  and RMSE for different regression functions (either linear or power depending on the site, and rational function), as well as median and maximum  $k$  and turbidity,  $k$  in clear water ( $k_0$ ), and the number of days the midday averaged turbidity exceeded 50 NTU at all study sites and aggregated across all Barrow Island sites during dredging

| Site | Linear or power function |       |      | Rational function             |       |       |
|------|--------------------------|-------|------|-------------------------------|-------|-------|
|      | Function equation        | $R^2$ | RMSE | Function equation             | $R^2$ | RMSE  |
| All  | $0.28T^{0.38}$           | 0.65  | 0.14 | $(2.3T + 10.15)/(T + 41.2)$   | 0.70  | 0.13  |
| AHC  | $0.04T + 0.23$           | 0.67  | 0.48 | $(101T + 567)/(T + 2489)$     | 63.2  | 301.8 |
| REFN | $0.05T + 0.18$           | 0.75  | 0.63 | $(1412T + 5570)/(T + 30.167)$ | 69.4  | 289.2 |
| ELS  | $0.05T + 0.19$           | 0.66  | 0.54 | $(226T + 975)/(T + 5019)$     | 44.6  | 294.6 |
| ANT  | $0.02T + 0.30$           | 0.06  | 0.71 | $(117T + 2501)/(T + 7248)$    | 42.8  | 167.7 |
| LOW3 | $0.07T + 0.24$           | 0.52  | 0.69 | $(1398T + 4849)/(T + 19837)$  | 55.8  | 173.1 |
| LOW1 | $0.06T + 0.23$           | 0.51  | 0.60 | $(553T + 2262)/(T + 9958)$    | 38.3  | 316.5 |
| LNG0 | $0.27T^{0.36}$           | 0.66  | 0.26 | $(1.7T + 8.7)/(T + 33)$       | 35.7  | 469.0 |
| LNGA | $0.23T^{0.35}$           | 0.63  | 0.15 | $(T + 2)/(T + 11.8)$          | 28.2  | 610.9 |
| LNG1 | $0.23T^{0.36}$           | 0.73  | 0.21 | $(1.7T + 7.5)/(T + 30.3)$     | 37.4  | 473.6 |
| LNGB | $0.24T^{0.34}$           | 0.72  | 0.17 | $(1.1T + 2.5)/(T + 13.8)$     | 30.5  | 536.2 |
| LNG2 | $0.04T + 0.3$            | 0.85  | 0.24 | $(10.3T + 71.2)/(T + 248)$    | 42.1  | 399.6 |
| LNGC | $0.26T + 0.34$           | 0.74  | 0.23 | $(1.2T + 2.7)/(T + 13.8)$     | 25.2  | 544.0 |
| MOFA | $0.32T^{0.4}$            | 0.79  | 0.23 | $(2.7T + 12)/(T + 39.3)$      | 44.3  | 365.9 |
| MOFC | $0.30T^{0.36}$           | 0.72  | 0.37 | $(1.6T + 4.9)/(T + 19.5)$     | 35.0  | 400.8 |
| MOF1 | $0.32T^{0.37}$           | 0.75  | 0.39 | $(2.8T + 17.5)/(T + 55.1)$    | 31.2  | 402.9 |
| MOFB | $0.28T^{0.35}$           | 0.71  | 0.39 | $(1.6T + 6.5)/(T + 25.7)$     | 31.9  | 406.9 |
| MOF3 | $0.04T + 0.33$           | 0.73  | 0.26 | $(225T + 1874)/(T + 5677)$    | 65.1  | 332.2 |
| LNG3 | $0.04T + 0.29$           | 0.85  | 0.32 | $(7.3T + 39)/(T + 146)$       | 45.6  | 355.0 |
| TR   | $0.04T + 0.32$           | 0.84  | 0.48 | $(10T + 71.9)/(T + 234.3)$    | 56.1  | 250.3 |
| DUG  | $0.03T + 0.26$           | 0.77  | 0.46 | $(4.4T + 22.1)/(T + 93.5)$    | 56.2  | 264.1 |
| BAT  | $0.38T^{0.28}$           | 0.67  | 0.59 | $(1.4T + 3.8)/(T + 13.8)$     | 79.5  | 170.7 |
| REFS | $0.05T + 0.24$           | 0.82  | 0.53 | $(2372T + 10442)/(T + 43224)$ | 58.5  | 205.4 |
| SBS  | $0.04T + 0.26$           | 0.45  | 0.55 | $(775T + 5103)/(T + 19818)$   | 58.6  | 194.4 |
| LONE | $0.04T + 0.18$           | 0.76  | 0.57 | $(617T + 2272)/(T + 15090)$   | 47.1  | 433.6 |
| DSGS | $0.03T + 0.16$           | 0.69  | 0.52 | $(4.3T + 21.4)/(T + 141)$     | 44.2  | 530.9 |

\* Distance to spoil ground = 0.1 km

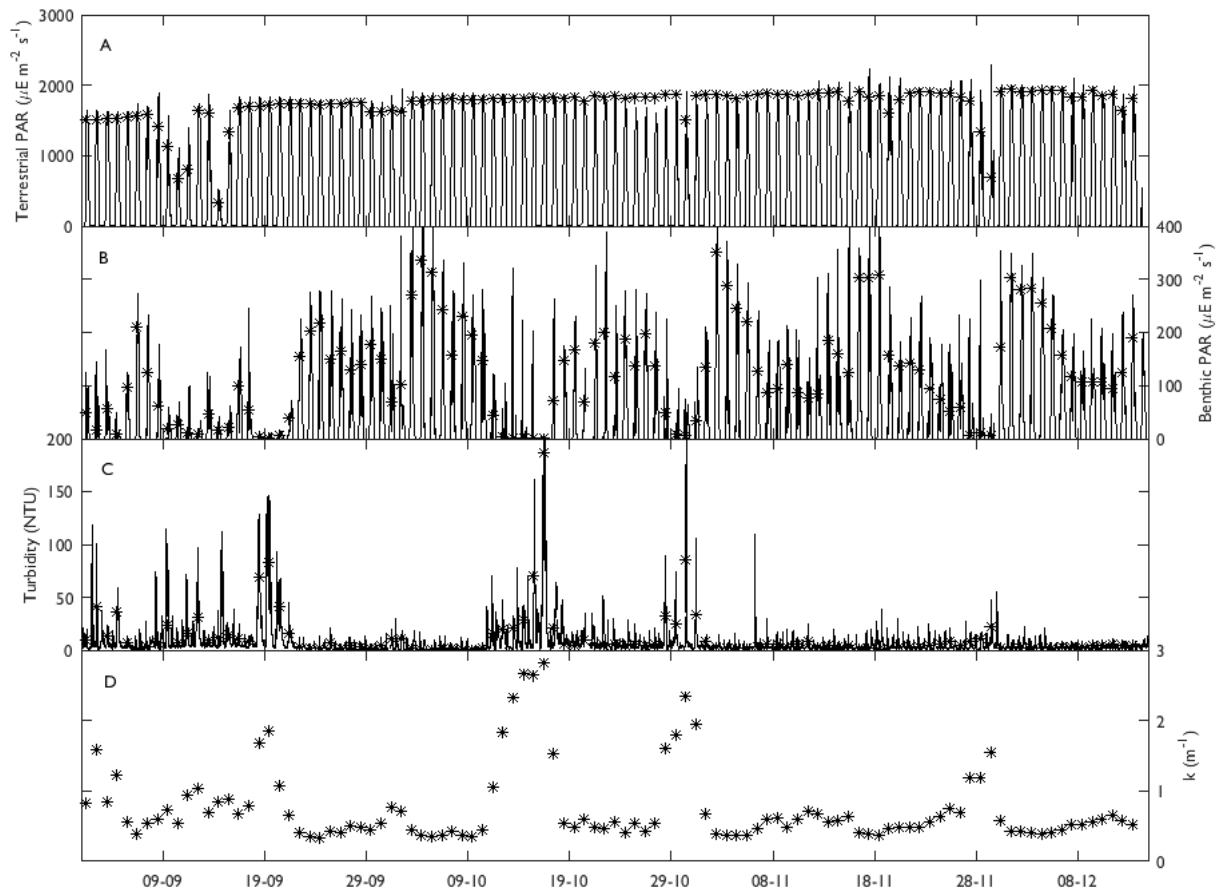


Figure 4-2 (A) Terrestrial PAR, (B) benthic PAR, (C) turbidity and (D) midday  $k$  values at MOFA (see Figure 2-1 for site locations) from September to December 2010. Raw terrestrial PAR (measured every 15 min), benthic PAR and turbidity (measured every 10 min) are represented by the black lines and midday (averaged between 10:00–14:00 h) values are represented by \*.  $K$  values in (D) have been calculated using the midday terrestrial PAR and benthic PAR, as well as the daily water depth (not shown) in the Beer-Lambert Law (equation 10).

In contrast to these high turbidity and  $k$  events at site MOFA, one of the furthest reference sites REFS (24.4 km south of the dredge zone, Figure 2-1 for site location) had only a few turbidity peaks (all of which were < 30 NTU, Figure 4-3 C). Further comparison between MOFA and REFS show that MOFA had the highest  $k$  of  $2.33 \text{ m}^{-1}$  and highest turbidity of 187 NTU of all sites, while REFS had a maximum  $k$  of  $1.86 \text{ m}^{-1}$  and maximum turbidity of 28 NTU (Table 4-1). Despite this, the depth corrected clear water  $k$  ( $k_0$ ) at MOFA was  $0.30 \text{ m}^{-1}$  while at REFS  $k_0 = 0.24 \text{ m}^{-1}$ . The correlation between turbidity and  $k$  at both sites was high (MOFA  $R^2 = 0.81$ , REFS  $R^2 = 0.82$ , Table 4-2).

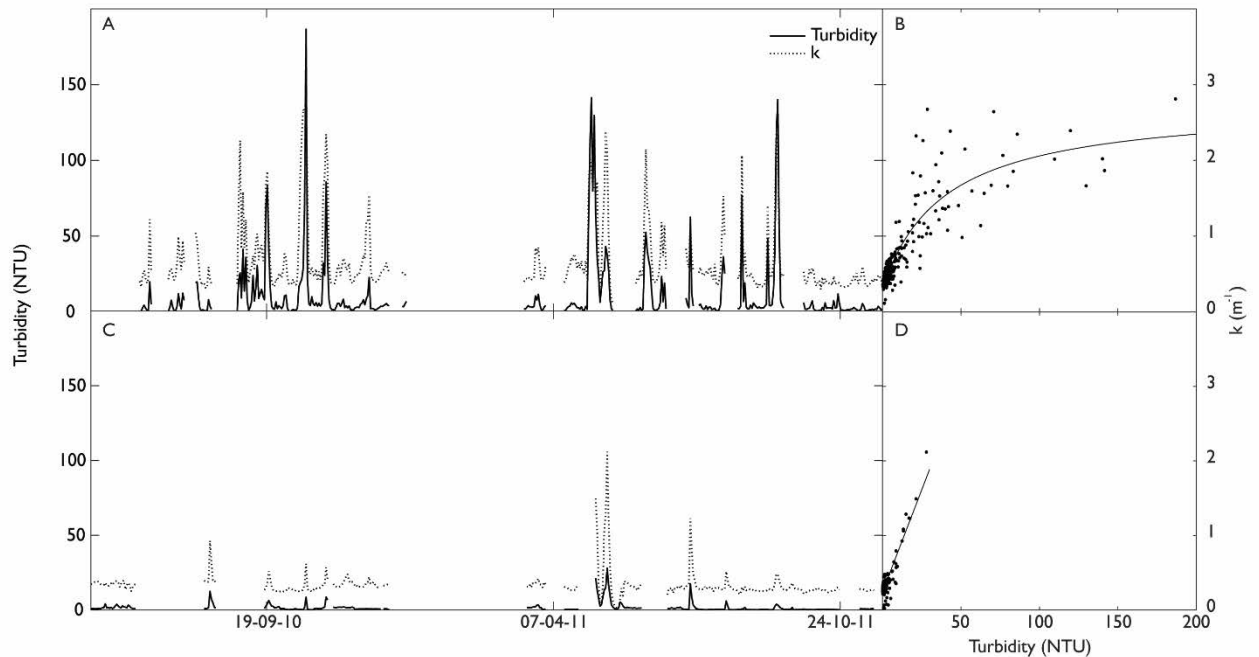


Figure 4-3 (A) Time series of midday (10:00–14:00 h) turbidity (primary vertical axis) and light attenuation coefficients ( $k$ , secondary vertical axis) at MOFA (located ~ 500 m south of dredge zone), (B) scatter plot of turbidity and  $k$  at MOFA, (C) time series of midday (10:00–14:00 h) turbidity (primary vertical axis) and light attenuation coefficients ( $k$ , secondary vertical axis) at reference site REFS, and (D) scatter plot of turbidity and  $k$  at REFS (~25 km south of dredge zone). See Figure 2-1 for site locations.

#### 4.3.2 Particle Size Distribution effects on light attenuation coefficients

The aggregated midday light attenuation coefficients were plotted against midday turbidity for all sites (Figure 4-4). To test whether a particle size dependency was influencing light attenuation for the Gorgon project, sites were grouped according to site distance and direction from dredging (assuming a higher proportion of fine particles were resuspended at sites closer to dredging). The MOF and LNG sites located within 1.4 km south of dredging (i.e. excluding site MOF3 and LNG3) were grouped together (nearfield sites, blue dots in Figure 4-4) and compared to all other sites (farfield sites, red circles in Figure 4-4). There was no significant difference in the range of light attenuation coefficients for the nearfield sites compared to the farfield sites, suggesting no particle size dependency in the light attenuation. To verify this, the PSD dependency was tested using



different site groupings including LNG sites within 1.4 km compared to all other sites (i.e. MOF sites plus all others), MOF sites within 1 km compared to all others, as well as the means and medians of all site groupings. These different analysis methods displayed the same results as in Figure 4-4 therefore are not included.

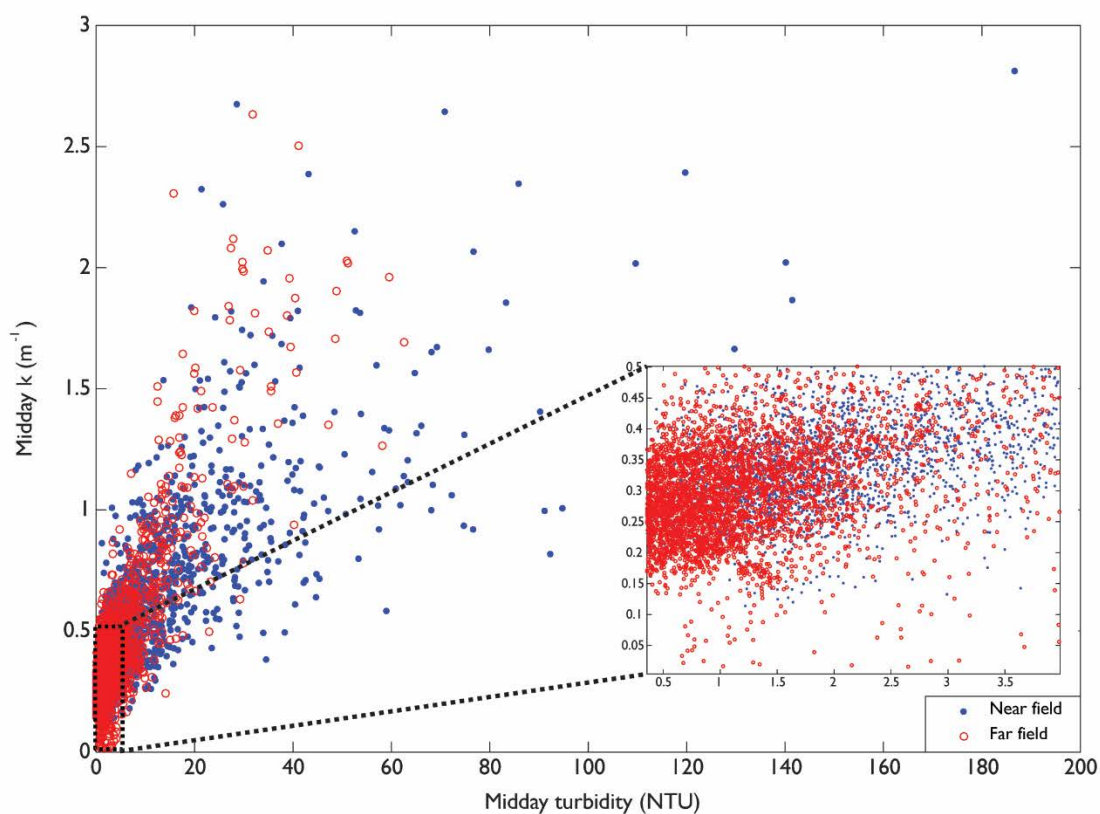


Figure 4-4 Scatter plot showing the relationship between midday turbidity and light attenuation coefficients for the aggregated data during dredging, separated into near field (MOF and LNG sites < 1.4 km south of dredging, blue dots) and far field sites (all other sites, red asterix). The inset shows the zoomed region between turbidity = 0 - 4 NTU and  $k = 0 - 0.5 \text{ m}^{-1}$  as they are difficult to compare in the main figure. Sites have been grouped to investigate whether a particle size dependency exists in the light attenuation coefficients.

### 4.3.3 Depth dependence of $k$

At two of the deeper sites (LNGA and LNGB) high turbidity events did not produce the higher  $k$  values that occurred at shallower sites (Figure 4-5). Sites LNGA and LNGB (~ 11 m depth, Figure 4-5 C and D and Table 2-1 for site depths) did not have  $k > 1 \text{ m}^{-1}$  for corresponding turbidity between

10 and 100 NTU. In contrast, at sites LNG2 and LNG3 (6.2 m depth, Figure 4-5 A and B, and Table 2-1 for site depths), turbidity often exceeded 20 NTU and  $k$  values reached  $2 \text{ m}^{-1}$ , with a linear relationship for all turbidity values ( $R^2 = 0.85$  and  $0.86$ , Table 4-1). Other shallow sites such as DUG (4.6 m) and TR (6.3 m) were within 10 km south-west of the dredging (Figure 2-1 for site locations and depths) also had higher corresponding  $k$  values of  $1.95 \text{ m}^{-1}$  and  $2.30 \text{ m}^{-1}$  for higher turbidity levels exceeding 20 NTU (Table 4-1).

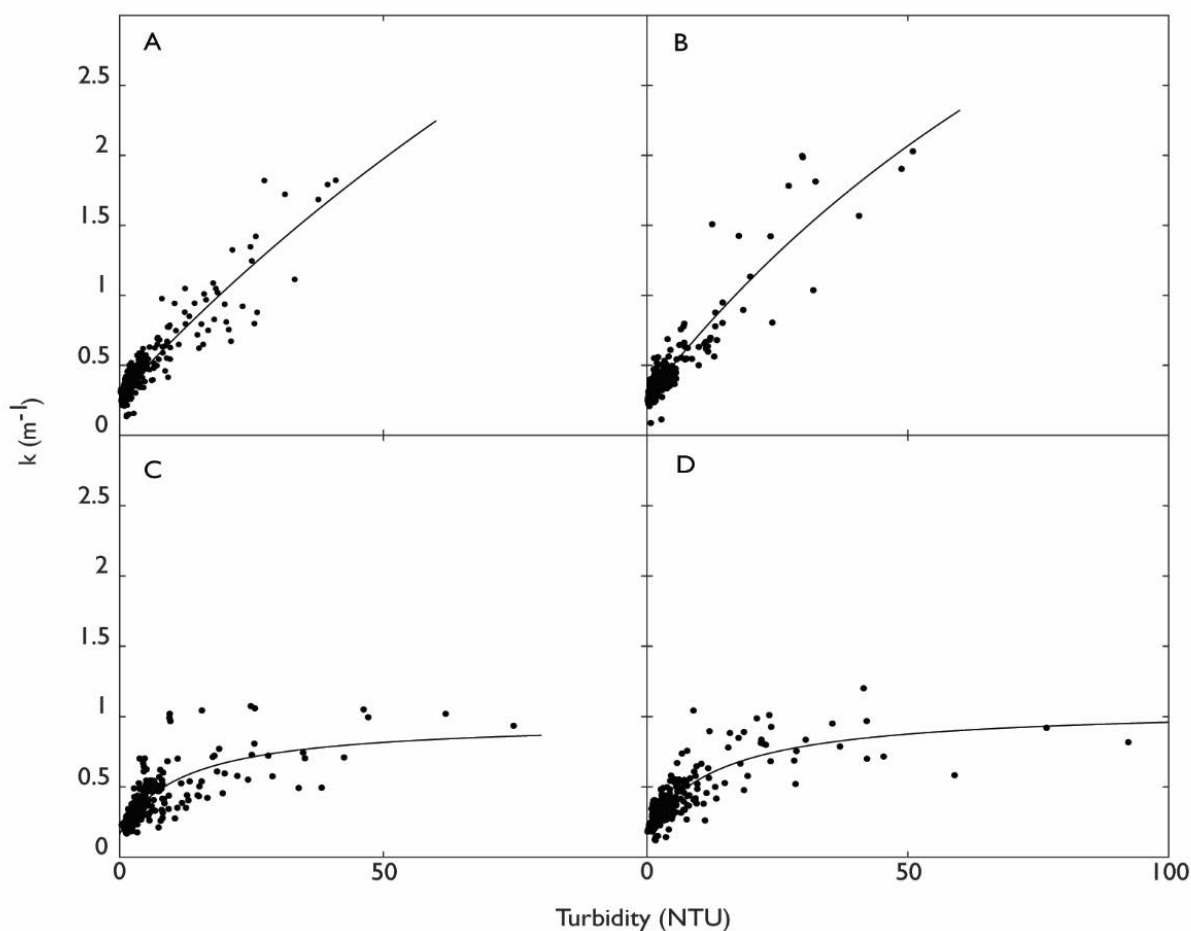


Figure 4-5 Relationship between turbidity and the light attenuation coefficient ( $k$ ) at four sites in the dredge impact zone. Sites are: (A) LNG2 (7.4 m depth), (B) LNG3 (6.8 m), (C) LNGA (12.2 m depth) and (D) LNGB (11.1 m depth). The  $k$  values at LNGB (D) and LNGA (C) did not exceed  $1 \text{ m}^{-1}$ , even for high turbidity levels  $> 20$  NTU, whereas sites LNG2 (A) and LNG3 (B) had linear relationships between  $k$  and turbidity with higher  $k$  values corresponding to high turbidity levels.

To investigate this depth dependence of  $k$ , the clear water  $k$  ( $k_0$ ) at each site was calculated using equation 3 and compared to the average dredge period logger depth (Figure 4-6). The result was a strong linear relationship with  $R^2 = 0.62$ . To remove the depth dependence from  $\hat{k}$  (so that the depth dependence did not interfere with the spatial analysis of light conditions during dredging), a single  $k_0$  value was derived using equation 15, averaged across all sites ( $k_0 = 0.25 \text{ m}^{-1}$ ), and used to replace  $k_0$  at each site.  $\hat{k}$  at each site were then recalculated using equation 18.

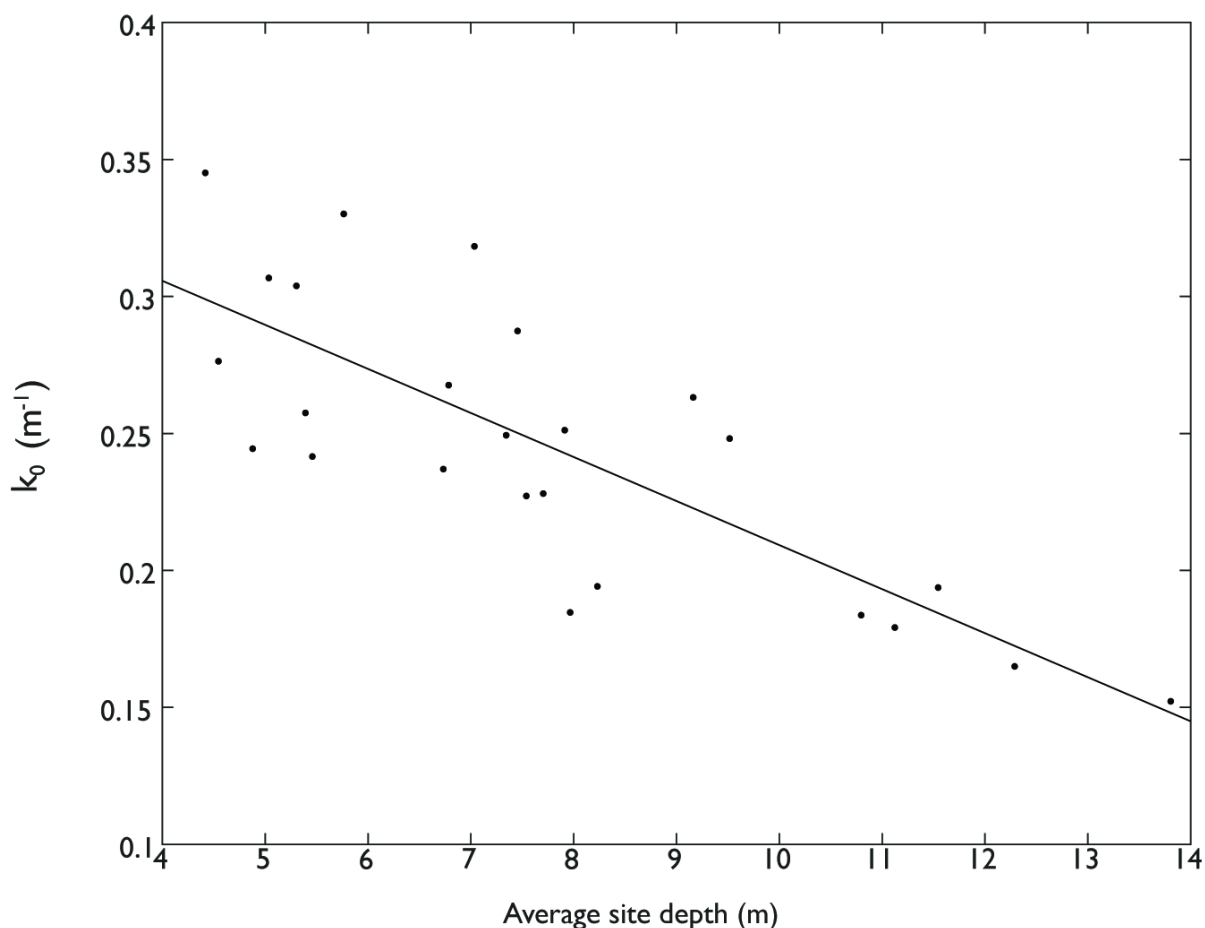


Figure 4-6 Clear water light attenuation coefficient ( $k_0$ ,  $k$  when turbidity = 0 NTU) plotted against the average of the dredge period midday logger depths ( $z$ ) at each site.

#### 4.3.4 Double exponential Paulson Simpson method

Terrestrial and submarine PAR data collected prior to dredging (21 April – 18 May 2010) were used to derive the coefficients of the Paulson and Simpson (1977) method. The regression coefficients were  $R = 0.555$ ,  $\zeta_2 = -6.4$  m and  $\zeta_1 = -2.53$  m. To improve the fit to observed  $I/I_0$  calculations,  $\zeta_1$  was adjusted to -1.5 m (the lower limit of the 95<sup>th</sup> confidence interval). Note that Paulson and Simpson report  $\zeta_2$  and  $\zeta_1$  as positive values although negatives were used in their model. The final regression equation was:

$$\widehat{I/I_0} = 0.55 e^{z/-1.5} + 0.45 e^{z/-6.4} \quad (22)$$

The performance of the PS method to replicate  $I_z$ , and comparison between PS method and the light attenuation and turbidity regression methods (linear / power and rational function) to estimate  $I_z$  are presented in and Figure 4-7.  $R^2$  between  $\hat{I}$  and measured  $I_z$  using the PS method at each site were between 0.15 and 0.71 (median 0.46), and RMSE were between 167 and 611  $\mu\text{E m}^{-2} \text{s}^{-1}$  (median 355  $\mu\text{E m}^{-2} \text{s}^{-1}$ , Table 4-3). In contrast,  $R^2$  between  $\hat{I}$  and  $I_z$  using the light attenuation and turbidity regressions (equations 11 - 12) were between 0.51 and 0.87 and 0.54 and 0.87 (medians 0.71 and 0.74), respectively, and RMSE were between 26 and 84  $\mu\text{E m}^{-2} \text{s}^{-1}$  and 25 and 80  $\mu\text{E m}^{-2} \text{s}^{-1}$  (medians 51 and 44  $\mu\text{E m}^{-2} \text{s}^{-1}$ , Table 4-3). Scatter plots comparing the three methods are presented at representative sites in Figure 4-7. The rational function method and the linear / power methods were very similar, with little difference visually or between  $R^2$  and RMSE.

Table 4-3 R<sup>2</sup> and RMSE between modelled  $\hat{I}_z$  and measured  $I_z$  for performance comparison of the three regression functions to replicate  $I_z$ : linear / power function method and rational function method (which models light attenuation on turbidity), and the double exponential Paulson Simpson method (which models light attenuation on depth).

| Site                                | Depth (m) | R <sup>2</sup> between $I_z$ model and observations |                          |           | RMSE between $I_z$ model and observations |                          |           |
|-------------------------------------|-----------|---|--------------------------|-----------|---|--------------------------|-----------|
|                                     |           | Linear / power function method                      | Rational function method | PS method | Linear / power function method            | Rational function method | PS method |
| <b>Northern sites</b>               |           |   |                          |           |   |                          |           |
| AHC                                 | 6.9       | 0.70  | 0.70                     | 0.48      | 62.9                                      | 63.2                     | 301.8     |
| REFN                                | 7.2       | 0.63  | 0.64                     | 0.63      | 74.1                                      | 69.4                     | 289.2     |
| ELS                                 | 7         | 0.73  | 0.74                     | 0.54      | 45.9                                      | 44.6                     | 294.6     |
| ANT                                 | 3.9       | 0.87  | 0.87                     | 0.71      | 66.5                                      | 42.8                     | 167.7     |
| LOW3                                | 4.5       | 0.87  | 0.87                     | 0.69      | 57.6                                      | 55.8                     | 173.1     |
| LOW1                                | 6.9       | 0.79  | 0.79                     | 0.60      | 41.9                                      | 38.3                     | 316.5     |
| <b>Southern sites</b>               |           |   |                          |           |   |                          |           |
| LNG0                                | 8.6       | 0.51  | 0.66                     | 0.26      | 42.5                                      | 35.7                     | 469.0     |
| LNGA                                | 11.1      | 0.52  | 0.55                     | 0.15      | 30.2                                      | 28.2                     | 610.9     |
| LNG1                                | 8.9       | 0.63  | 0.68                     | 0.21      | 58.7                                      | 37.4                     | 473.6     |
| LNGB                                | 10.2      | 0.67  | 0.76                     | 0.17      | 37.0                                      | 30.5                     | 536.2     |
| LNG2                                | 6.6       | 0.78  | 0.79                     | 0.24      | 46.6                                      | 42.1                     | 399.6     |
| LNGC                                | 10.7      | 0.74  | 0.76                     | 0.23      | 26.1                                      | 25.2                     | 544.0     |
| MOFA                                | 4.9       | 0.70  | 0.80                     | 0.23      | 65.9                                      | 44.3                     | 365.9     |
| MOFC                                | 6.2       | 0.64  | 0.72                     | 0.37      | 42.7                                      | 35.0                     | 400.8     |
| MOF1                                | 6.9       | 0.71  | 0.71                     | 0.39      | 37.7                                      | 31.2                     | 402.9     |
| MOFB                                | 7.5       | 0.66  | 0.70                     | 0.39      | 37.1                                      | 31.9                     | 406.9     |
| MOF3                                | 4.8       | 0.62  | 0.62                     | 0.26      | 65.0                                      | 65.1                     | 332.2     |
| LNG3                                | 6.2       | 0.78  | 0.78                     | 0.32      | 51.1                                      | 45.6                     | 355.0     |
| TR                                  | 4.5       | 0.84  | 0.84                     | 0.48      | 59.4                                      | 56.1                     | 250.3     |
| DUG                                 | 6         | 0.76  | 0.76                     | 0.46      | 53.9                                      | 56.2                     | 264.1     |
| BAT                                 | 3.7       | 0.73  | 0.72                     | 0.59      | 83.7                                      | 79.5                     | 170.7     |
| REFS                                | 5         | 0.82  | 0.81                     | 0.53      | 60.1                                      | 58.5                     | 205.4     |
| SBS                                 | 4.7       | 0.77  | 0.77                     | 0.55      | 59.2                                      | 58.6                     | 194.4     |
| <b>Dredge spoil disposal sites*</b> |           |   |                          |           |   |                          |           |
| LONE                                | 8.5       | 0.55  | 0.54                     | 0.57      | 47.1                                      | 47.1                     | 433.6     |
| DSGS                                | 14        | 0.55  | 0.56                     | 0.52      | 48.6                                      | 44.2                     | 530.9     |

\* Distance to spoil ground = 0.1 km

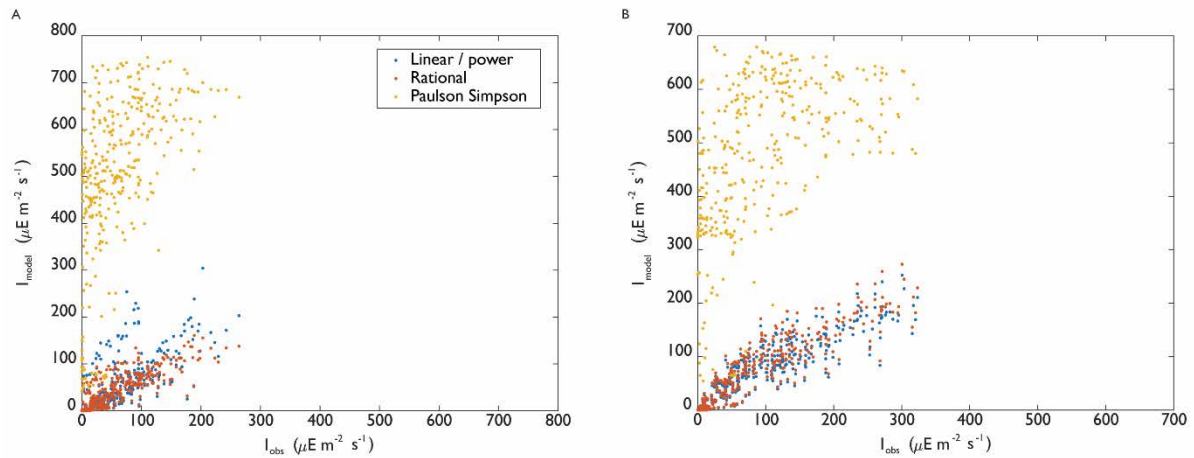


Figure 4-7 Relationship between observed  $I_z$  at depth  $z$  and modelled  $\hat{I}$  using the three regression methods: linear / power comparisons are blue dots, rational function method are red dots and the Paulson Simpson double exponential method are orange dots at sites A) LNG0 and B) LNG2 during the dredge period.

#### 4.3.5 Spatial dredging impacts on $k$ and turbidity

Scatterplots of the median midday turbidity and modelled  $k$  (depth corrected using equation 18) during the dredge period with distance from the dredge zone show a strong decay relationship between each variable and distance from dredging ( $R^2 = 0.67$  and  $0.83$  for  $k$  and turbidity, respectively) (Figure 4-8). Sites within 5 km south-west of dredging had median  $k$  between  $0.4$  and  $0.55 \text{ m}^{-1}$  while sites south-east, north and  $> 5$  km south of dredging (including LONE and DSGS on the perimeter of the dredge spoil disposal ground) had median  $k$  between  $0.36$  and  $0.4 \text{ m}^{-1}$  (Figure 4-8 and ). Median midday turbidity during the dredge period at sites within 10 km south-west of dredging were between  $1.5$  and  $3.5$  NTU (Figure 4-8, Figure 2-1 for site locations and Table 4-1 for  $k$  values), compared to sites south-east, north and  $> 10$  km south with  $0.5 - 1.3$  NTU. The two dredge spoil disposal perimeter sites (DSGS and LONE located  $< 10$  km south of the dredge zone) had lower median turbidity than two sites (DUG and TR) at similar distances but south-west of the dredge zone (Figure 4-8 B and Figure 2-1 for site locations).

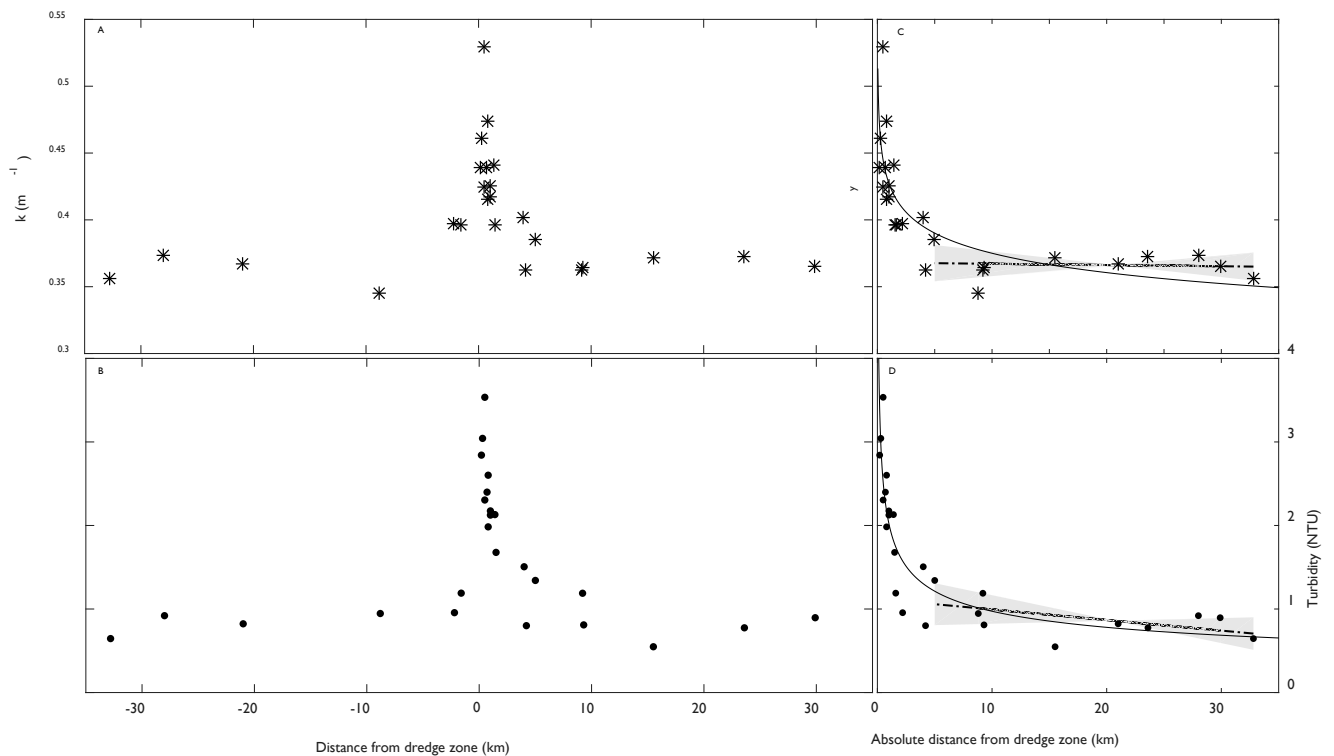


Figure 4-8 Median midday (A)  $k$  (depth corrected) and (B) turbidity plotted according to the distance of the site from the dredge zone, with negative values north of the dredge zone (which is at the origin) and positive values south. Figures (C) and (D) are the same  $k$  and turbidity midday values but plotted by absolute distance from dredging with a non-linear (rapid decay) regression fit (showing regression equations and  $R^2$  values) and only for the southern transect sites (i.e. southern sites excluding the dredge spoil perimeter sites). Impact sites are the MOF and LNG sites located within 2 km south of the dredge zone and reference sites are up to 30 km from the dredge zone in both north and south directions (see Figure 2-1). Non-linear regressions are fitted for  $k$  and turbidity at all distances from dredging for the southern transect sites (see Figure 2-1) while linear regressions are fitted only for median  $k$  and turbidity only for sites  $\geq 5$  km from dredging (C & D). The linear regressions also have 95 % confidence interval regions (grey shaded areas).

#### 4.4 Discussion

This study provides spatial analysis of dredging impacts on the underwater light environment by comparing light attenuation at increasing distances from a large scale dredging operation. Obvious dredge effects were observed in light attenuation coefficients and turbidity; median attenuation coefficients were 1.5 times higher and median (midday) turbidity 4 times higher at sites within 2 – 5 km south of dredging, compared to all northern sites and sites  $> 5$  km south (see Figure 2-1 for site locations) which were unaffected by dredging. There was a strong relationship between light

attenuation and turbidity at almost all sites; 24 of the 25 sites had  $R^2 > 0.5$  and 17 had  $R^2 \geq 0.50$ . Median light attenuation coefficients at sites closest to the main dredge zone (within 2 – 5 km) were between 0.4 – 0.55  $m^{-1}$  compared to all other sites which had levels 0.35 – 0.4  $m^{-1}$ . Clear water attenuation coefficients (approximate absorption coefficients) for coastal waters across the region ranged from 0.16 – 0.35  $m^{-1}$ , similar to the absorption coefficients in the 590 – 650 nm band of the spectrum reported by Kirk (2010).

Light attenuation coefficients were used in lieu of measured PARs for spatial analysis of dredging impacts, as the non-uniform PAR sensor depths introduces a depth dependence to the spatial analysis (depths ranged from  $\sim 3 - 14$  m, see Table 2-1 for sensor depths). Light continues to attenuate (by absorption and scattering) with increasing depth and, even in homogenous water quality conditions, sensors at different depths will record different PAR levels which would obscure the spatial analysis due to the sensor depth variations.

A further advantage of using the attenuation coefficients rather than measured PARs to analyse the dredging impacts is that it eliminates variations in irradiance that are not dredge related. For example, subsurface irradiance levels also vary due to cloud cover; Anthony et al. (2004) discovered that 14 – 17 % of annual benthic light variations were caused by cloud cover (while 74 – 79 % were from turbidity and 7 – 10 % due to the tidal cycle). The relationship between turbidity and light attenuation during this study was very similar to Anthony et al.'s results, with  $R^2 = 0.7$  for the aggregated data (across all sites) and  $R^2 > 0.6$  at 21 of 25 sites (Table 4-2). In contrast, previous



studies by Sofonia & Unsworth (2010) comparing PAR and turbidity showed a weaker relationship with only 41 % variation in PAR due to turbidity. While benthic PAR measurements include all light reducing effects, light attenuation measures only the proportion of surface light at depth  $z$  and therefore only includes the absorption and scattering of light in the water column, not atmospheric interference above the surface.

The relationship between light attenuation and turbidity was investigated using three different regression functions; linear, power and rational. The use of a linear or a power function was determined for each site visually and quantitatively using  $R^2$  and root mean square error (RMSE) values. Using either function the relationship was strong, with only 4 of the 25 sites with  $R^2 < 0.6$ . A rational function was also used at each site due to its flexibility and ease of use across multiple sites with varying regression functions. The form of the linear and power functions are simple and commonly used, but offer little flexibility in function shape (i.e. only the slope and intercept change for a linear function), but the rational function – although not typically used for water quality relationships – are much more flexible in their response to site specific water quality changes. There was little difference between the linear or power functions and the rational function, demonstrating its flexibility in responding to different, site specific, regression functions. The rational function was used as it only requires regression parameters to be changed between sites (and not the actual form of the regression) and also enabled investigation and removal of the depth dependence of the light attenuation coefficients in the Beer Lambert Law – by comparing and normalising the clear water  $k$  ( $k_0$ ) at each site (the regression parameters when  $T = 0$ ) to site depth.

The influence of particle size distribution (PSD) on light attenuation was also investigated by comparing the light attenuation values at near field sites (< 1.4 km south of dredging) to far field sites (all northern sites and southern sites > 1.4 km from dredging) however no effect was found (Figure 4-4). This is based on the assumption that dredging creates a higher distribution of fine particles at sites close to dredging, wh, as occurred at Cape Lambert and Burrup Peninsula dredging projects (Jones et al. 2016). The relationship between particle size and scattering is complex (Davies-Colley & Smith 2001, Jonasz & Fournier 2007, Bowers et al. 2009, Kirk 2010). Briefly, for suspended particles, it is the PSD per volume that affects scattering (Davies-Colley & Smith 2001), and depends on both the scattering cross section (projected area of scattered light) and the scattering efficiency (scattering cross section divided by geometrical cross section of particle, Kirk 1985) of individual particles. The scattering cross section decreases for larger particles but also for very small particles, and the ideal attenuation (scattering plus absorption, Jonasz & Fournier 2007) cross section particle size is around 1.2  $\mu\text{m}$  according to Davies-Colley (2001). Furthermore, scattering efficiency increases rapidly for particle sizes > 1.6  $\mu\text{m}$  but decreases at larger sizes (see Kirk 1985 for detailed explanation). The similar attenuation coefficients with site proximity to the dredge zone suggests either that there was no / minimal impact of PSD on light attenuation (possibly due to the size of the particles / distribution of particles with respect to the scattering cross section and scattering efficiency), there was no significant change in PSD at sites closer to dredging, or that there were other effects preventing changes in PSDs appearing in the attenuation coefficients.

To ensure that depth dependence was removed as much as possible from the spatial analysis, the depth dependence in the attenuation coefficients was also investigated. Light attenuation rates are

higher in surface layers, as red light absorption by water is much higher than any other colour – resulting in high absorption in the upper layers, and depleted red light in the underlying layers (Kirk 1977b). The absorption (attenuation) rate of the remaining green-blue light is therefore relatively low, causing differences in the attenuation rates at different depths. Analysis of the light attenuation coefficients at each site revealed this to be the case – the attenuation coefficients were depth dependent; coefficients at two of the deeper sites (LNGA and LNGB at 11 – 12 m) did not exceed  $1 \text{ m}^{-1}$ , unlike sites in a similar location with similarly high turbidity levels ( $> 20 \text{ NTU}$ ) but at shallower depths (LNG2 and LNG3 at 6 – 7 m), which had linear relationships between turbidity and  $k$  and  $k$  values up to  $2 \text{ m}^{-1}$ . Comparison of the average clear water attenuation (i.e. absorption by water) at each site to the site average sensor depth revealed a strong relationship ( $R^2 = 0.62$ ); deeper sites had lower absorption attenuation rates than shallower sites. This is because the attenuation coefficients are a vertical average over the water column, and, because attenuation rates are higher in the surface layers, shallower sites have relatively higher attenuation rates over the water column than the deeper sites. For spatial analysis the attenuation coefficient depth dependence was removed by modelling  $k$  on turbidity at each site and normalising  $k_0$ .

Due to this depth dependence of light attenuation, the use of an alternative function was investigated which aims to remove any difference in light attenuation rates between shallow and deep column layers. Paulson and Simpson (1977) have extended the Beer Lambert Law to a double exponential method which uses different exponential coefficients for the upper 6 m of the water column and for depths  $> 10 \text{ m}$ . The method first derives the regression coefficients for the deeper layers by a least squares fit of an exponential function to observations of surface and submarine

irradiance, then a further least squares fit using these derived coefficients to shallow observations of surface and submarine irradiance provides regression coefficients for the shallow layers. In Paulson and Simpson (1977) submarine light levels are measured at a single location (on multiple runs) just beneath the surface and then at increasing depths up to 40 m, whereas the data available for this study is measured at a single depth at each location, and the maximum depth is 14 m. Although there was a large amount of PAR data across the study region at multiple depths, the depths are non-linear and each depth, being at a different location, has possibly different water quality conditions to other sites. To minimise the variation in water quality at the different depths, only the baseline PAR measurements were used for model calibration, providing approximately 1 month of data due to the measurement period of the terrestrial light data. This difference in depth measurements to Paulson and Simpson (PS) made model calibration challenging and less accurate; most of the deeper sites were at  $\sim 10$  m depth and most shallow sites were  $\sim 5 - 6$  m depth. The lower performance of the PS method was due to the non-linear depths of the PAR measurements and the different water quality conditions for each depth measurement. Although only the baseline data was used, there is still variation in water quality conditions between sites due to different exposure to waves and the complex flows due to the bathymetry.

For the PS method, median  $R^2$  values between modelled  $\hat{I}$  and measured  $I_z$  was 0.46 compared to median  $R^2$  of 0.71 and 0.74 for the light attenuation and turbidity regressions. Also, the median RMSE for the PS method was  $355 \mu\text{E m}^{-2} \text{ s}^{-1}$  compared to 51 and  $44 \mu\text{E m}^{-2} \text{ s}^{-1}$  using the other regression methods. Although the PS method appears to be an effective alternative to the Beer Lambert Law to remove any selective depth dependence in light attenuation rates, it was not

suitable for this study due to the method of data collection, with only a single measurement depth at each monitoring site. The use of the rational function was chosen as the best method for this study to investigate the relationship between light attenuation and turbidity due to its flexibility, its ease of use across multiple study sites, and its performance at most sites. The depth dependence was removed from the modelled attenuation coefficients by normalising the clear water attenuation (attenuation due to absorption), and the resulting modelled attenuation coefficients were compared at increasing distance from the dredge zone. Results of the spatial impact of dredging (confined to 2 – 5 km south of dredging) were similar to other results in this study and of other studies using the same dataset (see Fisher et al. 2015).

## Chapter 5. Dredge deposition zone

### 5.1 Synopsis

Managing the environmental impacts of dredging requires a good understanding of the spatial extent of water quality changes and changes in coral health, and sediment deposition is believed to be one of the most harmful consequences of dredging to corals (Bak 1978, Brown et al. 1990, Rogers 1990) as it further reduces light, smothers corals and requires corals to expend excess energy by creating mucus sheets in an attempt to remove the sediment (Bak & Elgershuizen 1976, Cortes & Risk 1985, Stafford-Smith 1993, Riegl 1995, Torres 2001, Bégin et al. 2013). Being able to predict the spatial scale of potential deposition related impacts near coral reefs is important for dredging monitoring and management (Spearman 2015) as it will better inform dredging program design and the position of water quality monitoring sites.

During this chapter, a dredge related deposition zone was identified using both in-situ deposition data and overburden from the turbidity model described in section Chapter 3. The overburden method assumes that excess turbidity during dredging is likely to result in excess dredge related deposition – where suspended sediment quickly deposits in-situ, particularly if dredging occurs during calm conditions when entrainment hydrodynamics are non-existent. High natural turbidity events indicate the presence of turbulent conditions from waves and currents while low natural turbidity suggest calm sea states. Any excess measured turbidity above the natural turbidity is therefore likely to deposit because the hydrodynamics are insufficient to maintain suspension. The model overburden technique (i.e. assessing dredge induced deposition by overburden levels) provides an estimate or indication that excess deposition is occurring, and can therefore be used as

an early warning to dredge proponents to monitor dredging deposition threshold exceedance during future dredge operations.

The relationship between the turbidity model overburden and in-situ deposition data are compared in this chapter to validate the use of the overburden method to monitor dredge induced deposition. Also, deposition conditions prior to and during dredging are compared to characterise the natural and dredge related deposition conditions at Barrow Island, and spatial comparisons of the in-situ deposition data and daily overburden levels are compared at increasing distances from the dredge zone during dredging for dredge deposition zone identification.

## **5.2 Methods**

### **5.2.1 Overburden (from turbidity model)**

The turbidity model detailed in Chapter 3 was used here to estimate turbidity overburden (excess turbidity caused solely by dredging) and hence excess deposition due to dredging. Overburden was calculated by subtracting the daily averaged modelled turbidity (natural turbidity) from the daily averaged measured turbidity (natural + dredge turbidity) at each site. The spatial impacts of deposition caused by dredging were then analysed by comparing the overburden at each site with the site distance from the dredge zone.

The use of the overburden technique to monitor dredge related deposition threshold exceedance was analysed by comparing daily overburden to daily averaged SSD at each site as measured by the deposition sensor. As small overburden values could be caused by model errors, and deposition threshold exceedance is more likely to coincide with large overburden values, we also compared the daily overburden to daily averaged SSD only on days which had high overburden (> 5 NTU).

### **5.2.2 Daily surface sediment density (SSD)**

The deposition optical backscatter sensor (OBS), from which the SSD measurements are derived, has a two hour wiper which removes accumulated sediment on the sensor surface (see section 2.2.1 Turbidity and deposition measurements and calibration). This periodic SSD removal creates a sawtooth pattern in the data (for example Figure 5-1) where, during accumulation events, sediment continues to accumulate on the sensor, increasing the deposition reading (in  $\text{mg cm}^{-2}$ ), during the two hours between wiper activation. When the wiper activates, the sensor readings return to zero as all sediment is removed from the sensor. This sawtooth pattern was used to help identify significant accumulation events in the Barrow Island SSD data due to the size of the time-series and the difficulty identifying the two hourly sawtooth pattern in the raw data. Wavelet analysis (similar to the wavelet analysis used in the temporal analysis of turbidity data described in Chapter 3, section 3.2.2) can detect the two hourly periodic pattern and is easily identifiable in the wavelet analysis results as a dominant periodic event in the SSD data.



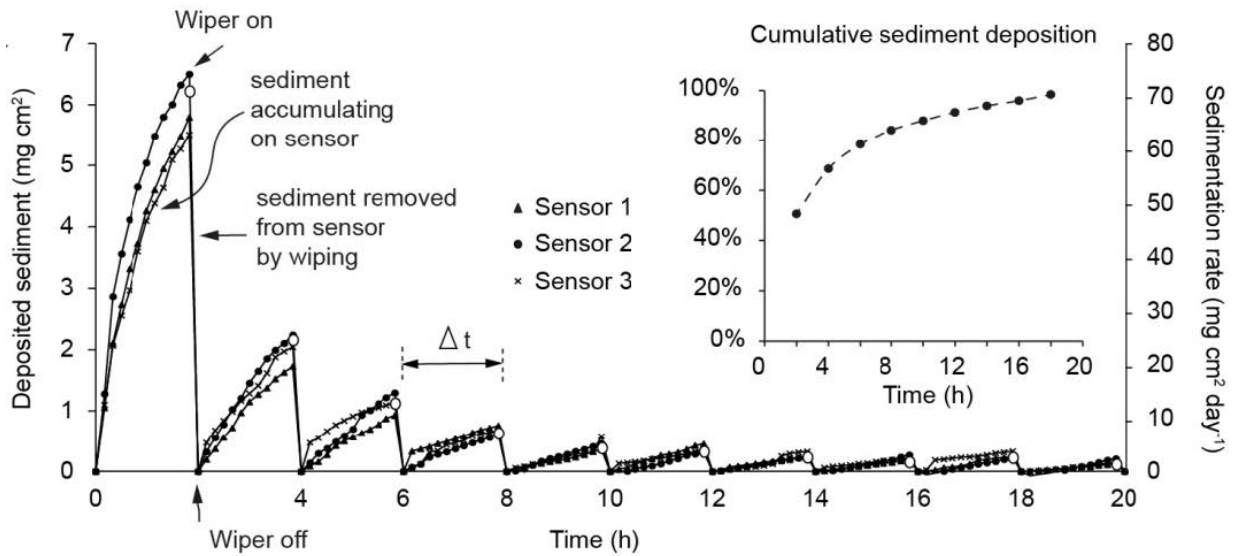


Figure 5-1 An example of the sawtooth pattern occurring in the SSD data during significant sediment accumulation events. Sediment deposits onto the sensor and accumulates every ten minutes during the two hours between sensor wiper activation (represented by the wiper off in the figure). The wiper removes any sediment or particles which have accumulated on the upwards facing optical backscatter sensor, returning the sensor reading to zero and thereby creating a sawtooth pattern. If this sawtooth pattern is present, it allows a deposition rate to be calculated from the slope for every two hour accumulation event (which has been normalised to a 24 hour period, secondary Y axis in units of  $\text{mg cm}^{-2} \text{d}^{-1}$ ). (Whinney et al. 2017)

As well as the spectral analysis of the SSD data to detect accumulation events, the SSD were also converted to daily measurements by averaging the daily values. To avoid false averages, no daily value was recorded if more than 20% of the data points per day were missing.

### 5.3 Results

#### 5.3.1 Surface sediment density

There was a large gradient in average SSD with increasing distance from the primary dredging sites (shown in Figure 5-2 in 2 dimensions and Figure 5-8 B in 3 dimensions – with time as an extra dimension). Average dredge period SSD values within a few km south of the dredging area was up to 7 times higher than the northern sites and sites > 5 km south (Figure 5-2). Sites within 5 km south had average dredge period SSD between 0.15 and 0.75  $\text{mg cm}^{-2}$  (Figure 5-2) and maximum daily SSD up to 13  $\text{mg cm}^{-2}$  (Figure 5-8 B and Table 5-1). All northern sites and sites > 5 km south had average

dredge period SSD  $< 0.1 \text{ mg cm}^{-2}$  (similar to average baseline levels of between 0 and  $0.2 \text{ mg cm}^{-2}$ , Figure 5-2 and Table 5-1) and maximum daily SSD up to  $6 \text{ mg cm}^{-2}$  (Figure 5-8 B). Higher average SSD at some sites during the baseline period (Figure 5-2, white circles near dredge zone) could be caused by variations in sensor deployment lengths resulting in exclusion of high natural resuspension to deposition events from the time series.

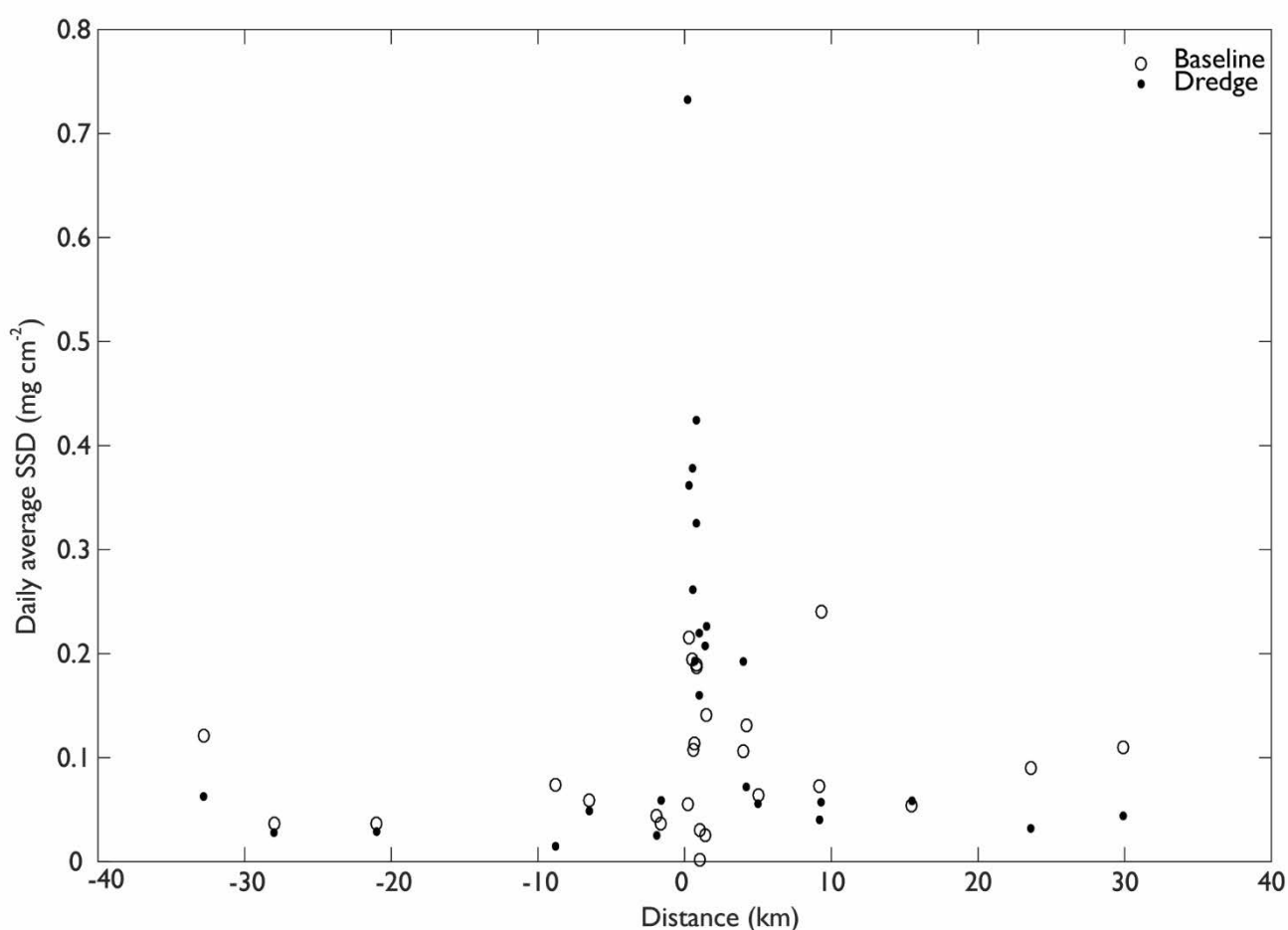


Figure 5-2 Average daily SSD ( $\text{mg cm}^{-2}$ ) during the baseline period (white circles) and dredge period (black circles) during the Barrow Island project plotted according to the distance of the sites from the dredge zone, with negative values north of the dredge zone (which is at the origin) and positive values to the south.

Table 5-1 Summary table showing mean, median and maximum SSD during the baseline and dredging periods listed according to site distances (km) from north to south of the dredge zone (with dredging at origin). The dredge spoil disposal ground sites are also listed; site LONE was 4.2 km south and site DSGS was 9.2 km south of the primary site of dredging and both were also 0.1 km from the dredge material placement site (Figure 2-1).

| Sites                              | Distance (km) | SSD (mg cm <sup>-2</sup> ) |        |      |        |        |       |
|------------------------------------|---------------|----------------------------|--------|------|--------|--------|-------|
|                                    |               | Baseline                   |        |      | Dredge |        |       |
|                                    |               | Mean                       | Median | Max  | Mean   | Median | Max   |
| <b>Northern sites</b>              |               |                            |        |      |        |        |       |
| AHC                                | 32.8          | 0.09                       | 0.05   | 1.11 | 0.06   | 0.03   | 0.59  |
| REFN                               | 28            | 0.03                       | 0.03   | 0.07 | 0.03   | 0.01   | 0.61  |
| ELS                                | 21            | 0.04                       | 0.03   | 0.12 | 0.03   | 0.02   | 0.55  |
| ANT                                | 8.8           | 0.06                       | 0.03   | 0.96 | 0.01   | 0.01   | 0.41  |
| DIW                                | 6.5           | 0.06                       | 0.04   | 0.56 | 0.05   | 0.02   | 5.15  |
| LOW                                | 1.9           | 0.04                       | 0.02   | 0.78 | 0.02   | 0.01   | 0.99  |
| LOW1                               | 1.6           | 0.03                       | 0.00   | 0.51 | 0.06   | 0.04   | 0.56  |
| <b>Southern sites</b>              |               |                            |        |      |        |        |       |
| LNG0                               | 0.2           | 0.06                       | 0.02   | 1.07 | 0.53   | 0.12   | 12.73 |
| LNGA                               | 0.3           | 0.21                       | 0.15   | 1.84 | 0.34   | 0.12   | 4.39  |
| LNG1                               | 0.5           | 0.19                       | 0.11   | 2.22 | 0.36   | 0.12   | 6.27  |
| LNGB                               | 0.7           | 0.11                       | 0.09   | 0.45 | 0.19   | 0.06   | 6.45  |
| MOFA                               | 0.6           | 0.10                       | 0.08   | 0.26 | 0.26   | 0.08   | 6.71  |
| MOFC                               | 0.7           | 0.18                       | 0.12   | 2.00 | 0.41   | 0.15   | 10.02 |
| MOF1                               | 0.8           | 0.16                       | 0.06   | 3.05 | 0.32   | 0.16   | 4.52  |
| MOFB                               | 1             | 0.03                       | 0.02   | 0.33 | 0.22   | 0.06   | 12.11 |
| LNG2                               | 1             | 0.14                       | 0.08   | 1.83 | 0.15   | 0.06   | 4.43  |
| LNGC                               | 1.4           | 0.03                       | 0.01   | 0.21 | 0.21   | 0.07   | 4.56  |
| MOF3                               | 1.5           | 0.13                       | 0.05   | 4.22 | 0.22   | 0.07   | 6.63  |
| LNG3                               | 4             | 0.09                       | 0.05   | 1.68 | 0.19   | 0.10   | 1.41  |
| TR                                 | 5             | 0.06                       | 0.02   | 2.10 | 0.06   | 0.03   | 1.30  |
| DUG                                | 9.2           | 0.14                       | 0.04   | 1.80 | 0.06   | 0.02   | 1.06  |
| BAT                                | 15            | 0.05                       | 0.02   | 1.75 | 0.06   | 0.04   | 0.98  |
| REFS                               | 24            | 0.09                       | 0.06   | 0.28 | 0.03   | 0.02   | 0.51  |
| SBS                                | 30            | 0.09                       | 0.01   | 3.04 | 0.04   | 0.02   | 0.44  |
| <b>Dredge spoil disposal sites</b> |               |                            |        |      |        |        |       |
| LONE                               | 4.2           | 0.12                       | 0.05   | 5.11 | 0.07   | 0.03   | 1.06  |
| DSGS                               | 9.2           | 0.07                       | 0.06   | 0.53 | 0.04   | 0.02   | 0.66  |

\* Distance to spoil ground = 0.1 km

A wavelet analysis technique was used to identify significant SSD events, however it was discovered that the deposition sensor underestimated accumulated sediment (Figure 5-4). The wavelet analysis technique is possible due to the sawtooth pattern occurring during accumulation events (Figure 5-4 A). Every two hours the antifouling wiper of the upwards facing OBS removes sediment that has

accumulated on the sensor surface, which resets the sensor reading to zero, creating a sawtooth pattern in the data indicative of sediment accumulation (Figure 5-4A). The sawtooth patterns appear as uniquely coloured stripes, shown in Figure 5-4 B for the site MOFC, where the yellow vertical bands represent  $5 \times 2$  h cycles (and harmonics at 1, 0.5, 0.25 h) over a 10 h period. Such occurrences were rare and further inspection of the raw data demonstrated that there were frequently periods when sediment accumulated on the flat sensor, moved off, and resettled again within the 2 h accumulation period (an example is presented in Figure 5-3). This created a broken sawtooth pattern and no 2 hourly period bands were evident in the spectral data, which prevented calculation of a sedimentation rate for each 2 h period. For this reason a different method was used to calculate SSD – by averaging the 10 minute SSD measurement over the day, providing an index of sediment deposition as  $\text{mg cm}^{-2}$ .

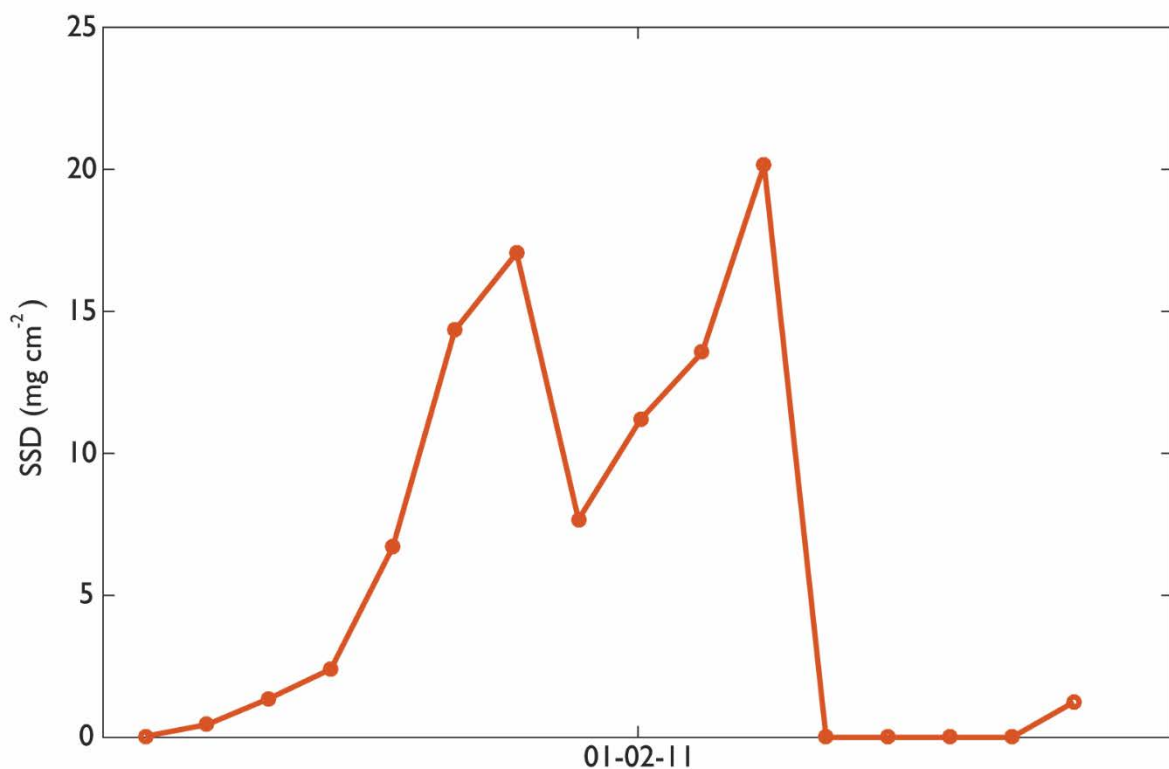


Figure 5-3 SSD data at MOFA demonstrating the rapid removal of accumulated sediment during a two hour accumulation period (i.e. between the two hour antifoul sensor wiper activation). Sediment has deposited on the sensor and begins accumulating every ten minutes. After one hour (i.e. 7 data points represented by the orange dots), some accumulated sediment is removed from the sensor, decreasing the SSD value and disrupting the sawtooth pattern and preventing calculation of deposition rate.

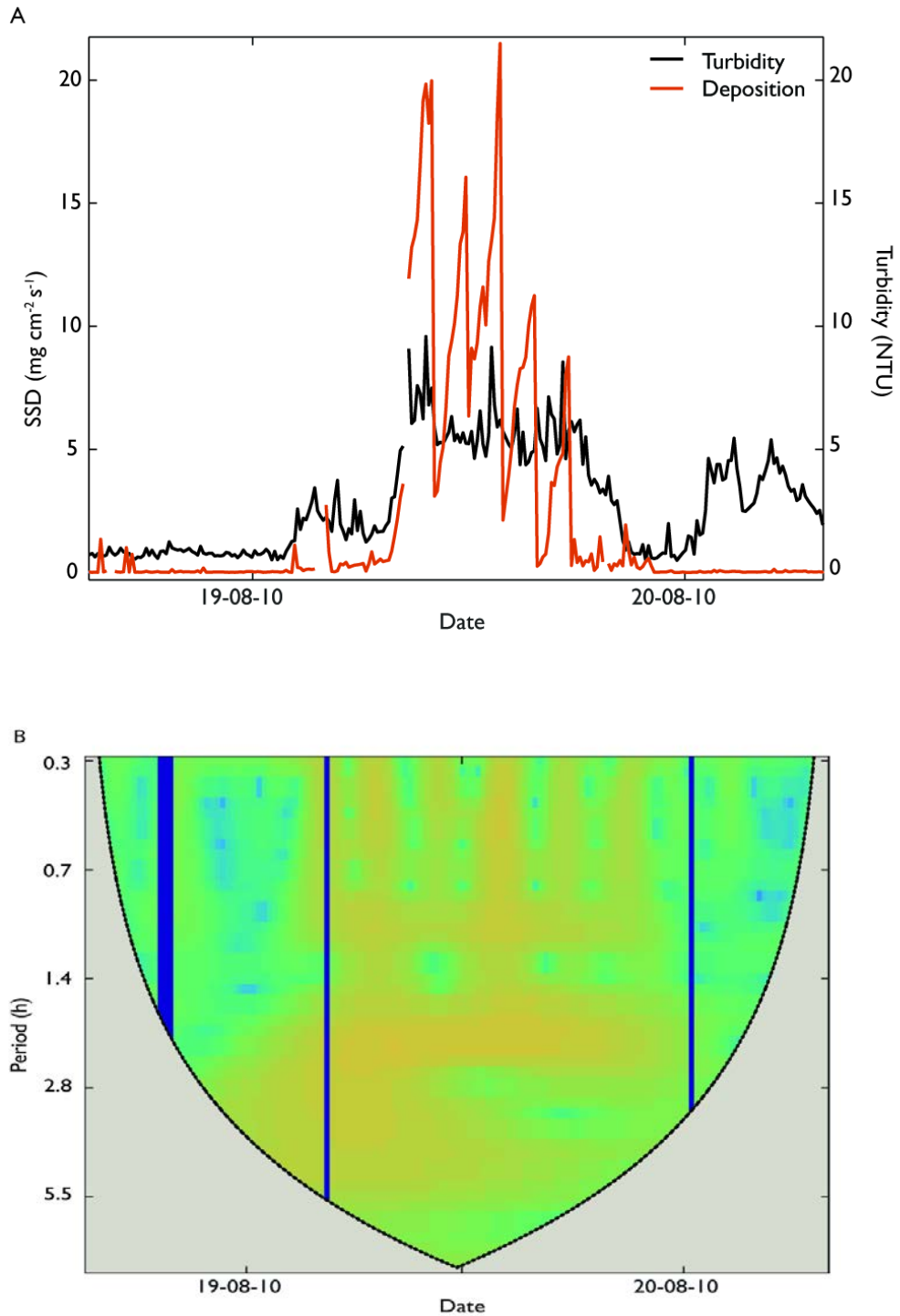


Figure 5-4 (A) Turbidity (black line) and deposition (orange line) at site MOFC from 19-20 August 2010, demonstrating the sawtooth pattern in the deposition data resulting from sediment accumulation and wiper action, and (B) the wavelet transform of the sawtooth pattern in deposition data, showing higher energy (yellow bands) in the 2,1 and half hour periods.

### 5.3.2 Overburden

By subtracting daily model estimates from the measured turbidity during dredging, the overburden could provide a monitoring tool to estimate excess turbidity and deposition induced solely by dredging. Average daily overburden was calculated for the Barrow Island sites (no dredging occurred at Hay Point). Daily overburden – up to ~5 NTU and maximum of up to ~70 NTU – was higher at sites close to dredging and decreased with increasing distance from dredging (Figure 5-5 and Table 5-2). Sites within 10 km south of the dredge zone, such as MOF1 (0.8 km from dredging) and LNG0 (0.2 km from dredging) with average overburden between 3.3 and 4.4 NTU (Table 5-2), had higher and more frequent overburden events during dredging in contrast to northern sites and sites > 10 km south (shown in Figure 5-5 in 2 dimensions and Figure 5-8 A in 3 dimensions (with time as an extra dimension)). Sites within 2 km north, and sites >10 km north and south of the dredging had average dredge period overburden  $\leq 0$  NTU, equivalent to or less than typical baseline period overburden across all sites ( $\leq 0.5$  NTU, Figure 5-5 and Table 5-2). The negative overburden values occur when daily measured turbidity > daily modelled turbidity and are likely a result of model error. The dredge spoil disposal perimeter site LONE (located south-east of the dredge zone, Figure 2-1) had infrequent overburden events > 2 NTU and low average overburden of 0.03 NTU, similar to the most southern reference sites and all sites during the baseline period (Figure 5-5 and Table 5-2).

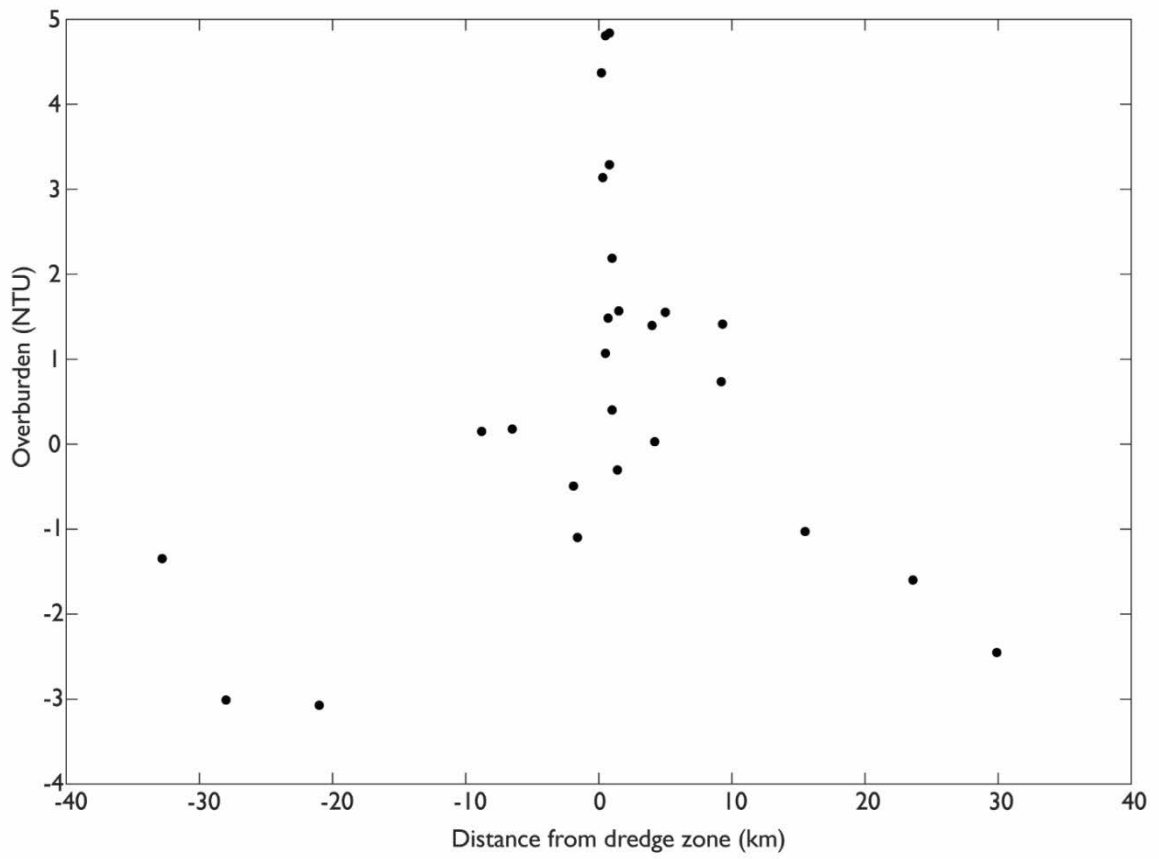


Figure 5-5 Daily average overburden (NTU) during the baseline period (white circles) and dredge period (black circles) during the Barrow Island project plotted according to the distance (km, see Figure 2-1) of the sites from the dredge zone, with negative values north of the dredge zone (which is at the origin) and positive values to the south.

Table 5-2 Summary table showing mean and maximum overburden (i.e. difference between measured and modelled turbidity in NTU) during the dredge period (overburden is only calculated during dredging), listed according to site distances (km) from north to south of the dredge zone (with dredging at origin). The dredge spoil disposal ground sites are also listed; site LONE was 4.2 km south and site DSGS was 9.2 km south of the primary site of dredging and both were also 0.1 km from the dredge material placement site (Figure 2-1).

| Sites                              | Distance (km) | Daily overburden (NTU) |       |
|------------------------------------|---------------|------------------------|-------|
|                                    |               | Max                    | Mean  |
| <b>Northern sites</b>              |               |                        |       |
| AHC                                | 32.8          | 6.29                   | -1.35 |
| REFN                               | 28            | 2.13                   | -3.01 |
| ELS                                | 21            | 0.04                   | -3.07 |
| ANT                                | 8.8           | 9.44                   | 0.15  |
| DIW                                | 6.5           | 12.94                  | 0.18  |
| LOW                                | 1.9           | 7.35                   | -0.49 |
| LOW1                               | 1.6           | 6.95                   | -1.1  |
| <b>Southern sites</b>              |               |                        |       |
| LNG0                               | 0.2           | 57.22                  | 4.37  |
| LNGA                               | 0.3           | 48.77                  | 3.14  |
| LNG1                               | 0.5           | 41.56                  | 1.07  |
| LNGB                               | 0.7           | 70.15                  | 1.48  |
| MOFA                               | 0.6           | 134.11                 | 4.81  |
| MOFC                               | 0.7           | 116.39                 | 4.84  |
| MOF1                               | 0.8           | 70.63                  | 3.29  |
| MOFB                               | 1             | 64.82                  | 2.19  |
| LNG2                               | 1             | 23.92                  | 0.4   |
| LNGC                               | 1.4           | 50.57                  | -0.3  |
| MOF3                               | 1.5           | 29.38                  | 1.57  |
| LNG3                               | 4             | 32.04                  | 1.4   |
| TR                                 | 5             | 32.7                   | 1.55  |
| DUG                                | 9.2           | 42.1                   | 1.41  |
| BAT                                | 15            | 12.14                  | -1.03 |
| REFS                               | 24            | 4.97                   | -1.6  |
| SBS                                | 30            | 3.1                    | -2.45 |
| <b>Dredge spoil disposal sites</b> |               |                        |       |
| LONE                               | 4.2           | 6.43                   | 0.03  |
| DSGS                               | 9.2           | 15.16                  | 0.74  |

\* Distance to spoil ground = 0.1 km



### 5.3.3 Surface sediment density and overburden

The relationship between daily average SSD and daily overburden was weak ( $R^2 \approx 0$ ) across all Barrow Island sites, however the relationship improved significantly at two sites (DUG and DSGS, see Figure 2-1 for site locations) when only higher overburden ( $>5$  NTU) days were analysed (Figure 5-6). At site DUG, the  $R^2$  increased from 0 to 0.5 and at site DSGS from 0 to 0.7 (Figure 5-6). The relationship remained weak at all other modelled sites. Sites  $> 10$  km south and the two northern modelled sites (AHC and ANT) had  $< 5$  days with overburden  $> 5$  NTU while sites within 10 km south of dredging had between 0 and 117 days with overburden  $> 5$  NTU. Comparisons between overburden and the following day SSD in case deposition of excess turbidity was delayed, however no improvement was found in the  $R^2$  values.

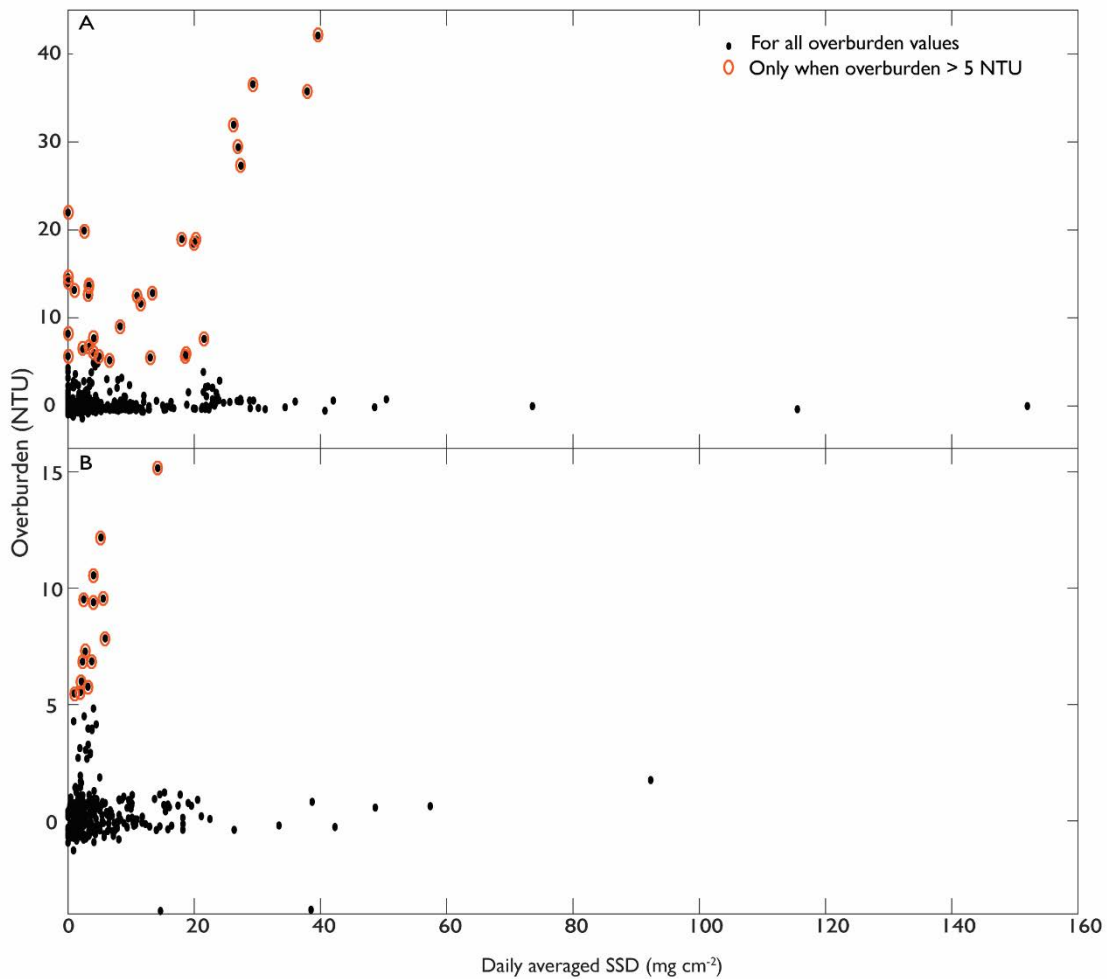


Figure 5-6 Overburden and daily averaged surface sediment density comparing all overburden values (black circles) and only days when overburden > 5 NTU (orange circles) at sites DUG (A) and DSGS (B). The relationship improved significantly at both sites when comparing overburden and SSD only on days when overburden > 5 NTU, from  $R^2 = 0$  (typical of all sites) to  $R^2 = 0.5$  at DUG and  $R^2 = 0.7$  at DSGS.

Most sites had a few instances with corresponding peaks in both overburden and deposition, however these were rare (see Figure 5-7) and due to storm activity, for example on 10 May 2011 at site DUG (Figure 5-7 A) during the highest overburden (> 140 NTU) event. MOF1 also had high overburden during this storm (up to 400 NTU, Figure 5-7 B), however there were no peaks in SSD. The highest peaks in SSD at site DUG (~1 mg cm<sup>-2</sup>) occurred in early November 2010 and mid-April 2011 (Figure 5-7 A). There were higher (~4 mg cm<sup>-2</sup>) and more frequent SSD peaks at site MOF1 (Figure 5-7 B), with only a few peaks corresponding to high overburden (up to 70 NTU) events in July and September 2011.

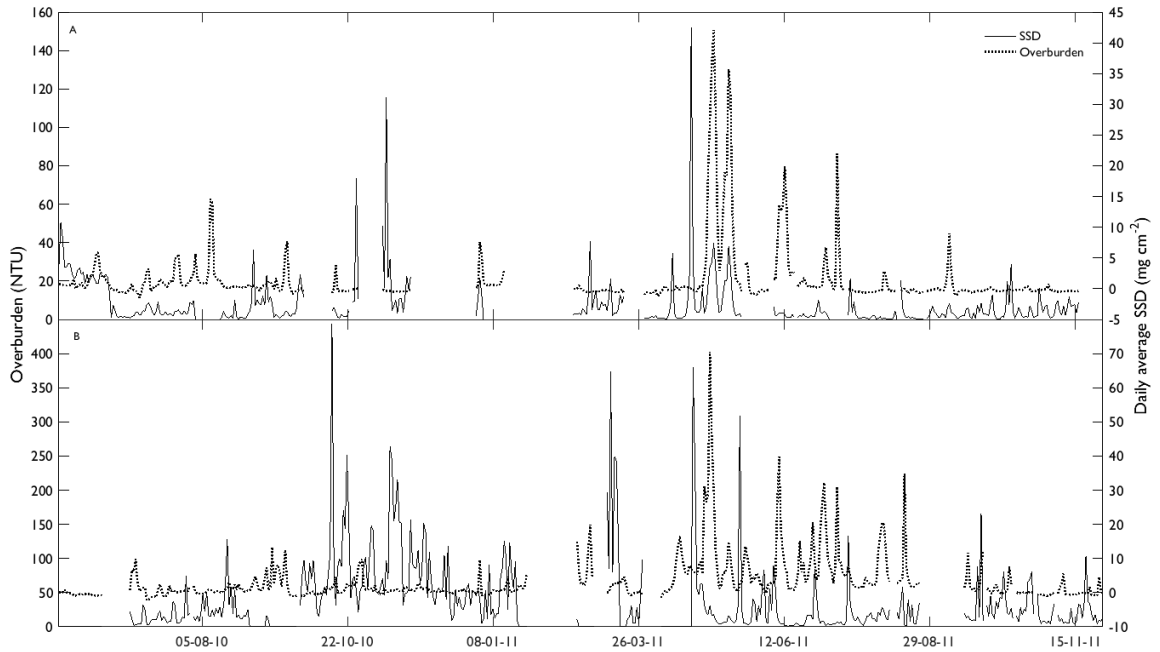


Figure 5-7 Daily averaged SSD (solid line) and daily overburden (broken line) at site DUG (A, 9.3 km south of the dredge zone) and MOF1 (B, 0.8 km of dredge zone and on the perimeter of the spoil disposal ground) during the dredge period. Corresponding peaks in SSD and overburden occurred at DUG (A) during a storm ~ mid May 2011, and corresponding peaks in SSD and overburden occurred at MOF1 (B) in July and September 2011, but not during the storm in mid May 2011. Higher and more frequent peaks in SSD occurred at MOF1 (B) than at DUG (A).

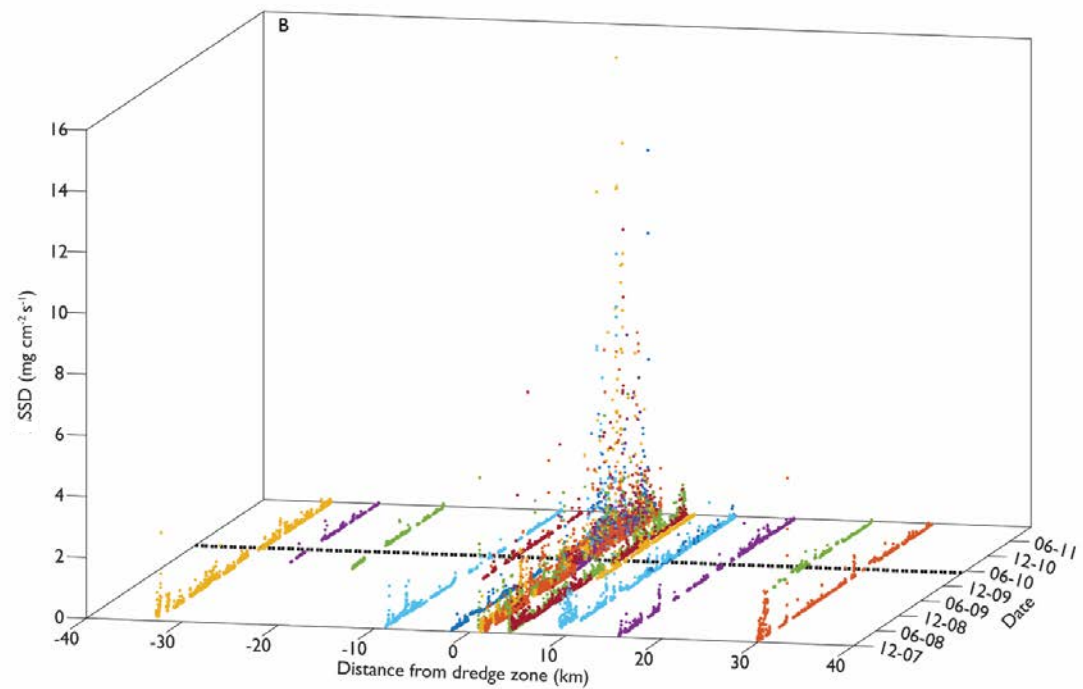
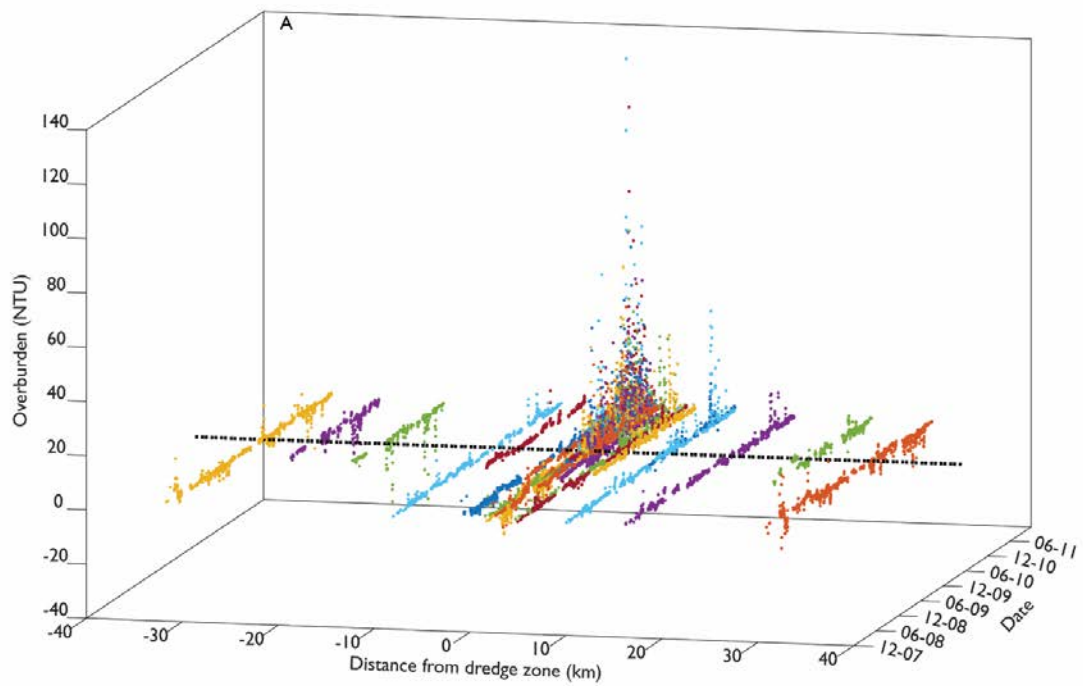


Figure 5-8 Daily overburden (A) and daily averaged sediment surface density (B) at Barrow Island sites from December 2007 to December 2011 plotted according to the distance of site from the dredge zone. Negative values are north of the dredge zone (which is at origin) and positive values are south. The black dotted line separates the baseline period (December 2007 to 19 May 2010) and dredge period (19 May 2010 to December 2011).

## 5.4 Discussion

Understanding the spatial extent of dredging impacts, particularly deposition events studied in-situ, is important in managing and mitigating their environmental impacts. This study demonstrated, using two different analysis methods, a clear deposition zone confined to within 2 – 5 km of dredging during 18 months of dredging at Barrow Island. Sites within 1 km north and 5 km south of the main dredge zone had median deposition levels up to 7 times higher and median overburden (dredge related turbidity) 3 – 4 times higher than reference sites further north and south. The reference sites had deposition and overburden levels similar to baseline (background) conditions. No significant deposition events occurred at two sites on the perimeter of the spoil disposal site, however this could be attributed to site placement. As explained in Fisher et al. (2015), these *in-situ* benthic spatial impacts of dredging are confined to a much smaller area than the spatial extent of the dredge plume analysed from satellite images and described in Evans et al. (2012).

A novel turbidity modelling technique was investigated to simplify deposition monitoring during dredge operations. Additional monitoring is required during a dredge operation if pre-determined water quality thresholds, set during the approvals process to minimise the environmental impact of the dredge, are exceeded (for example Chevron Australia Pty Ltd 2011a). The ability for turbidity and hydrodynamic data to predict potential deposition events by using the turbidity model would replace the need for additional data collection and monitoring (e.g. sediment trap deployment, see below). The use of the model to predict dredge related deposition events was tested at each Barrow Island site (no dredging occurred during the Hay Point study) by comparing the overburden with the daily in-situ SSD. Unfortunately, due to the clear ambient conditions at Barrow Island, model

performance was inadequate for this purpose. As a result the use of the model to predict dredge related deposition events could not be assessed at the Barrow Island sites and requires further testing.

Despite the poorer model performance at the Barrow Island sites, further investigation of model use for monitoring excess dredge related deposition is worthwhile. For one, the relationship between overburden and SSD – used to validate the use of the model to predict dredge related deposition – improved significantly at 2 sites, DUG and DSGS, from  $R^2 = 0$  to 0.5 and 0.7 (overburden > 5 NTU is likely to result in deposition levels significant to coral health). Both of these sites are located at the same latitude on the southern tip of Barrow Island (see Figure 2-1) and are probably more exposed to waves and tidal currents (see Hubbert et al. 2005) but are deep enough (with sensor depths of 5.5 m and 14 m, respectively – see Chevron Australia Pty Ltd 2011a for sensor depths) that wind driven water motion may not remove sediment from the deposition sensor plate as easily as the shallower sites further south (for example Wolanski et al. (2005) reported waves affecting only shallow sites < ~ 5.5 m on the leeward side of an island). Also, although the model performance was weak during the clear water Barrow Island study, the model performed well at most sites when applied to the more turbid environment of Hay Point (Queensland) (see Figure 2-1). The higher performance of the model at Hay Point demonstrates that the model is able to successfully predict natural turbidity events and therefore could estimate dredge related deposition levels when used in a more turbid environment.

Accurate deposition measurements are also necessary to assess the use of the model to predict and manage dredging deposition. The deposition sensor used during the Barrow Island study likely underestimated daily deposition levels due to the flat sensor plate; water motion could easily remove deposited sediment from the plate when it would normally remain on the rougher, more porous coral surfaces (Ridd et al. 2001, Chevron Australia Pty Ltd 2011a). Problems with the sensor were evident by infrequent sawtooth patterns occurring at sites close to the dredge zone despite high turbidity and deposition levels. The sawtooth pattern occurs when sediment accumulates on the plate and is wiped away every two hours (figure 2, Thomas & Ridd 2005), however sediment rapidly removed from the sensor plate disrupted this sawtooth pattern. Although sites close to the dredge zone had average deposition 4 to 5 times higher than sites > 2 km away, there were few sawtooth patterns in the data.

Despite data from the deposition sensor not being used throughout the project due to perceived doubts of its veracity, the data is still reliable for comparisons between sites and between pre-dredge and dredge conditions. Sediment accumulation levels may be lower than expected, but overall there were strong similarities to spatial trends using other analysis methods in this thesis, as well as by Fisher et al (2015) using the same dataset, and compared to other case studies into the impacts of dredging near coral reefs (Erftemeijer et al. 2012). Sites within 2 km of dredging had maximum daily SSD just over double the maximum daily SSD at sites > 2 km away. Similar results were found by Kettle et al. (2001); deposition rates of  $500 \text{ mg cm}^{-2} \text{ d}^{-1}$  within 500 m of dredging at Cleveland Bay were 10 times higher than sites 1.5 km from dredging, falling to  $50 \text{ mg cm}^{-2} \text{ d}^{-1}$  at 1.5 km radius. Furthermore, during dredging in Mermaid Sound, Dampier Archipelago in 2004, Stoddart

& Anstee (2004) found that coral mortality was confined to within 1 km of dredging, with average turbidity levels decreasing from 3.75 NTU to 1.24 NTU at the far field sites. Likewise Blakeway (2004) reported that Woodside found coral mortality was confined to 2 sites within 1.3 km. Monitoring changes in deposition levels during dredging requires comparisons to reference sites and/or ambient conditions prior to dredging, therefore relative daily SSD levels are sufficient for managing the impacts of dredging on the benthos.

To overcome problems with reduced absolute SSD levels, a new deposition sensor has since been developed by the James Cook University Geophysics Lab. The new sensor resolves issues by using an indented surface to better mimic coral surfaces and by increasing the number of sensors (see (Whinney et al. 2017)). Regular sawtooth patterns were observed for a range of turbidity levels using the new sensor.



## Chapter 6. Conclusion

### 6.1 Summary of work

This thesis studied the spatial and temporal water quality changes during a large scale capital (~ 7.6 Mm<sup>3</sup>) dredging operation on the eastern side of Barrow Island, Western Australia, during construction of a materials offloading facility and LNG jetty for development of the Gorgon LNG plant – the largest single resources project in Australia’s history. The comprehensive analysis used the largest global temporal and spatial water quality dataset ever collected prior to and during dredging, with 29 sites collecting water quality and water pressure measurements every 10 minutes along a 60 km north / south transect for up to 4 years. Dredging occurred for 18 months from 19 May 2010 – 31 November 2011.

The site locations of the Gorgon project allowed us for the first time to determine the spatial extent of the dredge impacts because there were many sites located within a few kilometres from the dredge so that gradients in turbidity, light, and sediment deposition could be measured and unequivocally related to dredging. We have now been able to very accurately determine the extent of the dredge impact field perhaps for the first time in Australia, and certainly for a location affecting corals.

Turbidity, light attenuation and sediment deposition conditions at Barrow Island were described prior to and during dredging, and spatially at increasing site distance from the dredge zone.

Turbidity metrics were up to 4 – 6 x higher, median light attenuation coefficients 1.5 x higher, median deposition levels up to 7 x higher and median overburden (dredge related turbidity, calculated using a simple statistical turbidity model which estimates natural turbidity during dredging) 3 – 4 x higher at sites within 2 – 5 km south of dredging. All northern sites and sites > 5 km south of dredging were unaffected by the dredge, as were the 2 dredge spoil disposal perimeter sites, located ~ 0.1 km from the spoil ground and 4.2 and 9.2 km south east of the main dredge zone.

Barrow Island is typically a clear water environment, with mean ambient turbidity levels 0.8 – 2.7 NTU and 1 – 7 NTU during dredging. During the baseline period turbidity metrics did not vary much with increasing site distance from the dredge zone, however during dredging mean, maximum and standard deviation levels were up to 5 x higher at the sites close to dredging, with maximums up to 550 NTU and maximum daily averaged turbidity up to 153 NTU.

Further temporal and spatial analysis of turbidity data included a running mean analysis over increasing temporal scales and spectral analysis – comparing conditions prior to and during dredging as well as at increasing distances from dredging. The running mean analysis revealed that sites close to the dredge zone had significantly higher average turbidity, even using a 30 day running mean window size, than the northern sites and sites > 5 km south). For example, at a site 0.5 km south of dredging the maximum of the 30 day running mean was greater than the maximum hourly mean during the baseline period. During dredging, the frequency of turbidity increases was also

evident in the running mean analysis with the 95<sup>th</sup> and 80<sup>th</sup> percentiles increasing with increasing running mean window sizes – requiring the presence of turbidity peaks in the larger window sizes.

The spectral analysis at Barrow Island decomposed the natural resuspension events into their periodic constituents – semi-diurnal, diurnal, spring-neap tide, as well as the presence of the weaker 10 day synoptic and Madden Julian Oscillation. The appearance of the semi-diurnal peak in the wave spectra and during the baseline period in the turbidity spectra suggests that the twice daily low water height amplifies wave resuspension, and the strengthening of the semi-diurnal peak during dredging at sites within 2 km of the dredge zone suggests that horizontal advection occurred at these sites.

A simple, statistical turbidity model was developed and tested in 2 different hydrodynamic settings – the clear waters of Barrow Island and the more turbid energetic waters of Hay Point, Queensland. The purpose of the model is to estimate natural turbidity, caused by waves and tides, using a simple model requiring collection of only 2 variables – in place of the more complex three dimensional hydrodynamic models typically used during dredging operations. The model can decouple the natural and dredge related sediment plume advection, which is useful for monitoring dredge related turbidity threshold exceedance as well as improving our understanding of turbidity changes during dredging. The model was successful at estimating daily turbidity at a few of the Hay Point and Barrow Island sites, with  $R^2 > 0.5$  between modelled and measured turbidity at 83% of sites during the model test phase at Hay Point (although model skill scores were  $> 0.5$  at only 1 site during the

test phase), and 38 % of Barrow Island sites had  $R^2 > 0.5$  at Barrow Island and , but improvements could be made to both the input data and possibly more sophisticated parameter estimation tools (such as Bayesian analysis).

The study of light levels during dredging shows that impacts were confined to sites < 5 km south of dredging while all northern sites and sites > 5 km south unaffected by dredging. It demonstrates spatial differences in both the magnitude of impacts (light attenuation was 1.5 x higher at sites directly affected by dredging), and the duration of reduced light levels (sites close to dredging experienced low light conditions for over 150 consecutive days). A method was successfully used to remove the depth dependence from light analysis (for studies where sensors are placed at non-uniform depths) to ensure spatial results were not obscured by differences in light sensor depths. The use of light attenuation coefficients is also useful for eliminating non-dredge parameters affecting submarine light levels, such as cloud cover. Further detailed spatial and temporal analysis of turbidity and SSC during this dredging project can be found in Fisher et al. (2015) and Jones et al. (2015).

A clear dredge related deposition zone, analysed using daily averaged SSD and turbidity model overburden (i.e. dredge related turbidity), was also confined to within 2–5 km south of dredging. The use of the turbidity model to estimate dredge related deposition and as a deposition threshold exceedance monitoring tool was investigated by comparing daily SSD measurements to the daily overburden values. Unfortunately due to low model performance in the clear water Barrow Island

waters, and the deposition sensor underestimating accumulated deposition, results are inconclusive. Despite this, there is still potential for the model to estimate dredge related deposition (and turbidity) and to monitor deposition threshold exceedance during future dredging operations; model performance was strong in the more turbid Hay Point environment, and the relationship between SSD and overburden improved significantly at 2 of the southern sites ( $R^2$  increased from ~ 0 to 0.5 and 0.7) when using only high overburden days (> 5 NTU, which are more likely to result in deposition events).

## **6.2 Recommendations and future work**

This research has provided a good basis for both spatial and temporal analysis methods, for studying light levels during dredging programs, for modelling light levels during future dredging operations, and for future threshold exceedance monitoring tools to be used during future dredging operations. The primary recommendation is that a high density of in-situ water quality monitoring sites are placed close to the dredge zone during future dredging operations to increase our understanding of dredging impacts. Previous studies into dredging impacts at Cape Lambert and Burrup Peninsula on the north west shelf did not find a similarly well-defined distance to dredge effects, but this could be because there were fewer monitoring sites deployed close to dredging rather than a lack of water quality spatial gradient during dredging operations (Fisher et al. 2015).

Due to the importance of distance to dredge impacts for the EIA process and while monitoring dredging impacts, it should also be recommended in the future that monitoring sites always be

located in geometrically increasing spacing's from within a few hundred meters of a dredge operation, and that a suite of oceanographic instruments be deployed to enhance our understanding of dredging impacts. This will enable the dredge impact field to be determined - even if there are no biologically sensitive sites at those close-in locations.

Also the performance of the turbidity model in different hydrodynamic settings, particularly during a dredge operation, is recommended to investigate the use of the model to monitor dredge related turbidity and deposition threshold exceedance. If the model is tested during a dredge operation, the new deposition sensor developed at the James Cook University Marine Geophysics Lab (Whinney et al. 2017) should also be deployed and used to validate the use of the model overburden in detecting dredge related deposition. The calculated overburden from the turbidity model (difference between measured and modelled turbidity) can be used to monitor excess dredge related turbidity – which can lead to excess dredge related deposition – however this method needs to be validated using accurate in-situ deposition measurements. The new deposition sensor is much more accurate than methods currently used and is therefore an important tool (see Whinney et al. 2017) to not only monitor deposition events during dredging and characterise dredge related deposition zones but to validate the overburden method and determine deposition levels caused solely by dredging.

## Chapter 7. References

- Anthony K, Fabricius KE (2000) Shifting roles of heterotrophy and autotrophy in coral energetics under varying turbidity. *J Exp Mar Bio Ecol* 252:221–253
- Anthony K, Larcombe P (2000) Coral reefs in turbid waters: sediment-induced stresses in corals and likely mechanisms of adaptation. *Proc 9th Int Coral Reef Symp I*:239–244
- Anthony K, Ridd P V, Orpin AR, Larcombe P, Lough J (2004) Temporal variation in light availability in coastal benthic habitats: Effects of clouds, turbidity, and tides. *Limnol Oceanogr* 49:2201–2211
- ANZECC (1994) National Water Quality Management Strategy Policies and Principles.
- Bak RPM (1978) Lethal and sublethal effects of dredging on reef corals. *Mar Pollut Bull*:1972–1974
- Bak RPM, Elgershuizen JHBW (1976) Patterns of Oil-Sediment rejection in corals. *Mar Biol* 37:105–113
- Baker ET, Lavelle JW (1984) The effect of particle size on the light attenuation coefficient of natural suspensions. *J Geophys Res* 89:8197
- Bégin C, Wurzbacher J, Côté IM (2013) Variation in benthic communities of eastern Caribbean coral reefs in relation to surface sediment composition. *Mar Biol* 160:343–353
- Blakeway DR (2004) Patterns of mortality from natural and anthropogenic influences in Dampier corals: 2004 cyclone and dredging impacts.
- Bolker BM (2008) Ecological models and data in R. Princeton University Press
- Bowers DG, Braithwaite KM, Nimmo-Smith WAM, Graham GW (2009) Light scattering by particles suspended in the sea: The role of particle size and density. *Cont Shelf Res* 29:1748–1755
- Bowers DG, Harker GEL, Smith PSD, Tett P (2000) Optical properties of a region of freshwater influence (the Clyde Sea). :717–726
- Brown BE, LeTissier M, Tissier MDA Le, Scoffin TP, Tudhope AW (1990) Evaluation of the environmental impact of dredging on intertidal coral reefs at Ko Phuket, Thailand, using ecological and physiological parameters. *Mar Ecol Prog ...* 65:273–281
- Bureau of Meteorology (2014) Wind data at Barrow Island Airport, Karratha Airport and Roebourne Airport 2006 to 2012.
- Burns K a. (2014) PAHs in the Great Barrier Reef Lagoon reach potentially toxic levels from coal port activities. *Estuar Coast Shelf Sci* 144:39–45
- Carter RM, Larcombe P, Dye JE, Gagan MK, Johnson DP (2009) Long-shelf sediment transport and storm-bed formation by Cyclone Winifred, central Great Barrier Reef, Australia. *Mar Geol* 267:101–113
- Chalker BE (1981) Simulating light-saturation curves for photosynthesis and calcification by reef-building corals. *Mar Biol* 63:135–141
- Chalker BE, Cox T, Dunlap WC (1984) Seasonal Changes in Primary Production and Photoadaptation by the Reef-Building Coral *Acropora Granulosa*, on the Great Barrier Reef. In: *Marine Phytoplankton and Productivity*. Springer-Verlag, p 73–87
- Chartrand KM, Bryant C V, Carter AB, Ralph PJ, Rasheed M (2016) Light thresholds to prevent dredging impacts on the Great Barrier Reef seagrass, *Zostera muelleri* ssp. *capricorni*. *Front Mar Sci* 3
- Chartrand K, Rasheed M, Sankey T (2008) Deepwater seagrass dynamics in Hay Point - Measuring variability and monitoring impacts of capital dredging. Final Report to the Ports Corporation

of Queensland.

- Chevron Australia Pty Ltd (2011a) Gorgon Gas Development and Jansz Feed Gas Pipeline : Dredging and Spoil Disposal Management and Monitoring Plan.
- Chevron Australia Pty Ltd (2011b) Gorgon Gas Development and Jansz Feed Gas Pipeline: Coastal and Marine Baseline State and Environmental Impact Report.
- Chevron Australia Pty Ltd (2011c) Gorgon Gas Development and Jansz Feed Gas Pipeline Coastal and Marine Baseline State and Environmental Impact Report : Offshore Feed Gas Pipeline System and the Marine Component of the Shore Crossing.
- Cloern JE (1987) Turbidity as a control on phytoplankton biomass and productivity in estuaries. *Cont Shelf Res* 7:1367–1381
- Condie SA, Andrewartha JR (2008) Circulation and connectivity on the Australian North West Shelf. *Cont Shelf Res* 28:1724–1739
- Condie SA, Andrewartha JR, Mansbridge J, Waring J (2006) Modelling circulation and connectivity on Australia’s North West Shelf.
- Connell JH (1997) Disturbance and recovery of coral assemblages. *Coral Reefs* 16:S101–S113
- Cooper TF, Ridd P V, Ulstrup KE, Humphrey C, Slivkoff M, Fabricius KE (2008) Temporal dynamics in coral bioindicators for water quality on coastal coral reefs of the Great Barrier Reef. *Mar Freshw Res* 59:703–716
- Cortes J, Risk M (1985) A reef under siltation stress: Cahuita, Costa Rica. *Bull Mar Sci* 36:339–356
- Dalyander PS, Butman B, Sherwood CR, Signell RP, Wilkin JL (2013) Characterizing wave- and current- induced bottom shear stress: U.S. middle Atlantic continental shelf. *Cont Shelf Res* 52:73–86
- Davies-Colley R, Smith D (2001) Turbidity, Suspended Sediment, and Water Clarity: A Review. *J Am Water Resour Assoc* 37:1085–1101
- DEC (2007) Management Plan for the Montebello/Barrow Islands Marine Conservation Reserves.
- Devlin MJ, Barry J, Mills DK, Gowen RJ, Foden J, Sivyer D, Tett P (2008) Relationships between suspended particulate material, light attenuation and Secchi depth in UK marine waters. *Estuar Coast Shelf Sci* 79:429–439
- Dodge RE, Vaisnys JR (1977) Coral Populations and Growth Patterns: Responses to Sedimentation and Turbidity Associated with Dredging. *J Mar Sci* 35:715–730
- Dollar SJ, Tribble GW (1993) Recurrent storm disturbance and recovery: a long-term study of coral communities in Hawaii. *Coral Reefs* 12:223–233
- Done TJ (1992) Effects of tropical cyclone waves on ecological and geomorphological structures on the Great Barrier Reef. *Cont Shelf Res* 12:859–872
- DSD (2016) Western Australia’s LNG: Fuelling the Future.
- Dunn R, Zigic S, Burling M, Lin H-H (2015) Hydrodynamic and Sediment Modelling within a Macro Tidal Estuary: Port Curtis Estuary, Australia. *J Mar Sci Eng* 3:720–744
- Environment and Communications References Committee (2014) Management of the Great Barrier Reef.
- EPA (2011) Environmental Assessment Guidelines for Marine Dredging Proposals.
- Erftemeijer PLA, Riegl B, Hoeksema BW, Todd P a. (2012) Environmental impacts of dredging and other sediment disturbances on corals: A review. *Mar Pollut Bull* 64:1737–1765
- Evans RD, Murray KL, Field SN, Moore JAY, Shedrawi G, Huntley BG, Fearn P, Broomhall M, McKinna LIW, Marrable D (2012) Digitise This! A Quick and Easy Remote Sensing Method to Monitor the Daily Extent of Dredge Plumes. *PLoS One* 7



- Fabricius KE, Logan M, Weeks S, Brodie J (2014) The effects of river run-off on water clarity across the central Great Barrier Reef. *Mar Pollut Bull* 84:191–200
- Falkowski PG, Dubinsky Z, Muscatine L, Porter JW (1984) Light and the bioenergetics of a symbiotic coral. *Bioscience* 34:705–709
- Fettweis M, Francken F, Eynde D Van den, Verwaest T, Janssens J, Lancker V Van (2010) Storm influence on SPM concentrations in a coastal turbidity maximum area with high anthropogenic impact (southern North Sea). *Cont Shelf Res* 30:1417–1427
- Fisher R, Stark C, Ridd P V, Jones R (2015) Spatial patterns in water quality changes during dredging in tropical environments. *PLoS One* 10:e0143309
- Flores F, Hoogenboom MO, Smith LD, Cooper TF, Abrego D, Negri AP (2012) Chronic exposure of corals to fine sediments: Lethal and sub-lethal impacts. *PLoS One* 7
- Foster T, Corcoran E, Erftemeijer P, Fletcher C, Peirs K, Dolmans C, Smith A, Yamamoto H, Jury M (2010) Dredging and port construction around coral reefs. *PIANC Environ Comm Rep No 108*
- Gagan MK, Chivas AR, Herczeg AL (1990) Shelf-wide erosion, deposition, and suspended sediment transport during cyclone Winifred, central Great Barrier Reef, Australia. *J Sediment Petrol* 60:456–470
- Gallegos CL (2001) Calculating Optical Water Quality Targets to Restore and Protect Submersed Aquatic Vegetation: Overcoming Problems in Partitioning the Diffuse Attenuation Coefficient for Photosynthetically Active Radiation. *Estuaries* 24:381
- Gattuso J-P, Gentili B, Duarte CM, Kleypas JA, Middelburg JJ, Antoine D (2006) Light availability in the coastal ocean: impact on the distribution of benthic photosynthetic organisms and contribution to primary production. *Biogeosciences Discuss* 3:895–959
- GHD (2009a) Environmental Impact Statement Townsville Marine Precinct Project.
- GHD (2009b) Report for Western Basin Dredging and Disposal Project: Marine Ecology Assessment. :171
- Gilmour JP, Cooper TF, Fabricius KE, Smith LD (2006) Early warning indicators of change in the condition of corals and coral communities in response to key anthropogenic stressors in the Pilbara, Western Australia. *Rangelands*:108
- Grant W, Madsen O (1986) The continental-shelf bottom boundary layer. *Annu Rev Fluid Mech*:265–305
- Graus RR, Graus RR, Macintyre IG (1989) The zonation patterns of Caribbean coral reefs as controlled by wave and light energy input, bathymetric setting and reef morphology: computer simulation experiments. *Coral reefs* 8:9–18
- Green M (1995) Storm sediment transport: observations from the British North Sea shelf. *Cont Shelf Res* 15:889–912
- Guillén J, Bourrin F, Palanques A, Durrieu de Madron X, Puig P, Buscail R (2006) Sediment dynamics during wet and dry storm events on the Têt inner shelf (SW Gulf of Lions). *Mar Geol* 234:129–142
- Hallock P, Schlager W (1986) Nutrient excess and the demise of coral reefs and carbonate platforms. *Palaios* 1:389–398
- Harmelin-Vivien ML, Laboute P (1986) Catastrophic impact of hurricanes on atoll outer reef slopes in the Tuamotu (French Polynesia). *Coral Reefs* 5:55–62
- Hubbert GD, Oliver S, Rouphael T (2005) Measurement and Model Prediction of Ocean Currents and Tides at Barrow Island.
- Humphrey C, Weber M, Lott C, Cooper TF, Fabricius KE (2008) Effects of suspended sediments,

- dissolved inorganic nutrients and salinity on fertilisation and embryo development in the coral *Acropora millepora* (Ehrenberg, 1834). *Coral Reefs* 27:837–850
- In-Situ Marine Optics (2011) MODIS Algorithm Development and Sediment Transport Model Validation: Field Data Collection Report.
- Jewson DH, Talling JF, Dring MJ, Tilzer MM, Heaney SI, Cunningham C (1984) Measurement of photosynthetically available radiation in freshwater: comparative tests of some current instruments used in studies of primary production. *J Plankton Res* 6:259–273
- Jing L, Ridd P V (1996) Wave-current bottom shear stresses and sediment resuspension in Cleveland Bay, Australia. *Coast Eng* 29:169–186
- Jonasz M, Fournier G (2007) *Light Scattering by Particles in Water: Theoretical and Experimental Foundations*. 1st
- Jones R, Bessell-Browne P, Fisher R, Klonowski W, Slivkoff M (2016) Assessing the impacts of sediments from dredging on corals. *Mar Pollut Bull* 102:9–29
- Jones R, Fisher R, Stark C, Ridd P V (2015) Temporal Patterns in Seawater Quality from Dredging in Tropical Environments. *PLoS One* 10:e0137112
- Jones R, Ricardo GF, Negri AP (2015) Effects of sediments on the reproductive cycle of corals. *Mar Pollut Bull* 100:13–33
- Kettle B, Dalla Pozza R, Collins J (2001) A Review of the Impacts of Dredging in Cleveland Bay, and Research Priorities for the Next Decade.
- Kinzie RA (1973) The zonation of west indian gorgonians. *Bull Mar Sci* 23:93–155
- Kirk JTO (1977a) Use of a quanta meter to measure attenuation and underwater reflectance of photosynthetically active radiation in some inland and coastal south-eastern Australian waters. *Mar Freshw Res* 28:9
- Kirk JTO (1977b) Attenuation of light in natural waters. *Mar Freshw Res*:497–508
- Kirk JTO (1985) Effects of suspensoids (turbidity) on penetration of solar radiation in aquatic ecosystems. *Hydrobiologia* 208:195–208
- Kirk JTO (2010) *Light and Photosynthesis in Aquatic Ecosystems*. Cambridge University Press, Cambridge
- Larcombe P, Ridd P V, Prytz A, Wilson B (1995) Factors controlling suspended sediment on inner-shelf coral reefs, Townsville, Australia. *Coral Reefs* 14:163–171
- Larcombe P, Woolfe KJ (1999) Terrigenous sediments as influences upon Holocene nearshore coral reefs, central Great Barrier Reef, Australia. *Aust J Earth Sci* 46:141–154
- Lawson S, Wiberg P, McGlathery K, Fugate D (2007) Wind-driven sediment suspension controls light availability in a shallow coastal lagoon. *Estuaries and Coasts* 30:102–112
- Liu Y, San Liang X, Weisberg RH (2007) Rectification of the Bias in the Wavelet Power Spectrum. *J Atmos Ocean Technol* 24:2093–2102
- Luger SA, Ballegooyen RC van (2000) Predictive Modelling Of Hydrodynamics And Marine Water Quality: Three Applications Along The South African Coastline. *WIT Trans Ecol Environ* 43
- Luger SA, Schoonees JS, Mocke GP, Smit F (1998) PREDICTING AND EVALUATING TURBIDITY CAUSED BY DREDGING IN THE ENVIRONMENTALLY SENSITIVE SALDANHA BAY
- Macdonald RK, Ridd P V, Whinney JC, Larcombe P, Neil DT (2013) Towards environmental management of water turbidity within open coastal waters of the Great Barrier Reef. *Mar Pollut Bull* 74:82–94
- Madden RA, Julian PR (1994) Observations of the 40-50-day tropical oscillation - a review. *Mon Weather Rev* 122:814–837

- Margvelashvili N, Andrewartha JR, Condie SA, Herzfeld M, Parslow J, Sakov P, Waring J (2006) Modelling suspended sediment transport on Australia's North West Shelf.
- Marszalek D (1981) Impact of dredging on a subtropical reef community, southeast Florida, USA. Proc Fourth Int Coral Reef Symp Manila
- Masselink G, Hughes MG, Knight J (2011) Introduction to coastal processes & geomorphology . 2nd
- Mathworks (2016a) Optimization Toolbox™ Users Guide R2016b.
- Mathworks (2016b) Rational polynomials.
- McCook L, Schaffelke B, Apte A, Brinkman R, Brodie J, Erftemeijer P, Eyre B, Hoogerwerf F, Irvine I, Jones R, King B, Marsh H, Masini R, Morton R, Pitcher R, Rasheed M, Sheaves M, Symonds A, M.St.J W (2015) Synthesis of current knowledge of the biophysical impacts of dredging and disposal on the Great Barrier Reef: report of an independent panel of experts. Gt Barrier Reef Mar Park Authority, Townsv
- McKinnon a. D, Meekan MG, Carleton JH, Furnas MJ, Duggan S, Skirving W (2003) Rapid changes in shelf waters and pelagic communities on the southern Northwest Shelf, Australia, following a tropical cyclone. Cont Shelf Res 23:93–111
- Mobley CD (2001) Radiative Transfer in the Ocean.
- Nelson D, Smith W (1991) Sverdrup revisited: Critical depths, maximum chlorophyll levels, and the control of Southern Ocean productivity by the irradiance-mixing regime. Limnol Ocean 36:1650–1661
- Newell RC, Seiderer LJ, Hitchcock DR (1998) The impact of dredging works in coastal waters: a review of the sensitivity to disturbance and subsequent recovery of biological resources on the sea bed. Oceanogr Mar Biol An Annu Rev 36:127–178
- NQBP (2015) Port of Hay Point Handbook.
- Ogston AS, Storlazzi CD, Field ME, Presto MK (2004) Sediment resuspension and transport patterns on a fringing reef flat, Molokai, Hawaii. Coral Reefs 23:559–569
- Onuf CP (1994) Seagrasses, dredging and light in Laguna Madres, Texas, USA. Estuar Coast Shelf Sci 39:75–91
- Orpin a. R, Ridd P V, Stewart LK (1999) Assessment of the relative importance of major sediment-transport mechanisms in the central Great Barrier Reef lagoon. Aust J Earth Sci 46:883–896
- Orpin AR, Ridd P V, Thomas S, Anthony K, Marshall P, Oliver J (2004) Natural turbidity variability and weather forecasts in risk management of anthropogenic sediment discharge near sensitive environments. Mar Pollut Bull 49:602–612
- Pattiaratchi C (2011) Coastal Tide Gauge Observations: Dynamic Processes Present in the Fremantle Record . Oper Oceanogr 21st Century :185–202
- Pattiaratchi CB, Collins MB (1984) Sediment transport under waves and tidal currents: A case study from the northern Bristol Channel, U.K . Mar Geol 56:27–40
- Paulson CA, Simpson JJ (1977) Irradiance measurements in the upper ocean. J Phys Oceanogr 7:952–956
- Pearce A, Buchan S, Chiffings T, Adamo ND, Fandry C, Mills D, Phillips R, Simpson C (2003) A review of the oceanography of the Dampier Archipelago , Western Australia.
- Piniak GA, Storlazzi CD (2008) Diurnal variability in turbidity and coral fluorescence on a fringing reef flat: Southern Molokai, Hawaii. Estuar Coast Shelf Sci 77:56–64
- Presto MK, Ogston AS, Storlazzi CD, Field ME (2006) Temporal and spatial variability in the flow and dispersal of suspended-sediment on a fringing reef flat, Molokai, Hawaii. Estuar Coast

Shelf Sci 67:67–81

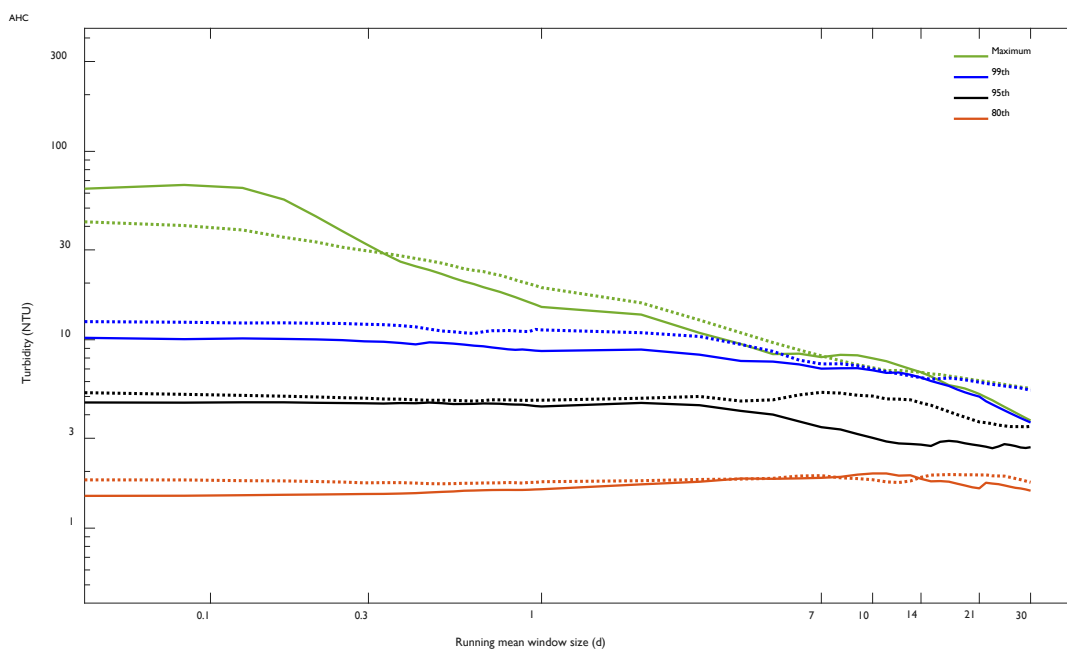
- Ridd P V, Day G, Thomas S, Harradence J, Fox D, Bunt J, Renagi O, Jago C (2001) Measurement of sediment deposition rates using an optical backscatter sensor. *Estuar Coast Shelf Sci* 52:155–163
- Ridd P V, Larcombe P (1994) Biofouling control for optical backscatter suspended sediment sensors. 116:255–258
- Riddle MJ (1988) Cyclone and bioturbation effects on sediments from coral reef lagoons. *Estuar Coast Shelf Sci* 27:687–695
- Riegl B (1995) Effects of sand deposition on scleractinian and alcyonacean corals. *Mar Biol* 121:517–526
- Rijn LC van (1986) Mathematical Modeling of Suspended Sediment in Nonuniform Flows. *J Hydraul Eng* 112:433–455
- Rogers CS (1990) Responses of coral reefs and reef organisms to sedimentation. *Mar Ecol Prog Ser* Oldend 62:185–202
- Saulquin B, Hamdi A, Gohin F, Populus J, Mangin A, Fanton O (2013) Estimation of the diffuse attenuation coefficient  $K_d$  PAR using MERIS and application to seabed habitat mapping. *Remote Sens Environ* 128:224–233
- Schanz F (1985) Vertical light attenuation and phytoplankton development in Lake Ziirichl. *Limnol Ocean* 30:299–310
- Shinn EA (1976) Coral reef recovery in Florida and the Persian Gulf . *Environ Geol* 1:241–254
- Smith RC, Baker KS (1978) The bio-optical state of ocean waters and remote sensing. *Limnol Oceanogr* 23:247–259
- Sofonia JJ, Unsworth RKF (2010) Development of water quality thresholds during dredging for the protection of benthic primary producer habitats. *J Environ Monit* 12:159–163
- Soulsby RL, Clarke S (2005) Bed Shear-stresses Under Combined Waves and Currents on Smooth and Rough Beds.
- Soulsby RL, Damgaard JS (2005) Bedload sediment transport in coastal waters. *Coast Eng* 52:673–689
- Spearman J (2015) A review of the physical impacts of sediment dispersion from aggregate dredging. *Mar Pollut Bull* 94:260–277
- Stafford-Smith M (1993) Sediment-rejection efficiency of 22 species of Australian scleractinian corals. *Mar Biol* 243:229–243
- Stoddart DR (1969) Ecology and morphology of recent coral reefs. *Biol Rev* 44:433–498
- Stoddart JA, Anstee S (2004) Water quality, plume modelling and tracking before and during dredging in Mermaid Sound, Dampier, Western Australia. *Corals Dampier Harb Their Surviv Reprod Dur Dredg Programs 2004*
- Storlazzi CD, Norris BK, Rosenberger KJ (2015) The influence of grain size, grain color, and suspended-sediment concentration on light attenuation: Why fine-grained terrestrial sediment is bad for coral reef ecosystems. *Coral Reefs*
- Storlazzi CD, Ogston AS, Bothner MH, Field ME, Presto M. (2004) Wave- and tidally-driven flow and sediment flux across a fringing coral reef: Southern Molokai, Hawaii. *Cont Shelf Res* 24:1397–1419
- Sverdrup H (1953) On conditions for the vernal blooming of phytoplankton. *J du Cons* 18:287–295
- Swanson JC, Isaji T, Galagan C (2007) Modeling the ultimate transport and fate of dredge-induced suspended sediment transport and deposition. In: *Proceedings of the 18th World Dredging*

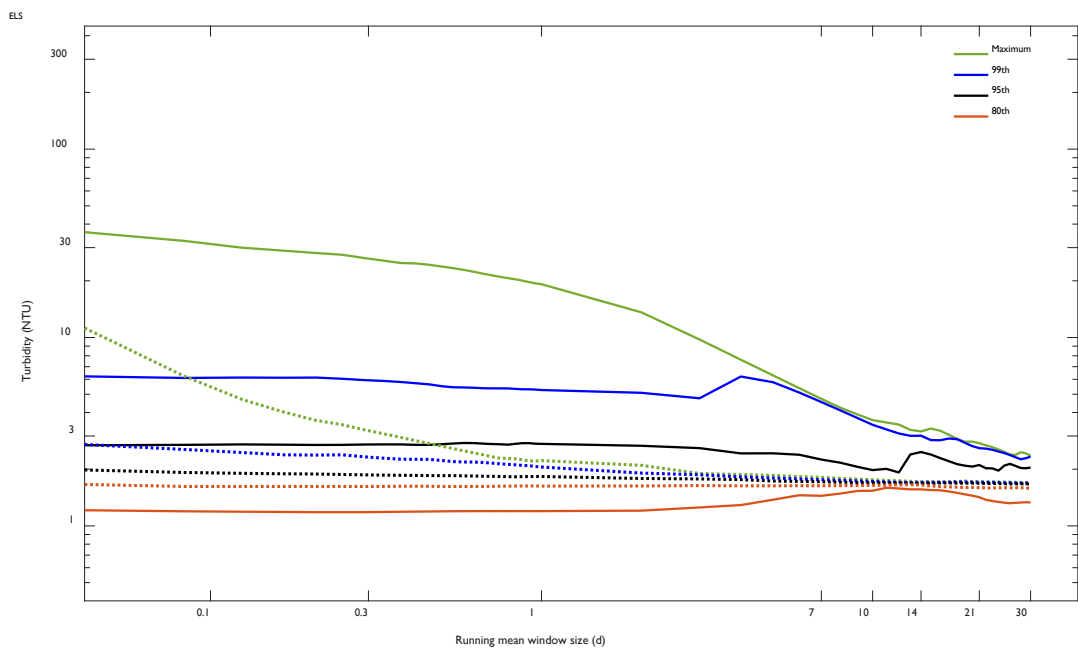
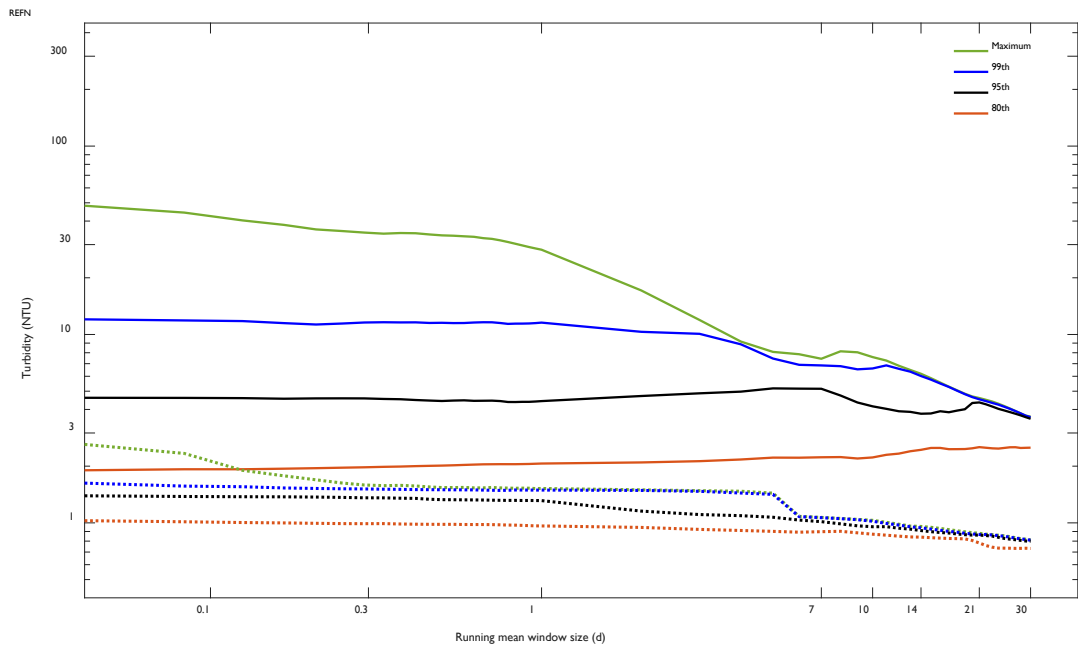
Congress. Florida

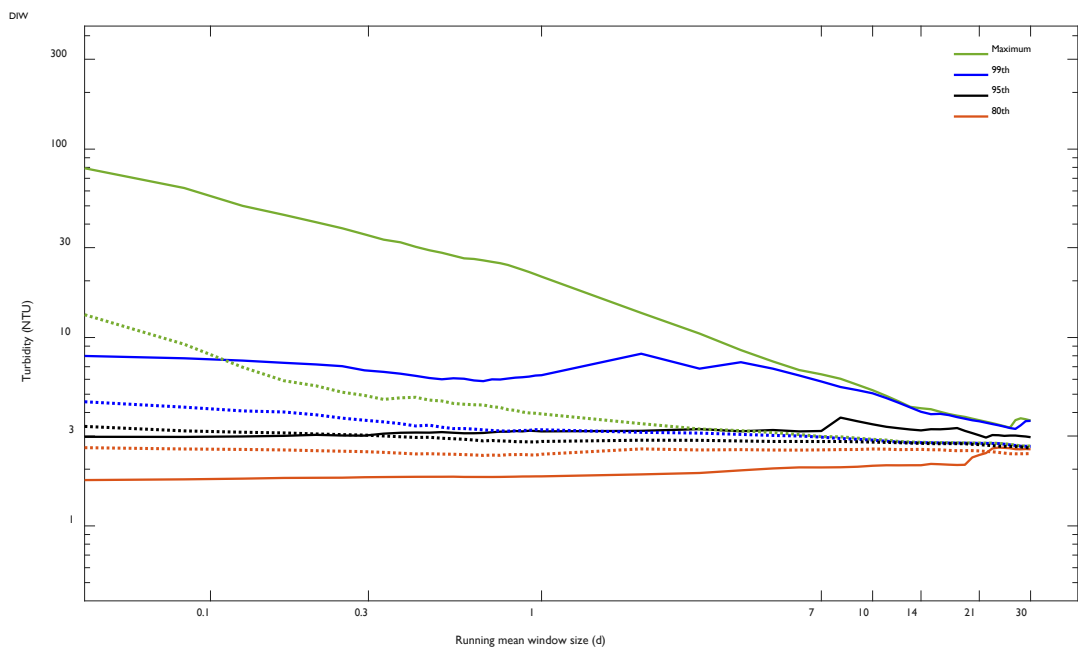
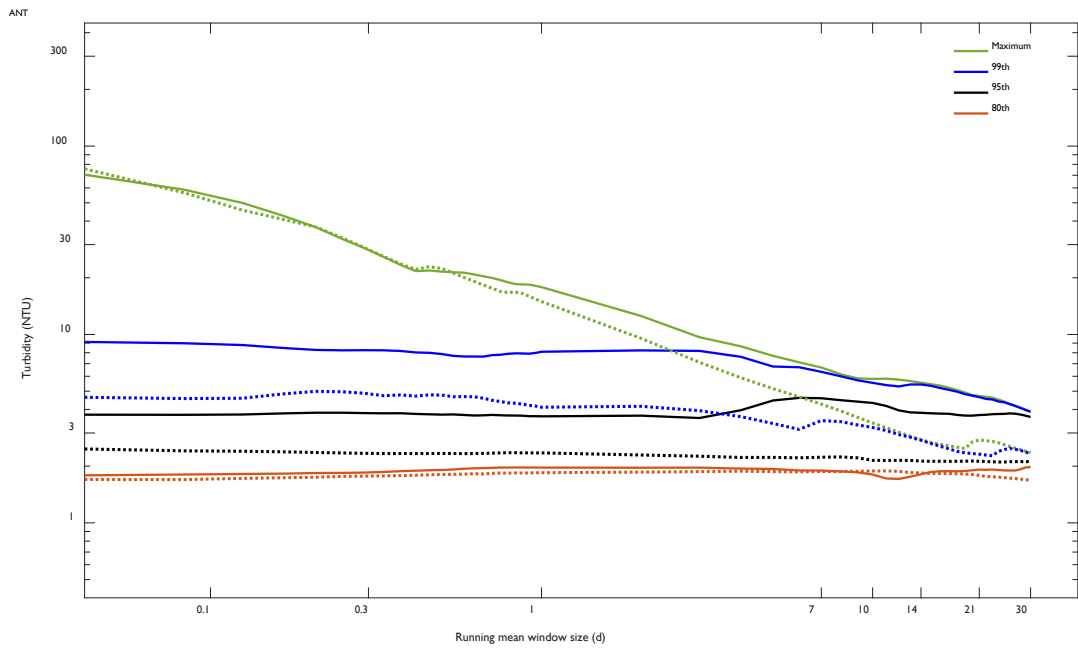
- Te FT (1997) Turbidity and its effect on corals: A Model using the extinction coefficient (K) of photosynthetic active radiation (PAR).
- Thomas S, Ridd P V (2005) Field assessment of innovative sensor for monitoring of sediment accumulation at inshore coral reefs. *Mar Pollut Bull* 51:470–480
- Thomas S, Ridd P V, Renagi O (2003) Laboratory investigation on the effect of particle size, water flow and bottom surface roughness upon the response of an upward-pointing optical backscatter sensor to sediment accumulation. *Cont Shelf Res* 23:1545–1557
- Tomascik T, Suharsono, Mah AJ (1994) Case histories: a historical perspective of the natural and anthropogenic impacts in the Indonesian Archipelago with a focus on the Kepulauan Seribu, Java Sea. *Proc Colloq Glob Asp Coral reefs Heal Hazards Hist* 1993:304–310
- Torrence C, Compo GP (1995) A Practical Guide to Wavelet Analysis.
- Torres JL (2001) Impacts of sedimentation on the growth rates of *Montastraea annularis* in southwest Puerto Rico . *Bull Mar Sci* 69:631–637
- VanSenden D, Taylor D, Branson P, Harbour D (2013) Realtime Turbidity Monitoring and Modelling for Dredge Impact Assessment in Darwin Harbour. In: *Coasts and Ports 2013: 21st Australasian Coastal and Ocean Engineering Conference and the 14th Australasian Port and Harbour Conference*. Engineers Australia
- Verspecht F, Pattiaratchi CB (2010) On the significance of wind event frequency for particulate resuspension and light attenuation in coastal waters . *Cont Shelf Res* 30:1971–1982
- Waltham N, McKenna S, York P, Devlin MJ, Campbell S, Rasheed M, Silva E Da, Petus C, Ridd P (2015) Port of Mackay and Hay Point Ambient Marine Water Quality Monitoring Program (July 2014 to July 2015).
- Weber M, Beer D de, Lott C, Polerecky L, Kohls K, Abed RM, Ferdelman TG, Fabricius KE (2012) Mechanisms of damage to corals exposed to sedimentation. *Proc Natl Acad Sci* 109:E1558–E1567
- Weeks AR, Simpson JH, Bowers D (1993) The relationship between concentrations of suspended particulate material and tidal processes in the Irish Sea . *Cont Shelf Res* 13:1325–1334
- Whinney JC (2007) Predicting Suspended Sediment Concentrations on Coral Reefs Using Meteorological Data. James Cook University, Townsville
- Whinney J, Jones R, Duckworth A, Ridd P (2017) Continuous in situ monitoring of sediment deposition in shallow benthic environments. *Coral Reefs* 36:521–533
- Wolanski E, Fabricius KE, Spagnol S, Brinkman RM (2005) Fine sediment budget on an inner-shelf coral-fringed island, Great Barrier Reef of Australia. *Estuar Coast Shelf Sci* 65:153–158
- Woodley JD, Chornesky EA, Clifford PA, Kaufman LS, Knowlton N, Lang JC, Pearson MP, Porter JW, Rooney MC, Rylaarsdam KW, Tunnicliffe VJ, Wahle CM, Wulff JL, Dallmeyer MD, Jupp BP, Neigel J, Sides EM (1981) Hurricane Allen's Impact on Jamaican Coral Reefs . *Sci* 214:749–755
- Wright LD (1995) Morphodynamics of Inner Continental Shelves. *CRC Marine Science Series*
- Zhang C (2005) Madden-Julian oscillation. *Rev Geophys*:1–36

## Appendix A Turbidity running mean percentiles Barrow Island

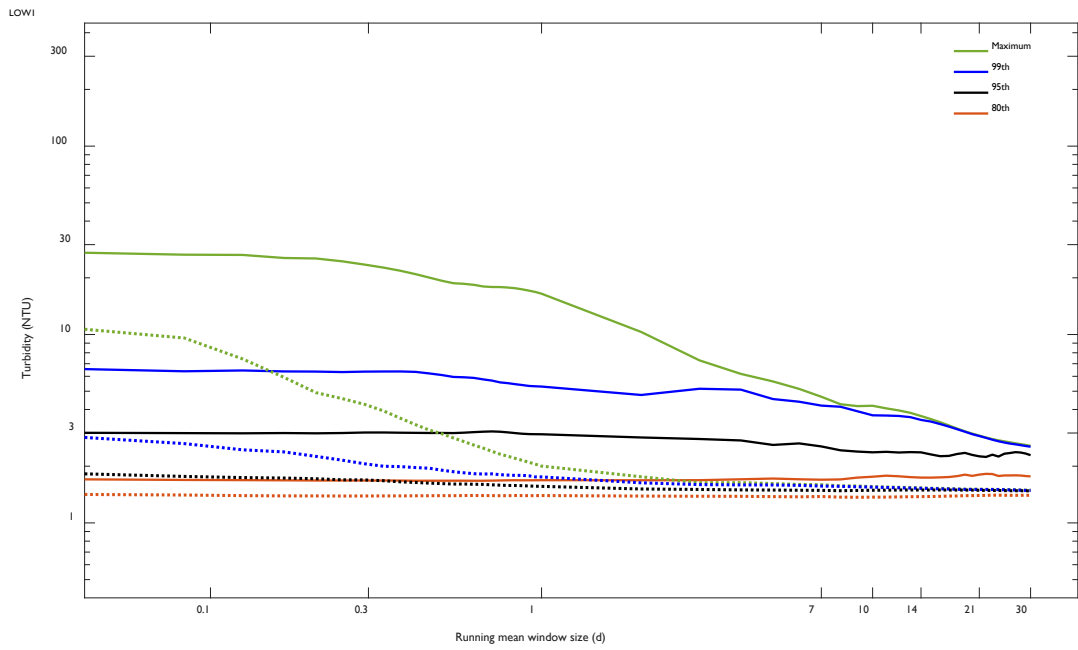
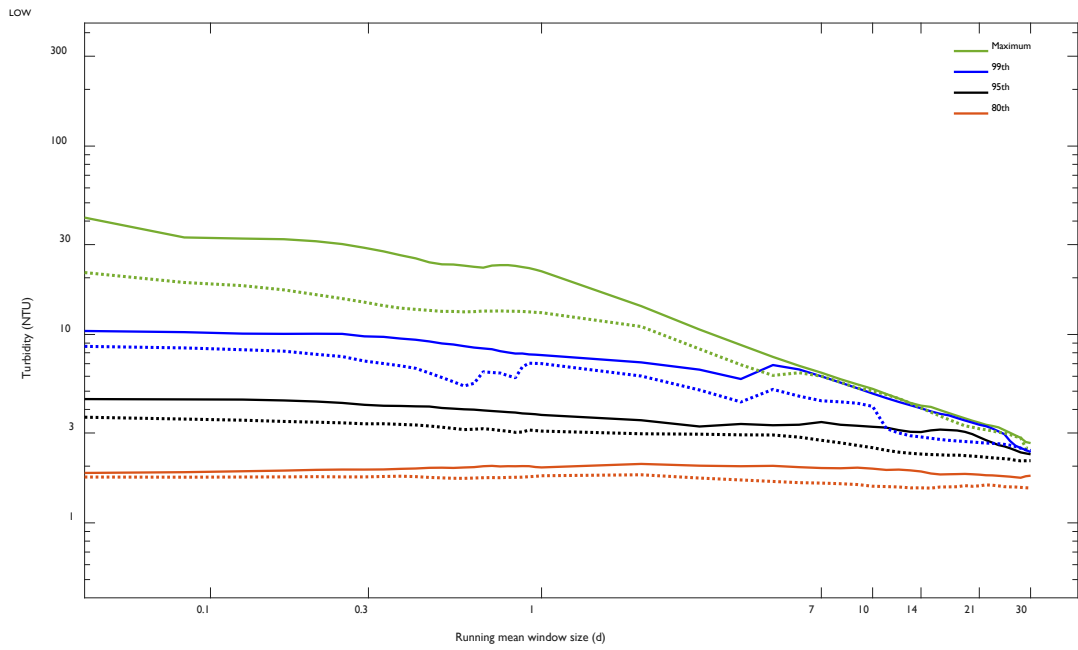
The remaining running mean turbidity figures from the other Barrow Island sites are presented here. Running mean figures for representative sites are shown and discussed in Chapter 3.

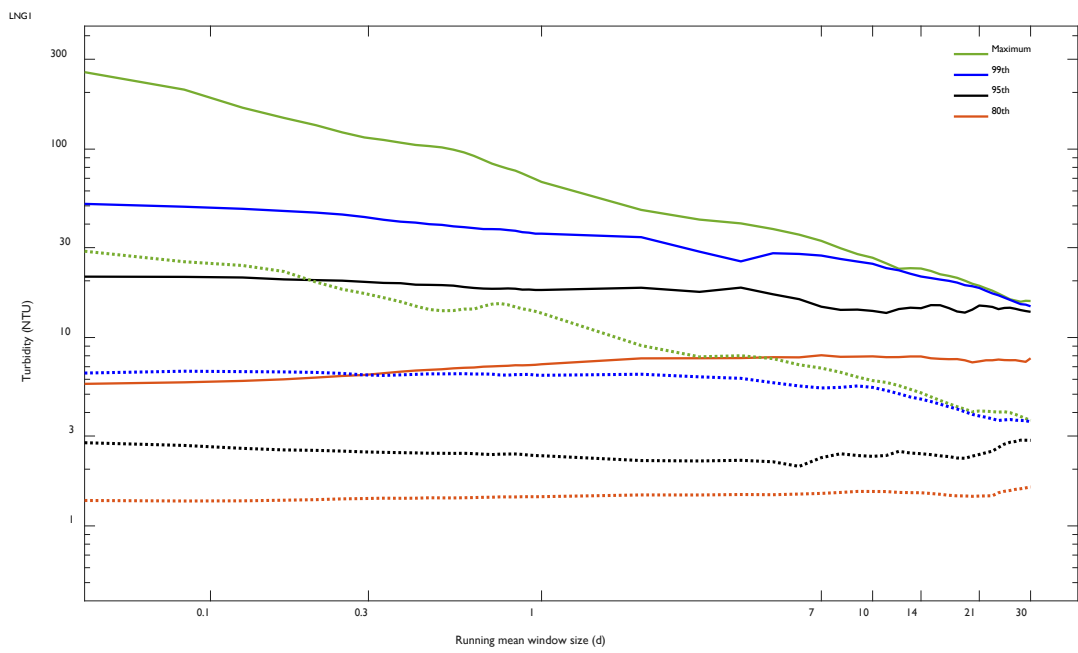
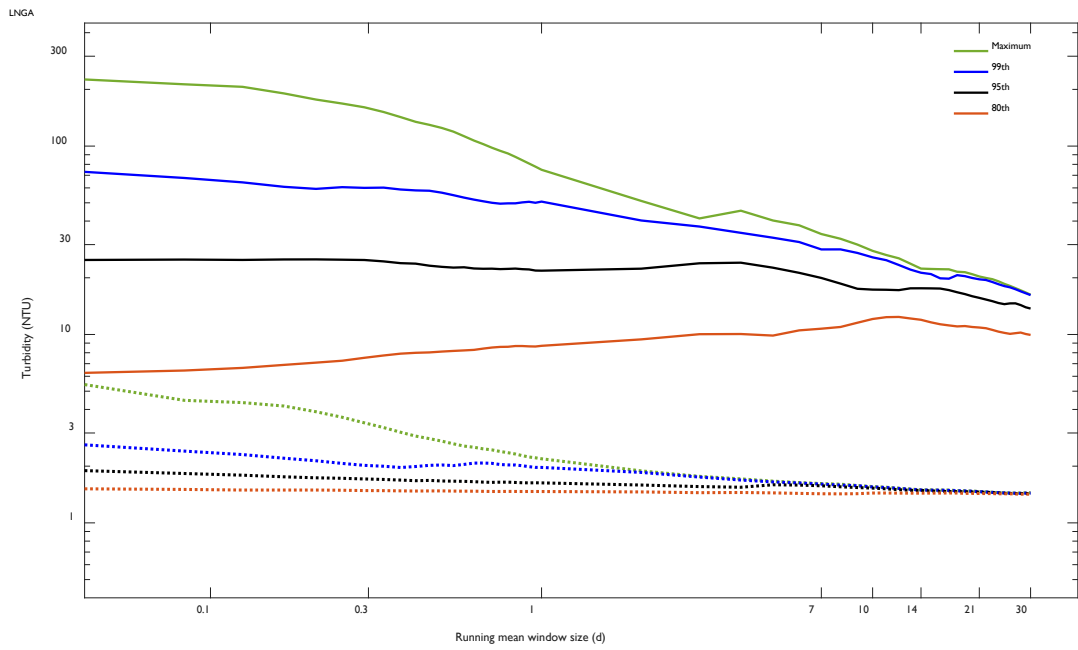


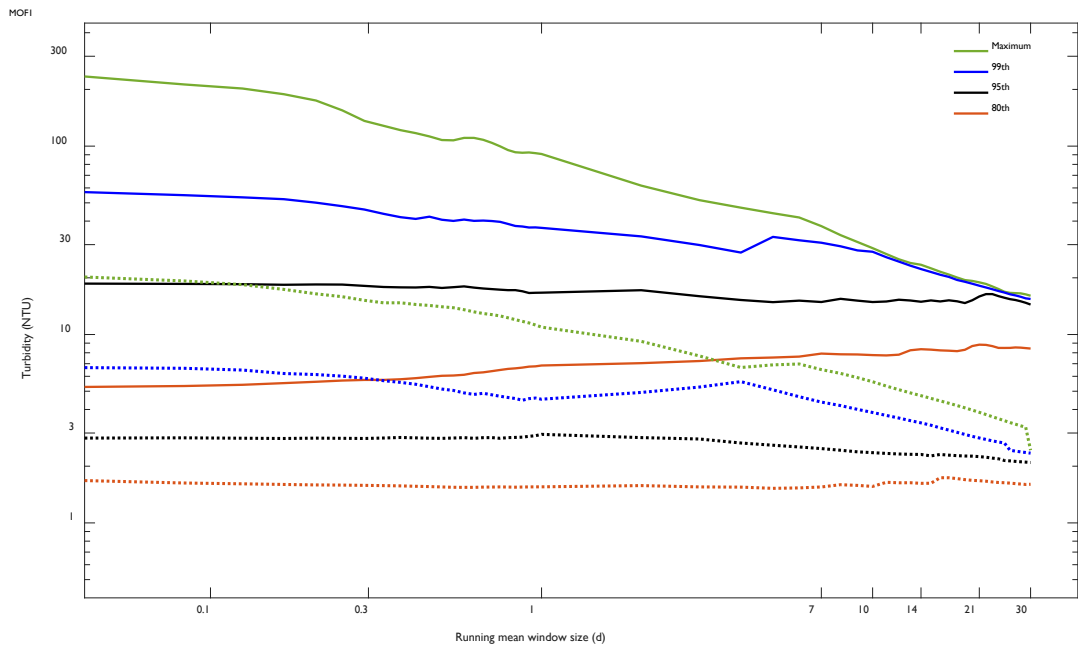
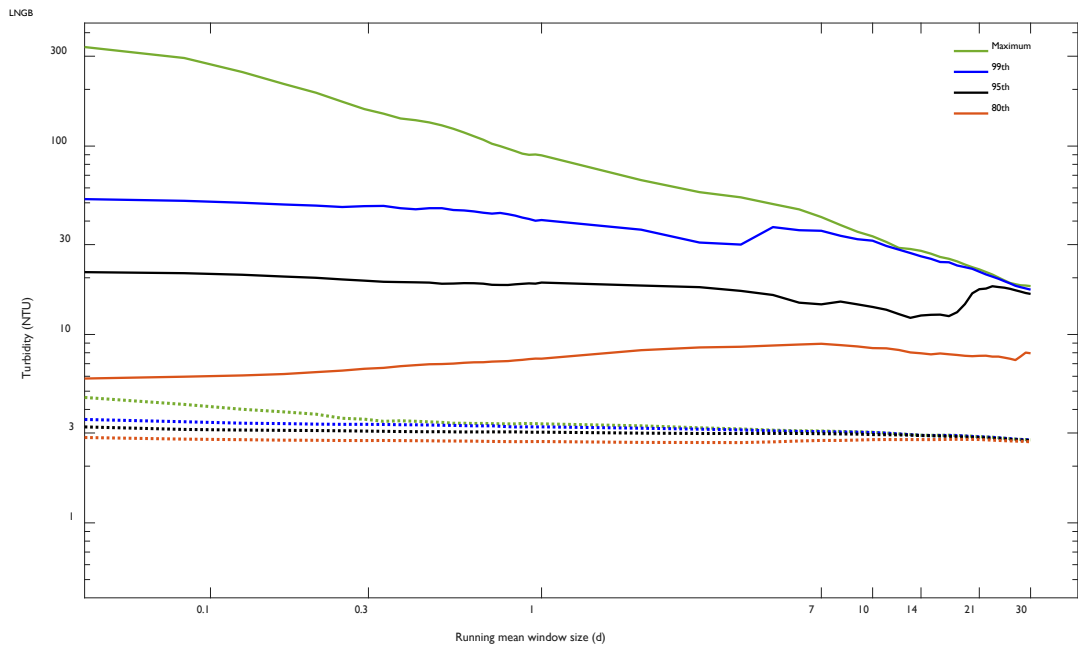


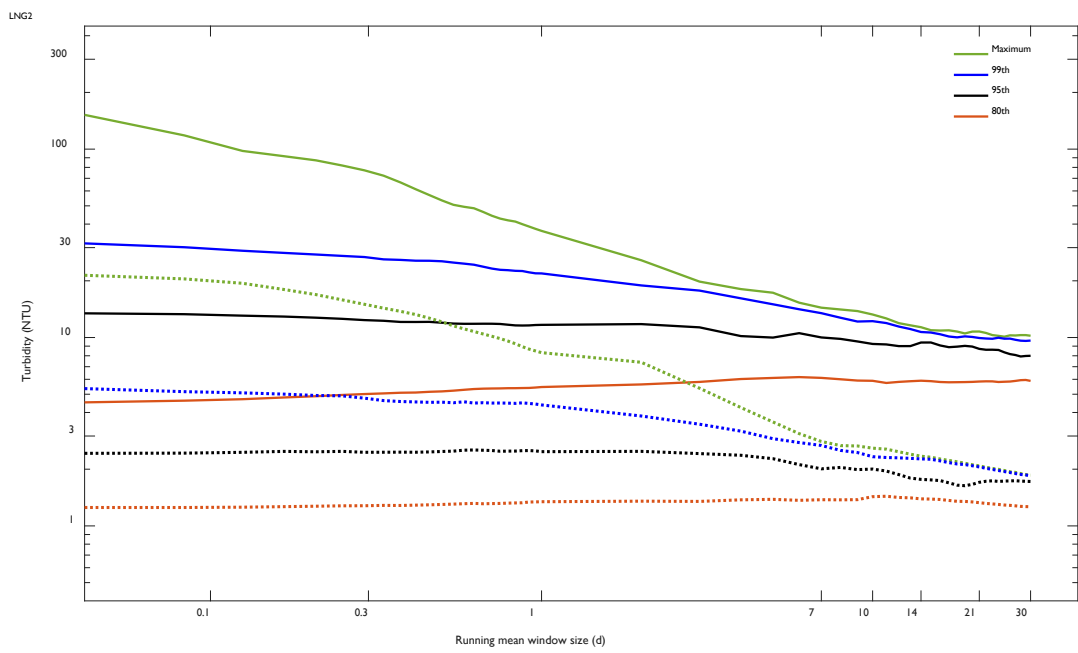
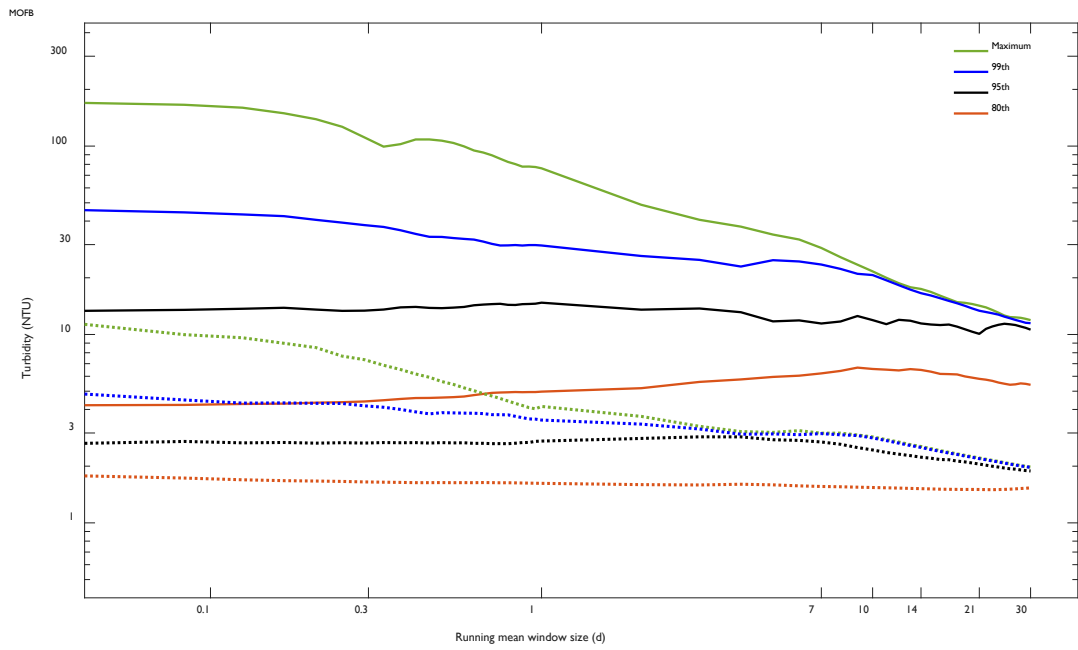


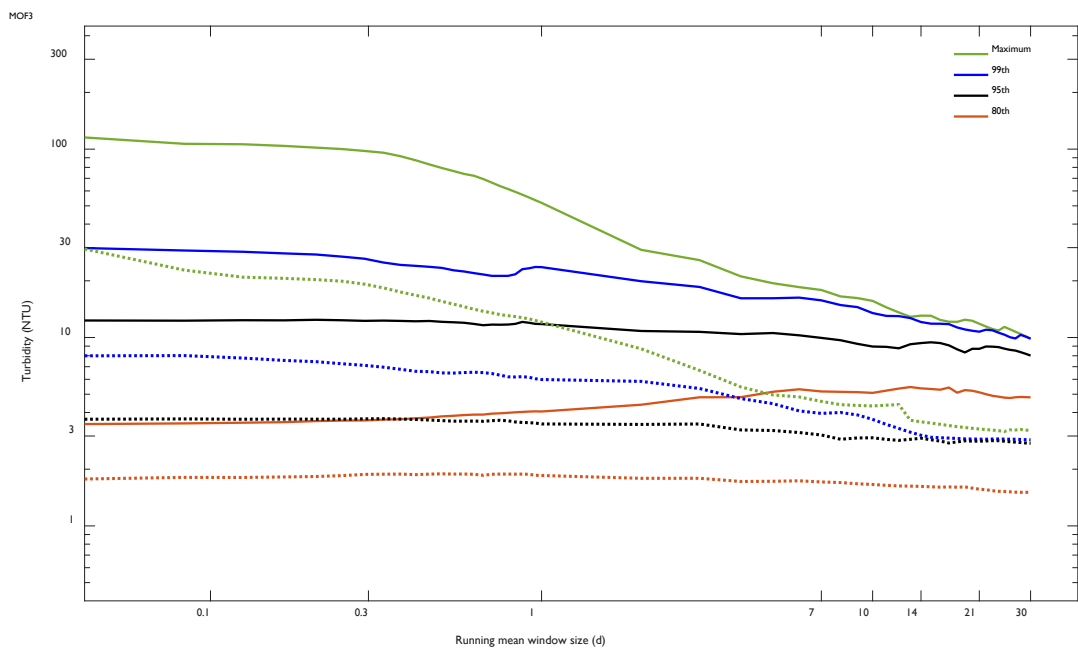
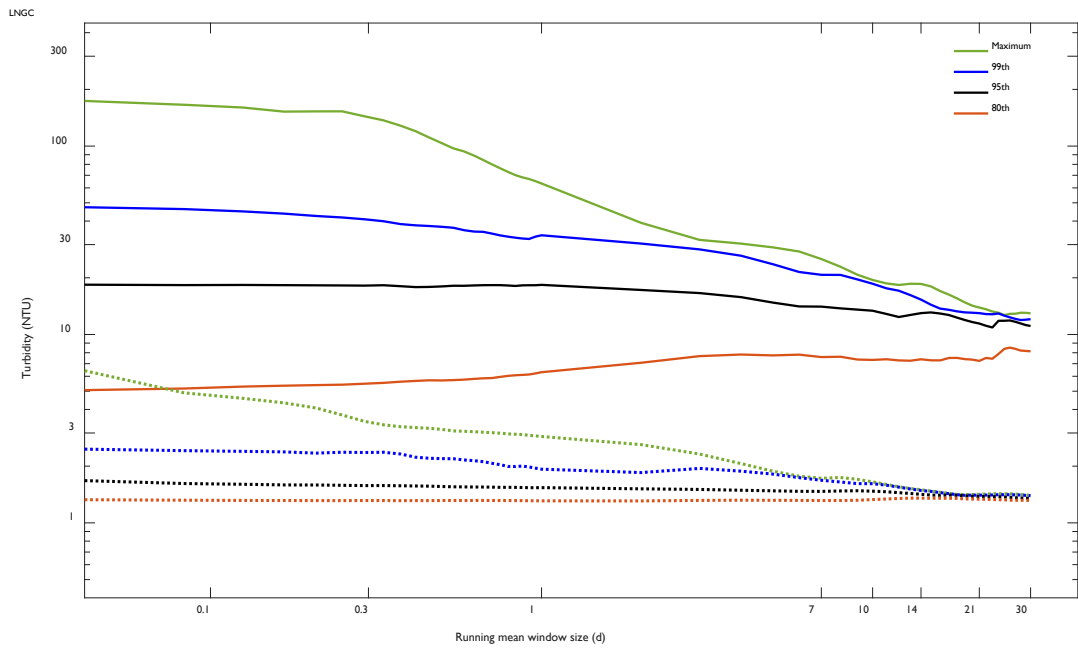


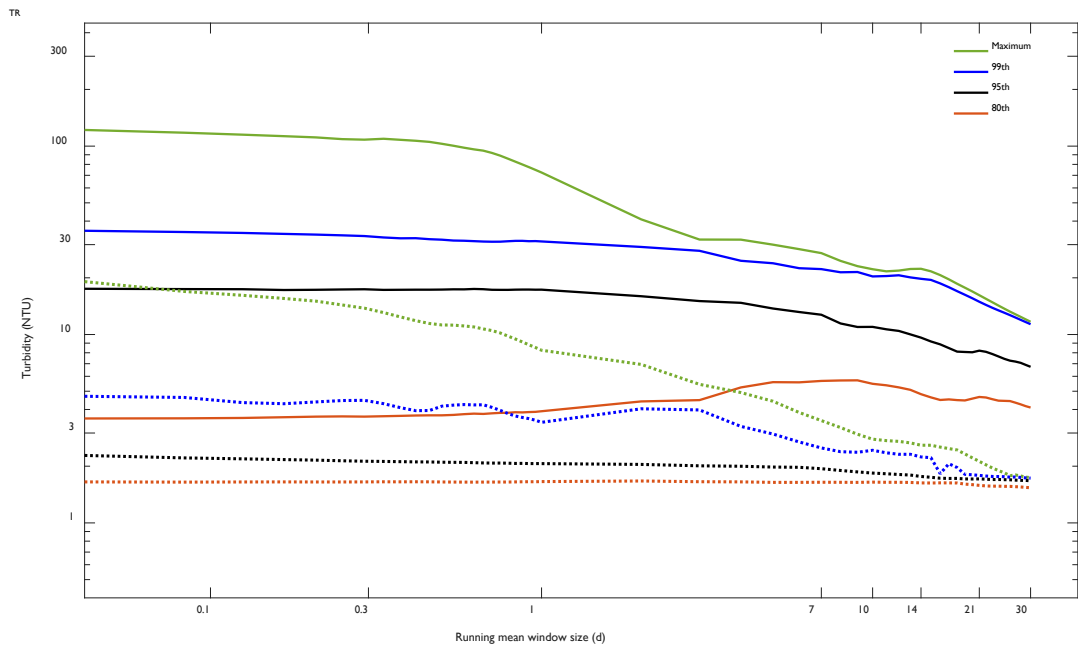
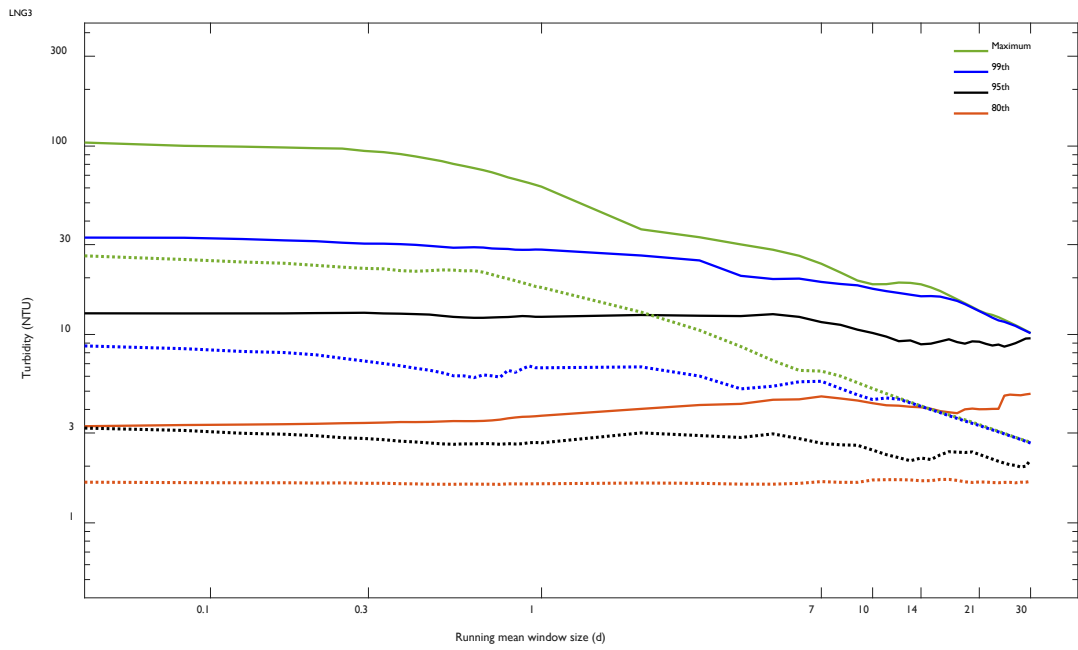


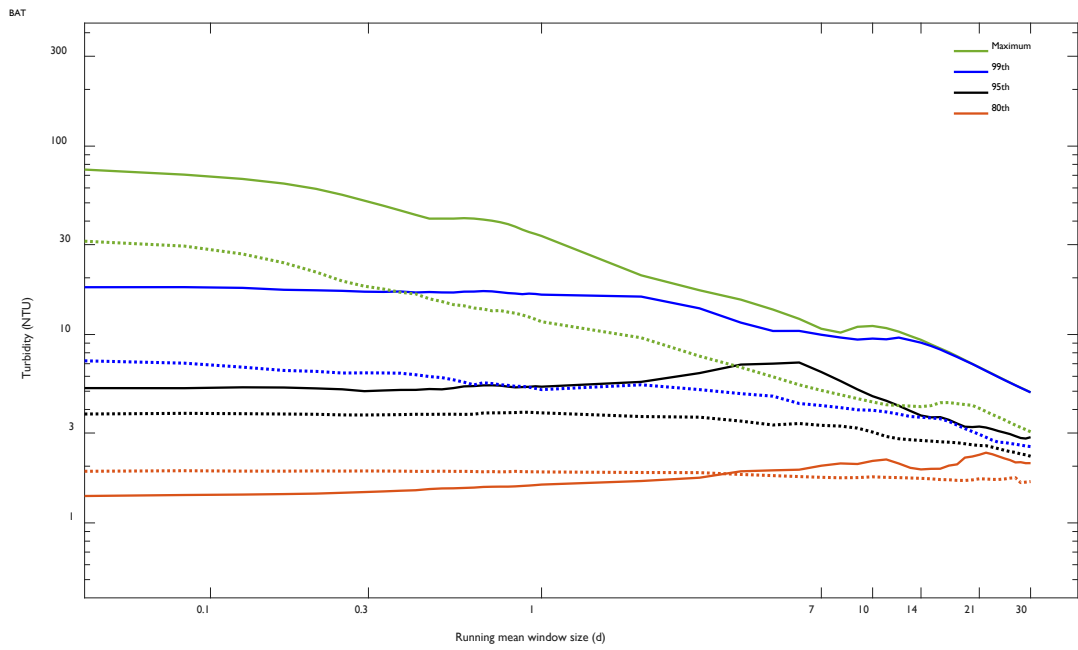
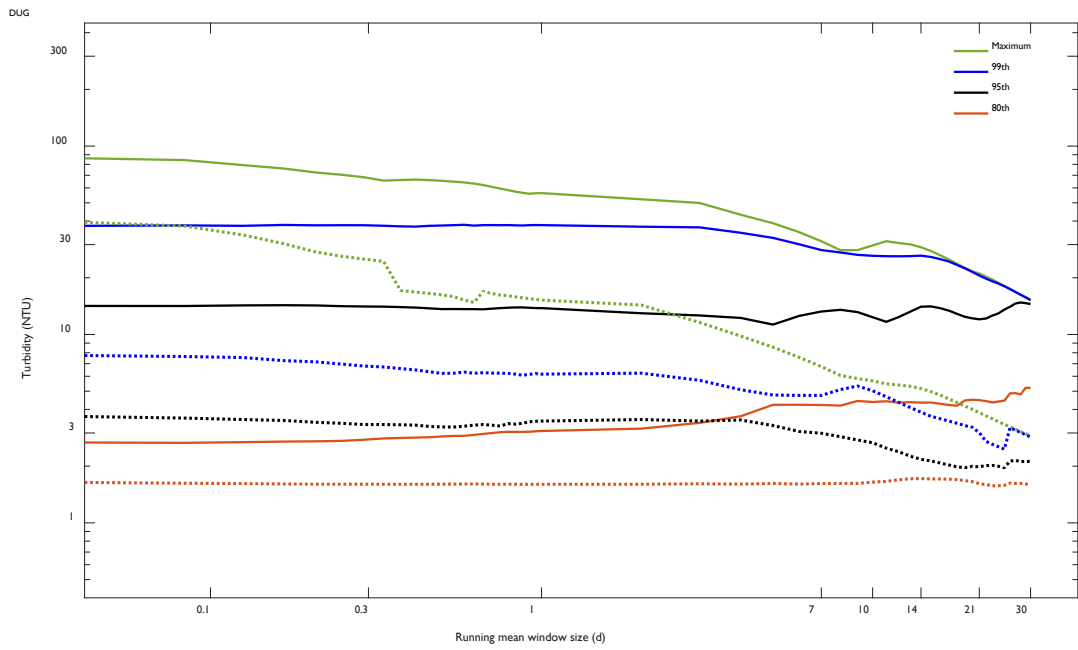












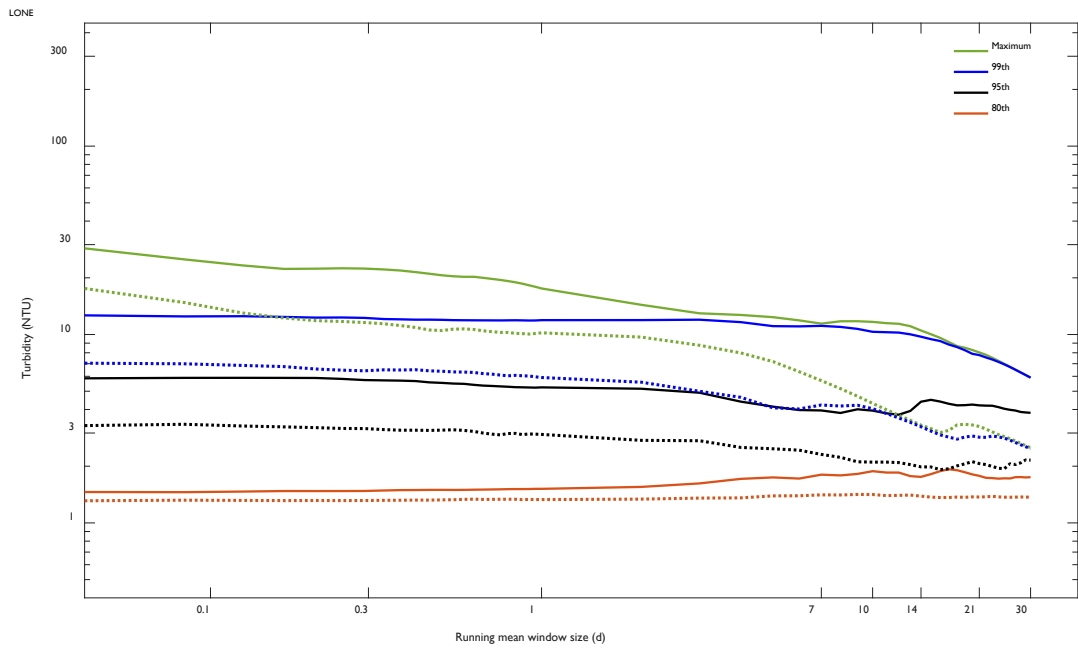
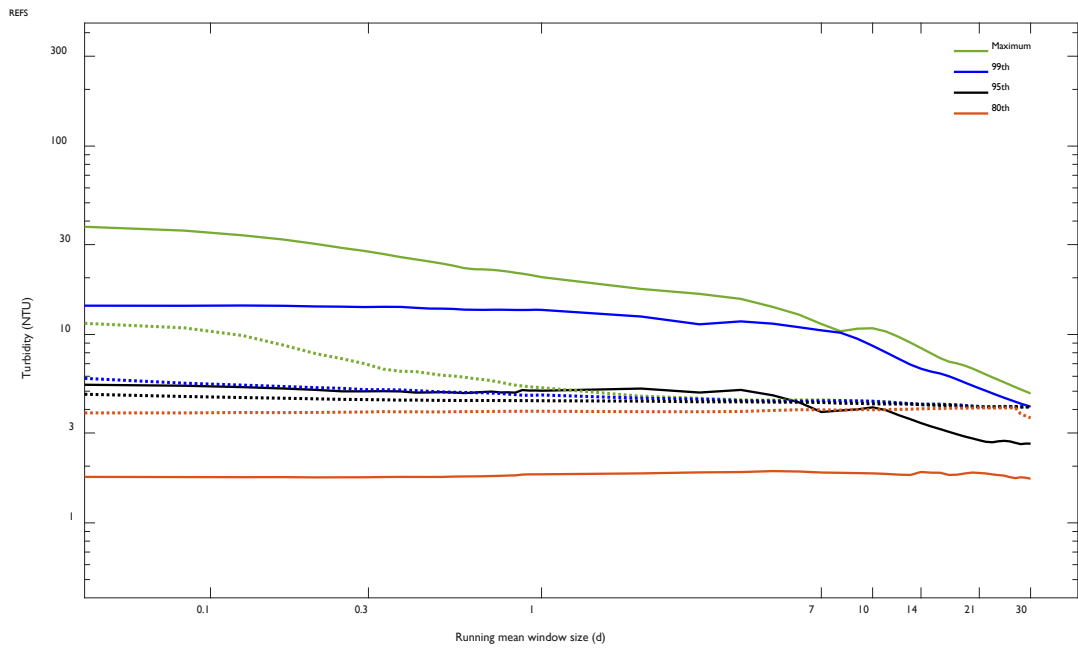


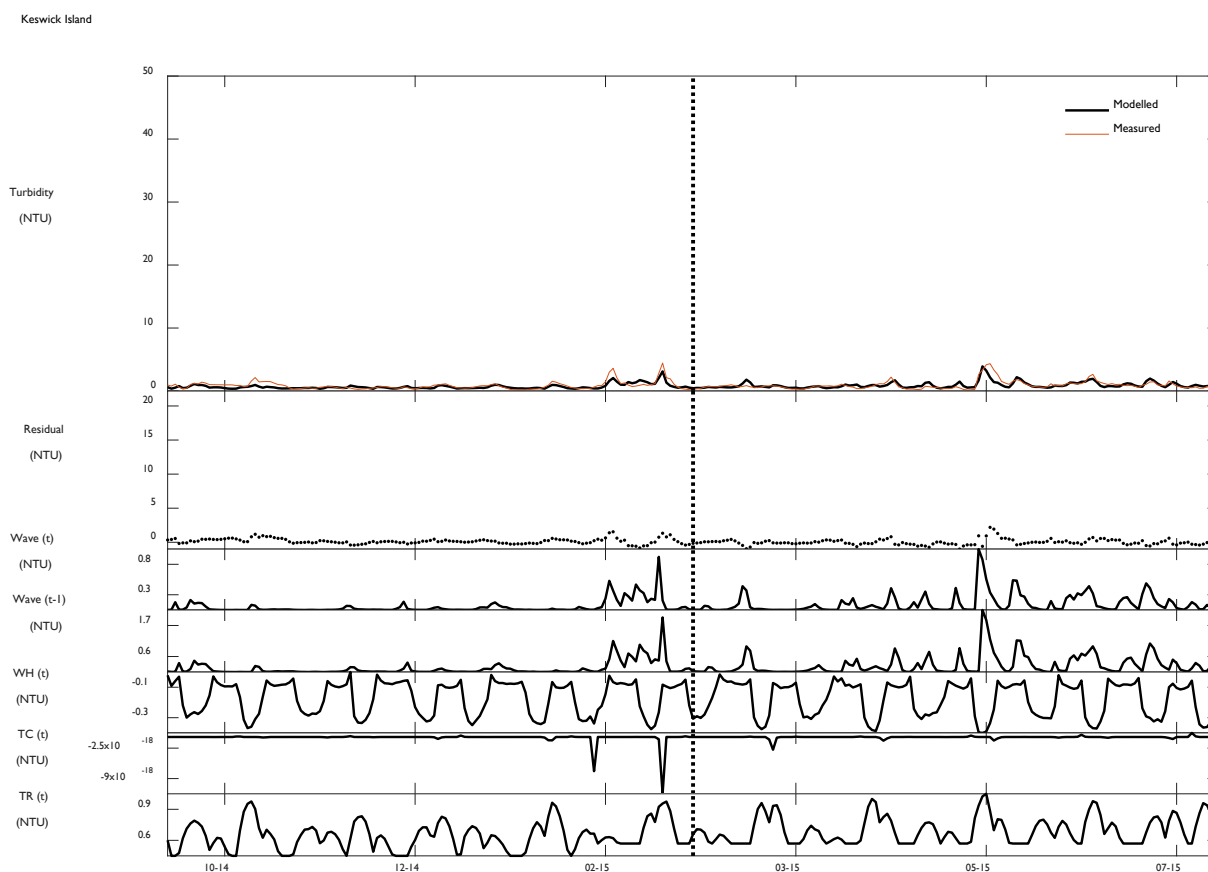
Figure A-I Turbidity running mean percentiles at remaining Barrow Island monitoring sites (excluding sites LNG0, MOFA, MOFC, SBS and DSGS which are presented in Figure 3-8). The running mean percentile analysis used increasing window sizes (from 1 hour to 30 days) comparing the baseline (dotted lines) and dredge periods (solid lines). The four lines for each period (baseline and dredge) are the maximum, 99th, 95th and 80th percentiles. Starting from the left of each figure to the right are the different running mean window sizes. Note that the 95<sup>th</sup> percentiles (black solid and broken line) represent the intensity of turbidity events. Only sites with data during both the baseline and dredging monitoring phases are included. Site codes are included in the top left of each figure.



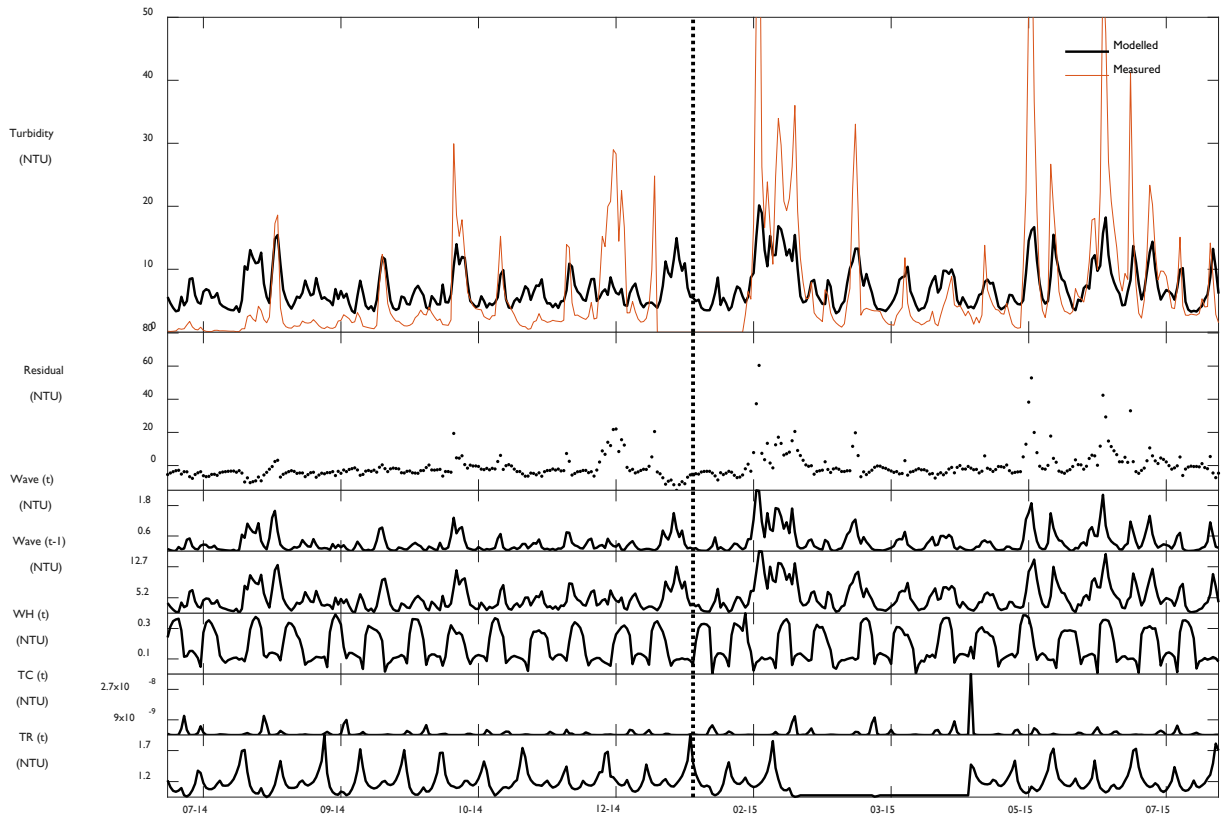
## Appendix B Turbidity model Barrow Island and Hay Point

Turbidity model as well as daily measured turbidity, model residuals (which is also the model overburden at the Barrow Island sites), and all model terms (with parameters applied) for the remaining Hay Point and Barrow Island sites are displayed here. See Chapter 3 section 3.3.3 for the model at representative Hay Point and Barrow Island sites.

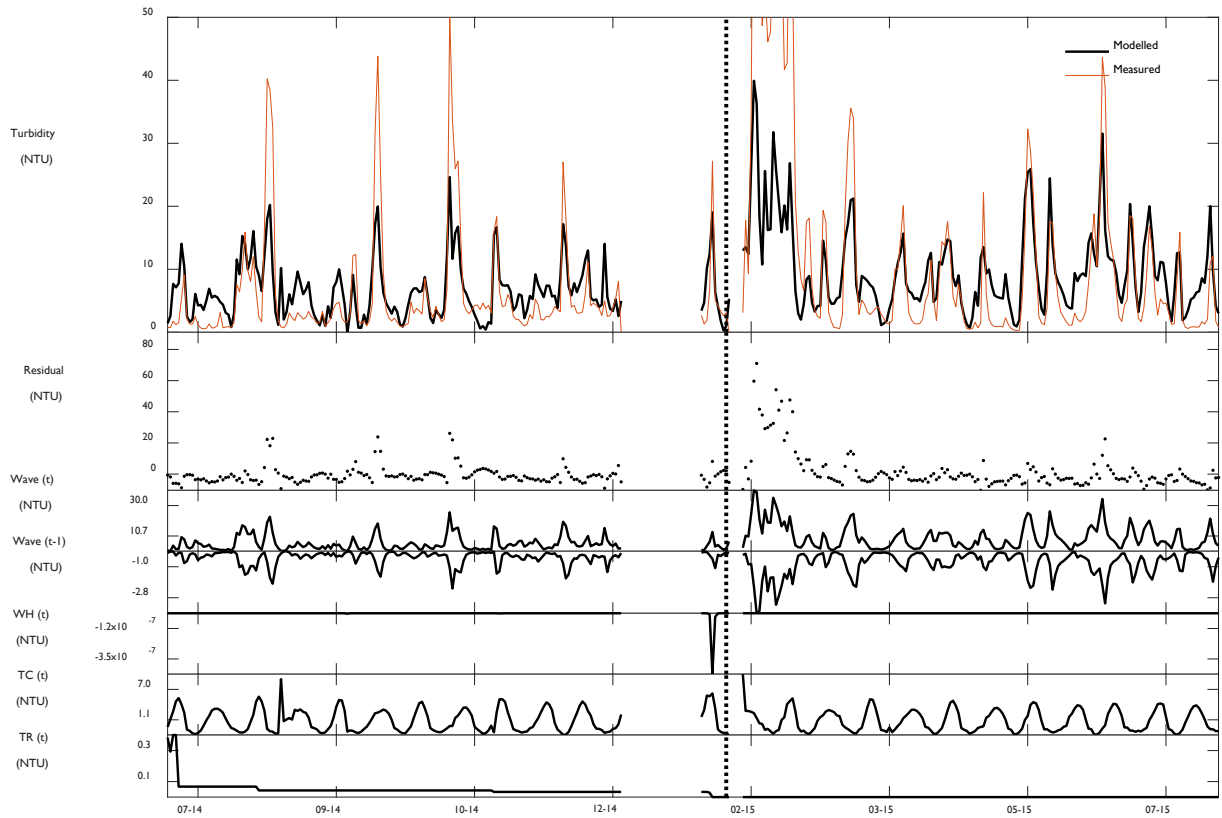
### Hay Point Sites:



Victor Island

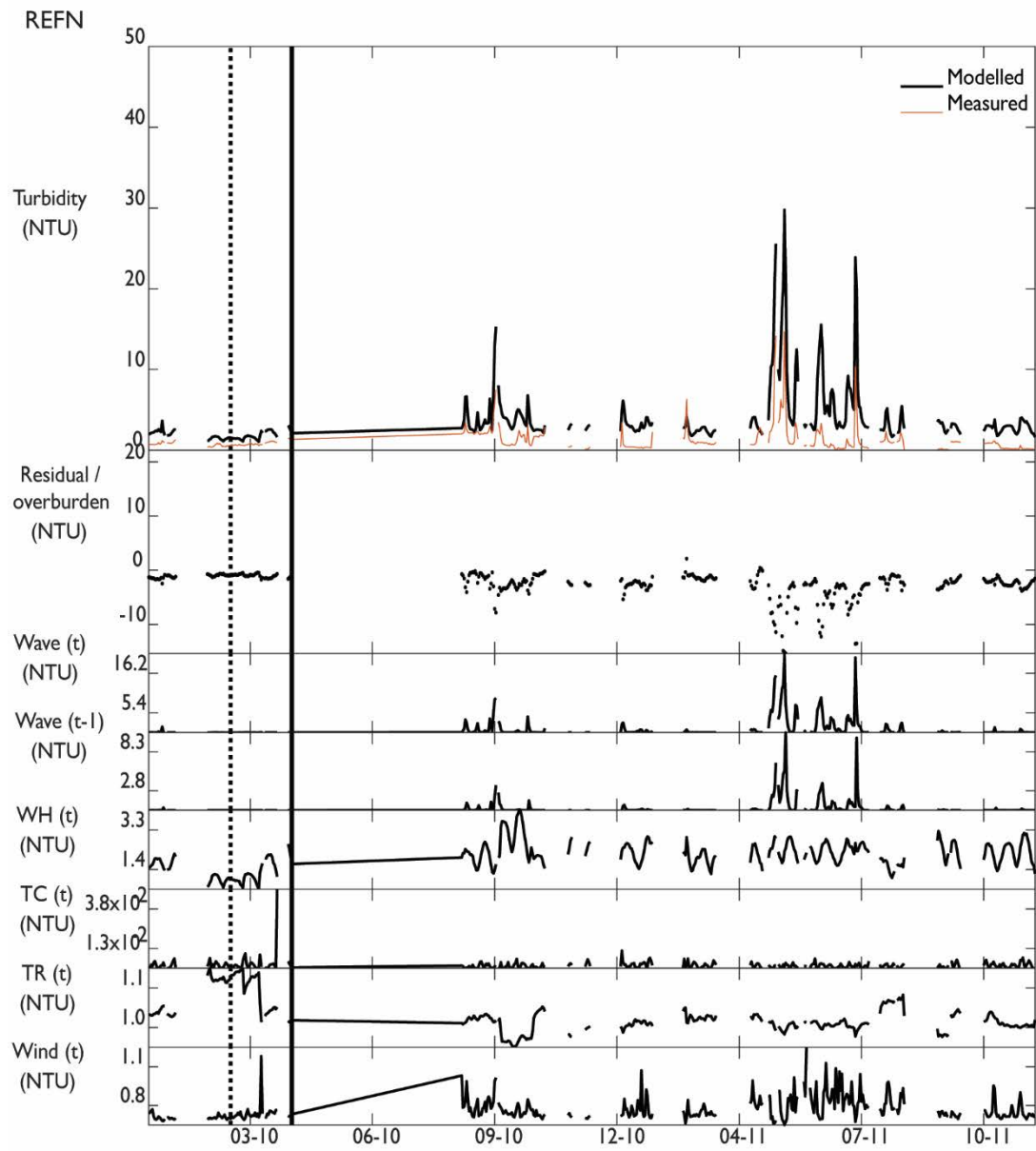


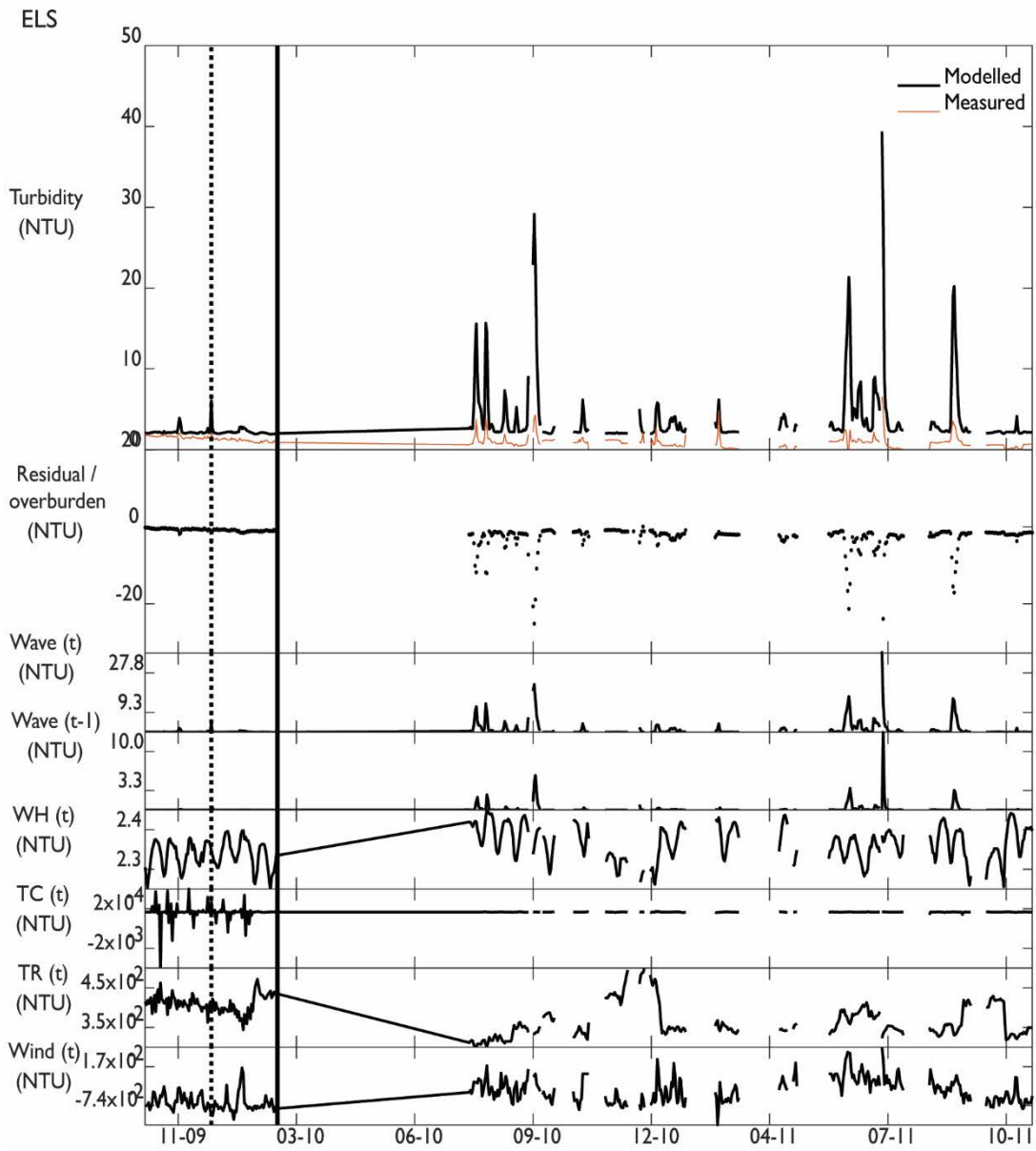
Freshwater Point



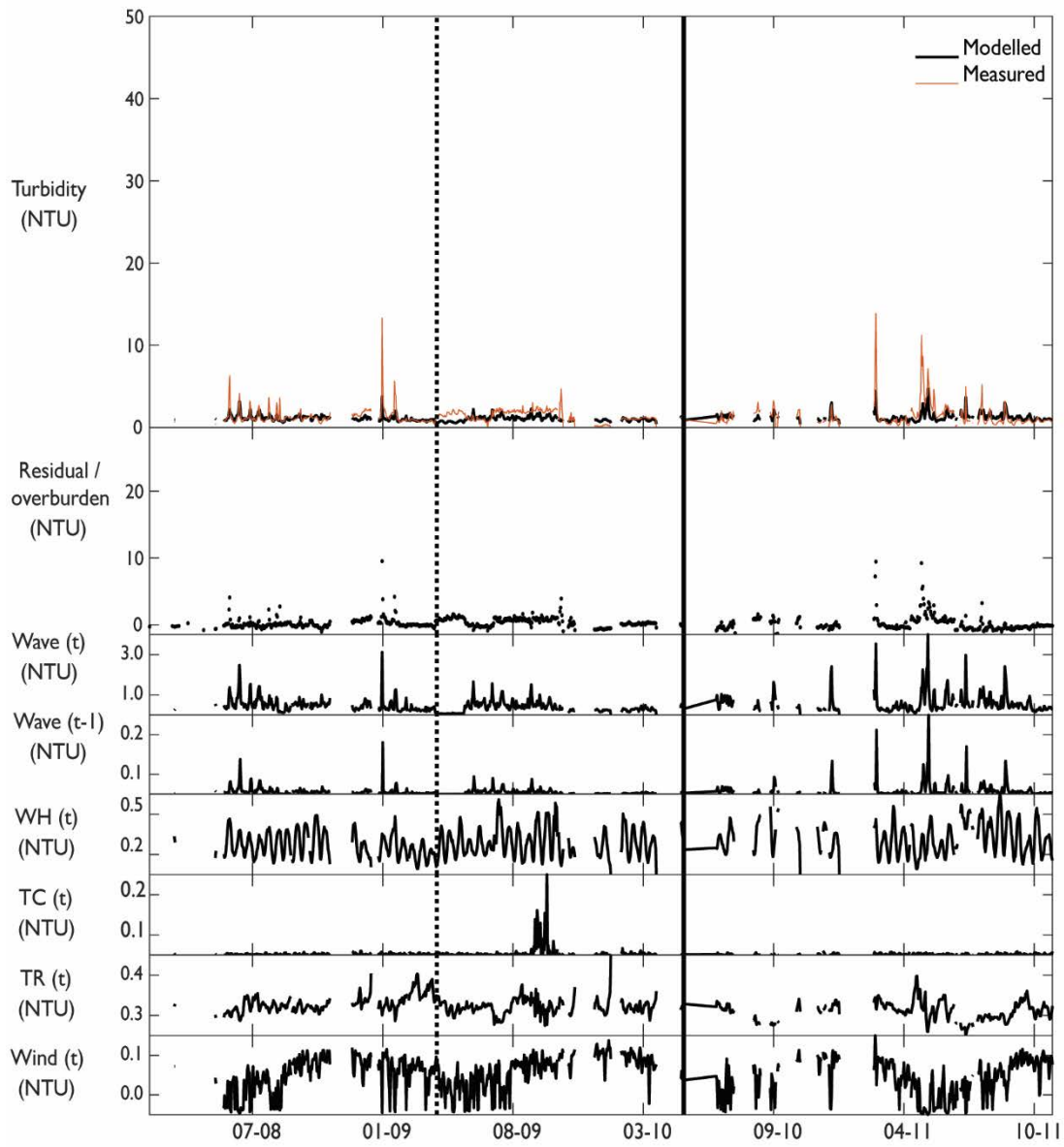
Hay Point project. Turbidity model (equation 5) performance at remaining Hay Point monitoring sites (excluding Hay Point Reef, Round Top Island and Slade Islet which are presented in Figure 3-4) during the baseline train (left of the dotted line) and test (right of the dotted line) periods showing (from top to bottom): the modelled (black line) and measured (orange line) turbidity levels, the residual turbidity, then each model term (with parameters applied) including RMS pressure fluctuations to represent the motion of surface gravity waves on the sea floor at time  $t$  (wave ( $t$ )), RMS pressure fluctuations from the previous day (wave( $t-1$ )), water height at time  $t$ , tidal current quasi estimates at time  $t$  and tidal range at time  $t$ , all in units of NTU. The top panel showing measured and modelled turbidity is the same in all figures and has been truncated to 50 NTU to show the smaller modelled turbidity levels. Site names are included at the top left of each figure

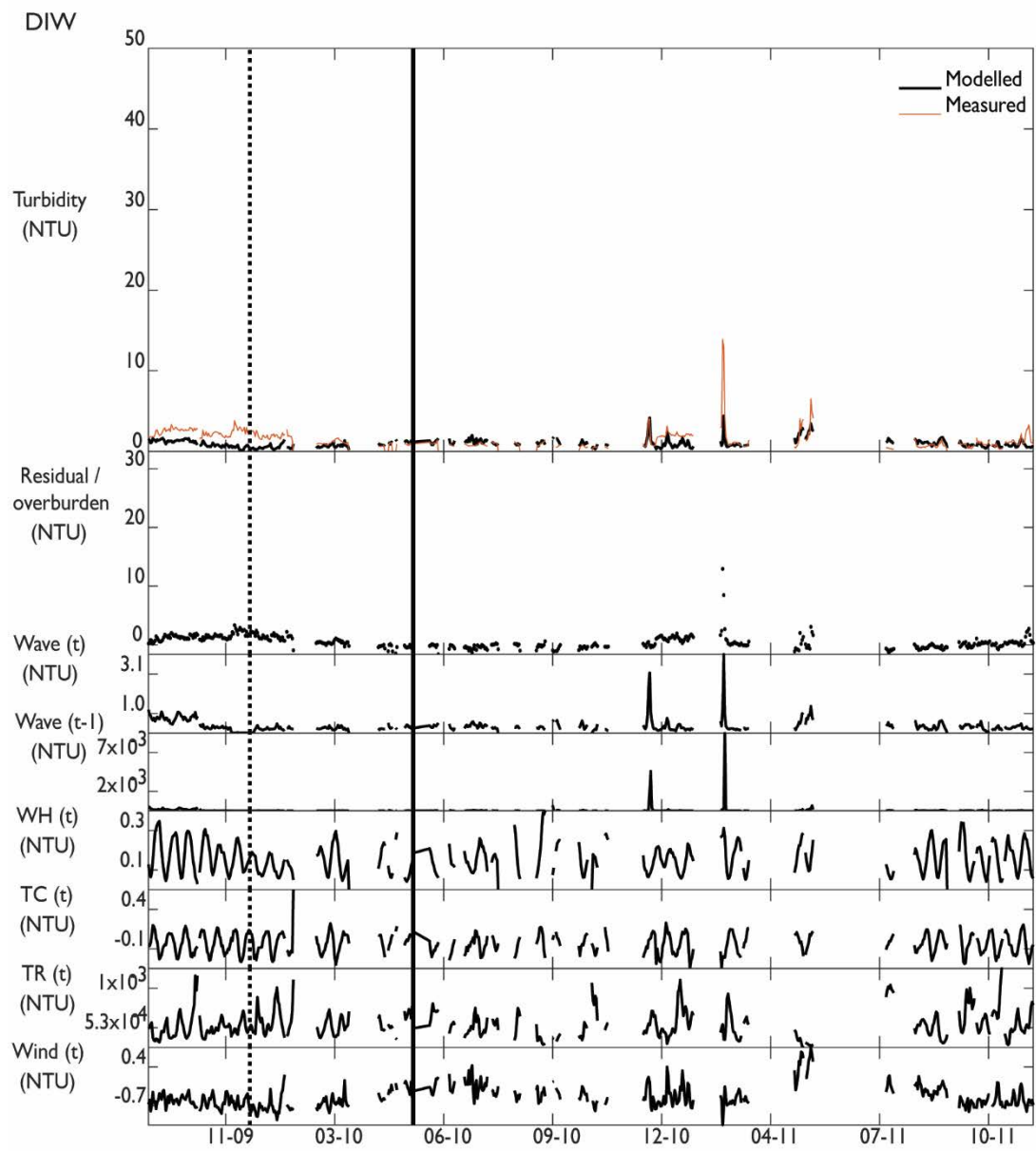
Barrow Island sites:

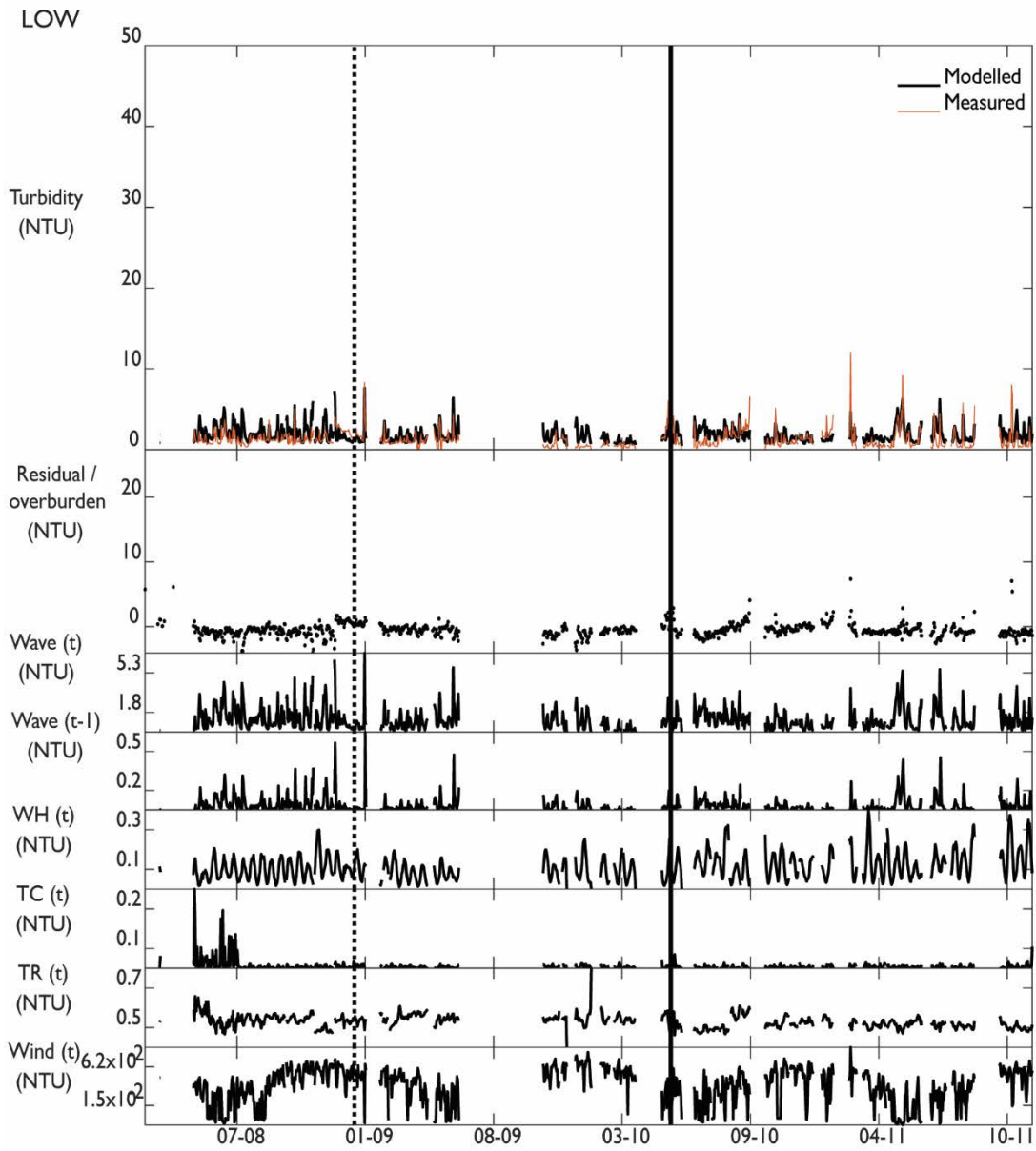




ANT

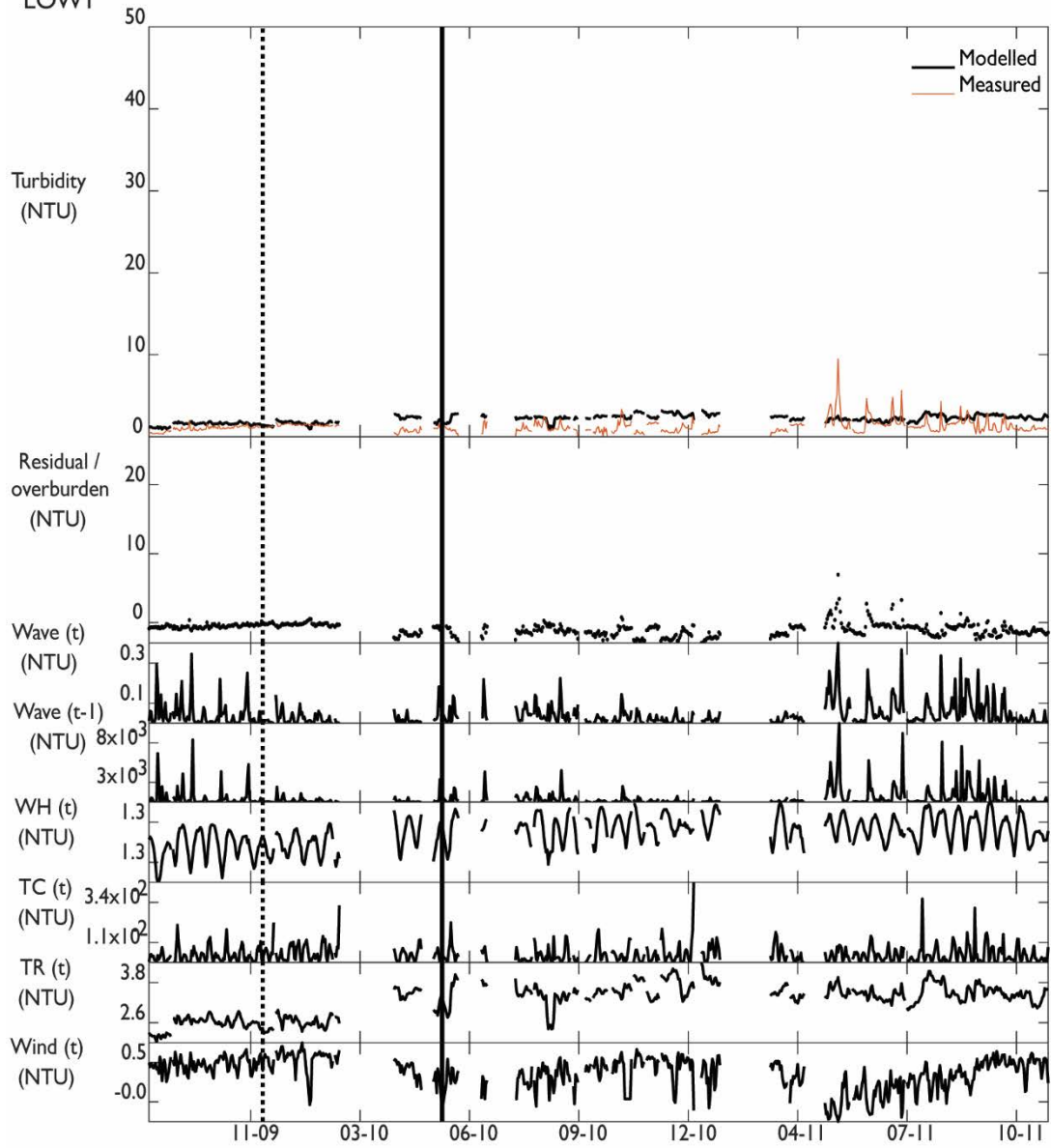




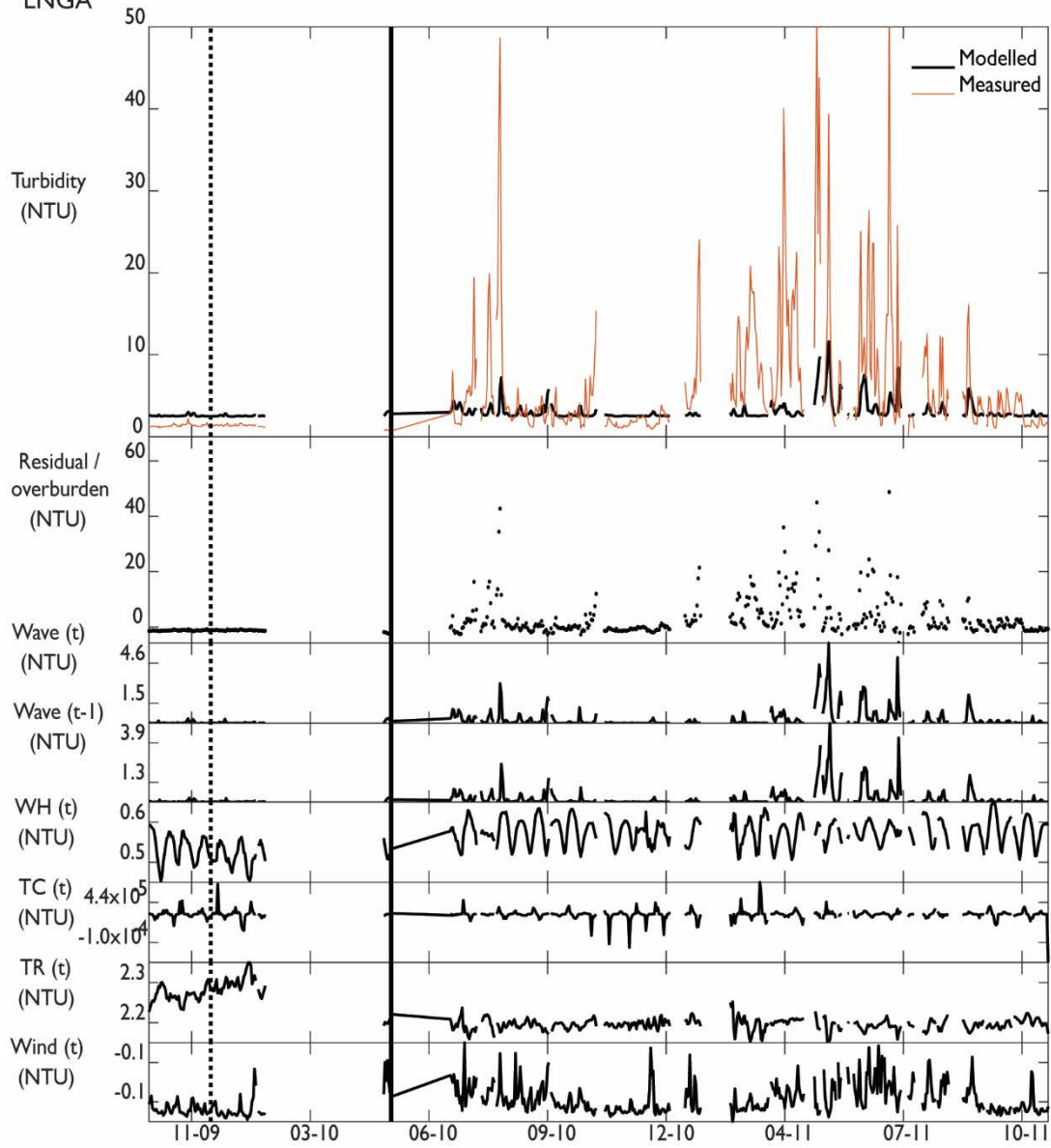


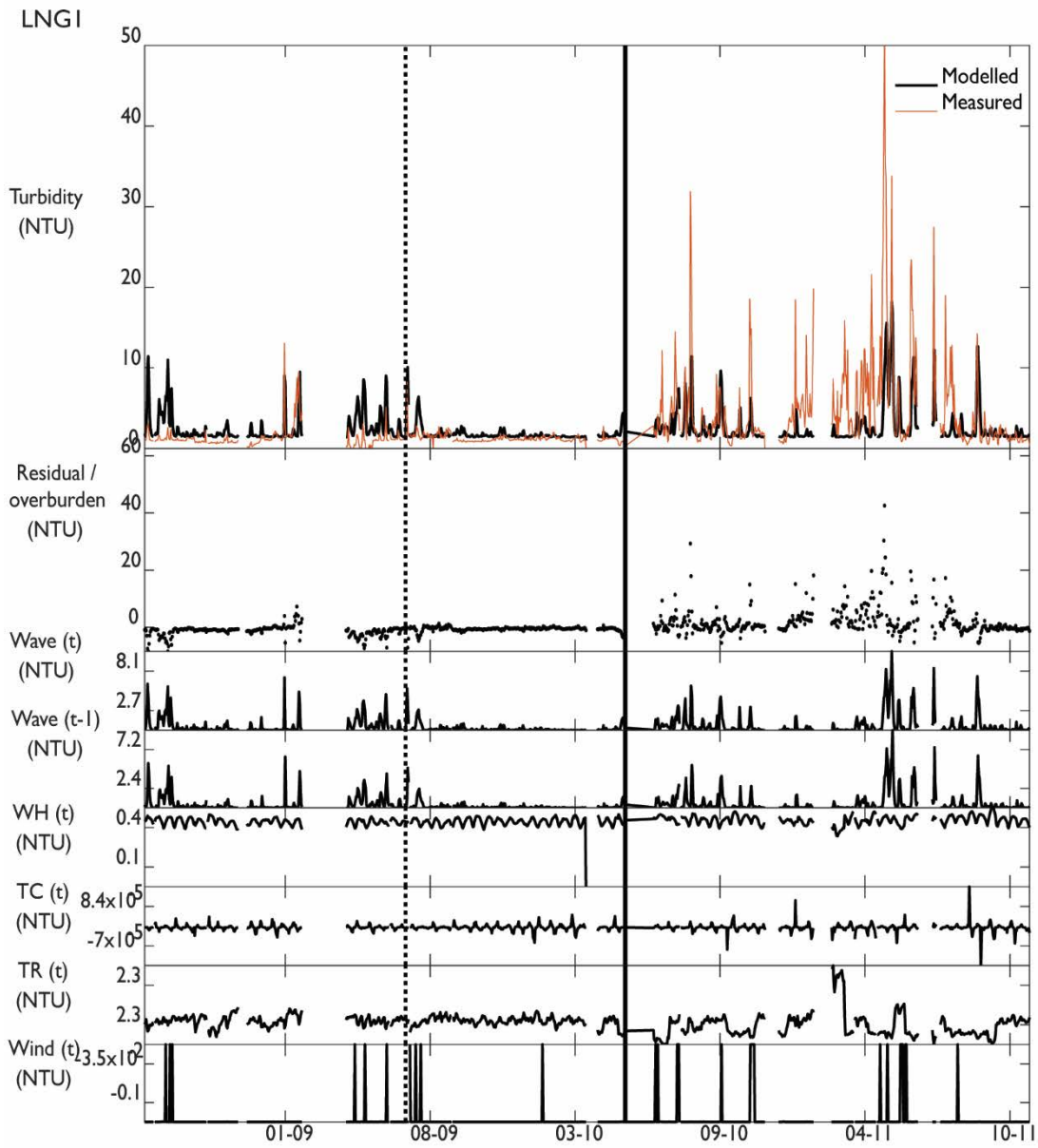


LOWI

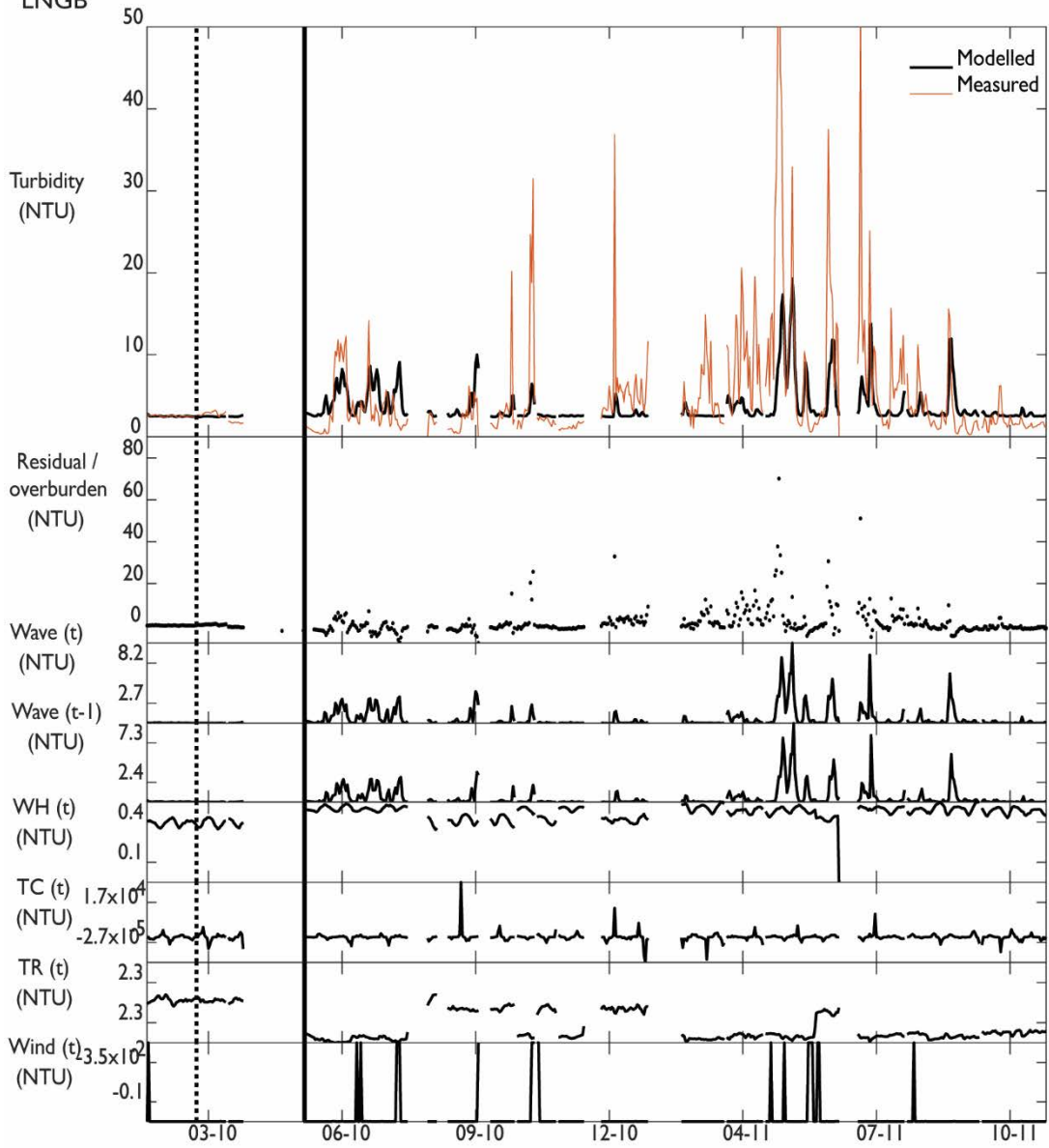


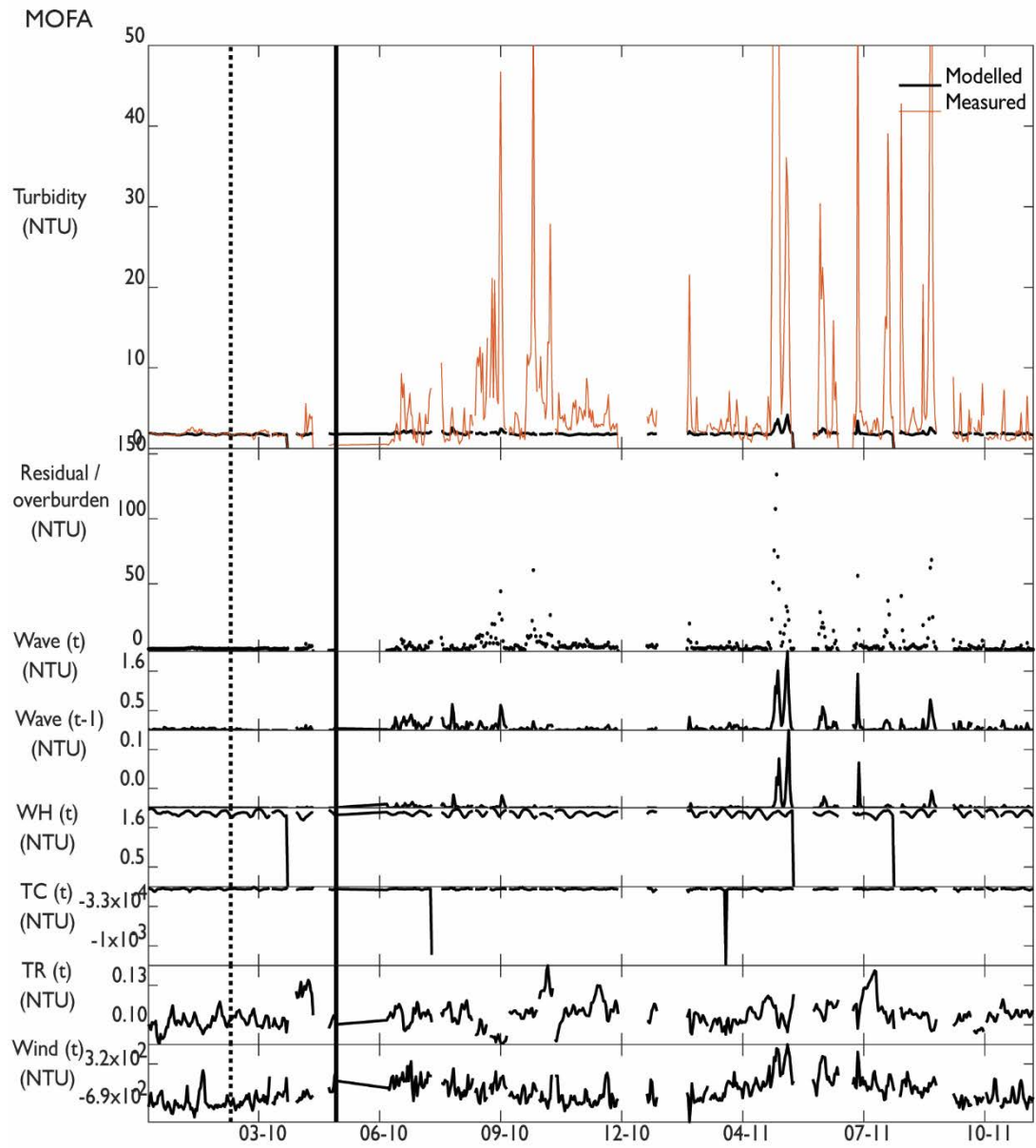
LNGA



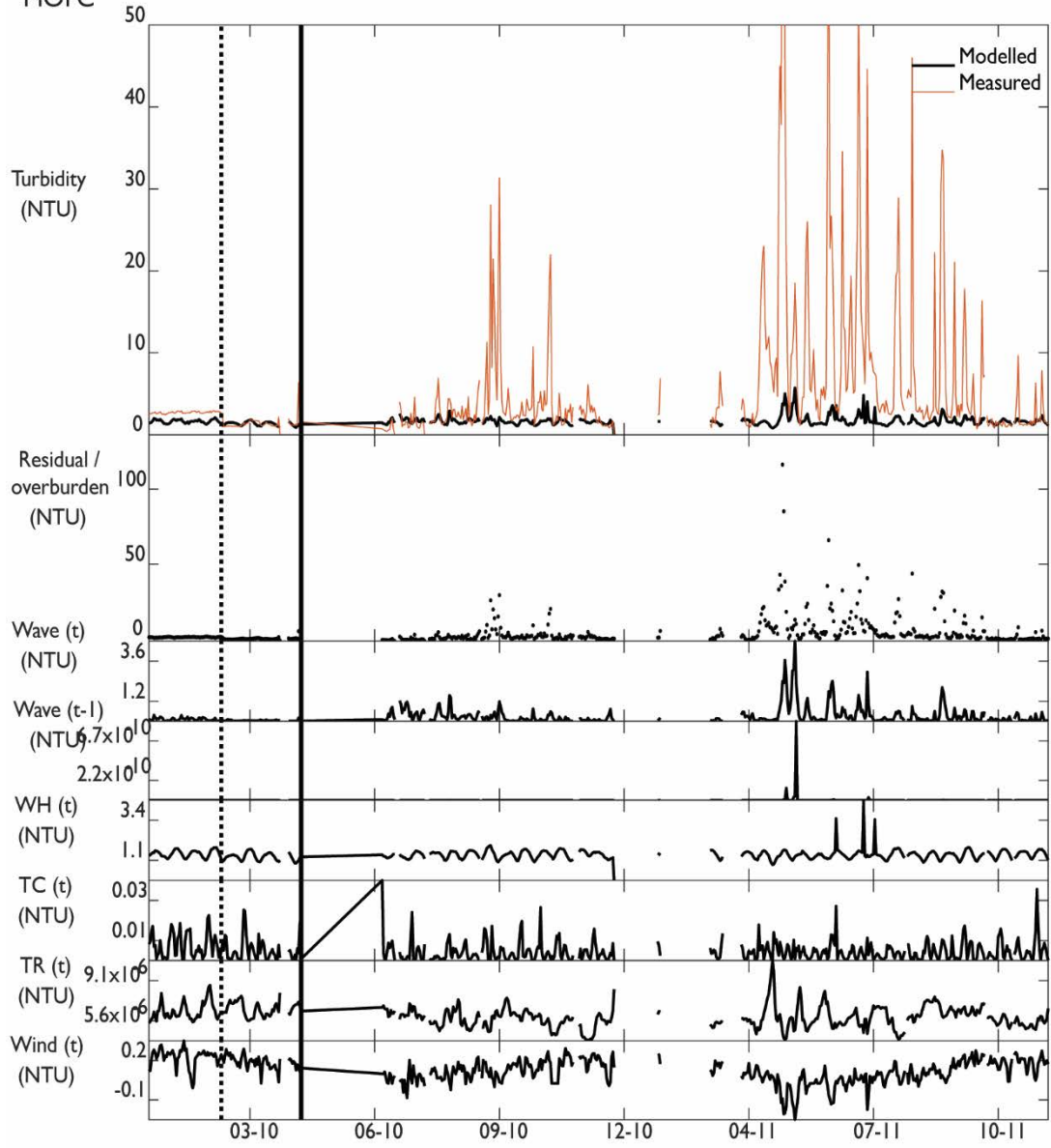


LNGB

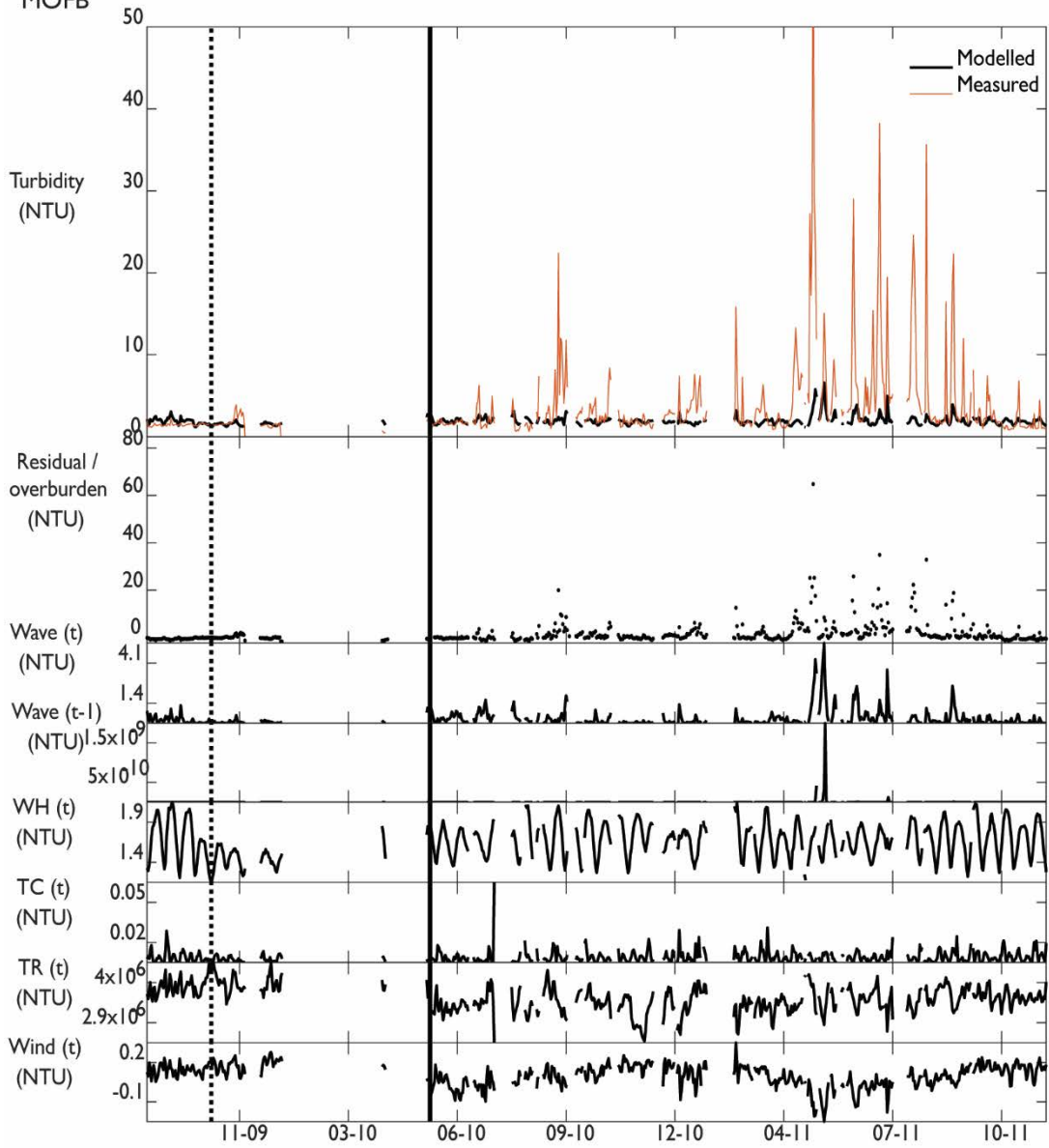




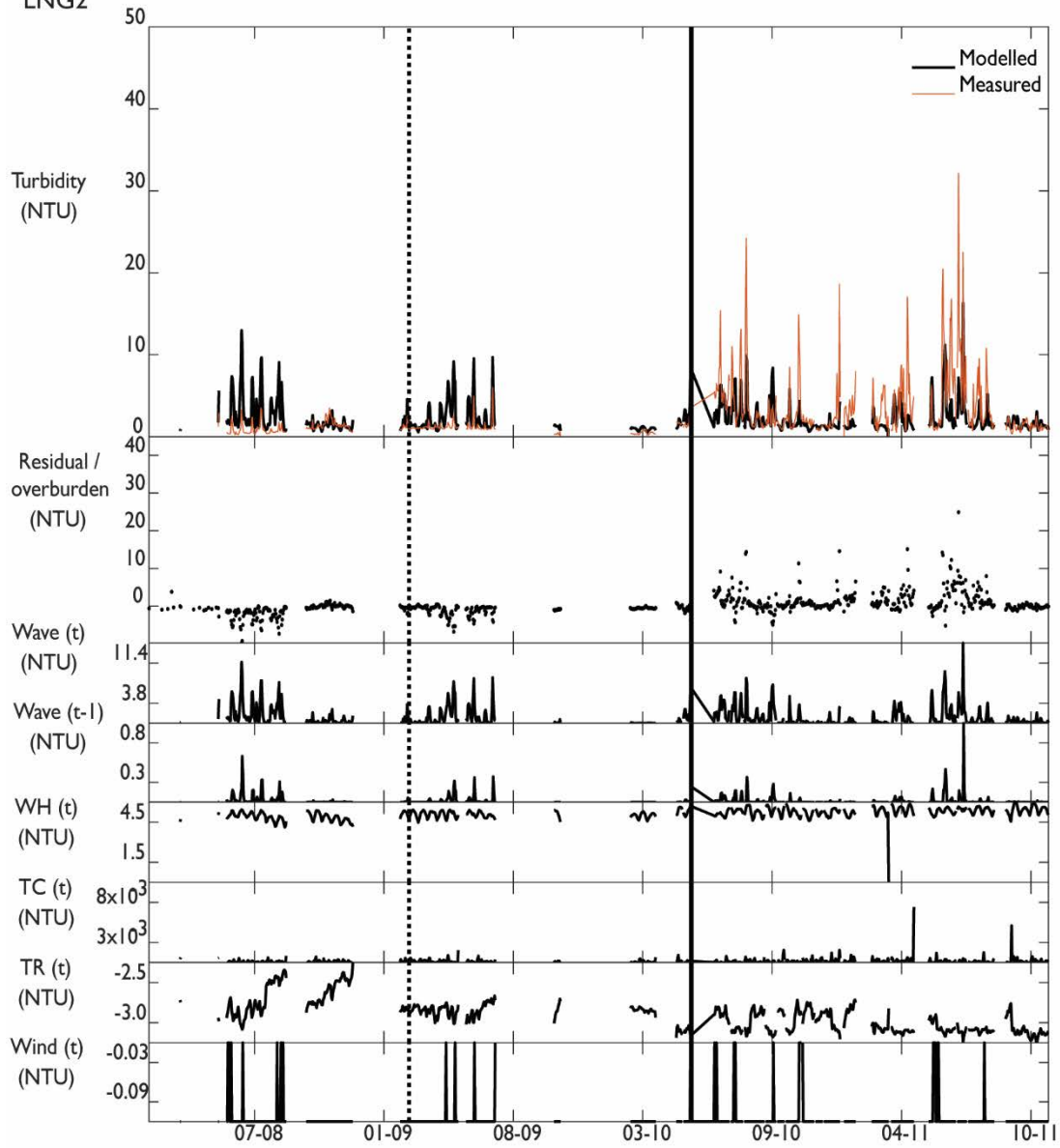
MOFC



MOFB

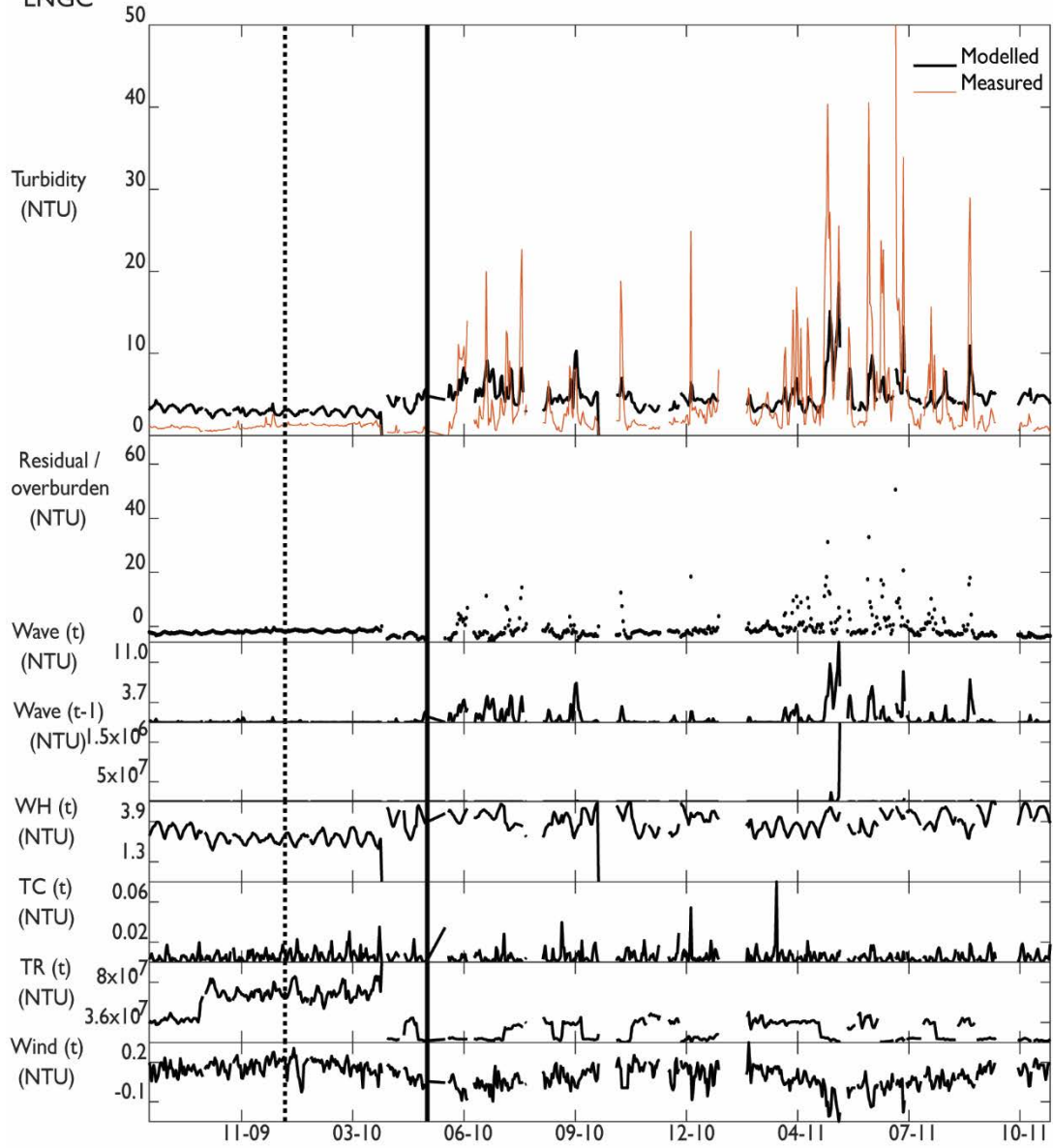


LNG2

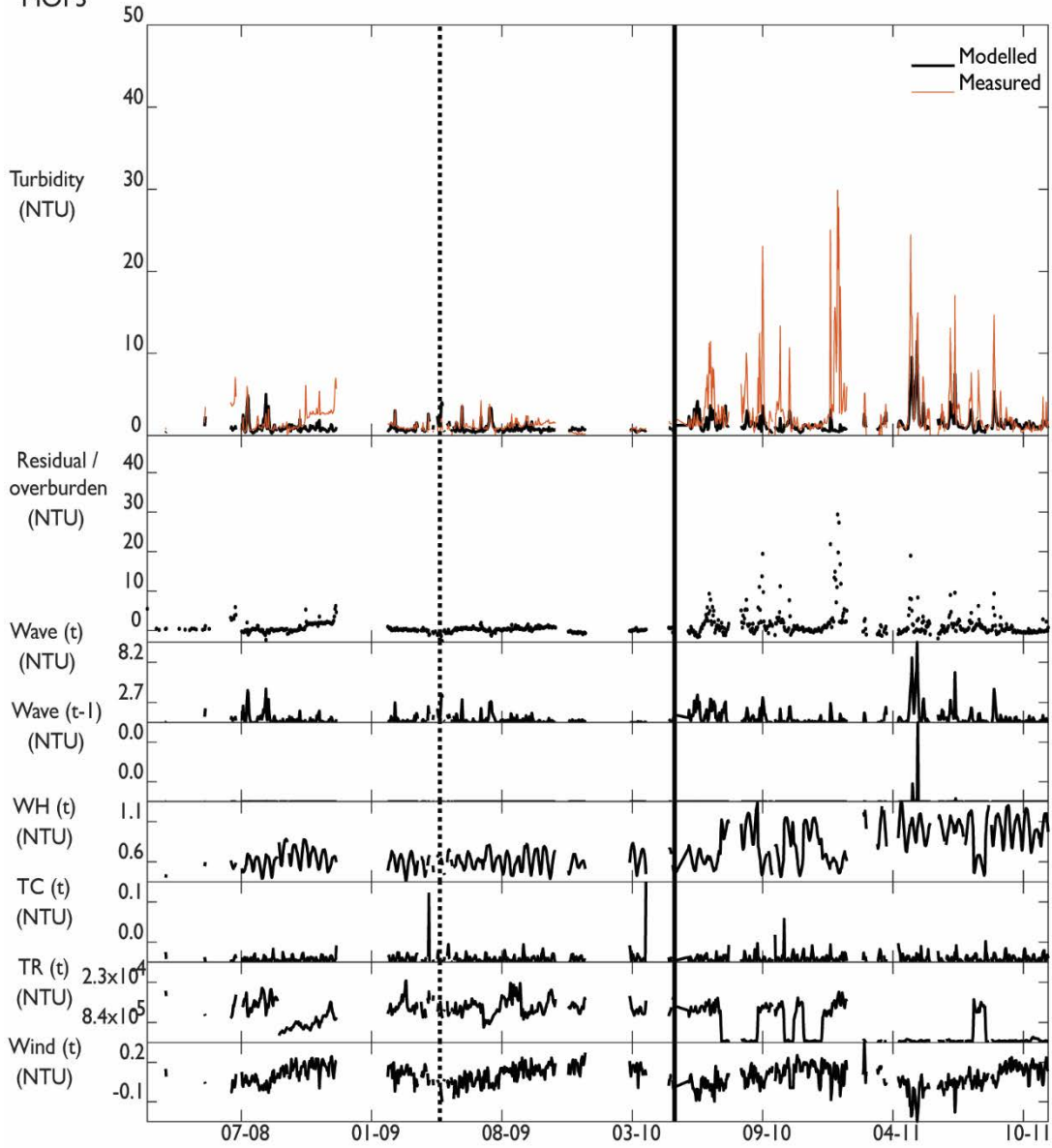




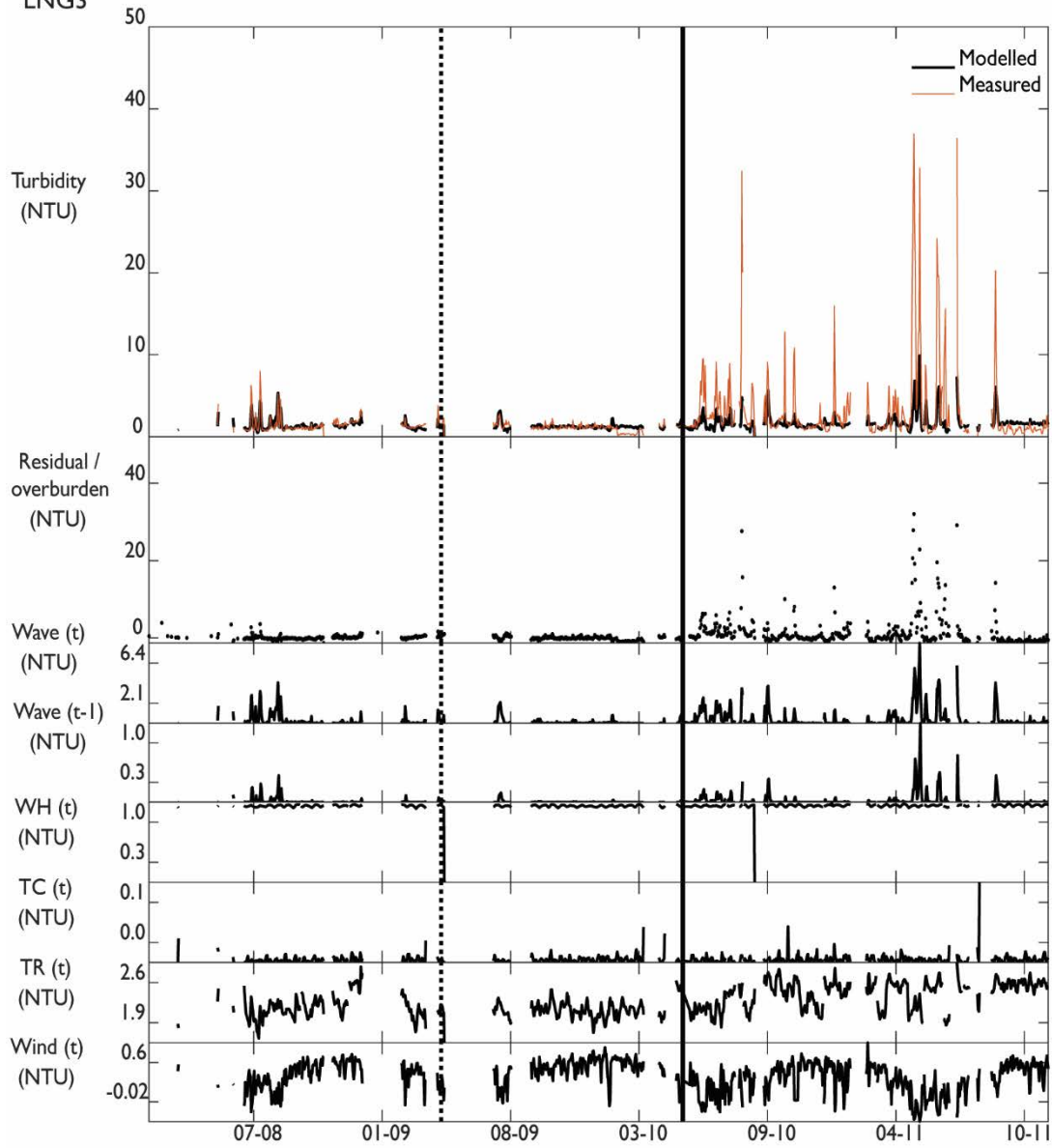
LNGC

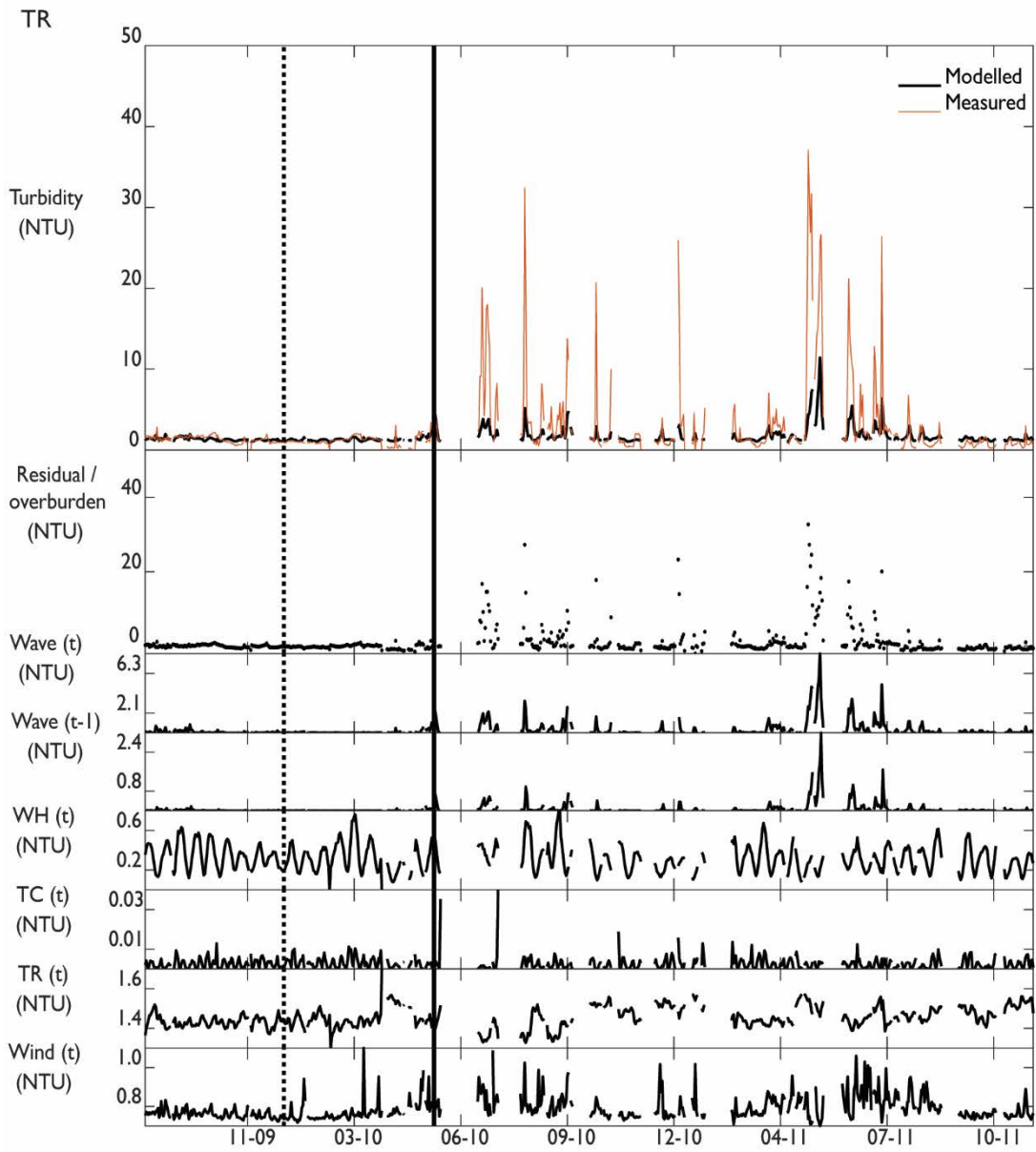


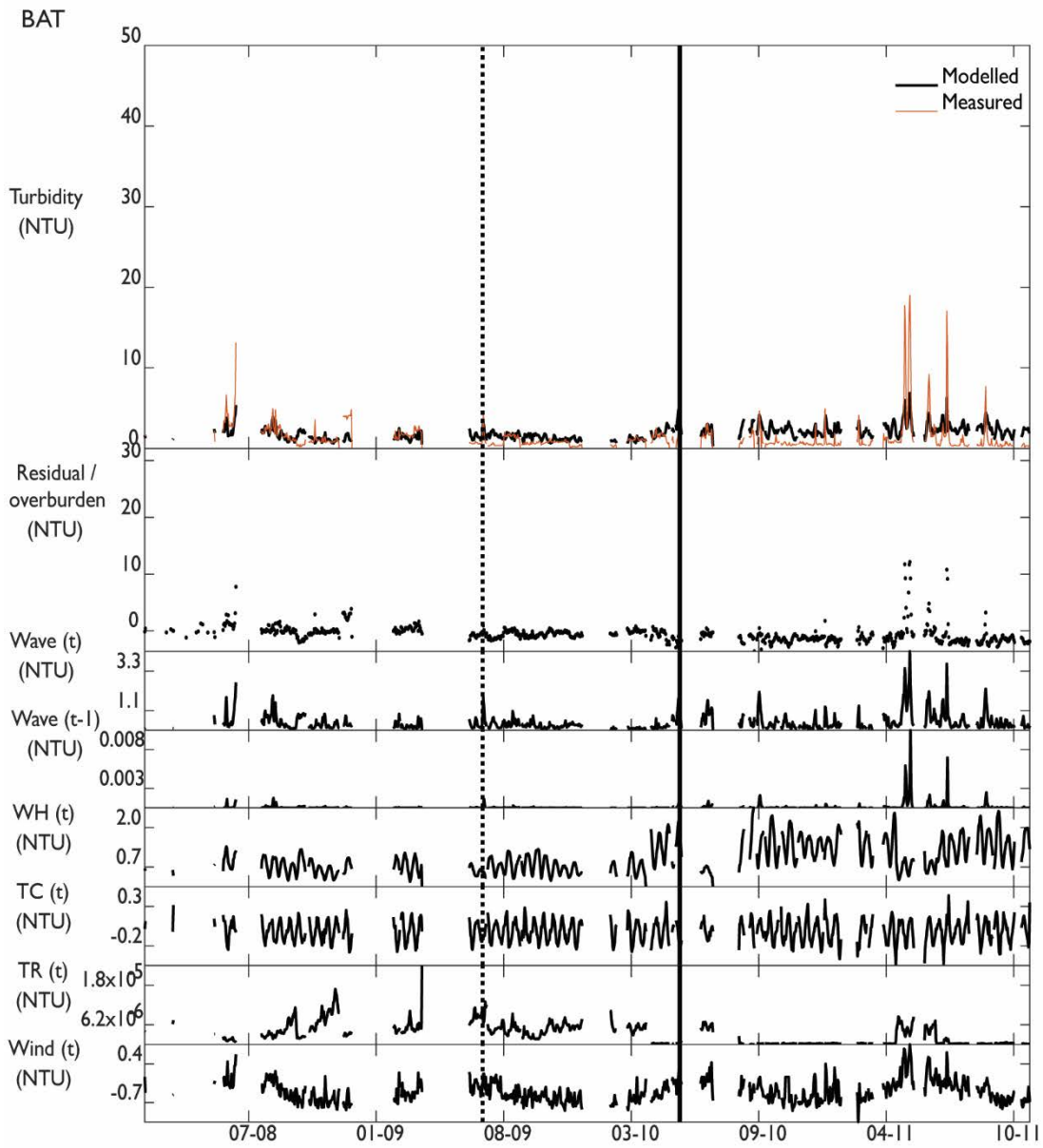
MOF3

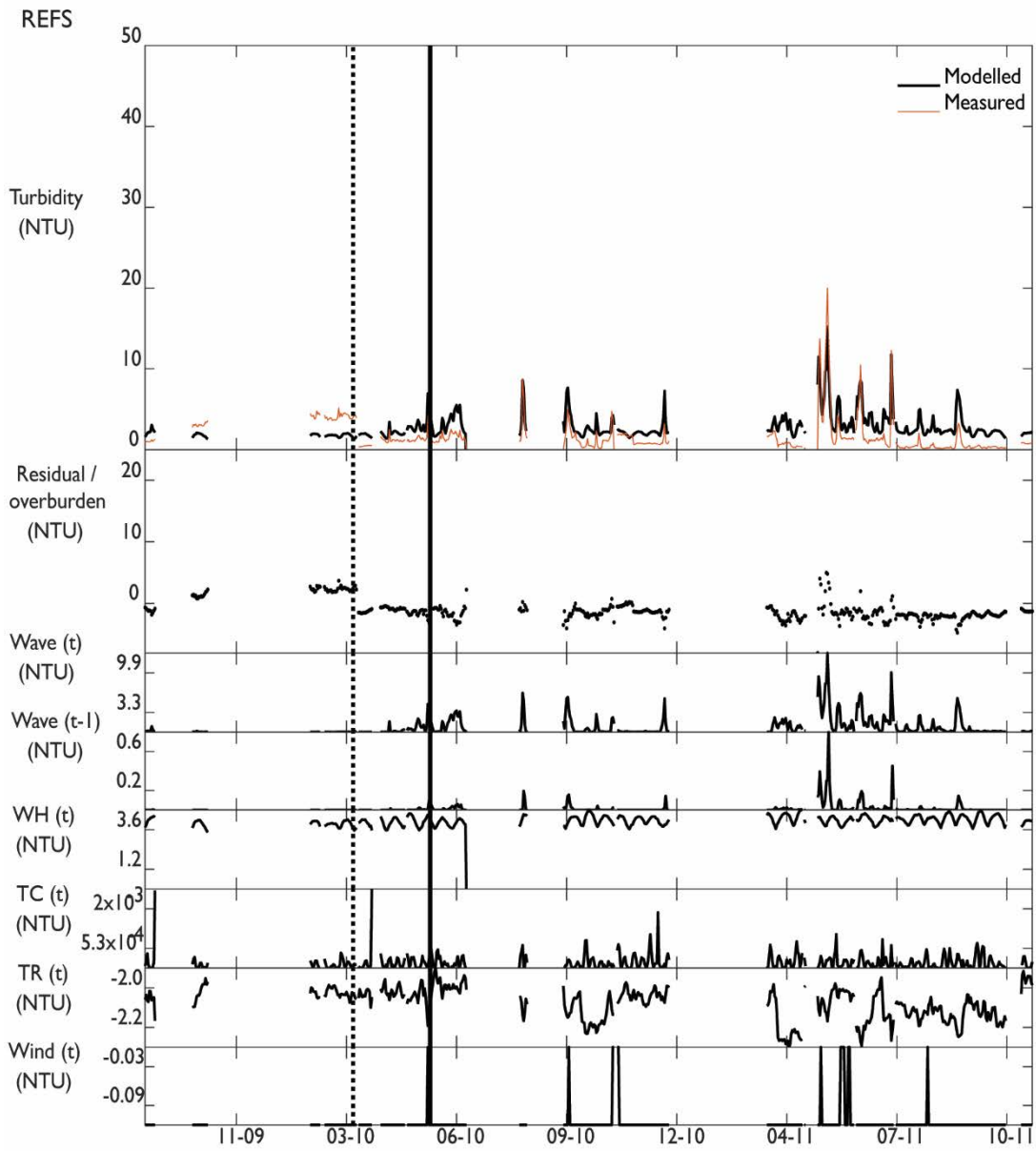


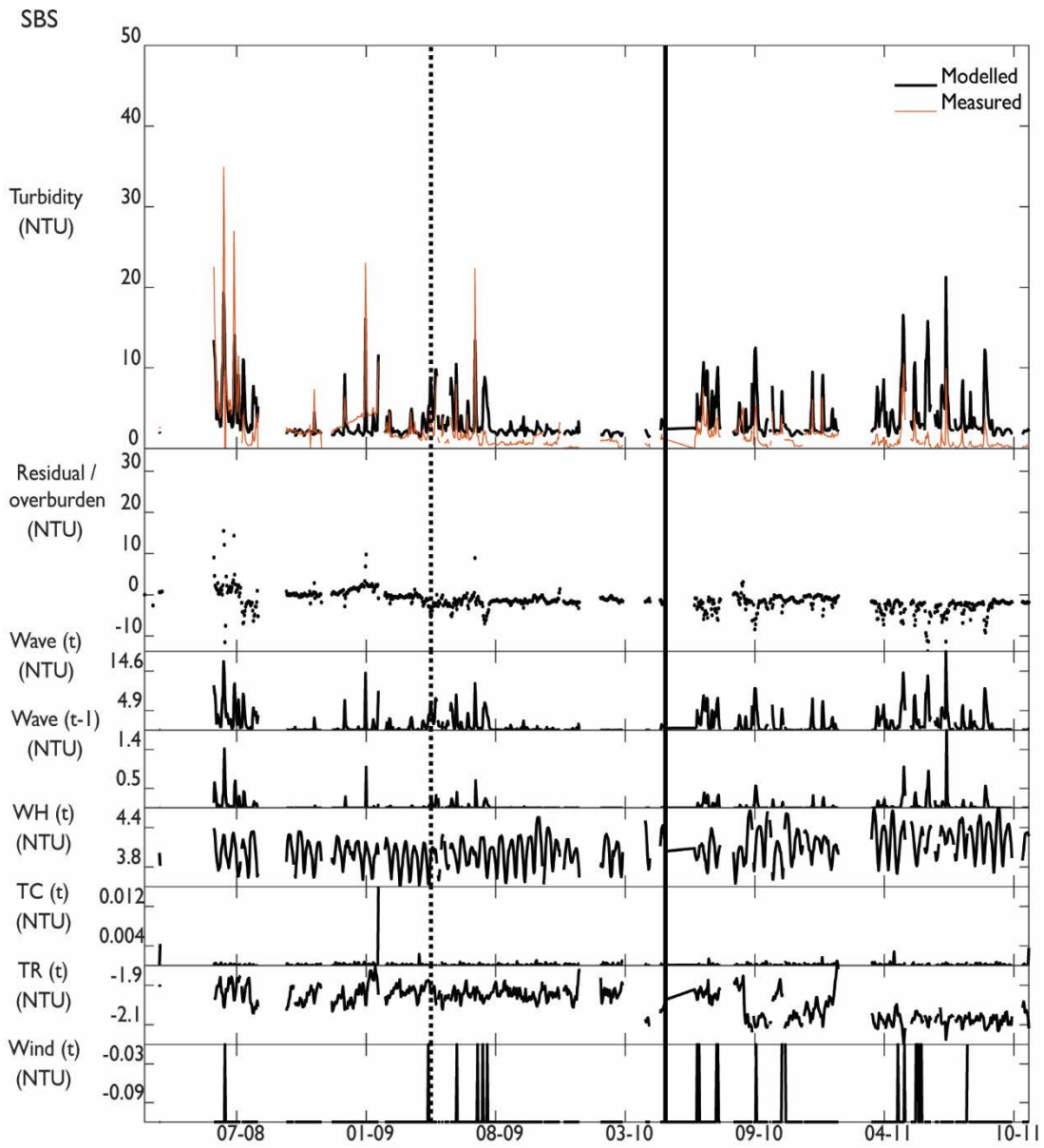
LNG3











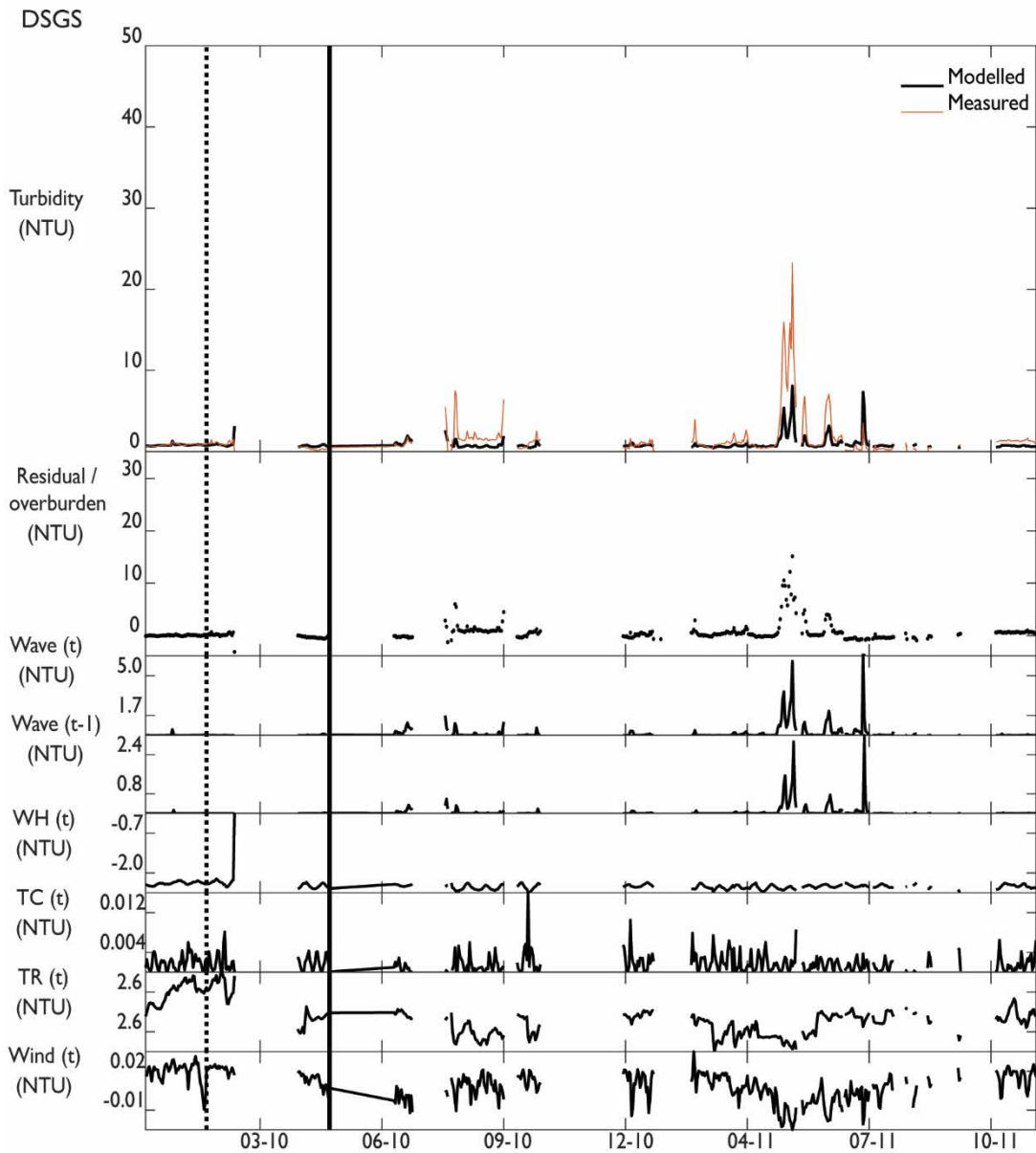
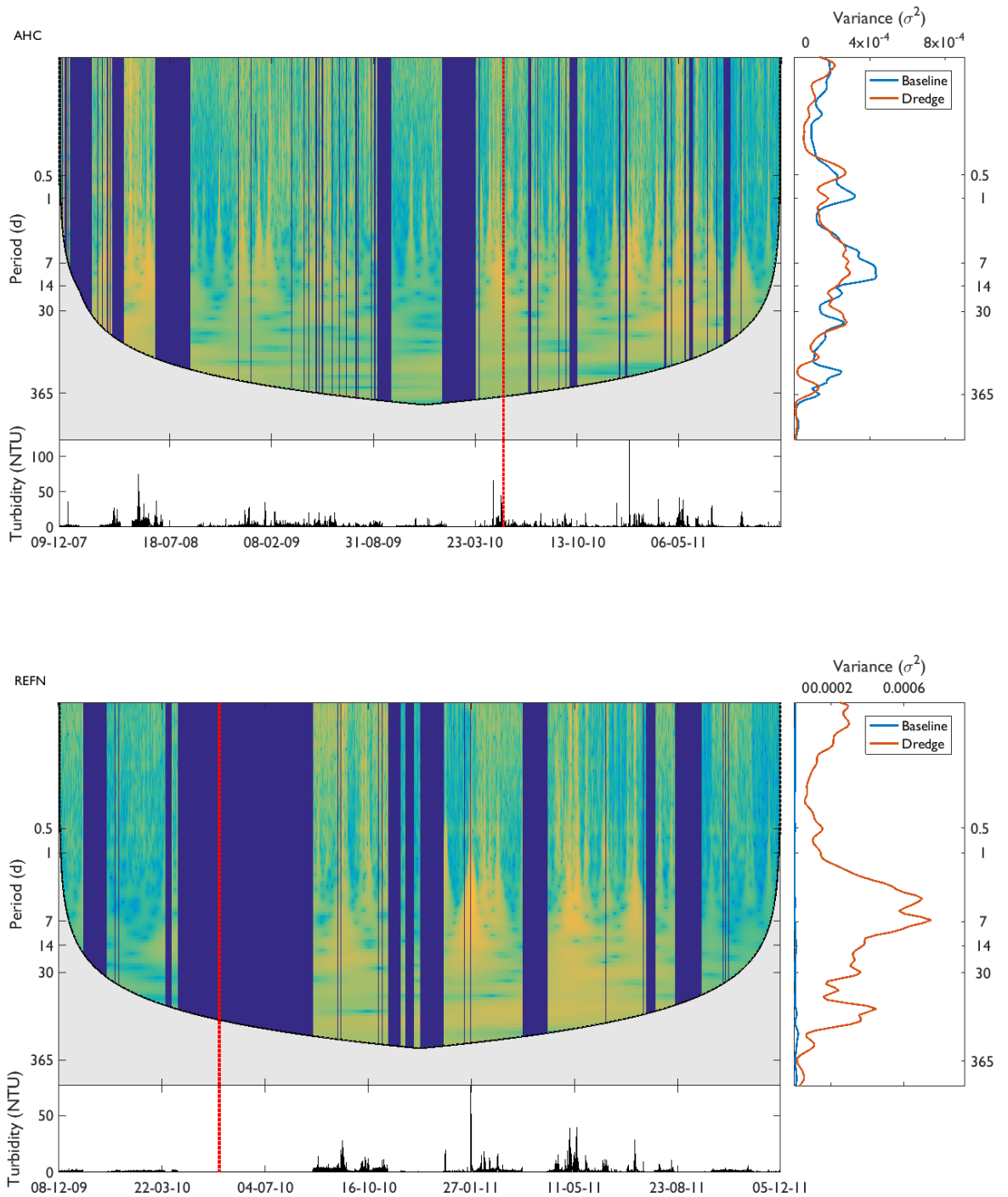


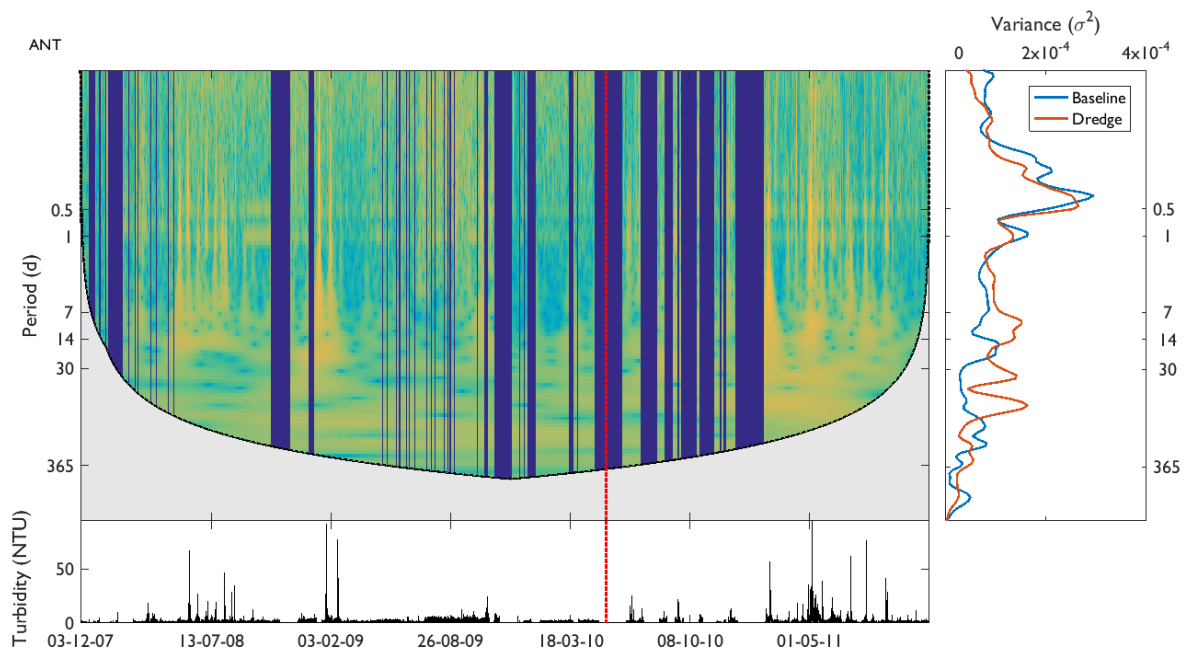
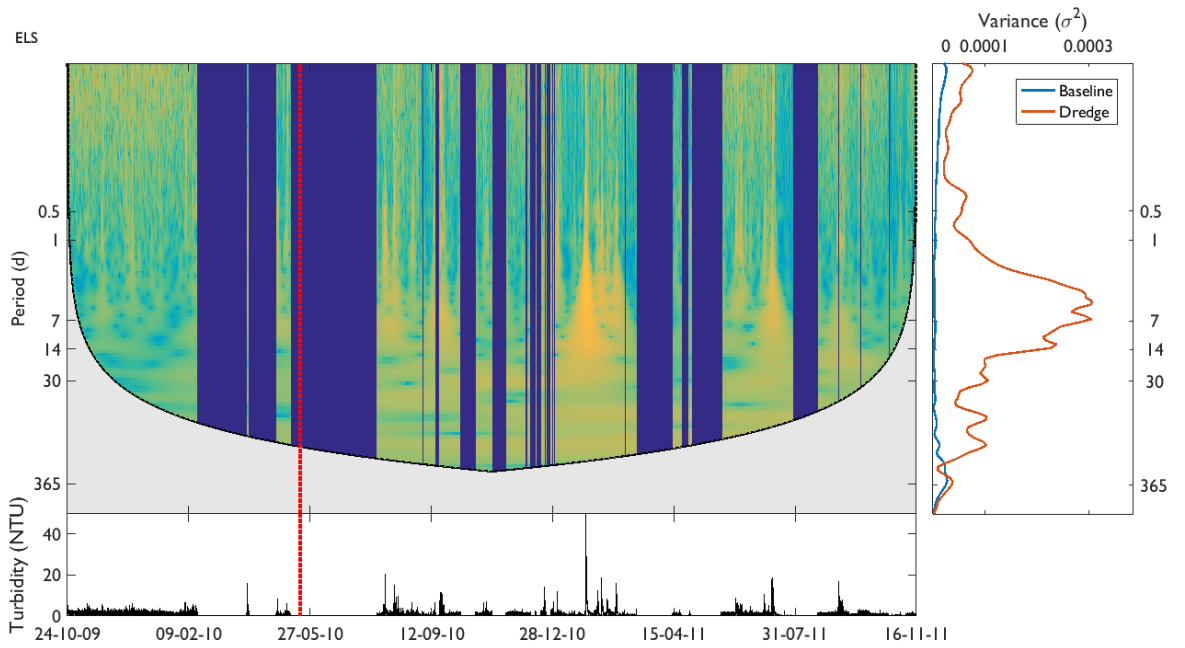
Figure B-I Turbidity model (equation 5) performance at the remaining Barrow Island monitoring sites (excluding LONE, MOFI, LNG0, AHC, and DUG which are presented in Figure 3-5) during the baseline train (left of the dotted line), test (between dotted and solid lines), and dredge period (right of the solid line) showing (from top to bottom): the modelled (black line) and measured (orange line) turbidity levels, residual turbidity, or 'overburden' (which is the difference between the measured and modelled turbidity), and each model term (with parameters applied) including: waves at time  $t$ , waves from the previous day (i.e. waves at  $t-1$ ), water height at time  $t$ , tidal current at time  $t$ , tidal range at time  $t$  and wind at time  $t$ , all in units of NTU. The top panel showing measured and modelled turbidity has the same scale in all 5 figures, truncated to 50 NTU to show the smaller modelled turbidity events (most of which are < 10 NTU during the baseline period). Site codes are included in the top left of each figure

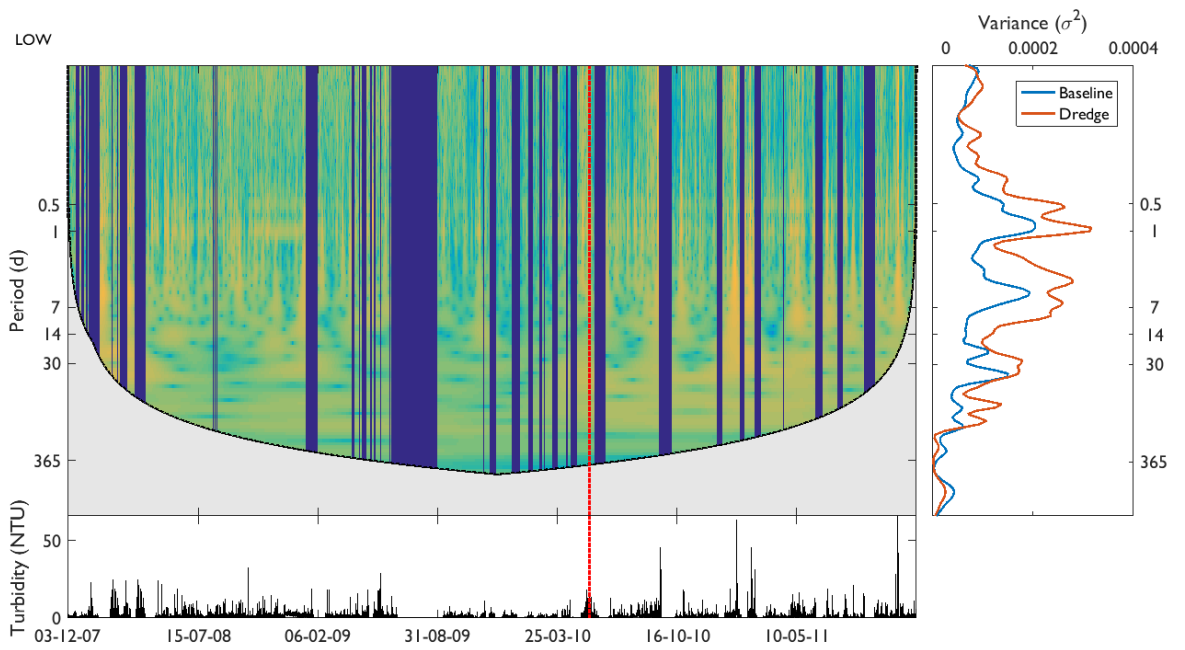
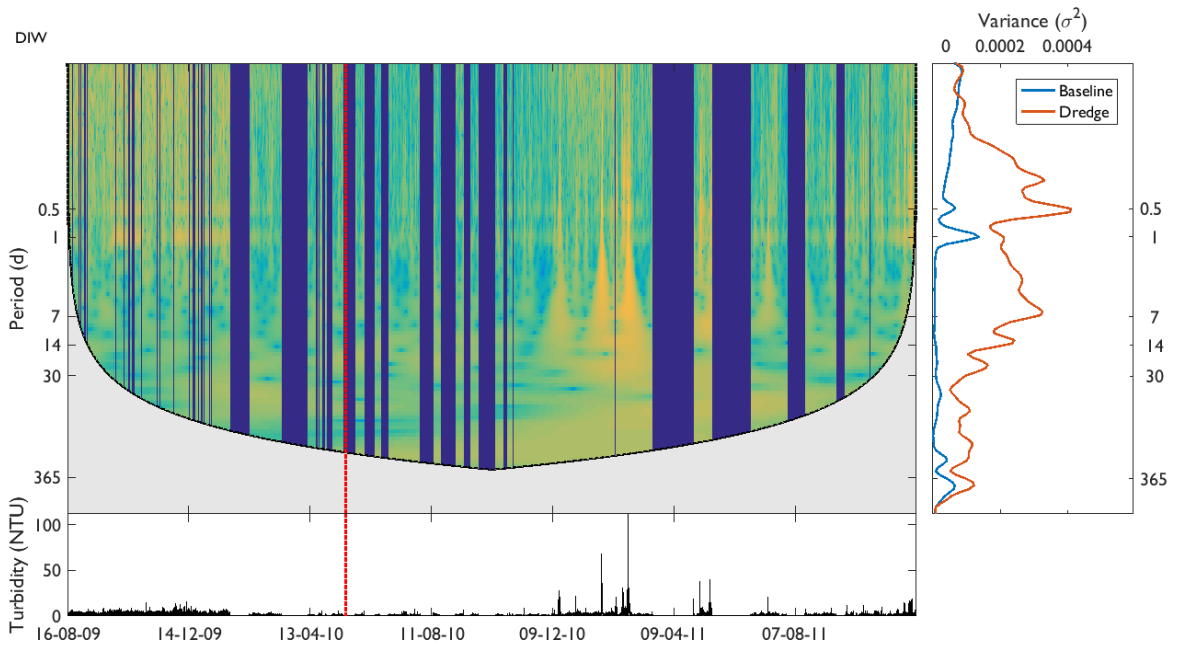


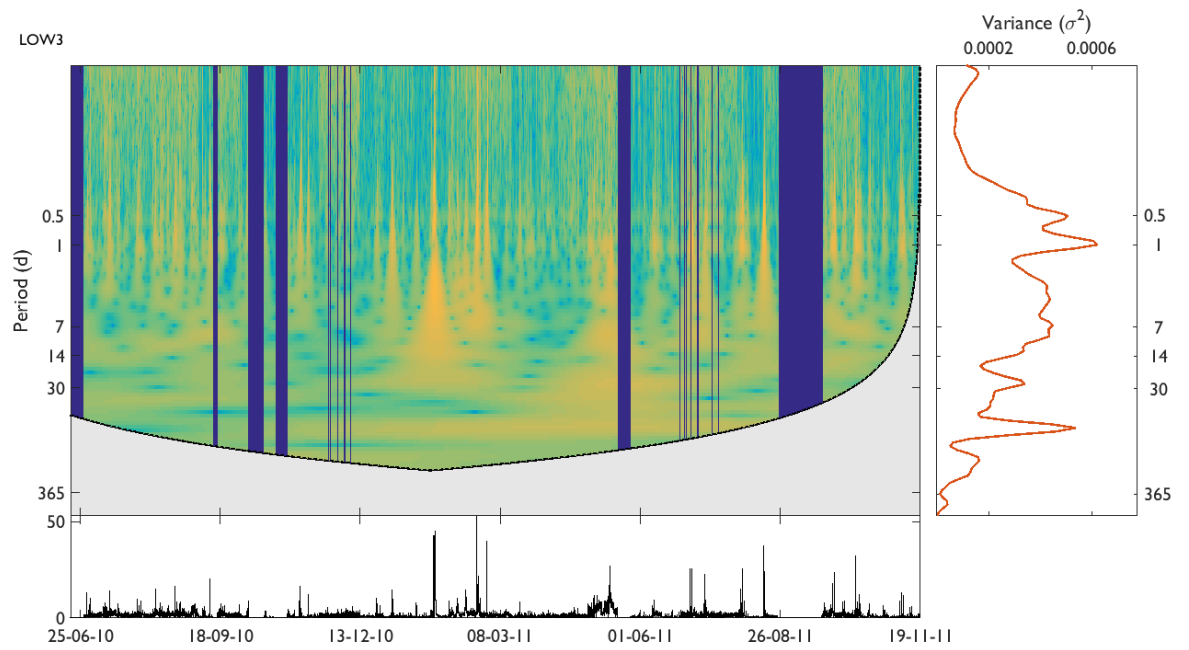
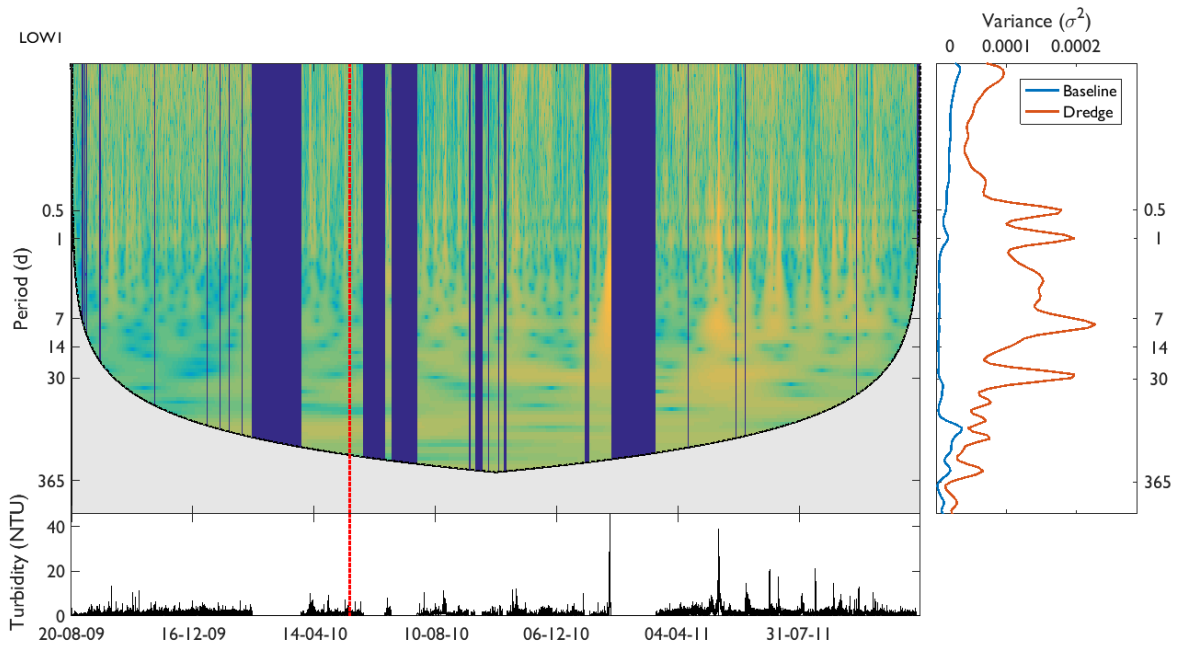
## Appendix C Turbidity spectral analysis for Barrow Island

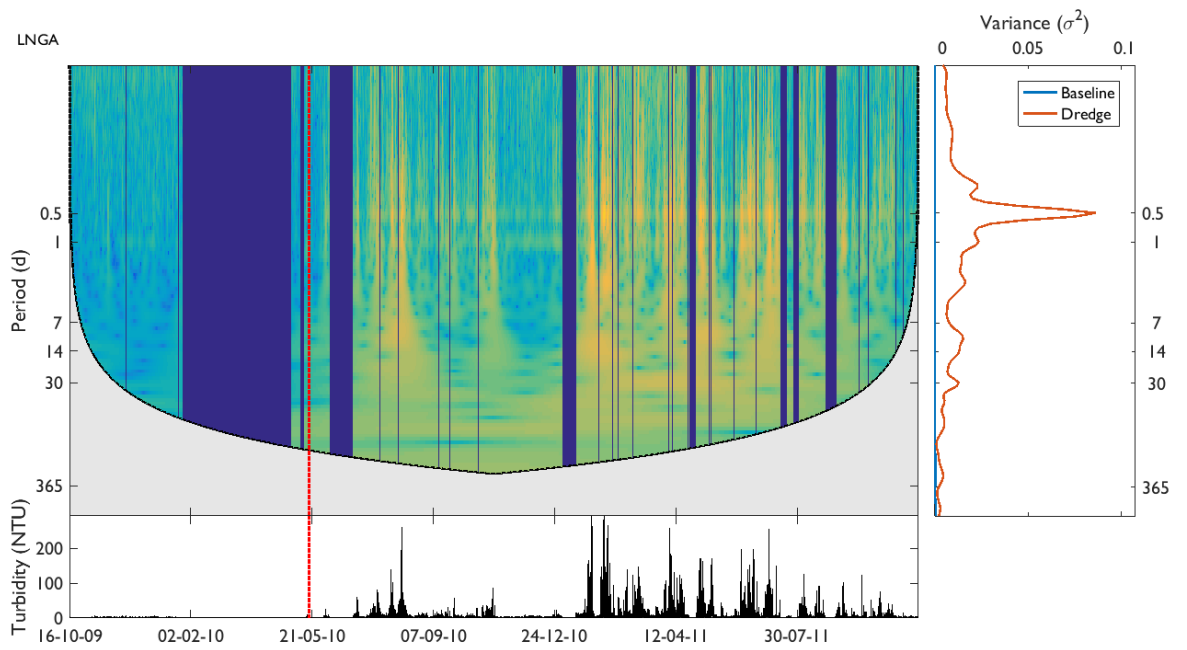
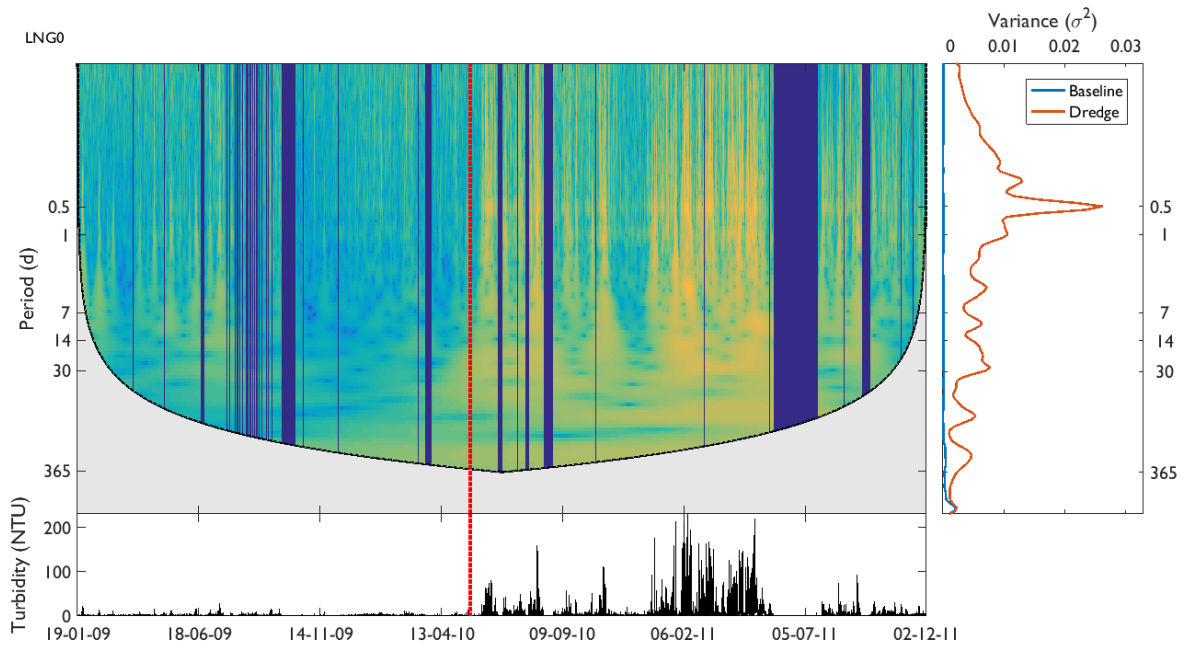
Wavelet analysis of turbidity at remaining Barrow Island sites. Other representative sites are included in Figure 3-12, Chapter 3 section 3.3.5.

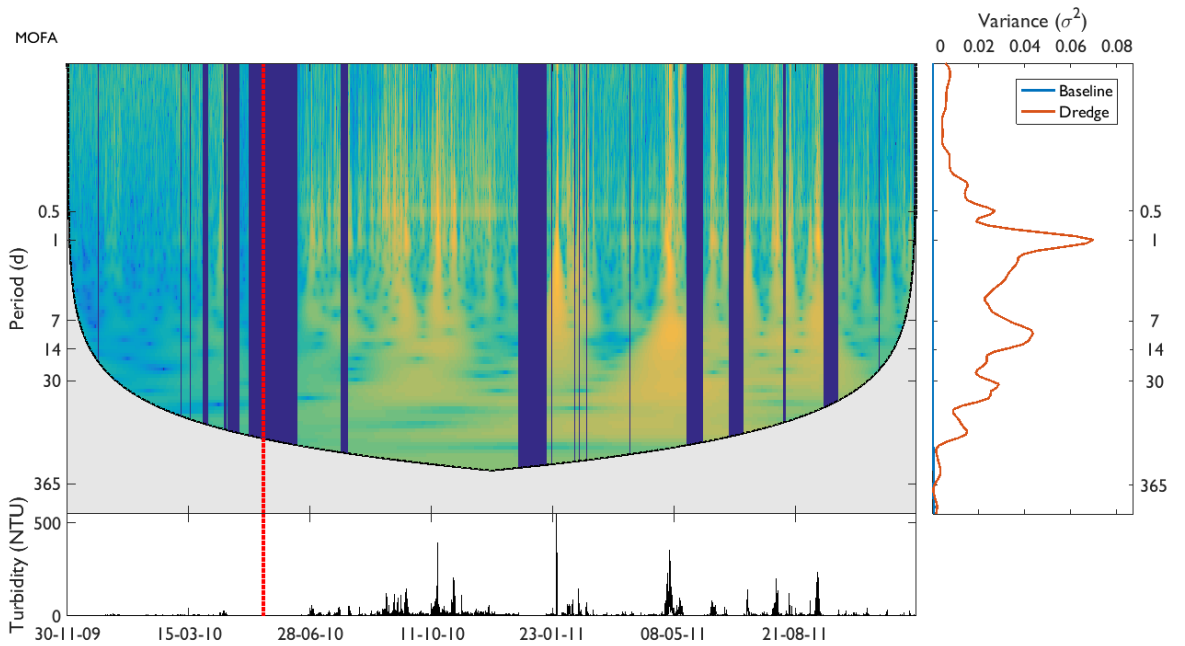
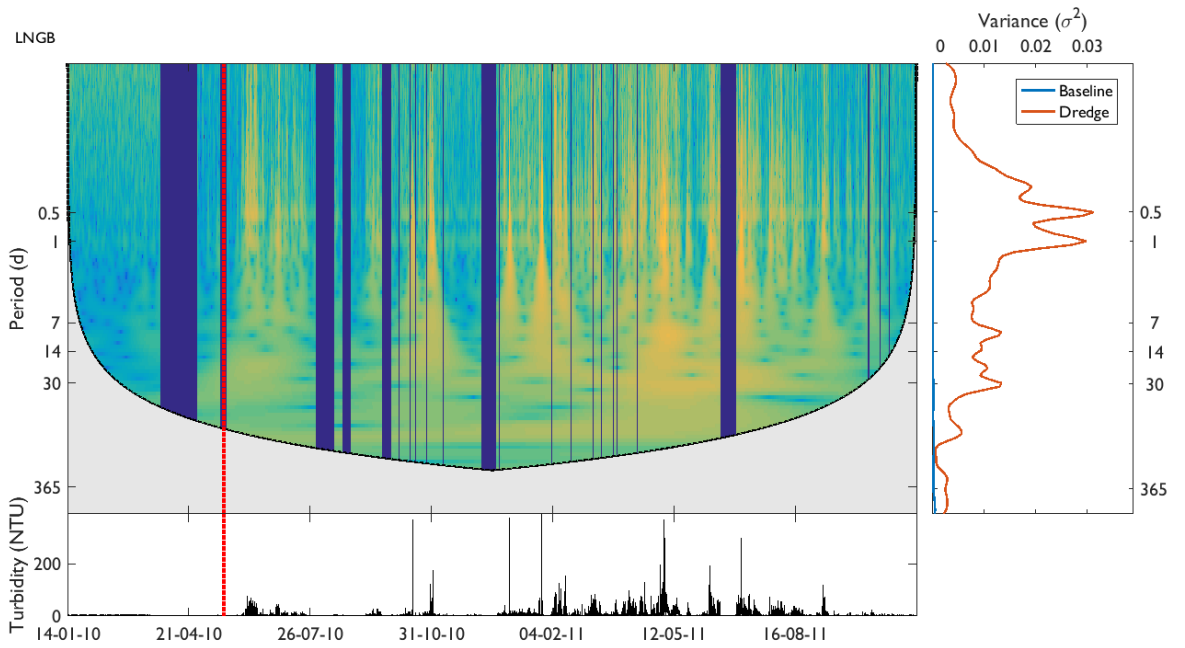


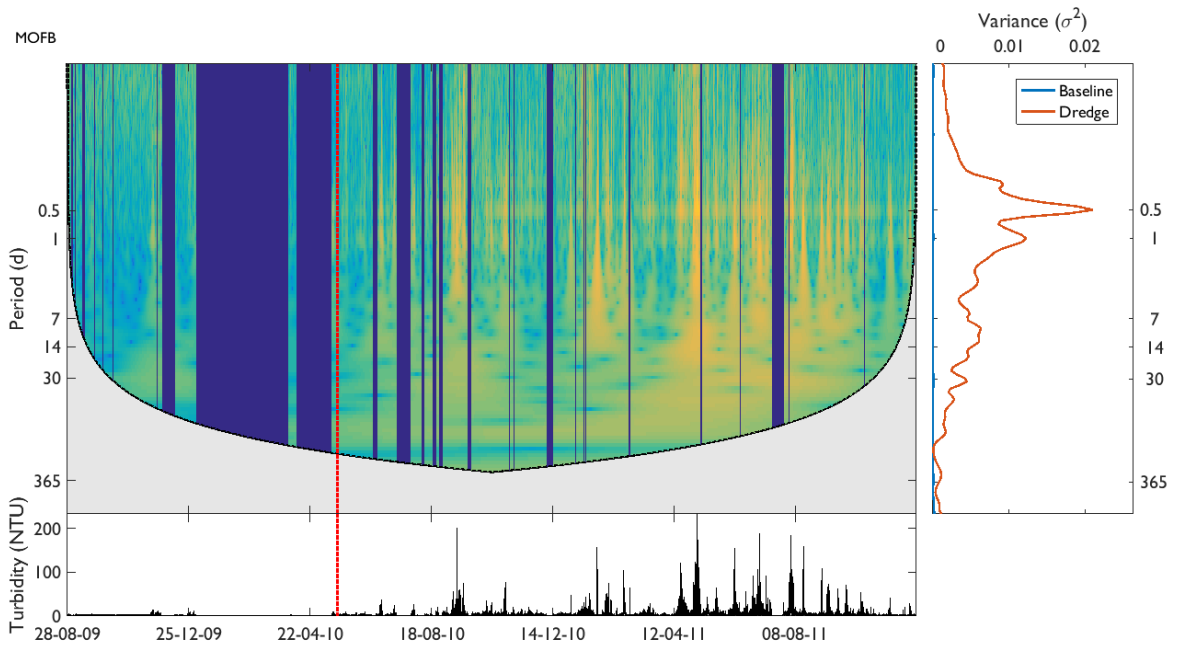
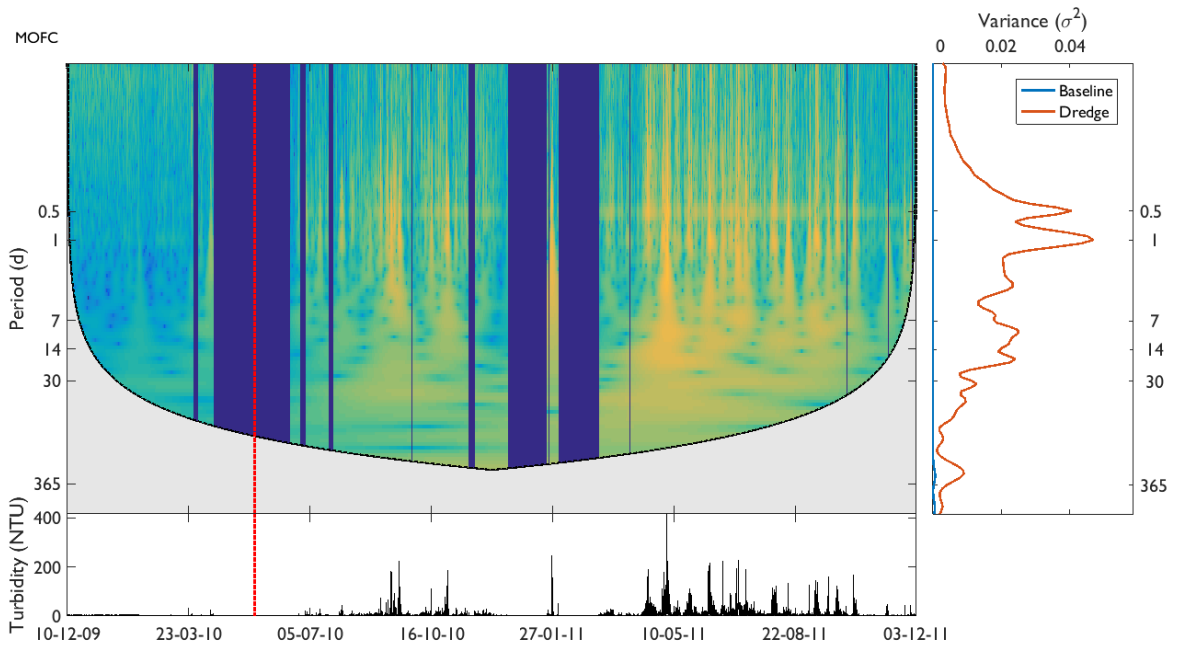


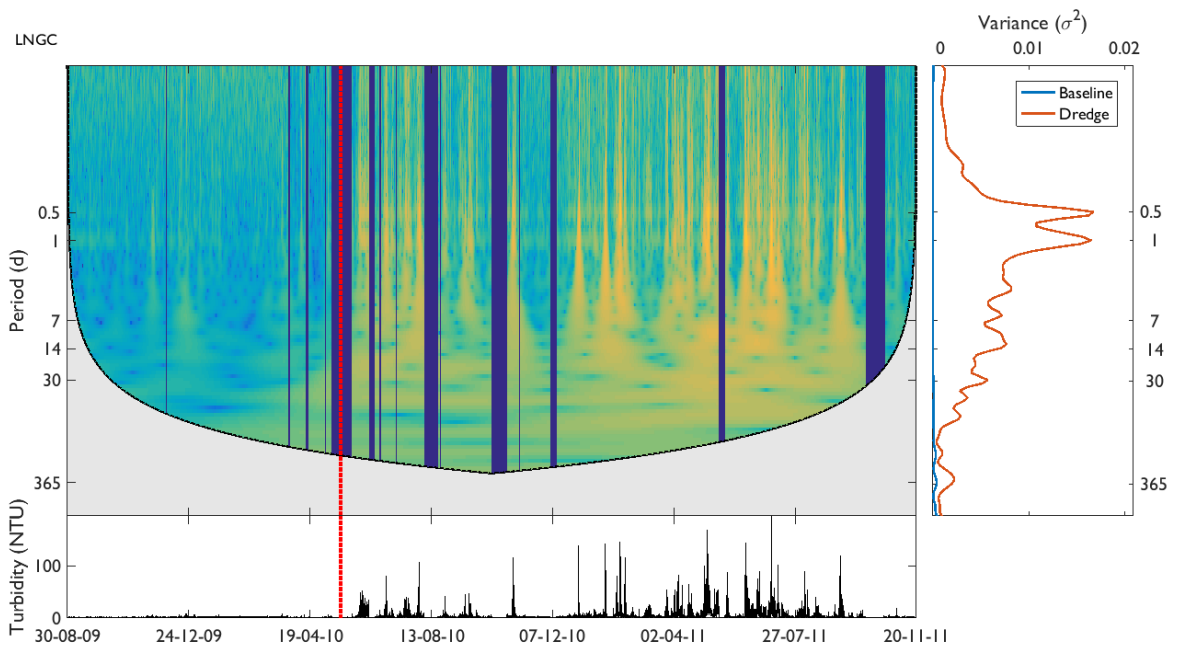
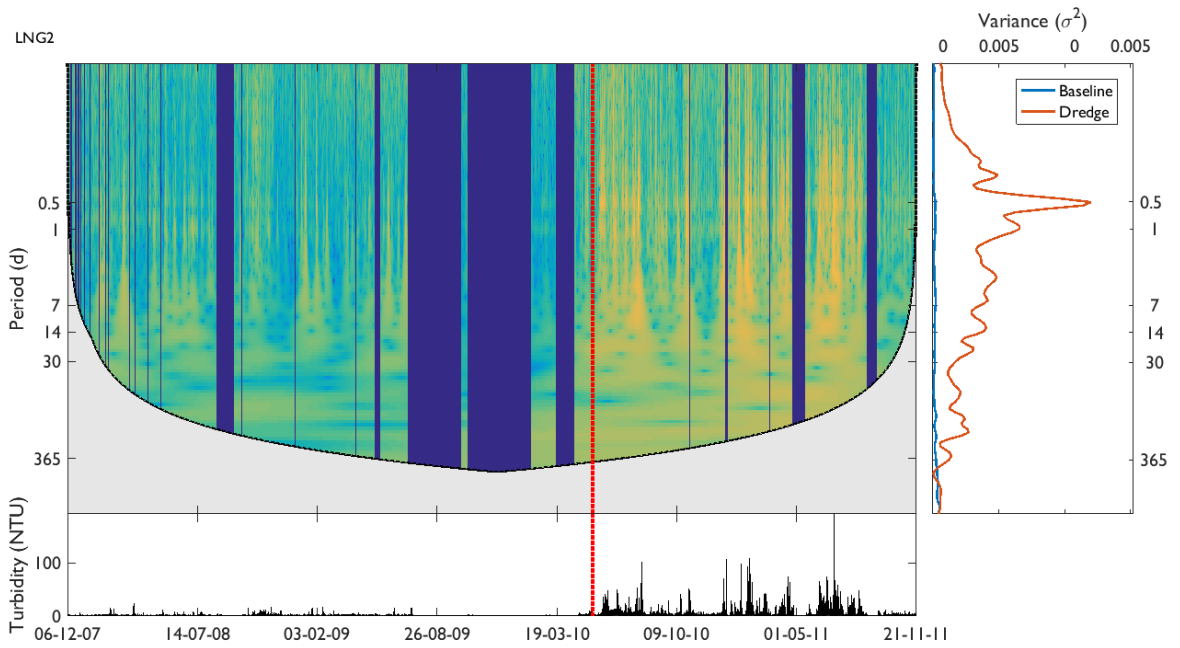




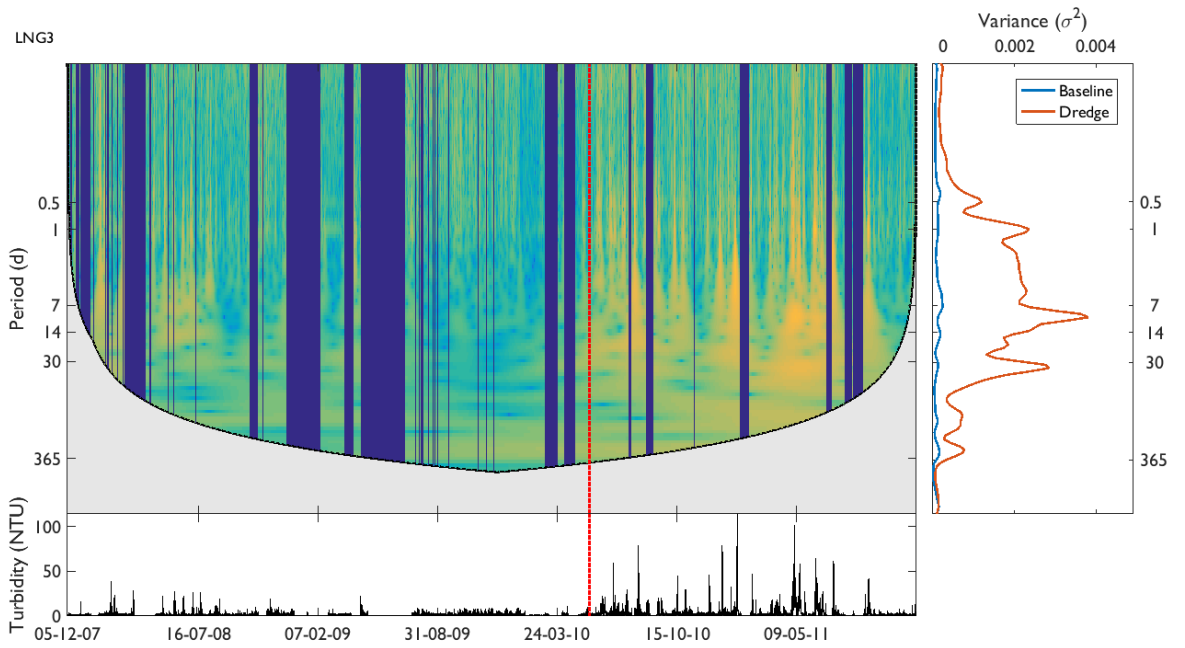
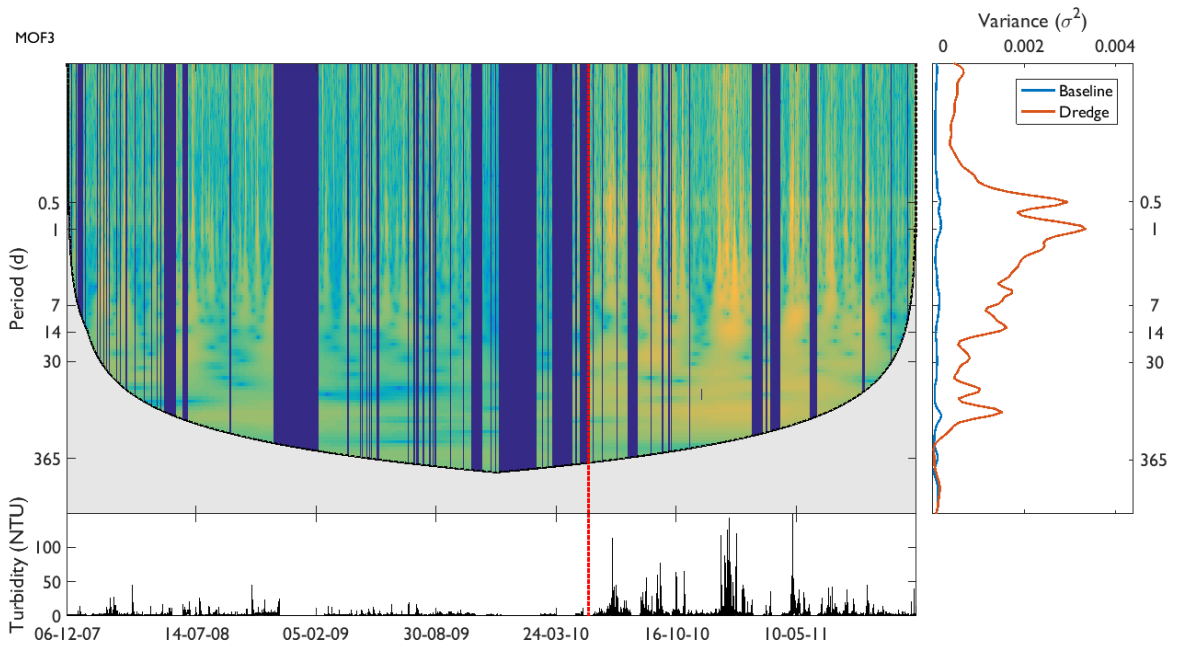


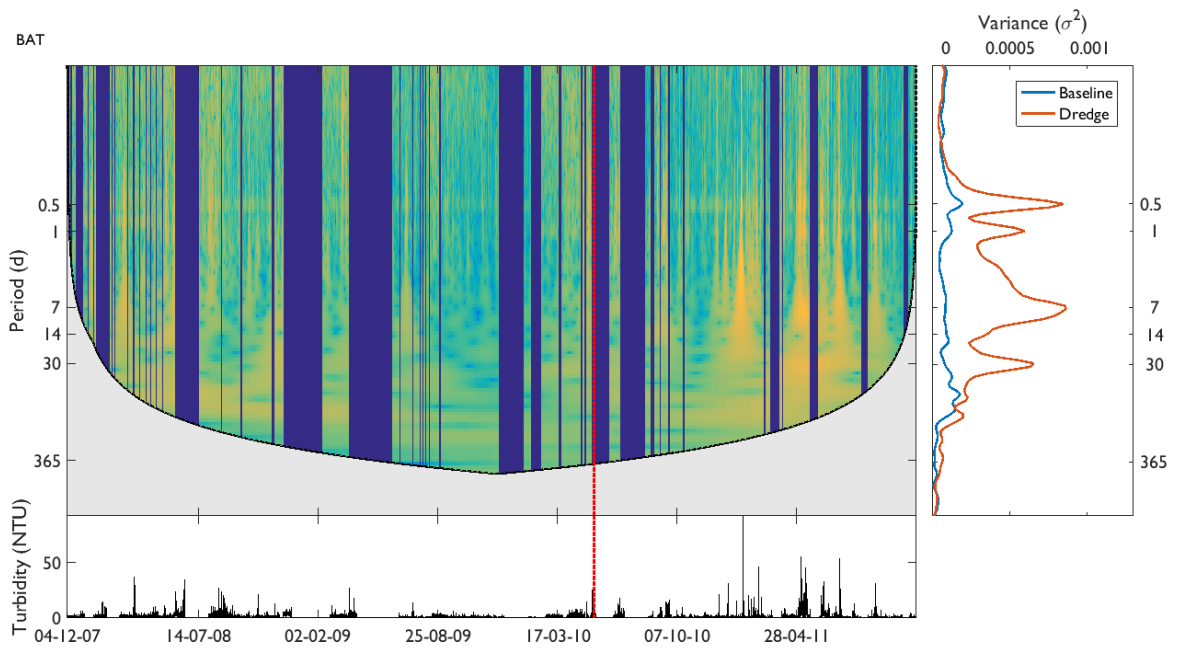
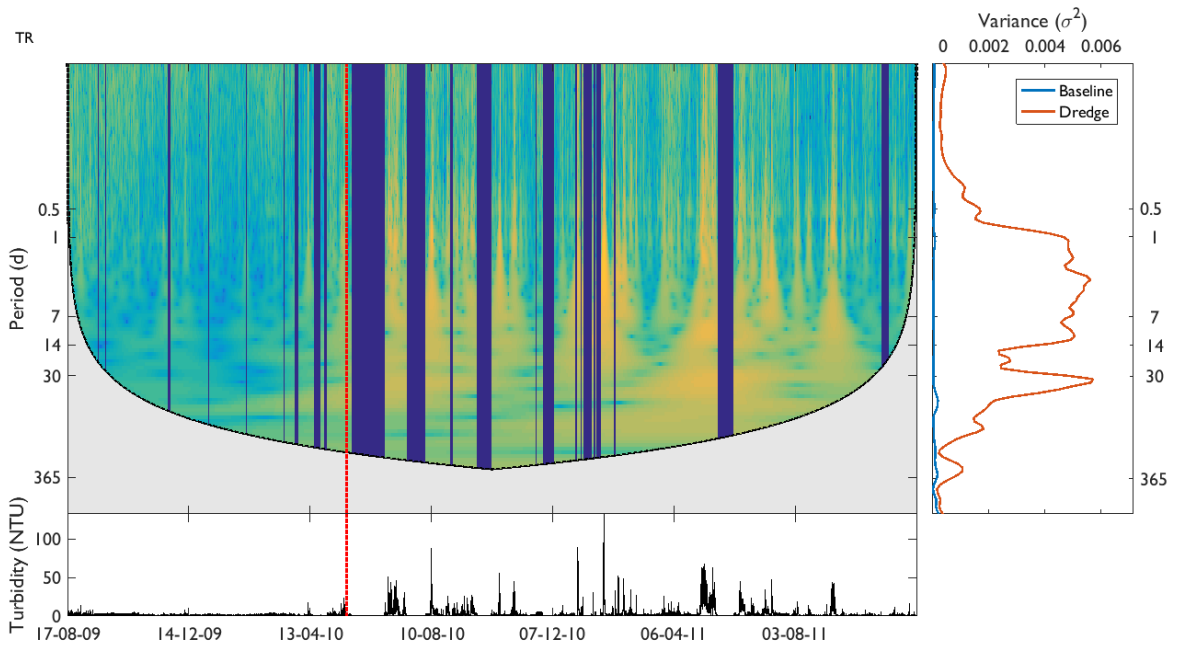


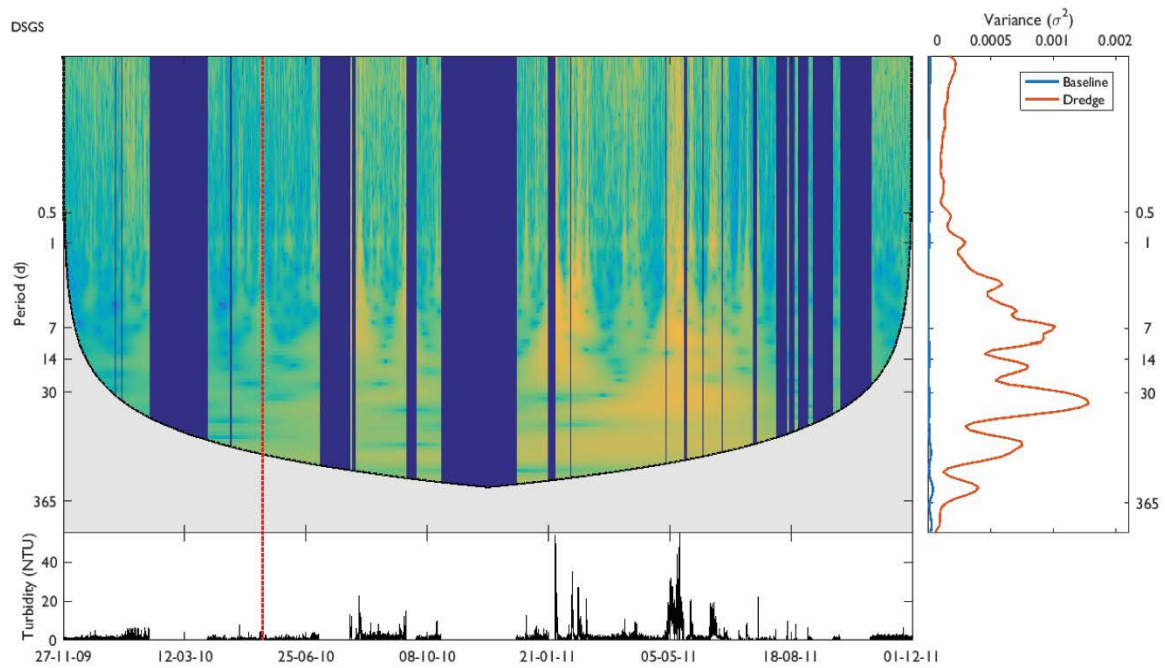
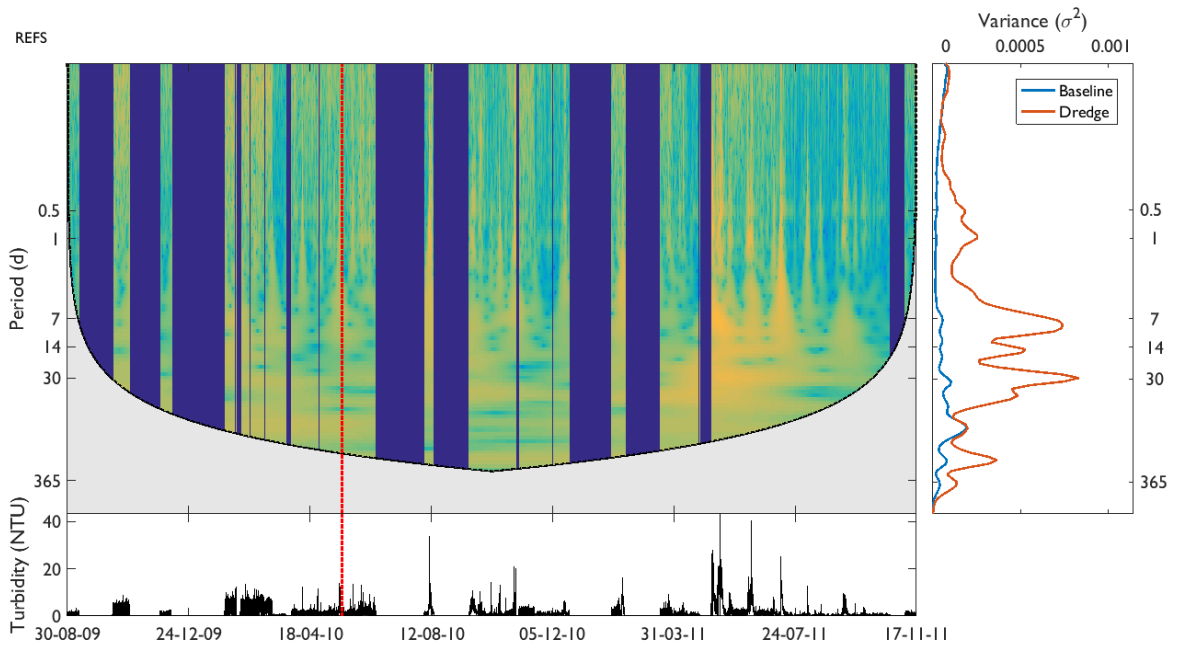












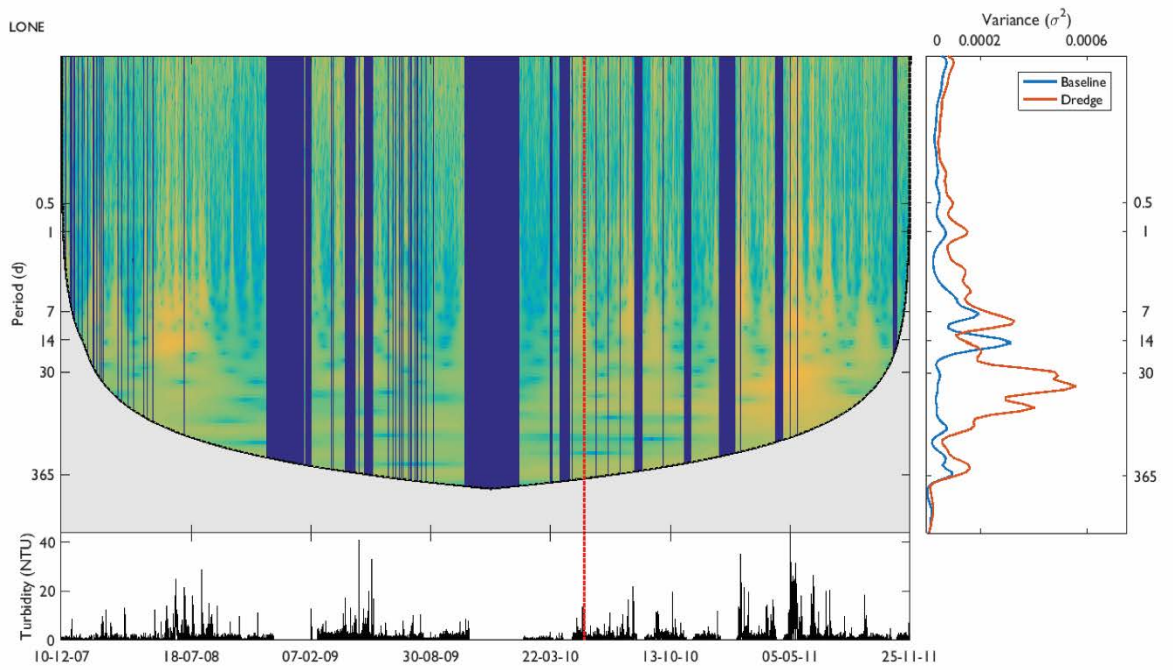


Figure C-1 Wavelet analysis of turbidity for the remaining Barrow Island sites (except sites LNG1, MOF, DUG and SBS which are presented in Figure 3-12). The three panels of each figure are: wavelet spectrum (top left), global wavelet spectrum (top right) and original time series (bottom). Areas of high energy are yellow, and low energy are light blue and green. The darker blue horizontal areas are gaps in the time series, and the grey curved area between the top and bottom plots is outside the cone of influence. The broken red line running from the wavelet spectrum through to the time series shows the start of dredging. The global wavelet spectral plot shows the peaks in the baseline data (blue line) and dredge data (orange line). 95% confidence contours have been removed as they obscure the high frequency energy regions.